

Ambient Vibration Based Model Updating Effects on the Earthquake Response of Tall Buildings

Betül Demirtaş¹, Alemdar Bayraktar¹, Aydın Dumanoglu²

¹Karadeniz Technical University, Department of Civil Engineering, Turkey

²Canik Başarı University, Department of Civil Engineering, Samsun, Turkey

ABSTRACT

The study investigates ambient vibration based model updating effects on the seismic behaviour of a RC tall building subjected to far and near-fault ground motions. A 17-storey building built in Giresun, Turkey is selected as an application. Firstly, 3D initial finite element model of the selected building is created and determined analytical dynamic characteristics. Then, experimental dynamic characteristics of the building (frequencies, mode shapes, damping ratios) are determined by Operational Modal Analysis Method from the ambient vibration tests. According to experimental results, initial finite element model is calibrated by using boundary conditions and material properties. Initial and calibrated finite element models of the building are analysed under far and near-fault ground motions. The displacements, velocity and accelerations from the analyses are compared with each other.

Keywords: Model Updating, Tall Buildings, Near-Fault Ground Motion, Ambient Vibration Testing, Seismic Response

1. INTRODUCTION

Nowadays, in developed and in developing countries, a considerable increase is observed in the construction of tall buildings. Safety evaluation of existing tall buildings to earthquake motions is very important. Dynamic characteristics such as natural frequencies, damping ratios and mode shapes are one of the most important parameters for the safety evaluation of tall buildings. The dynamic characteristics of engineering structures can be obtained by finite element method and experimental measurement methods. The most commonly used experimental measurement method is Operational Modal Analysis (OMA). In recent years, there has been an increasing interest in determination of dynamic characteristics of tall buildings by OMA. Ventura and Schuster [1], Wu and Li [2], Miyashita et al. [3], Xu and Zhan [4], Li et al. [5-8], Brownjohn et al. [9] implemented full-scale measurements of tall buildings. Li and Wu [10] created seven 3D FE models of a 78-story super-tall building, and numerical results were compared with their field measurements to identify the modelling errors for the purpose of updating FE models. Pan et al. [11] presented numerical studies on dynamic responses of the tallest building in Singapore with correlation with their field measurements. Chassiakos et al. [12] performed a study on ambient vibration data collected before, during, and after the structural retrofitting.

Near-fault ground motions which expose the structure to high input energy in the beginning of the earthquake have the potential to cause a large response and considerable

damage to structures [13]. Therefore, structural response to near-fault ground motions has received much attention in recent years. The effects of near-fault ground motions on civil engineering structures such as buildings and bridges, etc., have been investigated in many recent studies [14-19].

This paper aims to investigate the effect of ambient vibration based model updating effects on a tall RC building under far and near-fault ground motions. Firstly, the analytical dynamic characteristics are obtained by using the initial finite element model. Then experimental dynamic characteristics are extracted using Enhanced Frequency Domain Decomposition technique. Finite element model of the building is updated by changing of material properties and boundary conditions to eliminate the differences between analytical and experimental dynamic characteristics. Linear seismic behaviours of the building for both initial and updated finite element models are determined under the selected earthquake ground motions.

2. FORMULATION

The experimental dynamic characteristics of the structure were determined by Enhanced Frequency Domain Decomposition (EFDD) technique. In this technique, the natural frequencies, modal damping ratios and mode shapes were extracted from the power spectra by selecting peak values. The relationship between the unknown input and the measured responses can be written as [20-21],

$$G_{yy}(j\omega) = H(j\omega) * G_{xx}(j\omega) H(j\omega)^T \quad (1)$$

where G_{xx} is the Power Spectral Density (PSD) matrix of the input signal, G_{yy} is the PSD matrix of the output signal, H is the Frequency Response Function (FRF) matrix, and $*$ and T denote complex conjugate and transpose, respectively.

3. APPLICATIONS

3.1. Description of Selected Building

The seventeen-storey building that is constructed in Giresun, Turkey is one of the highest buildings in the city. It has a rectangular plan, two basements, a ground floor, fourteen normal floors, and an attic. The height of the building is 47.6m and its dimensions are 20 m x 30 m. The floor height of the building is 2.8m. The building has a raft foundation. While performing measurement, all floors except the basements were built with brick walls. The view, plan and section of the building are given in Fig. 1.

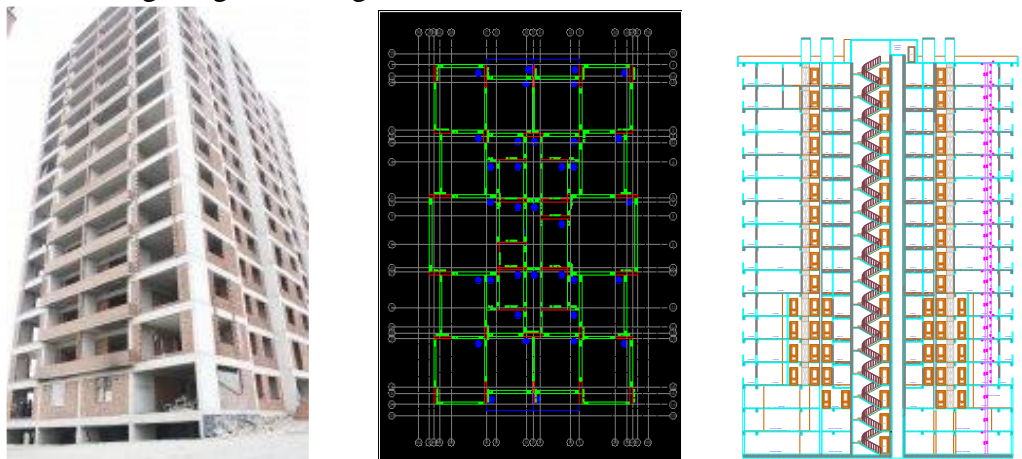


Fig. 1. The view, plan and section of the selected building

3.2. Theoretical Modal Analysis of the Building

Three-dimensional finite element model of the building was created by SAP2000 [22] program. The building was modelled by using plane and frame elements. The beams were modelled by the frame elements, and the shear walls and floors were modelled by the plane elements. 35053 joints, 4522 frames, and 41068 plane elements were used to model the building. All degrees of freedom under base of the building are assumed as fixed. The initial finite element model is given in Fig. 2.

Two different material properties were considered such as concrete and brick. The material properties assumed in the analyses are given in Table 1. The first three natural frequencies and mode shapes obtained from analytical modal analysis of the building are given Fig. 3, respectively.

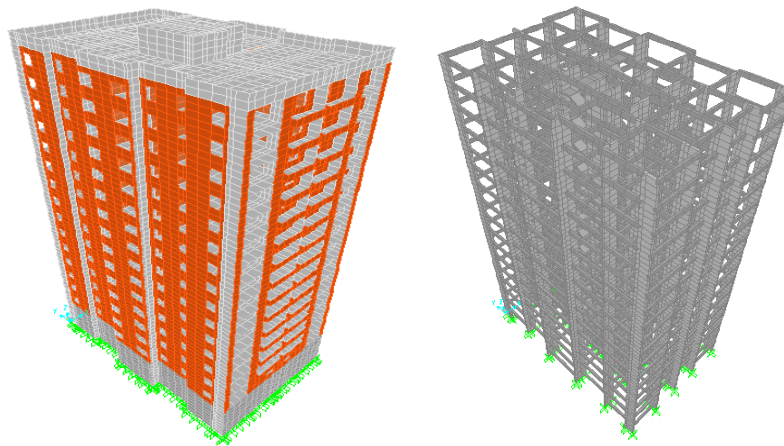


Fig. 2. The initial finite element model of the building

Table 1. Material properties used in theoretical modal analysis of the building

Materials	Modulus of Elasticity (N/m ²)	Poisson Ratio	Density (kg/m ³)
Concrete	3.2E10	0.2	2450
Brick	3.2E9	0.2	1600

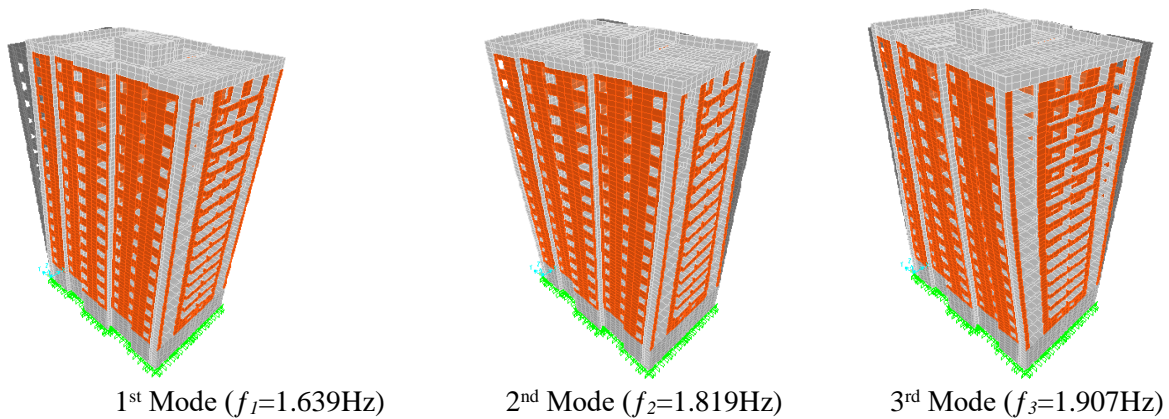


Fig 3. The first three analytical mode shapes of the building

3.3. Operational Modal Analyses of the Building

The full-scale vibration test of the building was conducted by Operational Modal Analysis (OMA) method under ambient vibrations. During the ambient measurements of the building, B&K 8340 type uni-axial accelerometers which have 10V/g sensitivity, B&K 3560 type data acquisition system with 17 channels, PULSE [23] and OMA [24] softwares were used.

The experimental dynamic behavior of the building was determined by taking the measurements from different floor levels. Total four different measurements with a reference sensor were implemented. The measurements were taken from the ground floor level, the sixth floor, the eleventh floor and the fifteenth floor, which is attic. All measurements were taken for 30 minutes. The total measurement setup and location of the accelerometers are given in Fig. 4. The power spectral density matrices of the building obtained using the EFDD technique are depicted in Fig. 5. The first three experimental natural frequencies and mode shapes of the building are given in Fig. 6.

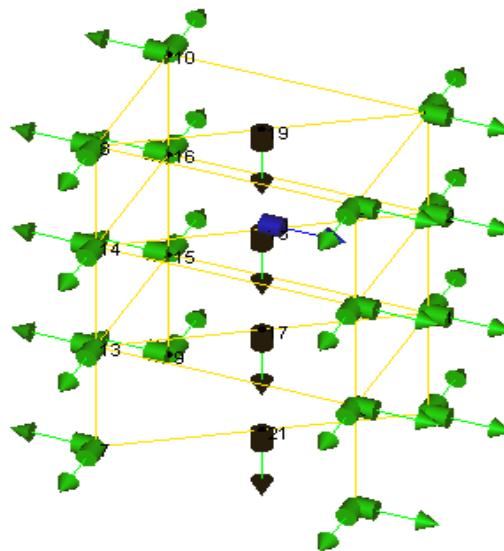


Fig. 4. Total measurement setup and location of the accelerometers

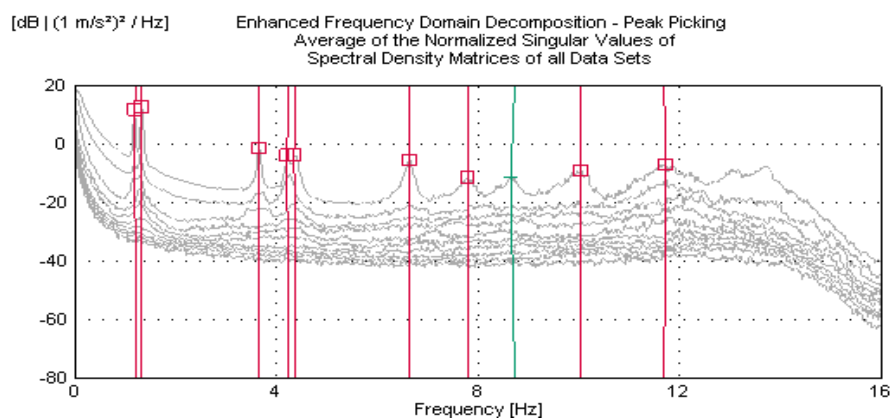


Fig.5. The power spectral density function from the EFDD technique

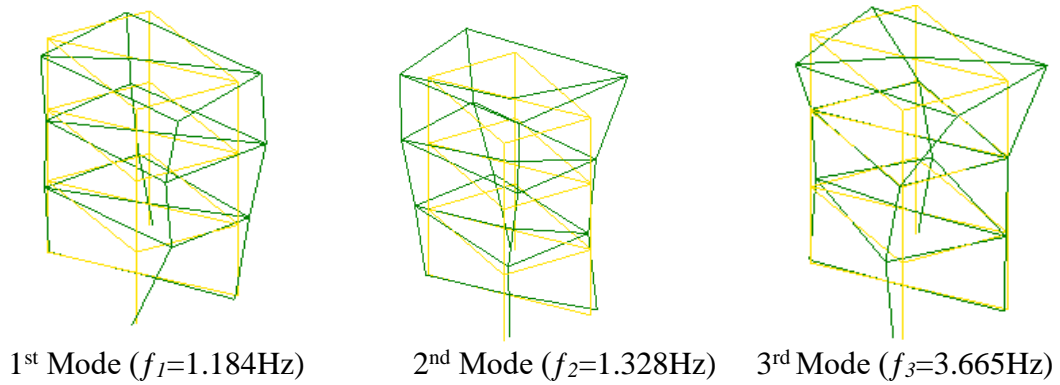


Fig. 6. The first three experimental mode shapes of the building

3.4. Finite Element Model Updating of the Building

When the natural frequencies and mode shapes obtained from the analytical and experimental studies are compared, it is seen that there are some differences between the results. Therefore, it needs to calibrate the initial analytical model in order to determine the real behavior of the building. For the calibration, modulus of elasticity of brick and boundary conditions are considered. The experimental, initial and updated natural frequencies are given in Table 2. The calibrated mode shapes are presented in Fig. 7.

Table 2. The experimental and analytical natural frequencies of the building

Mode Numbers	Natural Frequencies (Hz)			
	Experimental	Initial Model	Updated Model	Differences (%)
1	1.184	1.639	1.184	0.00
2	1.296	1.820	1.291	0.39
3	1.328	1.907	1.370	3.16

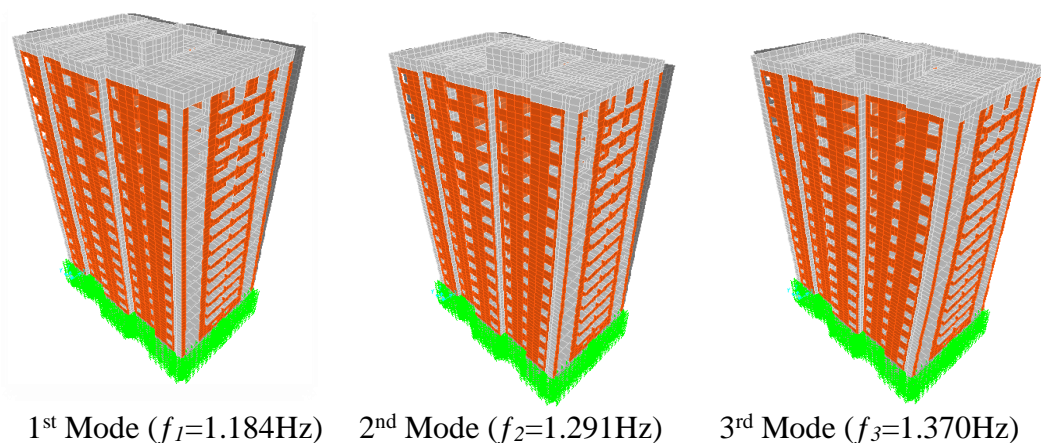


Fig. 7. The first three mode shapes of the updated building model

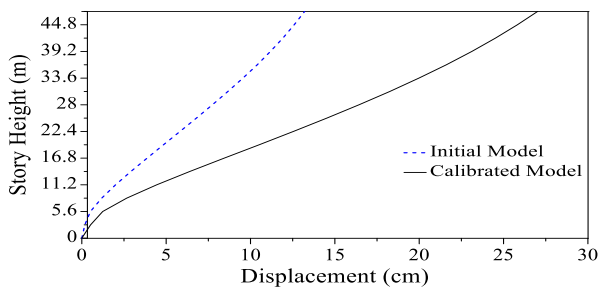
3.5. Analyses of the Building for Earthquake Motions

Duzce earthquake in 1999 as a near fault ground motion and Imperial Valley earthquake in 1979 as far fault ground motion are selected for the analysis. Some characteristics of these earthquakes are given in Table 3 (M: magnitude, d: distance, PGA: peak ground acceleration, PGV: peak ground velocity, PGD: peak ground displacement).

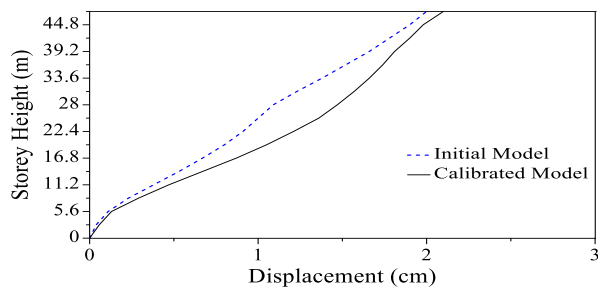
Table 3. Characteristics of the selected near and far-fault ground motions [25]

Earthquake	Record/Component	M	d (km)	PGA (cm/s ²)	PGV (cm/s)	PGD (cm)
1999 Duzce	DUZCE/DZC270	7.1	8.2	524.84	83.5	51.59
1979 Imperial Valley	IMPVALL/H-VCT345	6.5	54.1	163.83	8.3	1.05

The initial analytical and updated models of the building are analyzed under earthquake motions linearly. The ground motions are applied to the building in X-axis direction (in the weak direction of the building). The relationship between height and displacements under earthquake motions is given in Fig. 8. As can be seen from Fig. 8, the displacements increase with increasing story height. In addition, it is seen that the displacements obtained from the calibrated model are bigger than those of the initial model for both far and near-fault ground motions.



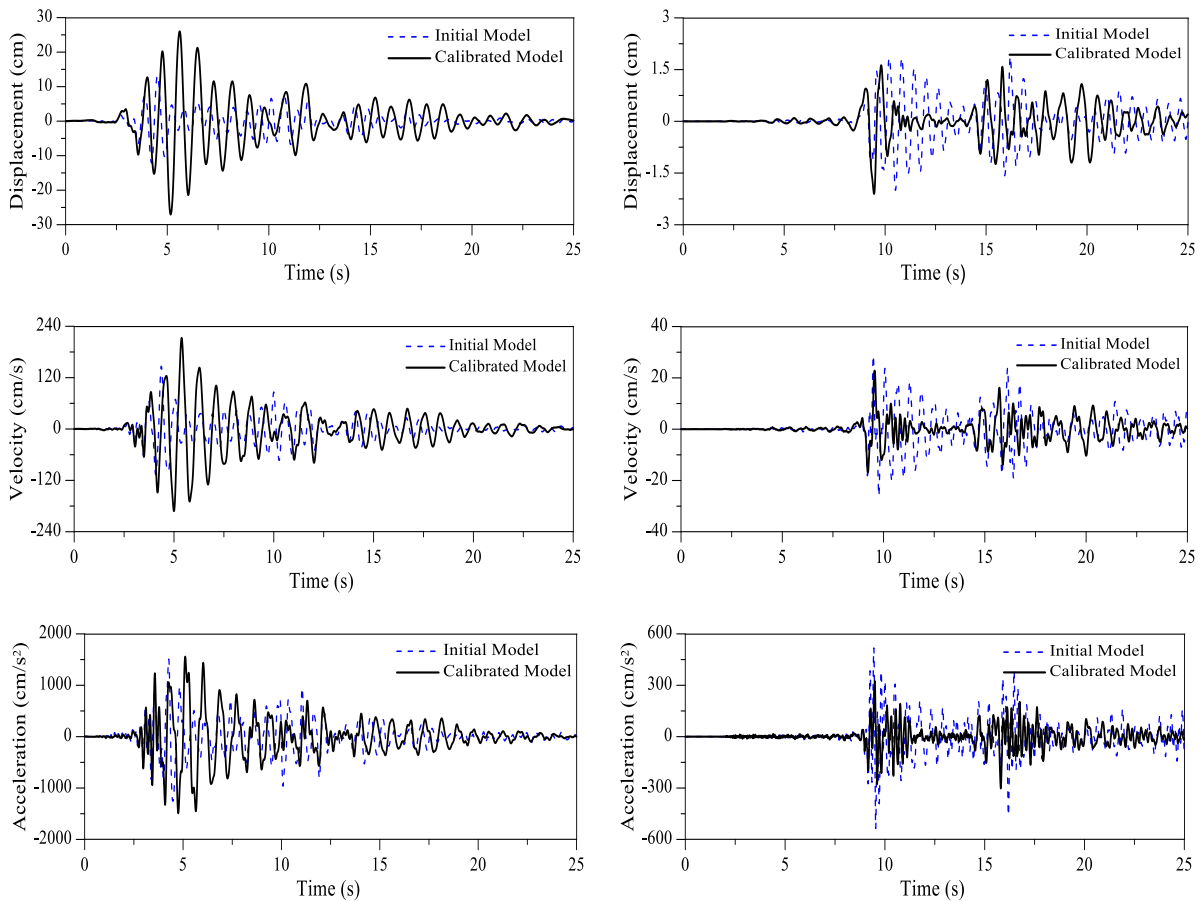
a) 1999 Duzce Earthquake



b) 1979 Imperial Valley Earthquake

Fig 8. The relationship between story height and displacements under earthquake motions

Displacements, velocities and accelerations occurring on the 17th floor of the building under far and near-fault ground motions are comparatively plotted in Fig. 9. Frequency contents of displacement, velocity and acceleration obtained from the initial and the calibrated models under near and far-fault ground motions are observed to be compatible with each other.



a) 1999 Duzce earthquake

b) 1979 Imperial Valley earthquake

Fig. 9. The time histories of the displacement, velocity and accelerations on the 17th floor

4. CONCLUSIONS

The paper investigates the effect of ambient vibration based model updating effects on a tall RC building under far and near-fault earthquake motions. The results obtained from the study are summarized below:

- Approximately 43% difference between the initial analytical and experimental natural frequencies of the building for the first three modes is observed. After model calibrating, the differences between calculated and experimental natural frequencies are reduced to approximately 3%. It is also observed that calibrated analytical and experimental mode shapes have a close harmony.
- Differences between displacements obtained from the initial and the calibrated models along the height of the building under the near fault ground motion are bigger than those of the far-fault ground motion.
- The displacements, velocities and accelerations calculated from the calibrated model for near-fault ground motion are generally larger than those of the initial model. However, it is observed opposite situation for the far-fault ground motion.
- Frequency contents of the displacement, velocity and accelerations obtained from the initial and the calibrated models are generally compatible with each other.

It can be generally said that the effects of finite element model updating and near-fault ground motion in the assessment of tall RC buildings must be taken into account.

5. REFERENCES

- [1] Ventura, C.E. and Schuster, N.D., (1996) Structural dynamic properties of a reinforced concrete high-rise building during construction. *Canadian Journal of Civil Engineering*, 23:950_72.
- [2] Wu, J.R., and Li, Q.S. (2004) Finite element model updating for a high-rise structure based on ambient vibration measurements. *Engineering Structures*, 26, 7, 979-990.
- [3] Miyashita, K., Itoh, M., Fujii, K., Yamashita, J. and Takahashi, T. (1998) Full-scale measurements of wind-induced responses on the Hamamatsu ACT tower. *Journal of Wind Engineering and Industrial Aerodynamics*, 74–76: 943–953.
- [4] Xu, Y.L. and Zhan, S. (2001) Field measurements of Di Wang tower during typhoon York. *Journal of Wind Engineering and Industrial Aerodynamics* 89: 73–93.
- [5] Li, Q.S., Fang, J.Q., Jeary, A.P. and Wong, C.K. (1998) Full scale measurements of wind effects on tall buildings. *Journal of Wind Engineering and Industrial Aerodynamics* 74–76: 741–450.
- [6] Li, Q.S. Yang, K., Wong, C.K. and Jeary, A.P. (2003) The effect of amplitude-dependent damping on wind-induced vibration of super tall building. *Journal of Wind Engineering and Industrial Aerodynamics* 91: 1175–1198.
- [7] Li, Q.S., Wu, J.R., Liang, S.G., Xiao, Y.Q., and Wong, C.K. (2004) Full-scale measurements and numerical evaluation of wind-induced vibration of a 63-story reinforced concrete tall building. *Engineering Structures*, 26, 12, 1779-1794.
- [8] Li, Q.S., Xiao, Y.Q., Fu, J.Y. and Li, Z.N. (2007) Full-scale measurements of wind effects on the Jin Mao building. *Journal of Wind Engineering and Industrial Aerodynamics* 95: 445–466.
- [9] Brownjohn, J.M.W. (2003) Ambient vibration studies for system identification of tall buildings. *Earthquake Engineering & Structural Dynamics*, 32(1), 71-95.
- [10] Li, Q.S. and Wu, J.R. (2004) Correlation of dynamic characteristics of a super tall building from full-scale measurements and numerical analysis with various finite element models. *Earthquake Engineering & Structural Dynamics*;33: 1311_36.
- [11] Pan, T.C, Brownjohn, J.M.W. and You, X.T. (2004) Correlating measured and simulated dynamic responses of a tall building to long-distance earthquakes. *Earthquake Engineering & Structural Dynamics*, 33:611_32.
- [12] Chassiakos, A.G., Masri, S.F., Nayeri, R.D., Caffrey, J.P., Tzong, G. And Chen, H.P. (2005) Use of vibration monitoring data to track structural changes in a retrofitted building. *Structural control and Health Monitoring*, 14:2, 219238.
- [13] Liao, W.I., Loh, C.H. and Lee, B.H. (2004) Comparison of dynamic responses of isolated and non- isolated continuous girder bridges subjected to near-fault ground motions. *Engineering Structures*, 26(14):2173–83.
- [14] Çavdar, Ö. (2012) Probabilistic sensitivity analysis of two suspension bridges in Istanbul, Turkey to near-and far-fault ground motion. *Natural Hazards and Earth System Sciences*;12(2):459–73.
- [15] Dicleli, M. and Buddaram, S. (2007) Equivalent linear analysis of seismic-isolated bridges subjected to near-fault ground motions with forward rupture directivity effect. *Engineering Structures*. 29(1):21–32.

- [16] Liu, T., Luan, Y. and Zhong, W. (2012) Earthquake responses of clusters of building structures caused by a near-field thrust fault. *Soil Dynamics and Earthquake Engineering*, 42:56–70.
- [17] Mazza, F. And Vulcano, A. (2012) Effects of near-fault ground motions on the nonlinear dynamic response of base-isolated RC framed buildings. *Earthquake Engineering and Structural Dynamics*, 41(2):211–32.
- [18] Mortezaeia, A., Ronaghb, H.R. and Kheyroddinc, A. (2010) Seismic evaluation of FRP strengthened RC buildings subjected to near-fault ground motions having fling step. *Composite Structures*, 92(5):1200–11.
- [19] Trifunac, M.D. (2009) The role of strong motion rotations in the response of structures near earthquake faults. *Soil Dynamics and Earthquake Engineering*, 29 (2):382–93.
- [20] Jacobsen, N.J., Andersen, P. and Brincker, R. (2006) Using enhanced frequency domain decomposition as a robust technique to harmonic excitation in Operational Modal Analysis. *Proceedings of ISMA2006: International Conference on Noise and Vibration Engineering*, Leuven, Belgium.
- [21] Bendat, J.S. and Piersol, A.G. (2004) *Random data: analysis and measurement procedures*. 3th Edition, John Wiley and Sons, USA.
- [22] SAP2000 (2008) *Integrated Finite Element Analysis and Design of Structures*, Computers and Structures, Inc., Berkeley, California, USA.
- [23] PULSE (2006) *Analyzers and Solutions*, Release11.2. Bruel and Kjaer, Sound and Vibration Measurement A/S, Denmark.
- [24] OMA (2006) *Operational Modal Analysis*, Release 4.0. Structural Vibration Solution A/S, Denmark.
- [25] URL_1, <http://peer.berkeley.edu/smcat/search.html>.

Regional and temporal evaluation of seismicity in the Vlorë-Elbasani-Dibrë Transversal Fault Zone, Albania

Rrapo Ormeni¹, Serkan Öztürk², Olgert Gjuzi¹

¹*Institute of Geosciences, Energy, Water and Environment Polytechnic University, Tirana*

²*Gümüşhane University, Department of Geophysics, Gümüşhane, Turkey*

ABSTRACT

Characteristics of seismic activity along the Vlorë- Lushnjë-Elbasani-Dibrë (V-L-E-D) Transversal Fault Zone are analyzed between 1964 and 2015. There are a total of 2814 events in the time interval 1964 and 2015 with $M_d \geq 1.7$. This study is focused on the correlation of seismotectonic b -value, precursory quiescence Z -value, and interrelationships between some other seismicity parameters. The distribution of the relatively low b -value coincides with the tectonic compression field which acts along the V-L-E-D Transversal Fault Zone. The distribution of the relatively low b -value coincides with the tectonic compression field which acts along the V-L-E-D Transversal Fault Zone. Anomalously low b -value areas coincide more or less with the spatial distribution of $M \geq 5.0$ earthquakes and their known rupture extents. Temporal changes in b -value may be related to the stress variations in these times before and after the main events. The lowest Z -values show that the variations in seismic activity rate are not significant, and the highest Z -values demonstrate a decrease in seismicity rate. In the Z -value maps for all parts of the V-L-E-D, three areas exhibit significant seismic quiescence: centered at 41.00°N-19.78°E (region A, around Lushnjë), 40.99°N-20.03°E (region B, in the Cërriku), 40.81°N-19.86°E (region C, including Kucovë). In addition to these three significant areas, there are some small quiescence areas in different parts of the V-L-E-D.

Key words: *Vlorë-Lushnjë-Elbasani-Dibrë Fault Zone, seismic activity, b -value, Z -value, decompose*

INTRODUCTION

The Albania region is a seismically active area with tens of destructive large earthquakes over the past twenty centuries as revealed from the historical sources [7] [16]. The main cause of Albanian seismicity is the collision of Adria with the Albanian orogen. This continental collision directly influences on the inner part of the country, on the longitudinal and transverse faults cutting across the eastern and north-eastern part of Albania [2] [9]. The Lushnjë-Elbasani-Dibrë (V-L-E-D) Transversal Fault Zone in Albania is a major tectonic feature with a well-defined fault trace and an established history of seismicity. Activity of the V-L-E-D during the 20th century began with the destructive Peshkopia earthquake in 1920 in northeast Albania and migrated westwards by a series of destructive earthquakes in 1921, 1930, 1935, 1942, 1959,

1962, 1967, 1982, 2009, and 2014 [2] [10] [16]. In the present study, our main goal is to analyze the spatial and temporal properties of seismicity pattern in the VLED Transversal Fault Zone in order to better understand the seismic hazards in this significant area.

I. GEOLOGIC, TECTONIC / NEOTECTONIC SETTINGS OF ALBANIA

The main geological structures found within the Albanian territory are called the Albanides, which are part of the Dinaric-Albanid-Hellenic arc of the Alpine orogen. They are located between Hellenides in the south and Dinarides in the north, which together form the Dinaric branch of the Mediterranean Alpine Belt. The Vlorë-Elbasan-Dibër (V-L-E-D) Transversal Fault Zone [10] [17] (Fig. 1) with north-east strike dislocates the structure of the Albanides along their entire width. It is expressed by Vlorë and Lushnjë flexure, Dumreë diapire dome, Elbasan Quaternary depression, Labinoti transversal structure, marked by important quaternary infill (Melo, 1986), Gollubordë transversal horst continues toward the Tetovë Quaternary graben in FYROM [17] (Fig. 1).

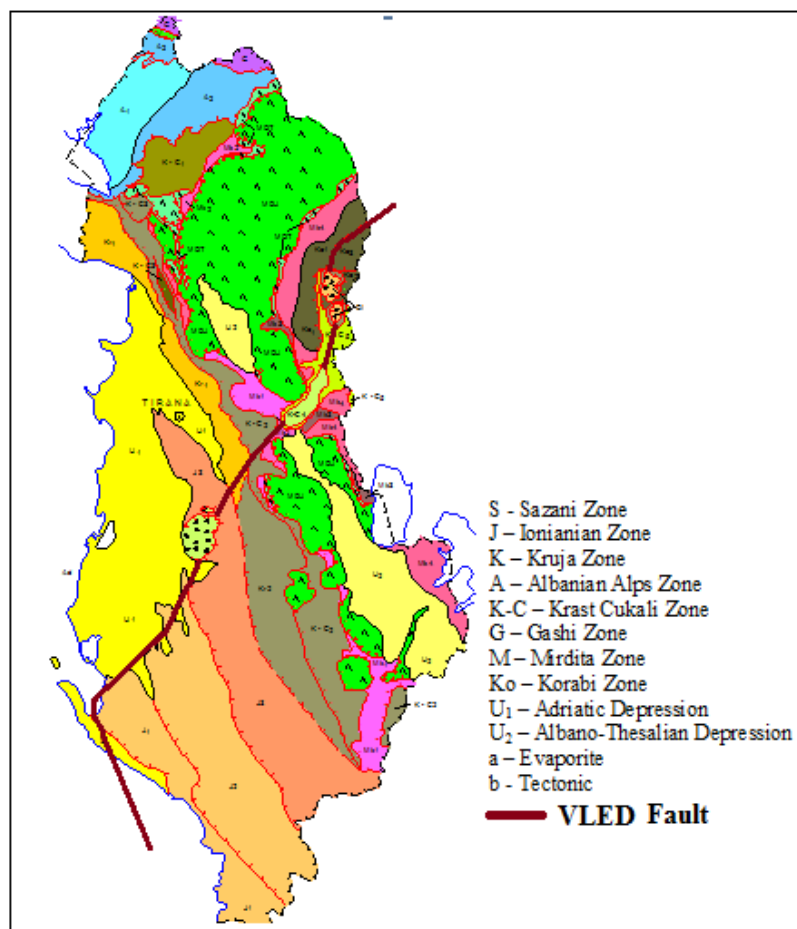


Fig. 1. Schematic tectonic map of Albania and seismic source zones in the VLED Transversal Fault Zone.

This fault zone, NE trending for approximately 100 km in Albanian territory, is composed of fragmentary normal faults cutting across the Krasta zone and dividing the Mirdita ophiolites zone in two main segments [2] (Fig. 1). Based on the analysis of the focal mechanisms of moderate and strong earthquakes, the V-L-E-D transverse fault zone plays an important role in the seismotectonics of Albania, as well as of the FYROM [2] [8] [15].

II. DATA AND DESCRIPTIONS OF THE METHODS

Epicenter distributions of all earthquakes ($M_d \geq 1.7$) and the principal main shocks ($M_d \geq 4.5$) in the study region are shown in Figure 2. The focal depth analysis reveals that this seismicity was mainly generated in the shallow upper crust under tectonic conditions that were described earlier [6-7]. The Vlorë-Lushnjë-Elbasan-Dibrë transverse fault zone has experienced many damaging earthquakes during the past 95 years [8], [9] [15] [16]. The Elbasan section has ruptured during earthquake occurred on 18 December 1920, (I=VIII degree), 31 March 1930 (M 5.7) and 19 May 2014 (M 5.2). The Dibrë earthquake of 30 November 1967 (M 6.7) is one of the greatest earthquakes that occurred in Albania.

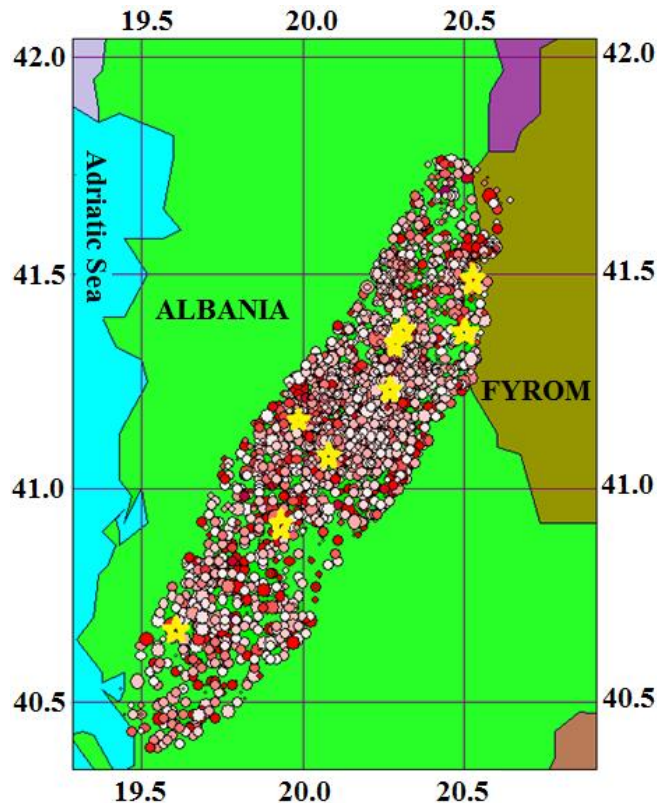


Fig. 2. Epicenter distributions of all earthquakes with $M_d \geq 1.7$ and depth < 70 km in the VLED Transversal Fault Zone between 1964 and 2015. Stars represent the principal main shocks with $M_d \geq 4.5$.

The Dibrë section have occurred other earthquakes 30 March 1921 Peshkopia (I=VIII-IX degree), 27 August 1942 Peshkopia (M 6.0), 6 September 2009 Gjorica (M 5.4). The Lushnjë-Fieri section have occurred 1 Shtator 1959 Lushnjë (M 6.2), 18 Mars 1962 Fieri (M 6.0), 16 November 1982 Fieri (M 5.4). The earthquakes that occurred in the Vlorë segment are: 21 November 1930 Qaf-Llogaras (M 6.0). The behavior of seismic activity analyzed in this study is restricted to shallow events (< 50 km). There are a total of 2814 events in the time interval 1964 and 2015 with $M_d \geq 1.7$. In order to characterize the seismic behavior, a number of statistical parameters are used; namely size-scaling parameters (such as slope of recurrence curve b -value), temporal and spatial distribution of earthquakes with characteristics of seismic quiescence Z -value as well as the histograms of temporal, spatial and magnitude distribution along the Vlorë-Lushnjë-Elbasan-Dibrë fault zone.

III.1. Magnitude-frequency relation (*b*-value) and magnitude completeness, *Mc*

The relationship between the size of an earthquake and its frequency of occurrence named as FMD (Gutenberg & Richter, 1944) [4] and defined as:

$$\log_{10} N(M) = a - bM \quad (1)$$

where $N(M)$ is the cumulative number of events with magnitudes equal to or larger than M . The parameters a and b are constants. The a -value shows the activity level of seismicity. The b -value is the slope of the frequency-magnitude distribution. The b -value has been shown to be inversely related to the shear stress in the crust [20]. b -value is positively correlated with the increasing heterogeneity in the crust [5] and shows strong heterogeneity in finer scales. The b -value can be estimated from the maximum likelihood method [1]:

$$b = 2.303 / (M_{\text{mean}} - M_{\text{min}} + 0.05) \quad (2)$$

where M_{mean} is the average value of magnitude and M_{min} is the minimum completeness magnitude in the seismicity catalogue to be analyzed. 0.05 value in this equation is a correction constant. The 95% confidence limits on the estimates of b -value are $\pm 1.96 b / n$, where n is the number of events used to make estimation. The completeness magnitude, Mc , is an important parameter for many seismicity studies [13]. In these studies, the usage of the maximum number of events available is necessary for high-quality results. Tendency of decreasing of b -values in temporal distributions before the large main shocks can be used as an indicator of the next earthquake [12]. Estimating of Mc can be made by the assumption of Gutenberg–Richter’s power-law distribution against magnitude [20].

III.2. Decomposing of catalogue and precursory quiescence *Z*-value

Some activities such as foreshocks, aftershocks, earthquake swarms, generally mask temporal variations of the number of events and the related analysis. The elimination of the dependent events from the catalogue is necessary for the reliable analysis of seismicity rate changes. In order to decompose (or decluster) the data based on the algorithm developed by Reasenber (1985), *ZMAP* software in Wiemer (2001) is preferred [21]. In study region, there are 2814 events with magnitudes greater than or equal to 1.7. Mc value for region is 2.5 and the number of earthquakes exceeding this completeness value is 1992. The decomposing process took away 460 events and 16% of the earthquakes were removed from the whole catalogue of region. Thus, the number of events for *Z*-value analysis was taken as 2354 for the VLED Fault Zone. In order to rank the significance of quiescence, the standard deviate *Z*-test is used [19], generating the Log Term Average (LTA) function for the statistical evaluation of the confidence level in units of standard deviations:

$$Z = (R1 - R2) (S1 / N1 + S2 / N2)^{1/2} \quad (3)$$

where $R2$ is the mean seismicity rate in the foreground window, $R1$ is the average number of events in all background period, S and N are the standard deviations and the number of samples, within and outside the window. The *Z*-value calculated as a function of time, letting the foreground window slide along the time period of catalogue, is called LTA.

III. RESULTS OF SEISMICITY ANALYSIS AND DISCUSSION

A detailed investigation of the seismicity behavior in the V-L-E-D Transversal Fault Zone in Albania is made by using the Gutenberg–Richter b -value, seismic activity rate changes, Z -value and also by evaluating the histograms of the temporal, spatial and magnitude distribution in time intervals between 1964 and 2015. As a result, this study is focused on the correlation of seismicity b -value, seismic quiescence Z -value, and interrelationships between some other seismicity parameters. The cumulative number of earthquakes *versus* time in the region for original catalogue and for decomposed events is shown in Figure 3. As shown in Figure 3, there is no significant change of reporting as a function of time between 1964 and 1974 for region. But further on, great seismic changes are seen in this area, especially after 1980. Also, time-number histogram for between 1964 and 2015 indicate an increase in the number of recorded events in the year of 2012 (Fig. 4).

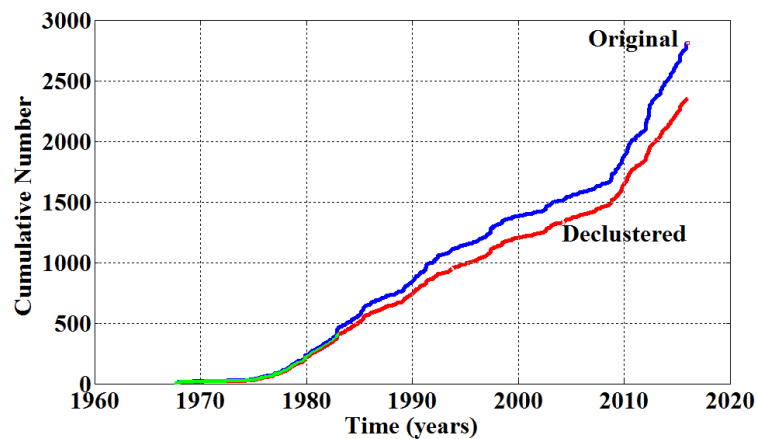


Fig. 3. Cumulative number of earthquakes versus time for the original and decomposed events.

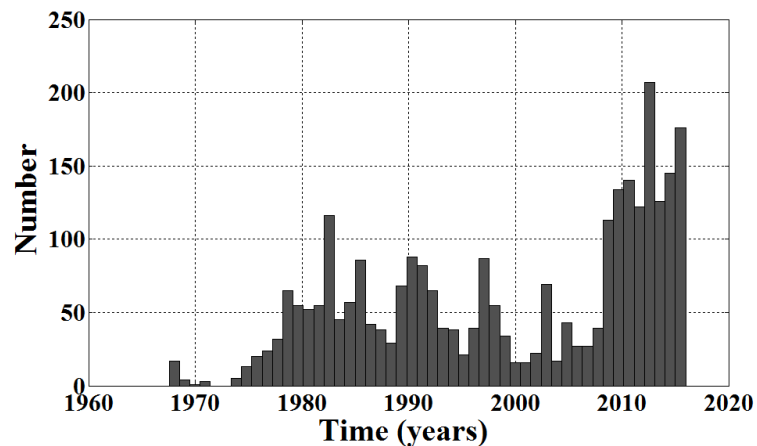


Fig. 4. Time-number histogram for the seismic activity in study region.

Because many stations have been constructed in recent years, especially after 2003 provides the real time data with the modern on-line and dialup seismic stations and V-SAT stations in Albania. Magnitude of earthquakes in this catalogue ranges from 1.7 to 6.7 with an exponential decay in their numbers from the lower to higher magnitudes. Figure 5 defines the magnitude-number histogram for the seismic activity of region. Most of the earthquakes are between 2.0 and 3.5, and a maximum M_d 2.5 is observed (Fig. 5). In order to investigate the seismic quiescence and the frequency-magnitude relationship, the change of M_c as a function of time is determined using a moving window approach. M_c is estimated for samples of 50

events per window for region by using the earthquake catalogue containing all 2814 events of $M_d \geq 1.7$.

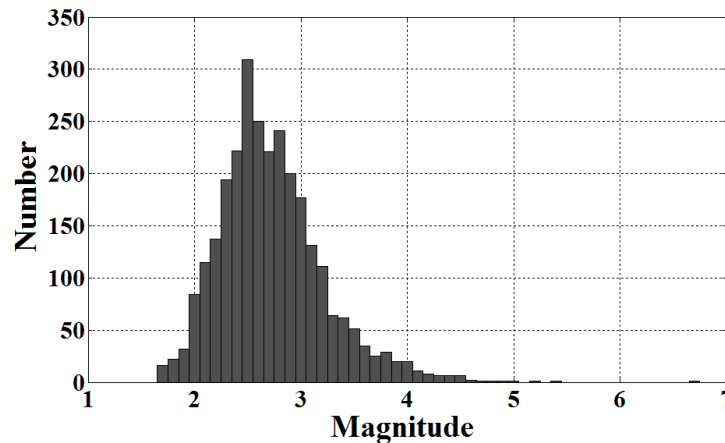


Fig. 5. Magnitude-number histogram for the seismic activity in study region

Figure 6 shows the variations of M_c with time for all parts of the V-L-E-D. For this region, M_c value is rather large and varies from 3.0 to 4.0 between 1964 and 1979 while M_c decreases to about 2.5 between 1989 and 1993 (Fig. 6). Then, it decreases to about 2.4 in the beginning of 1998. However, there is a great value about 3.3. This large value is observed after the 2007 Kukurman compound earthquake sequence. Therefore, it can be said that M_c generally shows a non-stable value in the different parts of the V-L-E-D. However, it can be easily said that M_c value varies between 2.5 and 3.7 in the V-L-E-D. Using ZMAP software, the b -value in Gutenberg–Richter (1944) relation calculated by the maximum likelihood method, because it yields a more robust estimate than the least-square regression method [1].

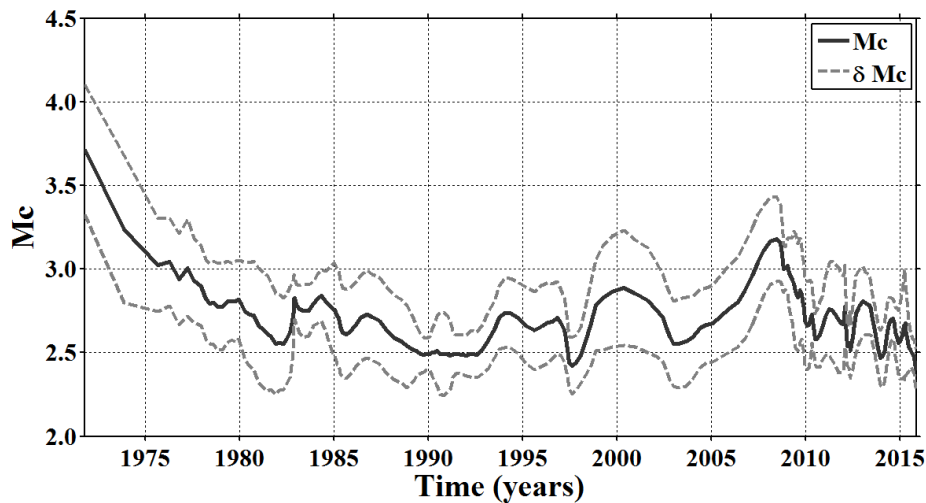


Fig. 6. Magnitude completeness, M_c , as a function of time. Standard deviation, δM_c , of the completeness (dashed lines) is also shown. M_c value is calculated for overlapping samples, containing 50 events.

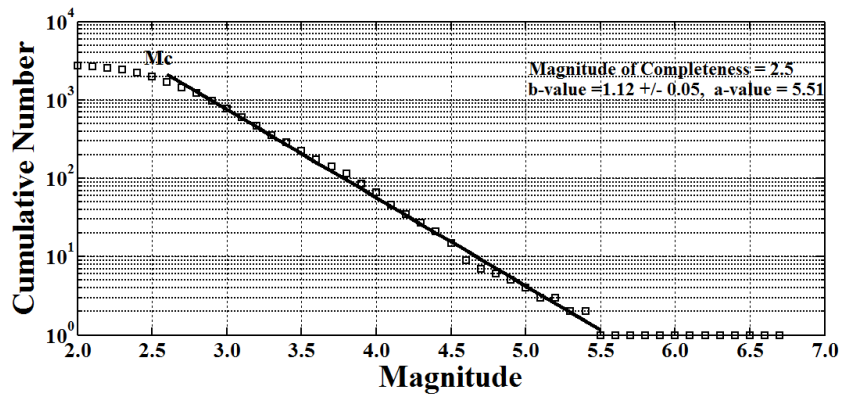


Fig. 7. Magnitude-frequency-relation for all earthquakes between 1964 and 2015. The b -value and its standard deviation, as well as the a -value in the Gutenberg– Richter relation are calculated.

Gutenberg–Richter (G-R) law describes the statistical behavior of seismic zones in energy domain using the frequency magnitude of earthquakes [3]. Figure 7 shows the plots of cumulative number of the earthquakes against the magnitude for all parts of the V-L-E-D. The whole catalogue includes 2814 earthquakes ($M_d 1.7$) for epicentral depths less than 50 km. The M_c value is calculated as 2.5 and using this value the b -value is calculated as 1.12 ± 0.05 and a -value 5.51 (Fig. 7). The b -value and its standard deviation are determined with the maximum likelihood method, as well as the a -value of Gutenberg–Richter relation. The tectonic earthquakes are characterized by the b -value from 0.6 to 1.5 and are more frequently around 0.9. It is clearly seen that the earthquake catalogue matches the general property of events such that magnitude-frequency distribution of the earthquakes is well represented by the Gutenberg–Richter law with a b -value typically close to 1. The variation of the b value as a function of time for the V-L-E-D Transversal Fault Zone is analyzed (Fig. 8). A systematic increase in b -value can be observed until 1983 with $b > 1.2$. The b -value shows a great decrease with $b \approx 0.7$ before the occurrence of 1985 February 21 earthquake and 1990 May 14 and a clear increase after the second main shock (Fig. 9). Such a kind of behavior is also observed for some strong earthquakes in region [10]. There is a clear tendency of decrease with $b \approx 0.8$ before the 2007 April 16 Kuturman compound earthquake and an increase with $b > 1.0$ after the main shock (Fig. 8). Many factors can cause perturbations of the normal b -value.

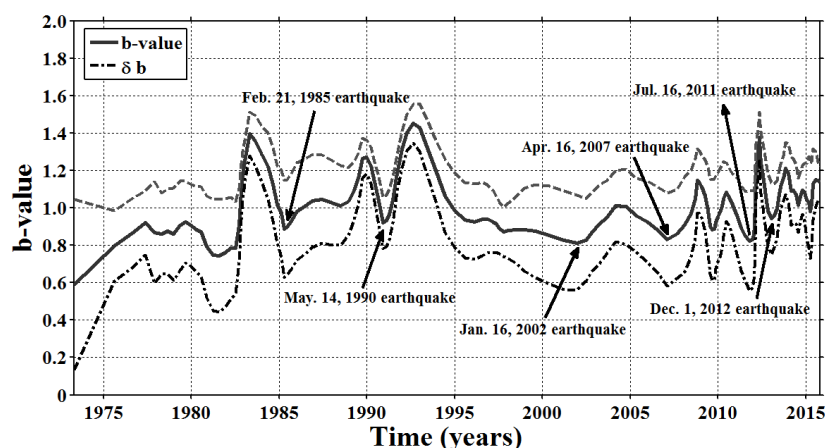


Fig.8. b -value variations versus time. b -value was estimated for overlapping samples of 75 events. Standard deviation, δb , of the b -values (dashed lines) is also shown. Arrows show the great decrease in b -values before the strong events in study region.

The b -value for a region does not reflect only the relative proportion of the number of large and small events in study area, but is also related to the stress condition over the region [18]. Therefore, it is considered that the anomalies of decreases in b -value before the main

shocks may be due to an increase in effective stress and can be used as an indicator of the next earthquake by observing the changes in b -value with time in the study region. Also, temporal increase in b -value may be related to the stress changes in these times before and after the main shocks [12], [13]. In the areas of increased complexity in the active fault system associated with lower b -value, the stress release occurs on fault planes of smaller surface area [11]. Spatial distribution of the standard deviate Z -value for the V-L-E-D Transversal Fault Zone is presented for the beginning of 2010 (Fig. 9). Each Z -value is represented with different colors: the lowest Z -values are displayed with blue and show that the change in seismicity rate is not significant, and the highest Z -values are represented with red and demonstrate a decrease in seismicity rate. Each Z -value in this representation is estimated in correspondence of a different grid point. The computed Z -values are then contoured and mapped. To obtain a regional variation of the seismic quiescence mentioned earlier, the Reasenberg (1985) [14] algorithm is applied to decompose the data. The areas under analysis were divided into rectangular cells spaced 0.02° in longitude and latitude. The nearest earthquakes, N , at each node are taken as 50 events after some preliminary tests for all regions and the seismicity rate changes are searched within the maximum radius changes by a moving time window, T_w (or iwl), stepping forward through the time series by a sampling interval as described by Wiemer & Wyss (1994) [19].

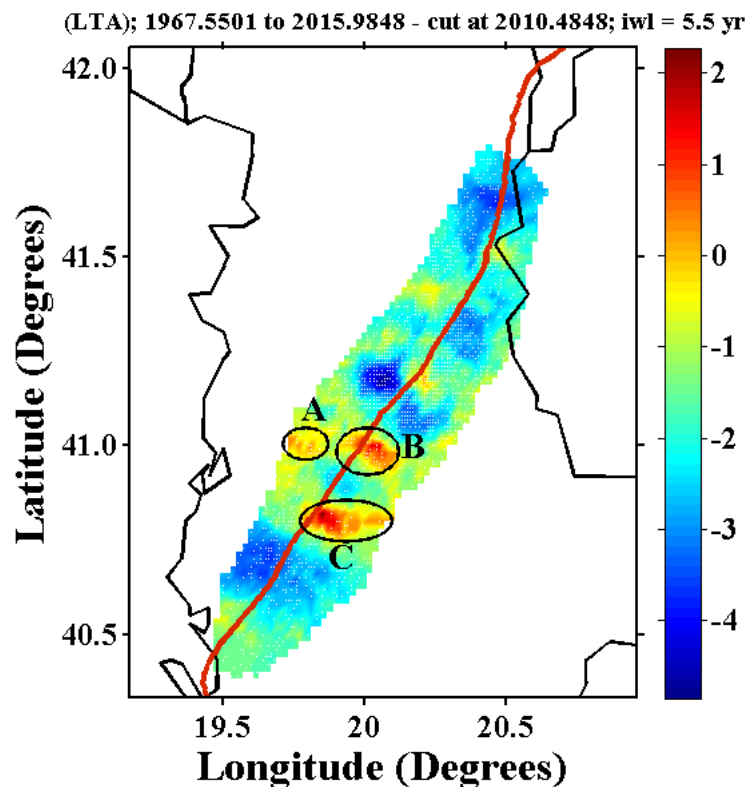


Fig. 9. Spatial distribution of Z -value in the beginning of 2010 with T_w (iwl) equal to 5.5 years. White dots show the decomposed events.

The shape of the LTA function strongly depends on the choice of the length of the foreground window (iwl). While the statistical robustness of the LTA function increases with the size of iwl , its shape becomes more and more smooth, if the iwl length exceeds the duration of the anomaly. The time window, T_w , equal to 5.5 years is used. Since the quiescence anomalies obtained in Figure 9 are the best represented at the epicentral areas for T_w equal to 5.5 years, this time window length is used to image the spatial variation of the seismicity rate changes. For each grid point we binned the earthquake population into many binning spans of 28 days for all regions in order to have a continuous and dense coverage in time. The N and T_w

values are generally selected accordingly to enhance the quiescence anomaly and this choice does not influence the results in any way. Figure 9 shows the spatial variation of Z -values for region. As shown in Figure 9, there are three areas (A, B, and C) exhibiting significant seismic quiescence. In addition to these three significant areas, there are some small quiescence areas. However, since these small quiescence areas are not very clear it is considered that they are not as significant as the other three quiescence areas. As a result, Z -value variation is represented in the beginning of 2010. Clear quiescence anomalies were identified at several seismogenic sources. In the Z -value maps for all parts of the V-L-E-D, three areas exhibit significant seismic quiescence. Covering the V-L-E-D, the first significant quiescence is estimated centered at $41.00^{\circ}\text{N}-19.78^{\circ}\text{E}$ (region A, around Lushnja) and the second one is estimated centered at $40.99^{\circ}\text{N}-20.03^{\circ}\text{E}$ (region B, in the Cerriku). The third significant anomaly is found centered at $40.81^{\circ}\text{N}-19.86^{\circ}\text{E}$ (region C, including Kucova).

IV. CONCLUSIONS

Temporal and regional assessments of the recent seismic activity are performed in order to put forth the seismic behavior in the V-L-E-D Transversal Fault Zone in Albania. So, a few seismic parameters are used such as size-scaling parameters (such as slope of recurrence curve b value), precursory quiescence Z -value, temporal and regional variations of earthquakes as well as the histograms of temporal, spatial and magnitude distributions. For this purpose, statistical analysis techniques based on the seismic tool *ZMAP* are used. The instrumental earthquake catalogues of ASN between 1964 and 2015 are compiled and finally 2814 crustal earthquakes of magnitude equal and greater than 1.7, with depths less than 70 km are obtained. Seismicity characteristics in the V-L-E-D Transversal Fault Zone show an important increase, especially after 2003. Analysis of completeness magnitude shows a value between 2.7 and 2.9 for the V-L-E-D Transversal Fault Zone. b -value for study is close to 1.0 and typical for earthquake catalogues. Temporal distributions of b -values show a strong tendency of decreasing before the large main shocks and this behavior can be used as an indicator of the future earthquake. Reasenber algorithm is used to separate the dependent events and the earthquake catalogue is decomposed for the standard deviate Z -value estimation. Importance of seismicity changes is measured at the nodes of a 0.02° grid space in longitude and latitude for the V-L-E-D Transversal Fault Zone. There are three regions exhibiting significant quiescence anomaly on the V-L-E-D Transversal Fault Zone in the beginning of 2010. These three anomalies are observed centered at $41.00^{\circ}\text{N}-19.78^{\circ}\text{E}$ (region A, around Lushnja), $40.99^{\circ}\text{N}-20.03^{\circ}\text{E}$ (region B, in the Cerriku), $40.81^{\circ}\text{N}-19.86^{\circ}\text{E}$ (region C, including Kucova). These areas of seismic quiescence recently observed, which started at the beginning of 2010 in three aforementioned regions, can be considered as the most significant. The V-L-E-D Transversal Fault Zone was struck with strong earthquakes in recent years. Therefore, spatial and regional prediction of the next strong earthquake in the V-L-E-D Transversal Fault Zone would be useful.

REFERENCES

- [1] Aki, K. (1965). Maximum likelihood estimate of b in the formula $\log N = a - bM$ and its confidence limits, *Bull. Earthq. Res. Inst. Tokyo Univ.* **43**, 237-239.
- [2] Aliaj, Sh. Sulstarova, E. Muco, B. Kociu, S. (2001) Seismotectonic map of Albania, schale 1:500.000. *Seismological Institute Tirane*.
- [3] Awad, H. M. Mekkawi, G. Hassib and M. Elbohoty. (2005) Temporal and three dimensional spatial analysis of seismicity in the Lake Aswan area, Egypt, *Acta Geophys. Pol.* **53**, 2, 153-166.

- [4] Gutenberg, R. and C.F. Richter. (1944) Frequency of earthquakes in California, *Bull. Seism. Soc. Am.* 34, 185-188.
- [5] Mogi, K. (1962) Study of the elastic shocks caused by the fracture of heterogeneous materials and its relation to the earthquake phenomena. *Bulletin of Earthquake Research Institute, University of Tokyo* 40, 125- 173.
- [6] Ormeni, Rr. (2007) The general model of construction of the Albanian earth crust and its seismoactive feature according to the seismological data. *PhD thesis, Tirana*.
- [7] Ormeni, Rr. (2010) Structure of P, S seismic wave velocities of the Albanian earth lithospheres and its seismoactive features. *Kumi publications, Tirana*.
- [8] Ormeni, Rr. (2012) Analysis of feature of recently earthquakes occurred in Elbasani-Dibra seismogenic zone and its associated hazard. *Jubilee Conference of Geology October 2012, Tirana, Albania*.
- [9] Ormeni, Rr. Kociaj, S. Fundo, A. Daja, Sh. Doda, V. (2013) Moderate earthquakes in Albania during 2009 and their associated seismogenic zones, *Italian Journal of Geosciences*.
- [10] Ormeni, Rr. (2015) Mapping b-value in the seismogenic zones of Albania region” *Proceeding of the 8th Congress of the Balkan Geophysical Society, 4-8 October 2015, Crete, Greece*.
- [11] Öncel, A.O. and Wilson, T.H. (2000) Space-time correlations of seismotectonic parameters: examples from Japan and from Turkey preceding the İzmit earthquake, *Bull. Seism. Soc. Am.* 92, 1, 339-349.
- [12] Öztürk, S. (2011) Characteristics of Seismic Activity in the Western, Central and Eastern Parts of the North Anatolian Fault Zone, Turkey: Temporal and Spatial Analysis. *Acta Geophysica*, vol. 59, no. 2, Apr. 2011, pp. 209-238 DOI: 10.2478/s11600-010-0050-5.
- [13] Öztürk, S. (2012) Statistical correlation between b-value and fractal dimension regarding Turkish epicentre distribution. *Earth Sci. Res. J.* Vol. 16, No. 2: 103 - 108
- [14] Reasenber, P. (1985) Second-order moment of central California seismicity, 1969- 1982, *J. Geophys. Res.* 90, B7, 5479-5495, DOI: 10.1029/JB090iB07 p05479.
- [15] Sulstarova, E & Kociaj, S. (1975) Catalog of earthquakes of Albania, *Published, Science Academy of Albania, Tiranë*.
- [16] Sulstarova, E. Kociaj, S. Aliaj, Sh. (1980) Seismic Regionalization of Albania”, *Published, Science Academy of Albania, Tirana*.
- [17] Sulstarova, E. Peçi, V. Shuteriqi, P. (2000) Vlora-Elbasani-Dibra (Albania) transversal fault zone and its seismic activity. Kluwer Academic Publisher, *Journal of Seismology* 4, 117-131, Netherlands.
- [18] Utsu, T. (1971) Aftershocks and earthquake statistics (III): Analyses of the distribution of earthquakes in magnitude, time and space with special consideration to clustering characteristics of earthquake occurrence (1), *J. Faculty Sci., Hokkaido University, Ser. VII (Geophys.)* 3, 379-441.
- [19] Wiemer, S. and M, Wyss. (1994) Seismic quiescence before the Landers (M = 7.5) and Big Bear (M=6.5) 1992 earthquakes, *Bull. Seism. Soc. Am.* 84, 3, 900- 916.
- [20] Wiemer, S. and M, Wyss. (2000) Minimum magnitude of completeness in earthquake catalogs: Examples from Alaska, the Western United States, and Japan, *Bull. Seism. Soc. Am.* 90, 4, 859- 869.
- [21] Wiemer, S. (2001) A software package to analyze seismicity: ZMAP, *Seism. Res. Lett.* 72, 2, 373-382.

Strong tsunamis and tsunamigenic zones in the Adriatic Sea (Albania coastline)

Adisa Daberdini¹, Rrapo Ormeni²

¹*Polytechnic University of Tirana,*

²*Institute of Geosciences, Energy, Water and Environment Polytechnic University, Tirana,*

ABSTRACT

We calculated the expected impact on the Albanian coast of the Adriatic sea of a large set of tsunamis resulting from potential earthquakes generated by major fault zones. Our approach merges updated knowledge on the regional tectonics and scenario-like calculations of expected tsunami impact. Historical documentary sources of the Adriatic sea region contain much information about earthquakes and associated phenomena like tsunamis. Until recently, however, it was a widely held belief that tsunamis either did not occur in the Adriatic sea or they were so rare that they did not pose a threat to coastal communities of Albania. Catastrophic tsunamis are more frequent on Pacific Ocean coasts where both local and transoceanic tsunamis have been documented. On the contrary, large tsunami recurrence in the Adriatic sea is of the order of several decades and the memory of tsunamis is short-lived. A catalogue of historical tsunamis generated by earthquakes is compiled. Realistic seismic sources, with tsunami potential, are found to model expected coseismic deformation, which is translated directly to the water surface and used as an initial condition for the tsunami propagation. We selected five elongated potential source zones. We suggest that our results be taken into account in the design of early-warning strategies.

Keywords: tsunami, waves, Adriatic basin, tsunamigenic sources, hazard

INTRODUCTION

The Adriatic sea is an elongated basin stretching NW-SE in the central Mediterranean sea (Fig. 1). It has been struck several times by tsunamis most often along the coasts of the Gargano promontory [4] [9] [14] [20] [26]. The Adriatic region (Figure 1) has an unexpected economic and tourist growth with an increase in coastal population and the development of large leisure areas during recent years, with many parts of coastal cities being a couple of meters above sea level, making them prospective targets of a large-scale disaster, even if the height of the tsunami wave is moderate. We have one of the most seismically active areas and the entire Adriatic region [12] [15] [19] [17]. This area of Ulqini-Budva has been repeatedly affected by large magnitude earthquakes ($M > 7.0$) (Figure 1) that have caused severe destruction and human loss in the past centuries. Large tsunami events require the presence of a thick water layer that can

be found only in the oceanic domain, but it can also occur in small basins such as the Adriatic sea where many tsunamis have been reported during historical times. This situation requires urgent solutions for an effective risk management and mitigation plan. For this reason, it is essential to define the tsunami potential of the region and this study presents results of such an attempt. The lack of direct records, however, makes the rigorous estimation of the expected tsunami amplitudes rather difficult, and the analysis of available documents remains, somehow, controversial. Any attempt to assess a tsunami hazard, based on pure statistical methodologies, will not give reliable results because of data deficiency and because they use relationships linking earthquakes to tsunamis that may not be empirically well grounded. This means that alternative approaches to evaluate a tsunami hazard are called upon [29]. This is the approach used in the present investigation, focusing on the tectonic deformation mechanics of the potential tsunamigenic faults and their effect on the tsunami hazard in the region.

I. The data and method

Reliability of the Adriatic Sea tsunami waves listed by Soloviev [26]. From this catalogue of tsunamis were compiled for Albania coast region containing 12 reliable events. The maximum intensity K for each one of the 16 tsunami events was given according to the new 12-point tsunami intensity scale introduced by Ambraseys [4]. To assess the potential threat posed by earthquake-generated tsunamis in the Adriatic Sea we adopted the method developed by Lorito [13]. We systematically carried out a number of simulations for all source zones that can possibly affect the target coastlines [8]. A Source Zone (SZ) includes an active tectonic structure at regional scale that is made up of a number of individual fault segments, each one capable of releasing a significant earthquake.

Table 1. Reliable Tsunami Events known in the Albania coast region

o	Year			Location Lat- Long	Region				Reference Cat
	15 8 BC			41.18 -19.36	Durres, Albania coast				PA, AM, TMS
	34 6 AD			41.24 -19.24	Durres, Albania coast	.8	X		PA,
	12 73	9			Durres, Albania coast	.9	III		AM, NT4.1
	18 33	1	9		Albania	.5	III		PA, AM
	18 51	0	2	40.42 -19.24	Vlora Albania	.8	III		PA, NT4.1,
	18 66	1	2	40.24 -19.36	Albania	.6	X		PA, AM, TMS
	18 66	1	6		Albanian coasts (Narta)				AM, TMS
	18 66	3	2	40.24 -19.30	Vlora Albania	.3	X		PA, AM, TMS
	18 66	3	6	40.50 -19.30	Albanian coasts (Himara)	.1	III		PA, AM, TMS
	18 66	3	3	40.30 -19.30	Albania	.6	III		PA, AM, TMS
1	18 69	2	8	38.51 -20-48	Vlora Albania	.4	X		PA, AM

2	93	18	6	4	40.06 -19.42	Albaniancoasts(Hi mara)	.6	X	PA, AM, TMS
3	20	19	1	6	40.18 -20.00	Sazani, Albania	.3	X	AM, TMS
4	79	19	4	5	42.02 -19.07;	Montenegro- Albania	.0	X-X	BC, PA,ASN
<p>• Key: k = tsunami intensity in the Sieberg-Ambraseys 6-point scale; M = magnitude of earthquakes, I = Intensity of earthquakes, M = month, D = day</p>									

A0.1 Reference catalogues used for tsunamigenic events

– AM: Ambraseys (1962); – CF: Caputo and Faight (1984); – BC: Bedosti and Caputo (1986);
 – PA: Papadopoulos (2001); – ITC: Italian Tsunami Catalogue (Tinti et al., 2004); – TMS: Soloviev et al. (2000)

A0.2 Reference catalogues used for related earthquakes

– CFT: Catalogo dei Forti Terremoti (Boschi et al., 2000); – NT4.1: NT4.1 catalogue (Camassi and Stucchi, 1998); – ASN: Albanian earthquake catalogue (Sulstarova et al 2005)

II. Tsunamigenic source zones in the Adriatic sea

The northwestern portion of the Adriatic basin is also the most vulnerable because of its large low-topography coastal area extending for over 150 km. This area also hosts the city of Venice, that is particularly vulnerable to sea-level rise. From the regional tectonics standpoint, the Adriatic Sea falls in the middle of the Adria plate that is being pushed by Africa northward against stable Europe. Overall, the Adria is affected by active compression and overridden by thrust belts on all sides. The Adriatic Sea is mostly surrounded by active fold-and-thrust belts and strike-slip faults (Fig. 1). Frequent earthquakes occur along these well-known fault zones, most of which run close to the coastlines or in the open sea and are thus potential sources for tsunamis. The largest earthquakes ($M > 7$) occurred near the eastern margin of the central Adriatic Sea, along the Montenegro portion of the Dinaride-Albanide chain. Most of the remaining structures exhibit a potential for earthquakes of magnitude 6 -7, thereby holding a significant tsunamigenic potential. Dinarides, Albanides and Hellenides belt longer than 1,000 km runs along the eastern margin of the Adriatic Sea from the southern Alps, to the north to the Kefallonia-Lefkada Fault.

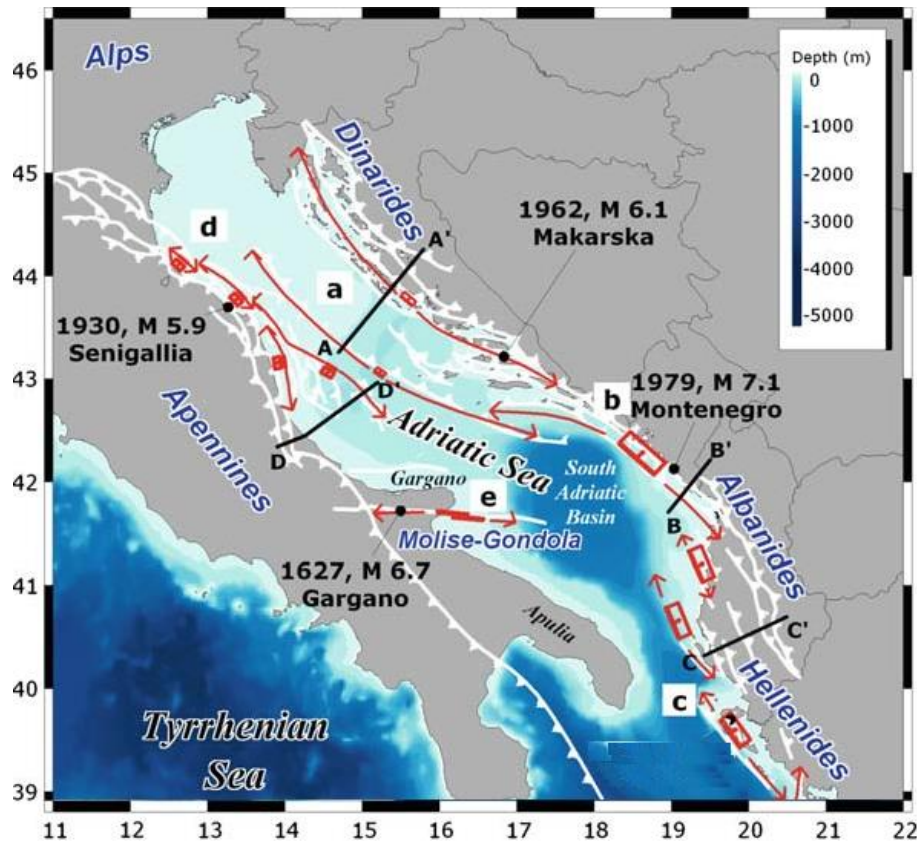


Figure 1. Tectonic sketch map of the Adriatic basin. The double-headed arrow indicates the floating path of the Typical Faults. a) Coastal and Offshore Croatia; b) Montenegro; c) Albania – Northern Greece; d) Northern Apennines; e) Apulia;. Selected some major earthquakes.

This fold-and-thrust belt is usually split into three different domains named Dinarides, Albanides and Hellenides, respectively from north to south, that started forming as a consequence of the subduction of Adria under the European plate. Adria acts as an indenter pushing northward into stable Europe [3] [11] [23]. GPS data document compressional strain across the chain at a rate of about 30 nanostrain/yr [25]. Stronger earthquakes mostly concentrate in the Albanides and Hellenides. The outer portion of these chains is partly located offshore and characterized by numerous thrust fronts that all seem to be currently active. Available focal mechanisms indicate predominant SW-NE shortening [16] [18] [19] [27] reverse faulting earthquakes dominate [22].

III.1. Selection of Seismic Sources in Albania coastline and its surrounding

The Albanian orogenic front thrust contact with the Adria-microplate. The convergent boundary between the Albanian orogen and the Adria microplate is now well constrained to be located in the Ionian and Adriatic offshore. A contractional belt longer than 300 km runs along the eastern margin of the Adriatic Sea from the southern Alps, to the north, to the Kefallonia-Lefkada Fault, (Fig 2). The Albanian orogenic thrust front is cut and displaced by the Othoni Island-Dhermi, the north of Sazani Island, and the Gjiri i Drinit-Lezha strike-slip faults, which divide the orogen into separate segments showing diachronous development (Aliaj et al, 2000). The following segments of the orogenic thrust front of the Albania orogen have been recognized (Figure 2):

- a. The NW-trending Karaburuni-Sazani Island offshore (KS)

- b. The ~N-trending Frakulla-Durresi mainly onshore segment (FD)
- c. The W-NW-trending Lezha-Ulqini offshore segment (LU)

a. The NW-trending Karaburuni-Sazani Island offshore segment

The orogenic front of the Sazani zone is present north of the Othoni Island-Dhermi strike-slip fault. The continental slope south-west of the Mountain Mali i Kanalit is deformed, and, as the result of minor thrusts, the transition from the Mali i Kanalit back-thrust monocline to the Apulian platform occurs along the Sazani zone orogenic front. Along this front Cretaceous carbonates are backthrust over Upper Triassic dolomites of the Çika anticline of Ionian zone, forming a triangular zone at the depth. North of the Gjiri i Ariut-Dukat strike-slip fault, there is a NW-trending thrust that marks the contact of the Karaburuni-Sazani thrust front with the Apulian platform (Figure 2; KS).



Figure 2. Southern convergent margin of Eurasia plate: Adriatic collision and Aegean Arc. Segments of Adriatic collision frontal thrust are noted by capital letters, as follows: KS- Karaburuni- Sazani Island, FD- Frakulla-Durresi, and LU-Lezha-Ulqini. The strike-slip faults cutting the orogen front, from south to north, are as follows: The north of Sazani Island and the Gjiri i Drinit-Lezha faults.

b. The ~N-trending Frakulla-Durresi (mainly onshore) segment

North of an E-W-trending transverse fault near Sazani Island, the transition from the Apulian platform to the Albanian Basin (=South Adriatic Basin) occurs in the Adriatic offshore (Figure 2; FD). The front of the orogen there is buried under molasses of Middle Miocene age exposed onshore on coastal terrains of the Periadriatic depression and may pass along the Frakulla-Durresi anticlinal line of quasi-northern extension [1]. Seismic data show that the Mio-Pliocene anticlines of Periadriatic depression are associated with thrust or back-thrust faults [2] [5]. These have been termed over-fault anticlines (Aliaj, 1971) or determined by Biçoku (1964) as having been “placed in narrow zones of some big faults found under the Neogene cover”. Some of these faults appear to be “flower” structures and “palm tree” structures associate with oblique thrusts [2]. The north-trending Frakulla-Durresi anticline (Figure 2) has been subjected to dextral transpressional deformation associated with oblique northeast-southwest regional

horizontal compression in post-Pliocene time. In the Durresi anticline the main fault is a west-dipping back-thrust that cuts marine Quaternary sediments that are still horizontal. The orogenic front along the Frakulla-Durresi segment is marked at the surface by thrusting and back-thrusting. Along the Ardenica and Durresi anticlines, the Oligocene to Quaternary age thick clastic sediments of South Adriatic Basin (Albanian Basin), have been detached from their carbonate substratum and have glided along a decollement at the level of the Oligocene clastics. The clastic sediments were largely backthrust on frontal thrust structures of the Ionian zone, forming triangular zones at depth.

c. The W-NW-trending Lezha-Ulqini offshore segment

The orogenic front, north of the Gjiri i Drinit-Lezha strike-slip fault, in the Adriatic offshore (Figure 2; LU), belongs to the Kruja Zone [2]. Local back-thrusting observed at Karaburuni-Sazani and Frakulla-Durresi segments of the frontal thrust of the Adriatic collision zone, is quite different from the regional back-thrusting in Western Alps caused by Eo-Alpine and Apulian lithospheric wedging [24]. In the Albanian case the Adria microplate (=Adriatic plate) is unaffected by such wedging; instead it was rigidly subducted during Alpine deformation beneath the Albanian orogen. The external margin of the fold and thrust belt in Albania was thrust on the Adria microplate, partly over the Apulian platform and partly over the Albanian Basin.

III.2. Seismicity and Tsunami Activity in Adriatic Region

In order to have a more complete picture of the tsunamigenic potential of the studied area, we performed accurate investigations on the earthquakes that occurred in the last century with the aim of identifying those potentially capable of generating tsunamis. We examined events occurred since 1900, with epicentre located in the sea or in land near the coast, namely not more than 10 km far from the shore. Eleven significant earthquakes have been identified (Fig. 3.), and only for two of them tsunami evidences have been found, respectively the 15 Aprile 1979 and the 1930 events. To this purpose, all the available material was gathered, with a scrupulous and careful search for the sources, including specific monographs and scientific papers, articles available in contemporary chronicles and in national and local newspapers. Seismicity in the Adriatic basin is strongly connected to the tectonic features outlined above. Albanian coastline region and the coastline region in the Ionian Sea that presents one of the most seismotectonically active regions of the Mediterranean. It is part of a region of intense deformation located between two major lithospheric plates, the European plate and the African plate. The African plate is moving northwards relative to Eurasia at a rate of 10 mm/year [10]. Its leading edge is being subducted along the Hellenic Trench in most of the cases. The major tectonic features, which set the Ionian-Adriatic Sea as an area of high seismicity are: the subduction of the African plate beneath the Aegean microplate and collision of Adria microplate to Albanian orogen. Fault plane solutions, for several shallow and intermediate depth earthquakes, have been published [16] [18] [20] [27] [28] and we have make an aproch of this study. Only the earthquakes with magnitude greater than 6.5 are plotted. Furthermore, only shallow (depth ≤ 30 km) earthquakes are plotted, since the tsunamigenic potential of deeper events can be neglected. Since tsunamis in the Adriatic basin, as well as in other parts of the world, are mostly generated by earthquakes, it is no surprise that the geographical distribution of the historical tsunamis in the region generally resembles the trend of seismicity. Taking into account the Ionian-Adriatic Sea tectonic regime and the tsunamogenic events depicted in Table

1, we have selected seven potential seismic sources that could represent a tsunami hazard in the region. The presence of tsunamis have been observed a few times in the past, associated with offshore earthquakes (i.e. 1633 and 1886, 1931), affecting near field as well as remote coastal segments (Table 2). The Adriatic offshore has repeatedly suffered large offshore earthquakes which have caused damage and human loss [1] [18] [19]. The damage was minor from these events, due to the sparse population of the region in the early years. The geographic location, strike, length and other parameters of each source were derived from existing fault maps, available reflection profiles and relevant seismological references and are presented. Today, a large earthquake along the Adriatic sea fault system would damage coastal communities, and its effect would be enhanced by sea waves triggered from the seafloor displacement [6] [7]. For each sub-region, will be possible tsunamigenic seismic sources, and take these as the basis to develop a scenario for the propagation of the tsunami from the source throughout the entire Adriatic basin.

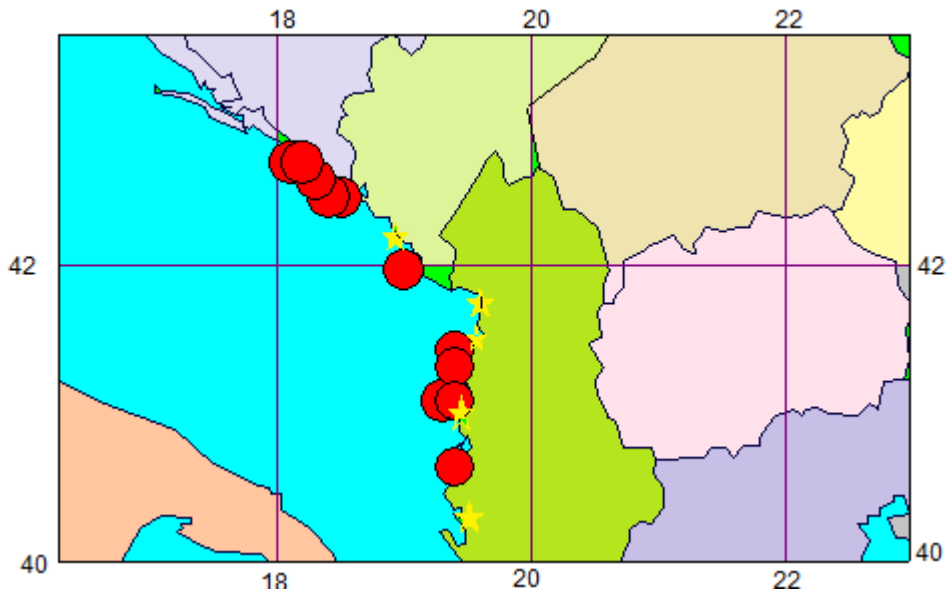


Figure 3. Earthquakes with $M > 6.5$ occurred along the Ionian and Adriatic Sea and the potential tsunamigenic sources (numbers in yellow squares) considered in the present investigation. Stars, denote tsunami reported sides.

III.2.1 Tsunami activity in Albania coastline

This zone includes the coastal region of Albania, from the border with Montenegro to latitude 40.50_ N. The seismicity is determined by the subduction of the Adriatic plate under the Albanides [1]. The typical focal mechanisms are thrust and strike-slip, the maximum historically reported magnitude is 7.3 (ECCSE), the strongest in the Adriatic region. The focal depth ranges from 5 to 25 km [7].

Table 2. Main parameters identifying the four sites of Zone 2.

Site	Latitude	Longitude	Epicentral dist. R
Ancona	43.63_ N	13.50_ E	519 km
Bari	41.12_ N	16.85_ E	184 km
Dubrovnik	42.63_ N	18.12_ E	150 km
Durres	41.32_ N	19.45_ E	55 km

The values of magnitude chosen for simulations are 6.5, 7.0 and 7.5, the values of focal depth are 10 km, 20 km and 30 km [21]. The representative epicenter is located at the point of coordinates 41.50 N, 19.00 E, in correspondence with the epicenter of the 346 AD earthquake of magnitude 7.3 as given by Shebalin et al. (1997). The liquid layer above the source is 180 m thick. The sites are chosen in correspondence of the cities of Ancona, Bari, Durres and Dubrovnik. The main parameters identifying each site are listed in Table 2. The synthetic mareograms calculated at the four sites for magnitude $M=7.0$ are shown in Fig. 3.

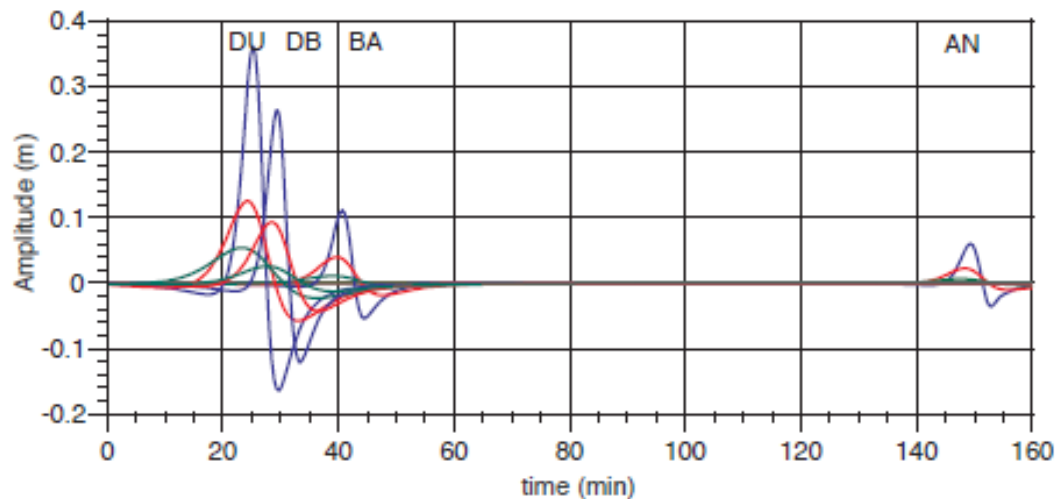


Fig. 3. Synthetic mareograms for Zone 1 and 2. Focal depth, $H=10$ km (blue), 20 km (red), 30 km (green). Magnitude: $M=7.0$.

III.3. Tsunamigenic Sources in Adriatic Basin

Most often, a solution to the problem is searched for, in terms of a scenario that considers the largest events known to have hit the area of interest in the past history and to simulate these events through numerical modelling. Because of the active lithospheric plate convergence, the Mediterranean Sea region is geodynamically characterized by high seismicity. Tsunamis are among the most remarkable phenomena associated with earthquakes, and landslides in the Ionian-Adriatic Basin. Until recently, however, it was a widely held belief that tsunamis either did not occur in the in the Ionian Sea or they were so rare that they did not pose a threat to coastal communities. Catastrophic tsunamis are more frequent on Pacific Ocean coasts where both local and transoceanic tsunamis have been documented. On the contrary, large tsunami recurrence in the Adriatic Sea is of the order of several decades and the memory of tsunamis is short-lived. The damage was minor from these events, due to the sparse population of the region in the early years. Today, a large earthquake along the Ionian sea fault system would damage coastal communities, and its effect would be enhanced by sea waves triggered from the seafloor displacement. Taking into account the Ionian Sea tectonic regime and the tsunamogenic events depicted in Table 1, we have selected four potential seismic sources that could represent a tsunami hazard in the region (Figure 4). For these reasons, the scientific study of tsunamis in the Adriatic Sea was rather neglected for a long period in comparison to other parts of the world. Up until the beginning of the 20th century tsunamis were sporadically mentioned in earthquake descriptions or catalogues. By the early and mid-20th century some research was carried out after large tsunami events such as the Messina event in southern Italy (28th December 1908). More systematic efforts to compile tsunami catalogues for the Adriatic Basin began in the 60's, when some progress was made in the fields of numerical wave modeling and tsunami hazard assessment. The beginning of 1990's marked a key turning point for tsunami science in the

Mediterranean Sea region and in Europe in general. Figure 4 illustrates a map of the known tsunamigenic sources in the Adriatic Basin region and a relative scale of their potential for tsunami generation calculated as a convolution of the frequency of occurrence and the intensity of tsunami events. The compilation of reliable tsunami data bases is of great importance for a wide range of tsunami related studies: statistics and hazard assessment, wave numerical modeling, risk evaluation, operation of early warning systems, public awareness.

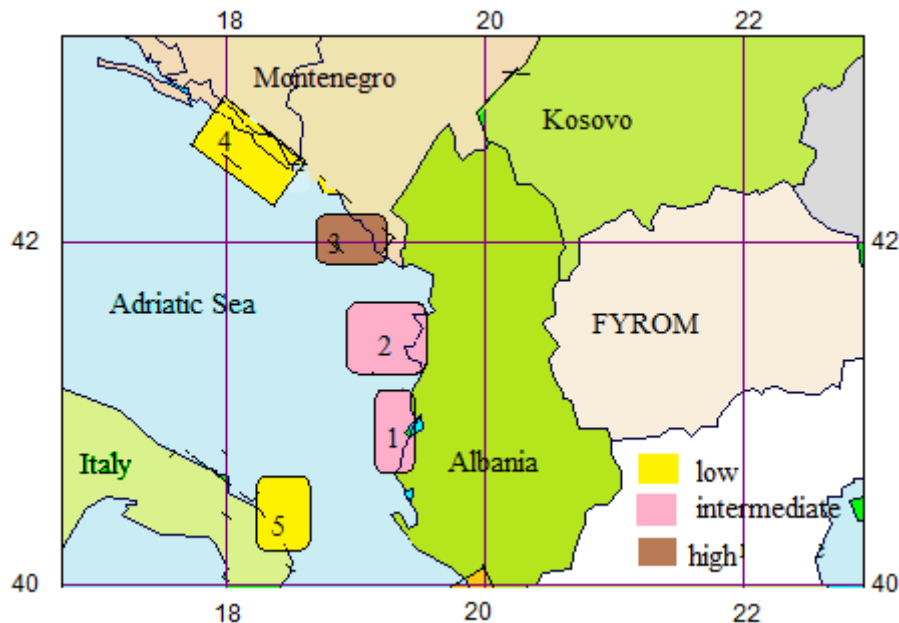


Figure 4. The tsunamigenic zones of the in the Adriatic Sea; 1 = Zverrrec-Rreth-Greth, 2 = Durres-Rodoni Bay, 3 = Ulqini, 4 = Bar-Budva , 5 = Gargano promontory, (the tsunami potential of each one zone is classified in a relative scale according to the frequency of occurrence and intensity of tsunamis)

III. Conclusions

For the offshore sources, as expected, the maximum tsunami amplitudes coincide with the highest magnitude of the generating event and with the minimum focal depth. In this study we investigate all the potential tsunamigenic earthquakes occurred in the central Adriatic Sea since 58 BC. These tsunamis were examined by following the catalogue guideline, therefore the present research is both a contribution for the updating of the catalogue itself and an improvement on the knowledge of the tsunamigenic potential of the central Adriatic region. For the offshore sources, as expected, the maximum tsunami amplitudes coincide with the highest magnitude of the generating event and with the minimum focal depth. Fault mechanism, focal depth and water layer thickness also affect tsunami generation and propagation. These coasts are characterised by flat and large beaches and the risk is especially high in the summer season, when the beaches and the water front resorts are crowded with tourists. Special emphasis was given to the tourist resorts, where we computed the corresponding activation of each of the five sources. From geographical point of view, the very strong events are associated either with highly seismogenic structures like the South Montenegro, Westen Albania, the South Italy. On the contrary, not very strong tsunamis were found in the rest tsunamigenic zones of the Adriatic Sea region. It should be noted, however, that these results are valid as much as the tsunami record over the last centuries could be extrapolated to longer periods of time. From this point of view, the incompleteness of the data along with the very long repeat time that may characterize the tsunami occurrence in some tsunamigenic zones, pose a serious problem in approaching reliably the repeat time of very strong tsunamis in the Adriatic Sea. Since these locations are heavily populated during the summer season, the need for special tsunami risk

mitigation measures is obvious. As a final consideration, our attention in this paper focussed on the time needed for the first tsunami signals to reach the remote coasts, but indeed deeper attention should be paid in a future study to the longterm features of the tsunami propagation for each scenario, in order to evaluate the expected total duration of the phenomena, the characteristic periods, the relative amplitude of the wave packets and the role of edge waves. Particularly in cases like this the identification of the tsunamigenic sources driving the hazard is of great importance for a proper tsunami risk assessment.

References

- [1] Aliaj Sh, Kociaj S., Sulstarova, E., Muço, B., (2010) “Neotectonic Structure of Albania” AJNTS, NR.4, Tiranë pp. 89-101.
- [2] Aliaj Sh, Sulstarova, E., Muço, B., Koçiu, S., 2000. Seismotectonic Map of Albania, scale 1:500.000. Seismological Institute Tirana
- [3] Aljinović, B., Prelogović, E., and Skoko, D. (1990), Tectonic processes on the contact of the Adriatic Platform and the Dinarides in the area of the Northern Dalmatia, Conf. on mechanics of jointed and faulted rock, Inst. of Mech/Tech. Univ. of Vienna, Proc. A. A. Balkema, Rotterdam/Brookfield, 179– 182.
- [4] Ambraseys NN, (1962) Data for the Investigation of the Seismic Sea Waves in the Eastern Mediterranean, B. Seismol. Soc. Am., 52(4), 895–913, 1962.
- [5] Biçoku T, (1964) Analysis and synthesis of seismic explorations in Periadriatic Depression. D. Sc. Thesis, Central Archive of Geology Tirana 271 p (in Albanian)..
- [6] Daberdini A, Ormeni Rr, (2013) Mechanical wave of earthquakes generated in Adriatic sea. International Geosciences Conference, GeoALB Kosovo, 2013
- [7] Daberdini A, Ormeni Rr, (2014) Modelimi numeric i vales se cunamit sipas modelit Boussinesq. International Geosciences Conference, GeoALB Kosovo, 2014
- [8] Daberdini A, Ormeni Rr, (2015) Scenarios and Tsunami Hazard Assessment of Tectonic Origin in the Ionian-Adriatic Seas. J. Int. Environmental Application & Science, “JIEAS” Selçuk University, Turkey
- [9] De Martini, P. M., Burrato, P., Pantosti, D., Maramai, A., Graziani, L., and Abramson, H. (2003), Identification of tsunami deposits and liquefaction features in the Gargano area (Italy): paleoseismological implication, Ann. Geophys.-Italy 46, 883-902.
- [10] DeMets C, Gordon RG, Argus DF, Stein S, (2001) Current plate motions, Geophys. J. Int., 101, 425–478, 1990.
- [11] Herak, M.J. (1999), Tectonic interrelation of the Dinarides and the Southern Alps, Geologica Croatica 52, 83– 98.
- [12] Jackson J, McKenzie D, (1988) Rates of active deformation in Aegean Sea and surrounding regions, Basin Res., 1, 121-128.
- [13] Lorito, S., Tiberti, M. M., Basili, R., Piatanesi, A., and Valensise, G. (2008), Earthquake-generated tsunamis in the Mediterranean Sea: Scenarios of potential threats to Southern Italy, J. Geophys. Res. 113, B01301, doi:10.1029/2007JB004943.
- [14] Maramai, A., Graziani, L., and Tinti, S. (2007), Investigation on tsunami effects in the central Adriatic Sea during the last century – a contribution, Nat. Hazards Earth Syst. Sci. 7, 15–19.
- [15] Makropoulos C, Burton PW, (1981) A catalogue of the seismicity in Greece and adjacent areas, Geophys. J. Roy. Astr. S., 65, 741-762.
- [16] Muço B, (1994) Focal mechanism solutions of Albanian earthquakes for the period 1964-1988. Tectonophysics, 231, 311-323

- [17] Ormeni, Rr., (2010).. "Structure of P, S seismic wave velocities of the Albanian earth Litosferes and its seismoactive features." Kumi publications", Tirana
- [18] Ormeni Rr, Kociaj S, Fundo A, Daja Sh, Doda, V (2013) "Moderate earthquakes in Albania during 2009 and their associated seismogenic zones", Italian Journal of Geosciences
- [19] Papazachos B, Papazachou C, (1997) The Earthquakes of Greece, Ziti Publication Co., Thessaloniki, 304 pp.
- [20] Papazachos BC, Dimitriu PP, (1991) Tsunamis in and near Greece and their relation to the earthquake focal mechanisms, Nat. Hazards, 4, 161-170.
- [21] Paulatto M, Pinat T, and F. Romanelli E (2007) "Tsunami hazard scenarios in the Adriatic Sea domain" Nat. Hazards Earth Syst. Sci., 7, 309–325.
- [22] Pondrelli, S., Salimbeni, S., Ekström, G., Morelli, A., Gasperini, P., and Vannucci, G. (2006), The Italian CMT dataset from 1977 to the present, Phys. Earth Planet. Int. 159, 286-303.
- [23] Prelogović, E., Aljinović, B., and Bahun, S. (1995), New data on structural relationships in the North Dalmatian area, Geologica Croatica 48, 167–176.
- [24] Roure F, Polino R, Nicolich R, (1990) Early Neogene deformation beneath the Po plain: constraints on the post-collisional Alpine evolution. Mem. Soc. Geol. France, N.S., n. 156.
- [25] Serpelloni, E., Vannucci, G., Pondrelli, S., Argnani, A., Casula, G., Anzidei, M., Baldi, P., and Gasperini, P. (2007), Kinematics of the Western Africa-Eurasia plate boundary from focal mechanisms and GPS data, Geophys. J. Int. 169, 1180–1200, doi: 10.1111/j.1365-246X.2007.03367.x.
- [26] Soloviev SL, Solovieva ON, Go CN, Kim KS, Shchetnikov NA, (2000) Tsunamis in the Mediterranean Sea 2000 B.C.– 2000 A.D., in: Advances in Natural and Technological Hazards Research, Volume 13, Kluwer Academic Publishers, Dordrecht, Netherlands, 237 pp.
- [27] Sulstarova E, Koçiaj S, Aliaj Sh, (1980) Seismic Regionalization of Albania. Shtypshkronja "Mihal Duri" Tirana, 297 p (in Albanian and in English).
- [28] Taymaz T, Jackson, JA, Westway R, (1990) Earthquake mechanisms in the Hellenic Trench near Crete, Geophys. J. Int., 102, 695-732.
- [29] Tselentis G-A, Gkika F, Sokos E, (2006) Tsunami hazards associated with the Perachora fault at eastern Corinth gulf, Greece, B. Seismol. Soc. Am., 96, 1649-1661.

Seismic design of an irregular structure with Adaptive Pushover Analysis.

Ervin Paçi¹, Altin Bidaj¹, Hektor Cullufi¹

¹Department of Construction and Infrastructures Engineering, Polytechnic University of Tirana, Albania,

ABSTRACT

Recently we are using the European Codes for the design of structures for earthquake resistance but in some cases even European Code doesn't give realistic results. For irregular structures the European Code gives very simplified recommendations that if will be used for the design gives results that could produce a very heavy and expensive construction.

The present paper in the first part will provide information about the EN-Eurocode 8 for Design of Structures for Earthquake Resistance and its limitations. After that will be presented adaptive pushover procedure for nonlinear analysis of irregular structures.

The APO theory will be used for the analyses of an existing structure. Firstly in the paper is given the information about the conditions of the existing structure. After that is performed the nonlinear analysis (adaptive pushover) and are given the structural measures suitable for retrofitting this type of structure.

In the end, the paper makes recommendations on the methodology of design and the most appropriate strategy of retrofitting these kinds of structures in order to achieve the required level of performance and increase their level of security based on European Codes.

Keywords: *Seismic retrofitting, Eurocodes, existing structure, Adaptive Pushover Analysis*

INTRODUCTION

In recent years in Albania had been constructed numerous buildings both private and public but despite several attempts the design and constructions standards for reinforced concrete structures are not renewed. The lack of adaptation of new design standards has forced a number of designers to work directly based on Eurocodes but meanwhile more designers continue to work with the old standards. This has led to a cacophony of design approaches and that for a very seismic country like Albania will lead to very large problems if a design earthquake occurs. In the article through the example of a building designed by the Albanian codes and retrofitted based on Eurocodes recommendations aimed to give the problems that could bring the use of existing codes and suggest to the entire community of engineers in Albania that is now essential to the designer of structures to apply not only European standards but to use the new methodologies as well.

The methodology of existing structures control and retrofit passes through the following stages:

- Dimensions and geometric data informations, reinforcement bars and detailing, material of the existing structure
- Static analysis design as a new structure but with geometry and characteristics of existing material (simulation design).

- Check of structure deformations, etc. Comparison of provided reinforcement with required reinforcement. If provided reinforcement is not sufficient then must be done the nonlinear analysis.
- Choose the strategy of intervention, analysis and control the retrofitted structure.

Below the article will give in detail all these stages.

EXISTING STRUCTURE

The design of existing building is done in 2009. The building is divided in two separate structures. The first structure which will be analysed in the article will serve as offices premises. It has 2 above ground stories with irregular form in plan. The dimensions are about 8m with 24.3m at max point.

The first structure is divided in 2 main axes in longitudinal direction (one main span) and 5 axes (4 spans) in transversal direction. Columns dimensions are 40 x 40cm and 40 cm diameter. The side beams and transversal beams are 40 x 60cm, while the beams for the port between axis “3” and “4” are 30x40cm and 25x60 cm. The slab height is 17 cm. We don't have data for other details and other possible changes during the construction.

From observations of the concrete elements is seen that the dimension of the structural elements are the same as in the design. We have done non-destructive and some destructive tests for taking the exact characteristics of the materials, and checking the height of the slab.

The building was designed based upon Albanian Design Codes “K T P 1985”. We have the final design drawings so taking into account also the real material characteristics we can consider that we have a very good level of recognition of the existing structure.



Figure 1. View of the structure

CONCRETE PROPERTIES INVESTIGATIONS

Up to now there are used 4 main methods for evaluation of Concrete properties. Based on their characteristics their results are more or less reliable.

We have done 2 core tests as described in UNI EN12504-1 standard and 6 Schmid hammer tests as described in UNI EN12504-2 standard.

For the core tests we have used the correction given by Masi (2005) [7]

$$F_{c,i}=(C_{h/D} \times C_D \times C_s \times C_d)f_{core,i}$$

Where $C_{h/D}$ correction for h/D different from 2.

C_D correction for D different from 100mm

C_s correction for steel presence influence

C_d correction for core disturbance

From this expression can have the following characteristics

Concrete properties from tests

Self weight

$$\gamma=2455 \text{ kg/m}^3$$

Cylinder concrete compressive strength

$$f_{ck}= 270 \text{ daN/cm}^2$$

Cubic concrete compressive strength

$$R_{ck}= 330 \text{ daN/cm}^2$$

Design compressive, tensile strength

$$f_{cd} = 180 \text{ daN/cm}^2$$

$$f_{ctm} = 28.5 \text{ daN/cm}^2$$

$$f_{ctk 0.05} = 19.4 \text{ daN/cm}^2$$

Structure evaluation based on Eurocodes

As recommended by the Eurocodes[] and the reference documents, structural evaluation of existing buildings in general requires an «additional» limit state. The new buildings are design to fulfil the hierarchy of resistances and appropriate ductility, and evaluated structures are design according to these requirements.

These requirements are based on the determination of three states of damage of the structure

- limit state with limited damage (immediate occupancy) IO
- limit state with significant damage (from damage control- life safety) LS
- limit state of structural stability (total or partial collapse) CP

The evaluation of the existing structure proceeds according to the following steps[5,7]:

- Identification of existing data
- Determination of levels of recognition and selection of computer models
- Determination of seismic loads in every limit stage
- Modelling and Analysis
- Verification of elements

The first two items we have described in the beginning of the article, the others are given below.

Seismic action

Seismic identification zone

Albania is a very seismic zone. In the existing Albanian code the seismic input is taken from an Intensity map multiplied by soil conditions and some other factors. According to EC8 seismic hazard should be given only with one parameter a_{gR} on ground type “A” that correspond to rock or rock like geological formations, including 5m weak formations (soil) at surface. The values of a_{gR} (maximum acceleration PGA) are taken from the Probabilistic hazard map of Albania recommended recently by a group of authors [6]. The return period of the reference event is $T_R=475$ years that corresponds to a life time of 50years.

The horizontal PGA in ground type A for the city of Tirana is taken $PGA=0,25g$

Based on the values of PGA in rock and for the specific type of terrain is calculated the design spectrum for three limit states based on EC8 formulations and soil condition classifications. The design spectrum is taken by reducing the corresponding elastic spectrum with the appropriate structure behaviour factor “q”. For the ultimate limit state for local soil conditions (ground type C) this factor is taken 3.2.

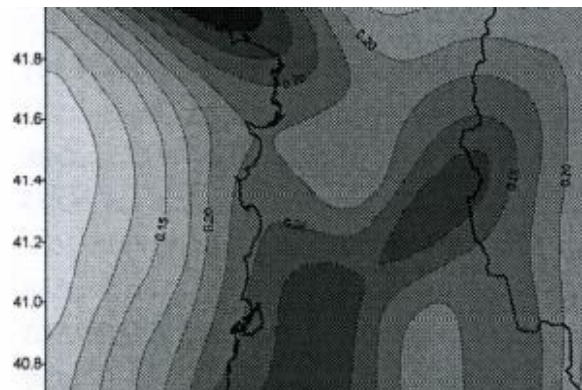


Figure 2. Peak ground acceleration Map of Albania

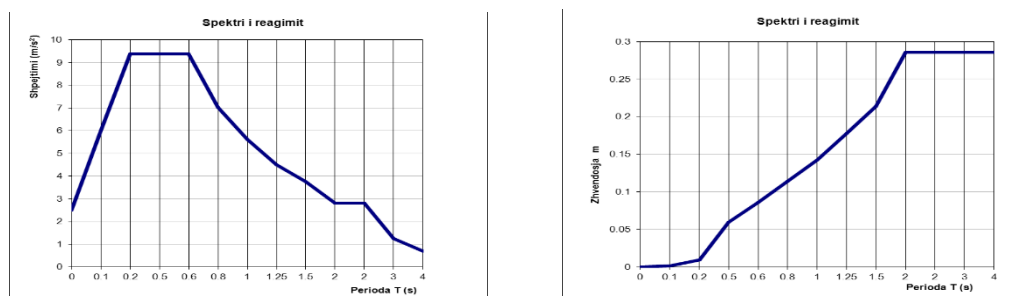


Figure 3. Graphical view of the elastic acceleration and displacement spectrum for soil type C

Dynamic linear analysis

Structural modelling aspects and the determination of seismic action given above is done in the same manner as for a new building according to EuroCodes 8 recommendations. The

analyse and the determination of internal forces is done by spectral method with concentrated masses in the centre of masses of each story. The combination of seismic loads and other actions is made according to EC1.

Model of the structure is the same as for a new building and the contribution of non-structural elements is neglected. The 3D model of the structure[4] is given below in fig. 3.

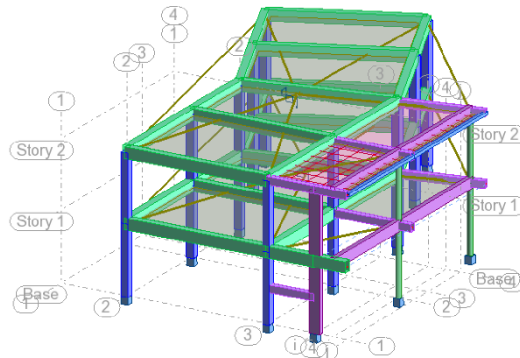


Figure 4. Graphical view of the linear model

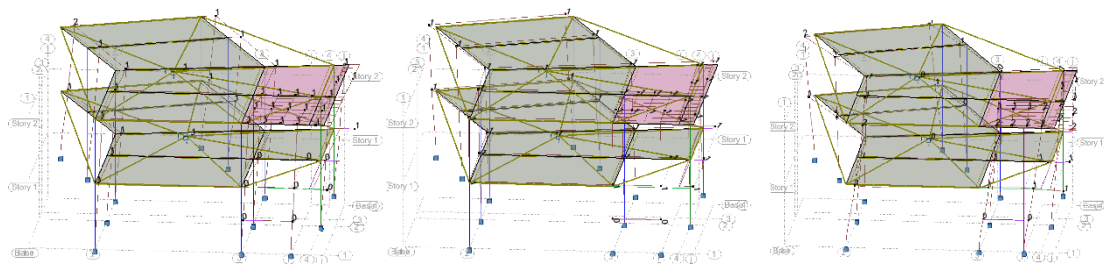


Figure 5. Graphical view of the three first modes

Table 1. Modal results of the structure

Case/ Mode	Frequency (Hz)	Period (sec)	Rel.mas. UX (%)	Rel.mas. UY (%)	Cur.mas UX (%)	Cur.mas UY (%)	Total mass (kg)
4/1	1.67	0.60	11.09	72.01	11.09	72.01	704610.46
4/2	1.68	0.59	80.78	88.76	69.69	16.75	704610.46
4/3	2.04	0.49	90.96	92.47	10.18	3.71	704610.46
4/4	4.71	0.21	91.08	98.70	0.13	6.23	704610.46

As seen from the modal results the structure is not regular and torsion influence its seismic behaviour. After the determination in advance the fragile or ductile behaviour for each element, with forces obtained from seismic combination is checked the strength of all the elements. From these results we can see that although nearly in limit the columns strength are assured (average safety coefficient is approximately around 1:03) while the beams meet the criteria of resistance

in shear but did not meet the criteria of flexural resistance. To get a more accurate picture of the way the structure behaves it is necessary to do nonlinear analysis.

Static nonlinear analysis

Nonlinear static analysis is the simplest method for nonlinear analysis of structures. This analysis can usually be done with concentrated plasticity models that are the classic uses but recently distributed plasticity models are used as well.

Without treating the aspects of the method we shall give only some problems which are also reflected in our analysis of the structure.

In difference from the linear analysis in this method cannot be made a combination of results in both directions but each direction must be considered separately. For each direction are taken into consideration two types of distribution of forces, one according to normalized first mode deformations and the second according to proportional mass of each floor.

The method cannot take into account the effects of progressive degradation of strength, the redistribution due to of the plastification and the change of modal characteristics. Also in torsionally eccentric structures the first mode has important effective mass participation in both directions and may not be disconnected from other modal forms. This mean simply that we cannot evidenced a first mode that effects only one direction to get real performance of the structure for each direction separately.

In these cases must be used nonlinear dynamics analysis or adaptive nonlinear static analysis [3]. Hereafter are given some figures that for the case of our structure illustrate the encountered problems.

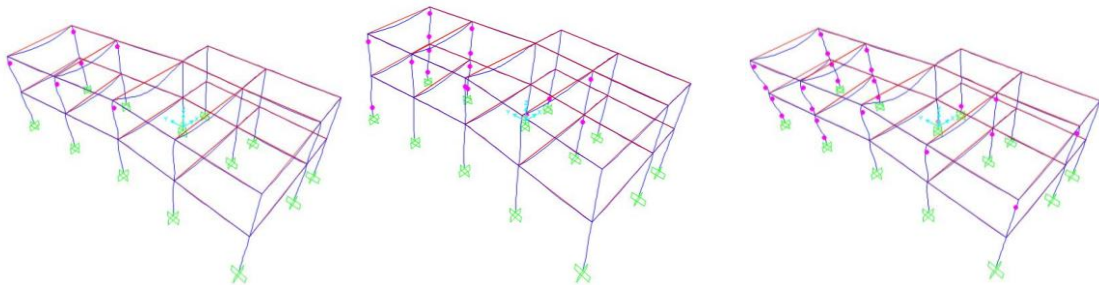


Figure 5. Graphical view of the structure for three incremental following steps

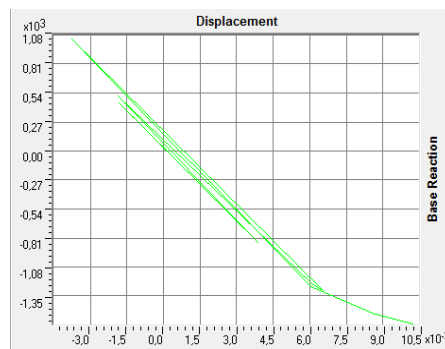


Figure 6. Graphical view of the base force versus displacement for the structure(capacity curve)

From the shown results can be clearly seen that the capacity curve, deformation base shear force relationship is not continuous in one direction and cannot be taken a performance point of the structure.

This means also that we can't determine the required maximum displacement and the corresponding base shear force with any of the known methods. (ATC40, FEMA 356)[2,1]

Consequently we cannot check the deformation capabilities (θ) or strength (M_{Rd}, V_{Rd}) of the elements of the structure.

Adaptive static nonlinear analysis (Adaptive pushover)

In this analysis, the distribution of horizontal incremental loading isn't held constant but varies according to modal forms and participation factors obtained from the analysis of its eigenvalues forms after each load step [3,8].

The analysis can consider the degradation (Softening) of structure elements strength, the change of eigenvalues forms after each load step and change the internal forces due to spectral amplification.

This type of analysis gives satisfactory results for torsionally eccentric structures and structures for which the higher modes influence the seismic response.

The used methodology is quite similar to the classical nonlinear static analysis (PO) so in the figures below are given only some results of deformation capacity the strength check of the most loaded frame (frame B).

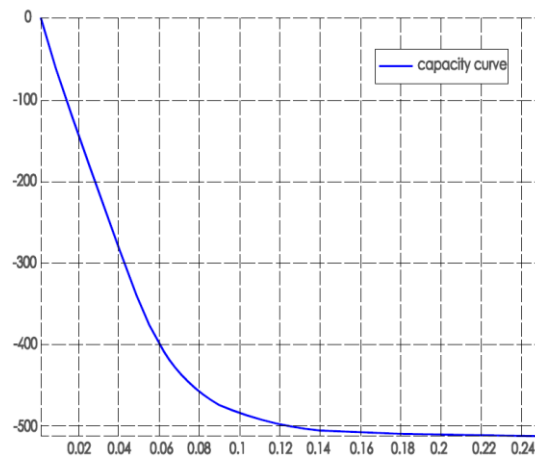
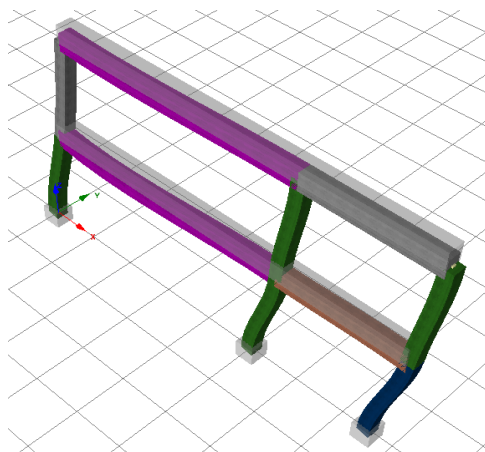


Figure 7. Graphical view of performance criteria check for frame B of the structure;

Figure 8. Graphical view of capacity curve only for frame B of the structure

From the curve of the relations in the function of displacement (incremental loading step) and the curve of the criterion of performance achieved for d_{max} is seen that the columns capacity to absorb the plastic deformation is greater than that of the beams so we have chosen to increase the flexural capacity of the beams and only confining the columns to achieve the performance that we have agree with the investor, that under the design earthquake the structure must achieve an acceptance criteria between Immediate Occupancy(IO) and Collapse Prevention(CP).

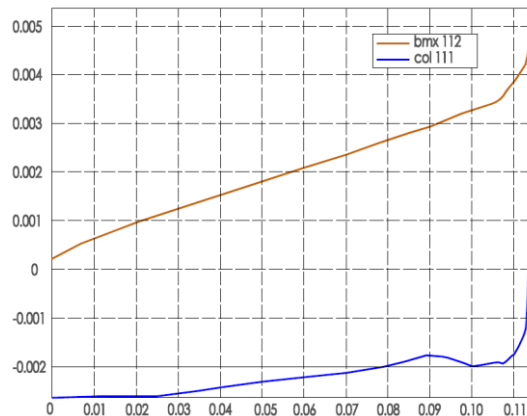


Figure 9. Graphical view of θ -incremental deformation for the side column and the first story beam.

Results

From the obtained results, as illustrated in the above figures the flexural strength of the beams is more problematic. To rehabilitate the structures we can use four different approaches.

1. Increasing the global capacity (strengthening). This can be done by the addition of cross braces or new structural walls.
2. Reduction of the seismic demand by means of supplementary damping and/or use of base isolation systems.
3. Increasing the local capacity of structural elements. This approach recognises the existing capacity of the structures, and adopts a more cost-effective approach to selectively upgrade local capacity (deformation/ductility, strength or stiffness) of individual structural components.
4. Selective weakening retrofit. This is an intuitive approach to change the inelastic mechanism of the structure.

From these four types of retrofit strategy approaches we have chosen to apply the third type, increasing the local capacity of structural elements because as it's seen from the results the structure has limit stiffness for accepted performance allowed drifts (cannot apply type 4), the addition of walls or braces is impossible due to architectural requirements, and the use of seismic base isolation systems is quite expensive.

In our case, for this purpose we have used for the reinforcement of the beams longitudinal carbon fiber strips both in middle and supports and for columns confinement carbon fiber web.

Fiber design and placement of needed fibers is done according to Italian recommendation CNR-DT 200/2004 and then we checked the structure with reinforced sections with distributed plasticity model.

From the obtained results can be seen that after strengthening of elements the structures performance is improved and all elements meet the performance criteria in flexure, shear strength, deformative capacity and the surface layer of column concrete that in the existing structure crush and spall out is now assured.

Below are given the results for the most loaded frame (frame B).

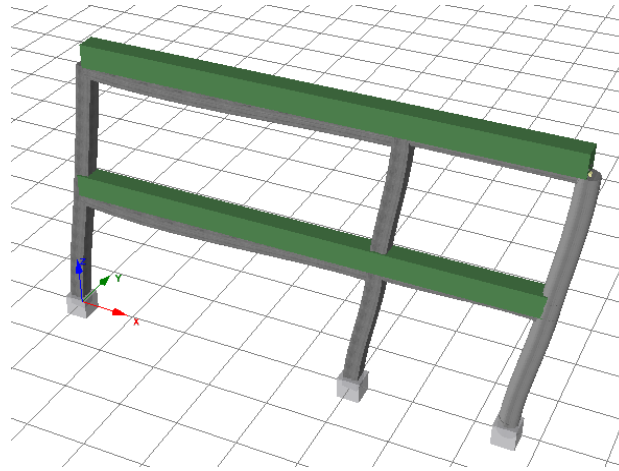


Figure 10. Graphical view of performance criteria check for frame B of the structure after the increasing of capacity of structural elements. (no performance criteria is reached)

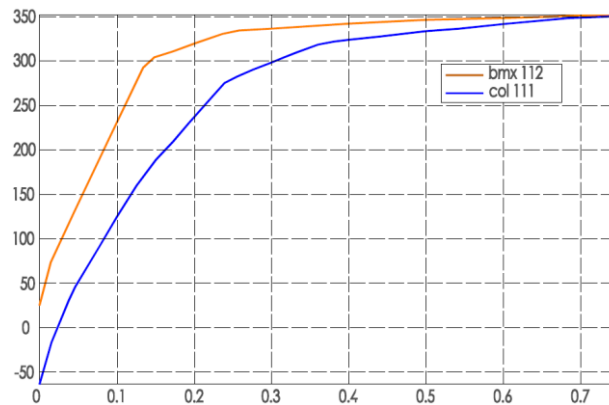


Figure 11. Graphical view of M-incremental deformation step percentuality for the side column and the first story beam after the increasing of capacity of structural elements

CONCLUSION

The use of Adaptive pushover analysis is highly efficient and the results are consistent and close to the results from nonlinear dynamical analysis. But the use of this method remains limited to specialized software and modelling requires plenty of time and care. If these analysis will not be implemented in ordinary commercial software the use of nonlinear dynamic analysis, although time-consuming will continue to remain the most widespread method for the calculation of torsionally eccentric structures.

REFERENCES

- [1] American Society of Civil Engineers (ASCE) [2000] “FEMA356: *Prestandard and commentary for the seismic rehabilitation of building*, Prestandard, Federal Emergency Management Agency (FEMA), Reston, Virginia, USA.
- [2] ATC. *Seismic evaluation and retrofit of concrete buildings*—volume 1 (ATC-40). Report No. SSC 96-01. Redwood City (CA): Applied Technology Council; 1996.
- [3] Beyer, K., Dazio, A., Priestley, M.J.N., [2008] “*Seismic design of torsionally eccentric buildings with U-shaped RC walls*”, IUSS Press, Pavia, Italy.
- [4] Computer and Structures, Inc. (CSI). SAP2000/NL-PUSH software, version 15, Berkeley (CA, USA): Computer and Structures, Inc., 2000.
- [5] Eurocode 8. Design of structures for earthquake resistance, 2006, EN 1998
- [6] Kuka N, Sulstarova E, Duni Ll, Aliaj Sh.; “Seismic Hazard assessment of Albania using the spatially smoothed seismicity approach”; International Conference in Earthquake Engineering; Skopje 26-29 August; 2003.
- [7] Manfredi, G., Masi, A., Pinho, R., Verderame, G., Vona, M., 2007 “*Valutazione degli edifici esistenti in Cemento Armato*”, IUSS Press, Pavia, Italy.
- [8] SeismoStruct version 6, Seismosoft Ltd., Via Boezio 10 27100 Pavia (PV) Italy

Repairing and Seismic Strengthening of Damaged Reinforced Concrete Structures with External Steel Shear Walls

Yavuz Selim Tama¹, Hasan Kaplan¹, Tarkan Görgülü², Zeki Ay²

¹Department of Civil Engineering, Pamukkale University, Turkey

²Department of Civil Engineering, Süleyman Demirel University, Turkey

ABSTRACT

In this study, a new strengthening technique for earthquake-damaged reinforced concrete (RC) structures was experimentally investigated. Within the scope of the study, three-dimensional, two-storey RC model was constructed. During the production of this model, some of the common structural inadequacies in existing RC structures were taken into consideration. For this purpose, initially a reference model was exposed to lateral loads up to 1.7 % drift. Then, the damaged structure was repaired with epoxy injection. Finally, the repaired model was strengthened with External Steel Shear Walls (ESSW) and subsequently tested under the same load pattern. Chevron braced system is selected as ESSW. The results show that existing RC structures damaged under earthquake effects can be strengthened rapidly by proposed strengthening technique and the lateral load capacity and stiffness of these structures can be increased significantly.

Keywords: *Earthquake, Repairing and strengthening, External steel shear wall, Chevron braced system.*

INTRODUCTION

Several techniques were developed for strengthening of the existing buildings [1-5]. Increasing the lateral load capacity and stiffness of the structures are the common aims of those techniques, which contribute to the performance of the structure by limiting the lateral drifts. Seismic strengthening of structures is mainly based on two strengthening schemes: Element-Based and System-Based. The former, bases on the strengthening of the structural elements, which are expected, undergo a brittle failure. The latter involves introduction of new structural elements to the system, such as reinforced concrete shear walls to improve the overall structural performance.

Element-based techniques may not always be sufficient to increase the seismic performance of the strengthened structure [3]. In this case, it is better to introduce system-based strengthening methods, which improve base shear capacity as well as lateral stiffness. These methods usually compensate for the local deficiencies, which reduce the structural performance before strengthening, by decreasing the displacement demand.

The use of RC infill walls has a wide range of applications for the strengthening of earthquake-damaged structures. Its efficiency was proved by numerous experimental studies [6-14] showing that strengthening with RC infill increases the lateral load capacity and stiffness while it reduces lateral drifts. In previous studies, the effect of connection capacity between existing and new concrete [9] and the effect of wall openings [8] were investigated. According to these studies, properties of reinforced concrete frames (column reinforcement ratio, column and beam transverse reinforcement and column compressive strength) and connection between frame and infill walls were effective in strengthened frame behavior. The use of external RC shear walls was also tested on RC specimens. External wall schemes that are perpendicular [15-17] or parallel [18] to the side of the building were examined. As found in these studies, external RC walls behaved like monolithic walls. Only minor cracks were observed between wall and connecting elements after 2 % drift ratios.

Additionally, many theoretical and experimental studies were carried out on the use of steel shear walls as an alternative method of strengthening [19-22]. Most of the experimental studies on the use of steel braced shear walls were performed on single-storey and single-span frame models. According to the studies, strengthening the structures with steel shear walls increased the strength of the structure and better performance was achieved considering the ductility and energy dissipation. The performance of the technique was directly related to that of the dowels [14].

In this study, seismic performance improvement of earthquake-damaged RC structures with External Steel Shear Walls (ESSWs) was investigated experimentally. The reference and repaired and strengthened models were tested under imposed lateral sway to simulate seismic behavior. Chevron braced system is selected as external steel shear wall for strengthening. Repaired and strengthened model was tested under lateral loads again. The results obtained were compared with the results of un-strengthened reference model. The results of the study, demonstrate that reinforced concrete structures damaged in earthquakes can be strengthened with external steel shear walls after being repaired.

EXPERIMENTAL STUDY

Within the scope of this study, two-storey three dimensional RC structural models were produced in one-third scale and tested under lateral loads. The prepared RC model structure (Reference Model-RM) was tested, after then the damaged structure was repaired by epoxy injection and strengthened with ESSWs. Subsequently, the repaired and strengthened model was subjected to deformation.

Production and Properties of Reference Model

A one-third scale RC Reference Model was constructed as two-storey, one bay at one side, and three bays at the other side. The plan view and sections of the model are shown in Fig. 1. Structural deficiencies, which are widely observed in many existing RC structures in Turkey, like strong beam-weak column, cold joints with low sliding shear capacity and inadequate development length, were duplicated in the reference model. The final view of reference structure is given in Fig. 2.

The details of column and beam sections in the reference model are given in Fig. 3. Column dimensions were chosen to be 200×200 mm and Ø6 (S220) steel bars were used for reinforcement. End regions of the columns and beams were poorly confined by 90° hooked stirrups. At the upper ends of the second storey columns, steel bars were placed straight without providing necessary development length. The beam dimensions were chosen to be 140×200

mm, see Fig. 3. Similar to the columns, $\varnothing 6$ steel bars (S220) were used as reinforcements. Meanwhile, $2\varnothing 8$ plain bars were used as top and bottom reinforcements in the longitudinal direction. At the supports, an additional $\varnothing 8$ steel bar was used for top reinforcement. Like the columns, poor confinement was evident.

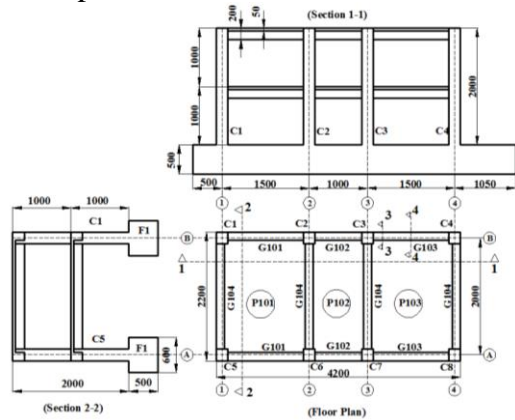


Figure 1 Plan view and sections of the RC structure model



Figure 2 Final view of the RC Reference Model (RM)

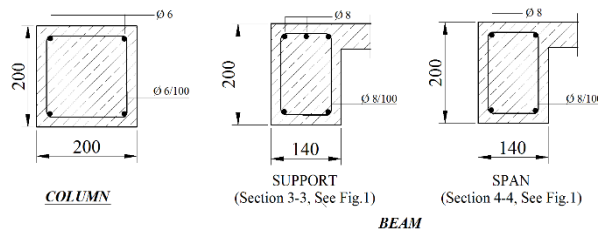


Figure 3 Details of the column and beam section

Material Properties

The properties of materials, concrete and steel bars, were also investigated in this study. Concrete samples taken during the production of the RC model were subjected to the uniaxial compression tests. Compressive strength was found to be 29.60 MPa and 32.18 MPa for the first and second storey, respectively. While, S220 reinforcement steel bars were used for the construction of RC models. S235 steel was used for SSW elements. Strength characteristics of these reinforcements and steel sections obtained from the tensile tests are given in Table 1. The technical properties of epoxy used for injection and anchor bonding are given in Table 2.

Experimental Setup

Experimental models fixed to the rigid floor with anchor bolts were loaded laterally by a servo-hydraulic actuator supported by the reaction wall. Fig. 4 illustrates the side view of the loading setup. Displacement of various points and deformation of some sections were measured to observe the behavior of the models. Linear Variable Differential Transformers (LVDT) and Linear Position Transducers (LPT) were used for measuring the displacements. They were also utilized for curvature measurements of RC elements and elongation of bracing elements.

Table 1 Strength characteristics of reinforcement steel bars and SSW members

Material Type	f_{sy} (MPa)	f_{su} (MPa)
Ø6 Reinforcement	328.30	398.70
Ø8 Reinforcement	386.50	532.00
St 37 (S235)	293.00	395.00

Table 2 Specifications of epoxy and anchorage resin, [23].

Material	Epoxy	Anchorage cement
Mixing ratio	A /B	A /B /C
Percentage by weight	60 /40	30 /20 /50
Percentage by volume	57 /43	40 /27/ 33
Mixing density (g/cm ³ , at 20 ^o C)	1.0 – 1.1	1.70 ± 0.10
Mixing race (min., 25 ^o C, 25 ^o g)	60- 90	50- 70
Color	Colorless	Gray
Desiccation duration (23 ^o C)		
Dust holding (min.)	120- 180	50- 60
Touching (hour)	5- 7	3- 4
Full hardening (date)	7	7

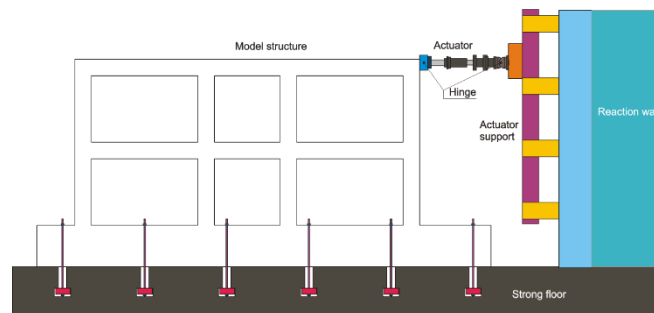


Figure 4 Side view of the loading setup

The Reference Structure Experiment

Reference model was tested under cyclic lateral load as shown in Fig. 4. The model was pushed up to 1.72% second floor drift level. At the end of the experiment, extremely smooth "load-displacement" conversion curves were obtained for the first and second floors of the structure (Fig.5). Until the end of the experiment, there was no significant decline in load carrying capacity of the structure. At the end of the experimental study, the second floor roof displacement of the model reached 34.40 mm, and capacity reached 67.35 kN (Fig.5). Damages mainly occurred in the upper and lower ends of the column. The cracks in the lower end of the column, shifted to floor joints expressed as cold joints and occurred in the form of a straight line. The cracks on the second floor column emerged as larger than the cracks on the first floor columns. The formation of cracks observed in the reference model after the experiment is shown in Fig.6.

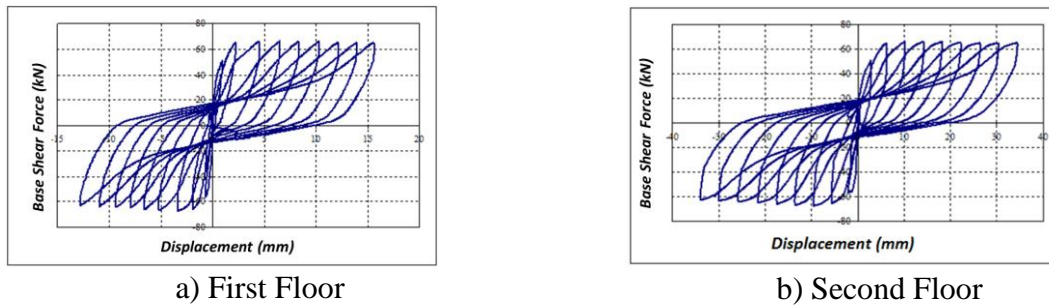


Figure 5 Reference Structure “Load-Displacement” Conversion Curve



Figure 6 Particular cracks on the RC reference model

Repairing of the Damaged RC Reference Model

The reference model damaged by pushing the second storey to drift ratio of 1.72 %, was repaired by injection of bi-component epoxy material to the RC structure in order to fill and repair the cracks formed on the RC members (Fig.6).

In order to repair the deformed model, initially, damaged zones were immobilized and all the cracks including micro fissures were enlarged and cleaned by oil-free dry compressor. Then, packers were placed into the holes which were perforated to the lower and upper parts of the cracks forming a 45° angle with the concrete surface for epoxy injection. Afterwards, cracks were closed completely with repair cement and epoxy material was pierced to the cracks under pressure (maximum with 5 bar pressure). This treatment continued to the point where the epoxy material goes out of the control packer. At this stage, it was understood that micro fissures were completely filled when epoxy left the control packers. Details of the repairing procedure for the reference model and the appearance of the repaired model are given in Fig.7 and Fig.8, respectively.



Figure 7 Repairing of the damaged RC reference model with epoxy injection



Figure 8 Repaired RC reference model before strengthening

Strengthening of the Repaired RC Reference Model

The repaired RC model was strengthened by SSW externally. External SSW strengthening system made out of circular hollow sections was designed and produced as a diagonally braced frame. Elements of the SSW were connected to each other with bolts to allow a prefabricated production. The aim of use of the existing structures was taken into consideration and braces of the SSW were arranged as reverse V (Δ). Fig. 9 illustrates the side view of the SSW and connection of the joints. As seen in section (1-1) of this figure, bolted joint connections of steel elements were constructed by squeezing the ends of circular hollow sections. Section properties of the steel elements used in SSW are given in Table 3, where A_s is cross-sectional area of steel, D is the diameter of circular tube section, i_x is the radius of gyration, I_x is the moment of inertia, S_{kx} is the buckling length and W_x is the section modulus.

The connection between the RC model and SSW needs a careful design to achieve load transfer from model to SSW elements. Therefore, the space between the strengthening system and RC system was minimized to provide a better connection. The connection elements (R),

which provide the connection between SSW and the reference model, were designed such that they transfer shear forces safely. Connection element linked to other elements with fillet welds is designed as 50x50x5 box section. Anchor holes were drilled into the RC model by using a template that fits the prefabricated SSW. The holes were cleaned by oil-free air and anchor bolts were fixed to the columns, beams and foundations. The connection details and the installation stages of External SSW to the RC structures are shown in Fig.10 and Fig.11 respectively.

Table 3 Sectional properties of the steel shear wall elements

Steel member types (See Fig. 10)	Section		As (mm ²)	ix (mm)	Wx (mm ³)	Ix (mm ⁴)	Skx (mm)
	D (mm)	t (mm)					
D1	33.70	3.0	289	10.90	2040	34400	860
D2	33.70	3.0	289	10.90	2040	34400	960
U1	60.30	3.0	868	19.60	11100	334800	930
U2	60.30	3.0	868	19.60	11100	334800	930
V1	60.30	5.0	868	19.60	11100	334800	880
V2	60.30	5.0	868	19.60	11100	334800	1000

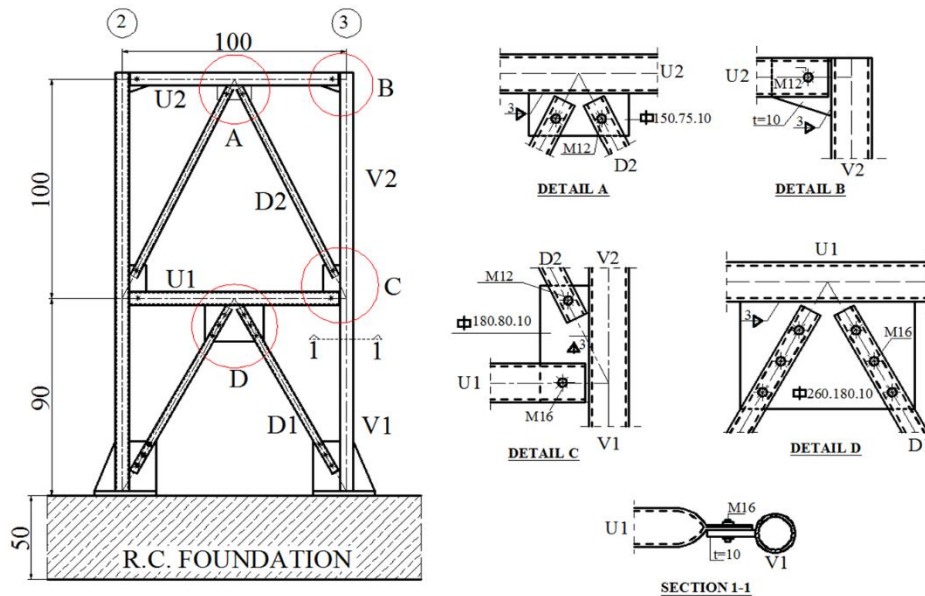


Figure 9 Connection details of the SSW

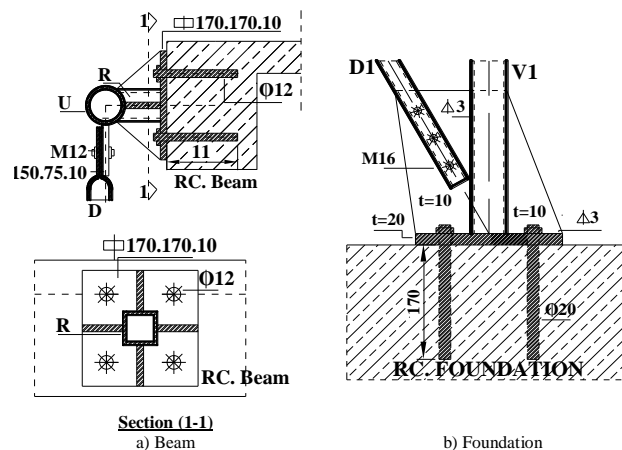


Figure 10 Details of the connection between the external SSW to the RC structure

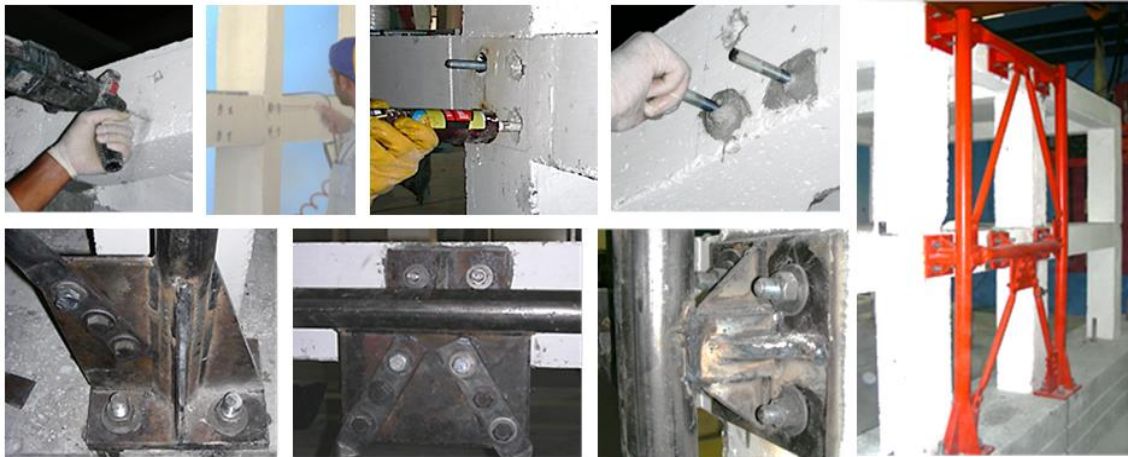


Figure 11 Installation of the External SSW to the RC structure.

Repaired and Strengthened Structure Experiment

The reference model was repaired and strengthened with External SSW, and then tested under lateral load applied to the second floor level. The experiment continued until the second floor displacement rate reached 3.13%. At the end of the experiment, the second floor peak displacement reached 62.55 mm and the maximum base shear reached 178.26 kN. Until the end of experiment, no significant decrease was observed in the carrying capacity of the structure.

For the strengthened model, initial damages in the RC system occurred at the upper ends of the second floor columns. The damage at the lower and upper ends of the columns became intense in the final stage of loading. Like the reference model, the cracks formed at the lower ends of the columns moved along cold joints and appeared as a straight line. The view of the damage formations at the RC system of the repaired and strengthened model is given in Fig. 12. Most cracks on the RC structure formed nearby the repaired cracks.

When the second storey drift ratio reached 0.8 %, diagonal member (D2) of the SSW buckled about the weak connection point, i.e. squashed end, due to the presence of compressive force. Meanwhile, crushing was observed as a result of the tensile force around the bolt hole of the other diagonal member (D2), see Fig.13.

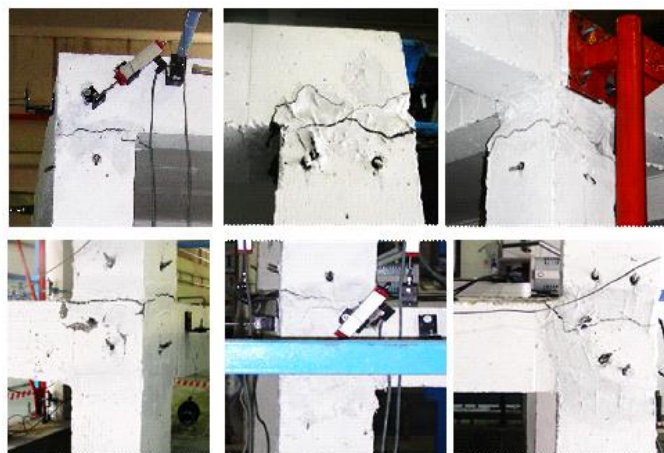


Figure 12 Particular cracks on the repaired and strengthened model

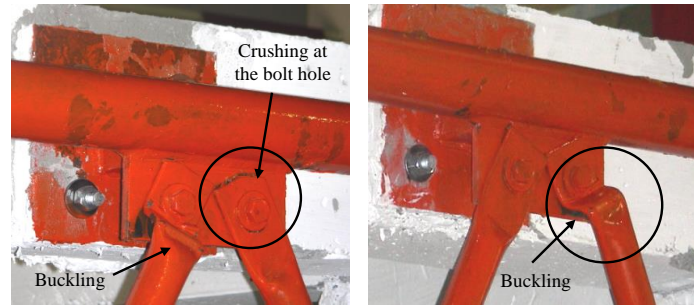


Figure 13 Damages formed in the strengthening SSW system

conclusion

In this study an alternative technique for strengthening of the earthquake-damaged RC structures with external SSWs was proposed. The experimental study was based on two models, namely reference model and repaired-strengthened model. The reference model was tested under lateral loads. The damaged reference model was repaired with epoxy injection and strengthened with external SSWs and then tested under incrementally reversed cyclic lateral loads. Here, it was aimed to increase the lateral load capacity of the structure to a sufficient value by new SSWs connected to the exterior surface of the system. For this purpose, the strengthening was performed externally. Compared to the conventional techniques, functionality of the structure was slightly affected and duration of construction was very short. Apart from these, the loss of space, architectural functional failures and repair costs are at a minimum level. For these reasons, the use of external SSW in strengthening to the damaged RC structures offers an economical and practical alternative. The main results of this study are as follows:

1. The application of external SSWs increased the lateral load capacity and stiffness of the reference structure substantially. The lateral load capacity of the model strengthened with SSW reached to the value of 178.26 kN showing 265 % increase in the capacity with respect to the reference model (67.35 kN). Similarly, initial stiffness of the strengthened model also increased by 315 % relative to the reference model.
2. Repaired and strengthened model was forced approximately to 3.0 % drift level during which no significant capacity loss occurred.
3. In the reference model, there is no considerable difference between the first and the second floor displacement ratio throughout the experiment. In contrast to that, in the strengthened model, the ratio of the second floor displacements to that of the first floor showed 100% increase. This was observed as shear walled system behavior and loading pattern were effective.
4. When the second storey drift ratio of the strengthened system reached 0.8 %, diagonal member (D_2) of the SSW was buckled about the squeezed end due to the compressive force. Besides, around the bolt hole of the other diagonal member (D_2), crushing occurred because of the tensile force. These demonstrate that, diagonal elements and their connections should be designed carefully.
5. In order to minimize the forces at the intermediate members (R) connecting SSW and RC structure, the exterior SSWs were positioned close to the RC structure, eliminating damage of the elements.
6. There was no damage at the anchorages, which successfully conducted the load transfer between RC system and SSWs.

Acknowledgement

This study was supported by Suleyman Demirel University and State Planning Organization of Turkey under project number BAP-08-11-DPT.2004K120760.

REFERENCES

- [1] Rodriguez, M. Park, M. (1991) Repair and Strengthening of Reinforced Concrete Buildings for Seismic Resistance, *Earthquake Spectra*, Vol. 7, No. 3.: 439-459.
- [2] Elnashai, A. S. Pinho, R. (1998) Repair and retrofitting of RC walls using selective techniques. *Journal of Earthquake Eng;* vol. 2, iss. 4, p. 525-568.
- [3] Moehle, J. P. (2000) State of research on seismic retrofit of concrete building structures in the US. *In: Proc. of US-Japan symposium and workshop on seismic retrofit of concrete structures - state of research and practice.*
- [4] Jirsa, J. Q. (2006) Learning from earthquakes to improve rehabilitation guidelines for reinforced concrete buildings. *Advances in earthquake engineering for urban risk reduction;* vol. 66, p. 209-227.
- [5] Tsionis, G. Apostolska, R. Taucer, F. (2014) Seismic strengthening of RC buildings, *JRC Science and Policy Report, European Commission*, Report EUR 26945 EN.
- [6] Canbay, E. Ersoy, U. Ozcebe, G. (2003) Contribution of reinforced concrete infills to seismic behavior of structural systems, *ACI Struct Jour;* 100:637-43.
- [7] Erdem, I. Akyuz, U. Ersoy, U. (2006) Ozcebe G, An experimental study on two different strengthening techniques for RC frames, *Eng Struct;* 28:1843-51.
- [8] Anil, O. Altın, S. (2007) An experimental study on reinforced concrete partially infilled frames, *Eng Struct;* 29:449-60.
- [9] Altın, S. Anil, Ö. Kara, M. E. (2008) Strengthening of RC nonductile frames with RC infills: an experimental study. *Cem Conc Comp*, 30: 612-21.
- [10] Griffith, M. (2008) Seismic retrofit of RC frames buildings with masonry infill walls: Literature review and preliminary case study, *JRC Scientific and technical Reports*, EUR 23289 EN.
- [11] Pujol, S. Climent, A. B. (2008) Rodriguez M E, Pardo J P S, Masonry Infill Walls: An Effective Alternative For Seismic Strengthening Of Low-Rise Reinforced Concrete Building Structures, *The 14 th World Conference on Earthquake Engineering October 12-17, Beijing, China.*
- [12] Essa, A. S. A. T. Badr, M. R. K. El-Zanaty, A. H. (2010) Effect of infill wall on the ductility and behavior of high strength reinforced concrete frames, *Housing and Building National Research Center, HBRC Journal*, 10, 258-264.
- [13] Grubisic, M. Sigmund, V. (2014) Comparison of Different Strengthening Techniques of Damaged and Weak Reinforced-Concrete frames, *Second European Conference on Earthquake Engineering and Seismology, Istanbul, Aug. 25-29.*
- [14] Abdel-Hafez, L. M. Abouelezz, A. E. Y. Elzefery, F. F. (2015) Behavior of masonry strengthened infilled reinforced concrete frames under in-plane load, *Housing and Building National Research Center, HBRC Journal* 11, 213-223.
- [15] Kaltakçı, M. Y. Yavuz, G. (2006) The behavior of the reinforced concrete frames strengthened with partially reinforced concrete shear wall under the affect of lateral load similar to earthquake. *In: Prof. of 7th Int Conf on Adv in Civil Eng.*

- [16] Kaltakçı, M. Y. Arslan, M. H. Yılmaz, U. S. (2008) Arslan H D, A new approach on the strengthening of primary school buildings in Turkey: An application of external shear wall., *Build and Environ*; 43: 983-990.
- [17] Kaltakci, M. Y. (2012) Ozturk M, An experimental study on the strengthening of non-ductile reinforced concrete frames via external shear wall, *European Journal Of Environmental And Civil Engineering*, Volume:16, Issue:1, Pages:59-76.
- [18] Yılmaz, S. (2007) Strengthening reinforced concrete buildings with exterior shear walls, *Denizli Pamukkale University Institute of Natural Sciences*.
- [19] Bush, T. D. Wyllie, L. A. Jirsa, J. Q. (1991) Observations on two seismic strengthening schemes for concrete frames. *Earthq Spec*; 7:511-27.
- [20] Masri, A. Goel, S. (1996) Seismic design and testing of an RC slab-column frame strengthened with steel bracing. *Earthq Spec*; 12:645-66.
- [21] Tama, Y. S. Yılmaz, S. Kaplan, H. Görgülü, A. T. (2005) An application of strengthening of the existing reinforced concrete structures with external steel shear wall. *In Proc. of the forth int. advanced technologies symp.*; 1194-1197.
- [22] Ohmura, T. Hayashi, S. Kanata, K. Fujimura, T. (2006) Seismic retrofit of reinforced concrete frames by steel braces using no anchors. *In Proc. of eighth national conference on earthquake engineering*.
- [23] Gorgulu, A. T. (2008), Application of external steel construction shear wall at strengthening of the present structures, Suleymen Demirel University, Institute of Natural Science, PhD Thesis.

Damage limitation requirements according Eurocode 8 for flexible reinforced concrete low-rise buildings

Altin Seranaj¹, Forcim Softa², Agim Seranaj³, Fanjola Koroveshi⁴

¹ Department of Building Construction and Transportation Infrastructure, Polytechnic University of Tirana,

² Department of Mechanics of Structures, Polytechnic University of Tirana, Albania

³ Department of Mechanics of Structures, Polytechnic University of Tirana, Albania

⁴ Department of Civil Engineering, Epoka University, Albania

ABSTRACT

This study presents an analytical assessment for the reinforced concrete frame constructed with flat beams. The typology is known as frame with “embedded beam in the slab”, with a total height 25cm. Many similar structures have been constructed all around Balkans regions and Middle East. Sometime these structures have only in the perimeter the normal beam (thickness more than the slab). As it is well known the main advantages of using this type of reinforced concrete frames are that, they provide both, low economical cost for initial construction and a good architectural flexibility. Anyway in some literature, these types of structures are not recommended as being the only system for seismic forces resistance of a building.

The response of the frame with flat beams is compared with two other structural typologies, classical frame and uncoupled wall systems. Structures with 3 and 5 floors are selected for this analyse. The effect of infill masonry hallow clay bricks is also considered.

The criterions of comparisons are based mostly on Eurocode 8 and especially on damage limitation states. This criterion is chosen in this study due to the fact that this parameter is connected not simply to deformation but to the financial loss to. This investigation is made by using software ETABS. The investigation as was expected show that the frame with flat beams has much deformation than the classical frame and the uncoupled wall systems. The interstory drifts are much difficult to accommodate as per Eurocode 8 requirements. When infill walls are symmetrical in plan and well distributed in height the effect is positive in all structures. When are not continues on the ground story only the uncoupled wall systems represent consistent interstory drifts. Two other structural typologies are similar on their ability to present the negative effect of soft story.

Keywords: Flat beams, Hallow brick masonry infill, soft story, damage limitation, construction cost.

INTRODUCTION

In the last decades, huge numbers of the reinforced concrete structures are constructed using beams inside reinforced concrete slabs made with hollow clay/concrete/polymers block. However, in most cases, due to lack of deep strong beams, which can form with columns strong frame actions, the resulted transverse stiffness may be low. This may lead to potential damage even when subjected to earthquakes with moderate intensity.

These types of structures are representing low initial cost for construction and very good architectural flexibility on buildings, but on the other side this structures are flexible and the deformation that follow the earthquake response even for moderate earthquake can cause a lot of damages on non-structural elements and so, an important economical losses.

Substantial research efforts have been devoted to investigating the performance of engineering structures during earthquakes such as reinforced concrete buildings, minarets, masonry and wooden buildings. It was reported that hundreds of thousands of buildings suffered different types of damage during these earthquakes.

This study presents an analytical assessment for the reinforced concrete frame constructed with flat beams. The depth of the beams on the examples studied in this article is 25cm, as normal practices in Albania. Typical buildings are shown on Figure 1.



Figure 1 Reinforced concrete frame structure with embedded beams into the slab

Their reaction under earthquake forces is compared with the reaction of classical reinforced concrete frame and wall systems. We have analyzed also these structures even taking into consideration the effects of infills with hollow bricks. According to the Eurocodes requirements, the designer has to take into consideration the infills during the analysis on the cases they have a negative influence on the reaction of the structures. In the literature the infills are called, as non-structural elements. This may lead to big problems, not only to the other professionals, but even to the civil engineers. They calling so (non-structural) would lead to do “dangerous” modifications during the constructions of building, due to the changing of the considerations that the designer has taken during the design.

On many recent earthquakes on Turkey, Italy, Taiwan, Haiti, India, Pakistan, Algeria, Greece etc., have shown that the mistakes made during the design and construction due to the negative influence of infill walls have led to considerable damages.

Due to the similarity of these typologies of structures we are here below on the figure presenting some photos from the structures affected by the earthquake “Izmir (Kocaeli), Turkey earthquake, Aug. 17, 1999, with intensity 7.4 Richter [1]. Typical buildings are shown on Figure 2.

The same types of structures are constructed these last 20 years in Albania. The future strong earthquake will come and similar pictures as above (even worse) we may see after that earthquake (if we will). An urgent need is to emphasize the problem that the flexible structures present and after increasing the requirement on the design and constructions have to be decided. Central and local authority have to collaborate in efficient way in order to do vulnerability analysis and other studies in order to construct a sustainable strategy for earthquake disaster preparedness and management.



Figure 2 Reinforced concrete frame structure with embeded beams into the slab, after earthquake Gölcük, Turkey.

2 DESCRIPTION OF THE BUILDINGS

The investigated buildings are 3 and 5 floors multi-story reinforced concrete structure with beams depth 25 cm embedded on slabs. For the normal classical frame and wall systems the beams have the normal high 60cm. The elevation of the building and the floor plan are shown in Figure 3 and Figure 4. The ground floor is 4.2m height and for other story height is 3.15m. The total height of the building above the basement is 10.5 m for the structure with 3 floors and 16.8m for the structure with 5 floors. The dimensions in plane are the same for both buildings 13.8x10.4m.

Footings with tie beams represent the foundation. Concrete C25/30 is used. The corresponding modulus of elasticity amounts to $E_{cm} = 31 \text{ GPa}$ (EN1992/Table 3.1). Steel S500 Class C is used. The structure will be designed for ductility class DCM.

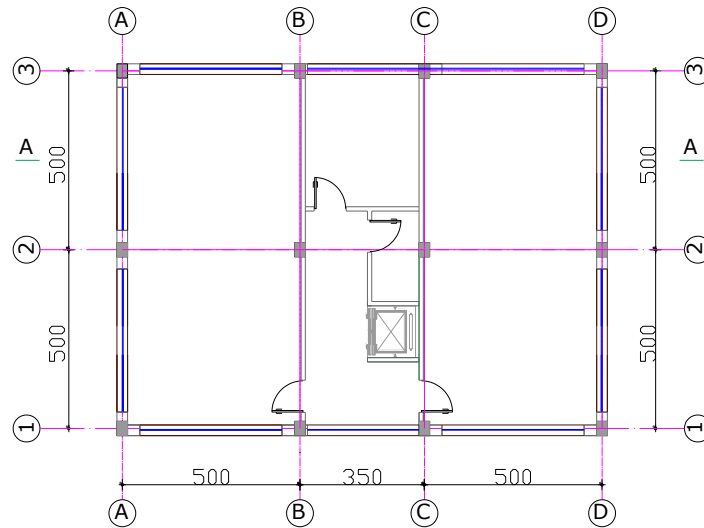


Figure 3 Plane of the model (3 floors and 5 floors)

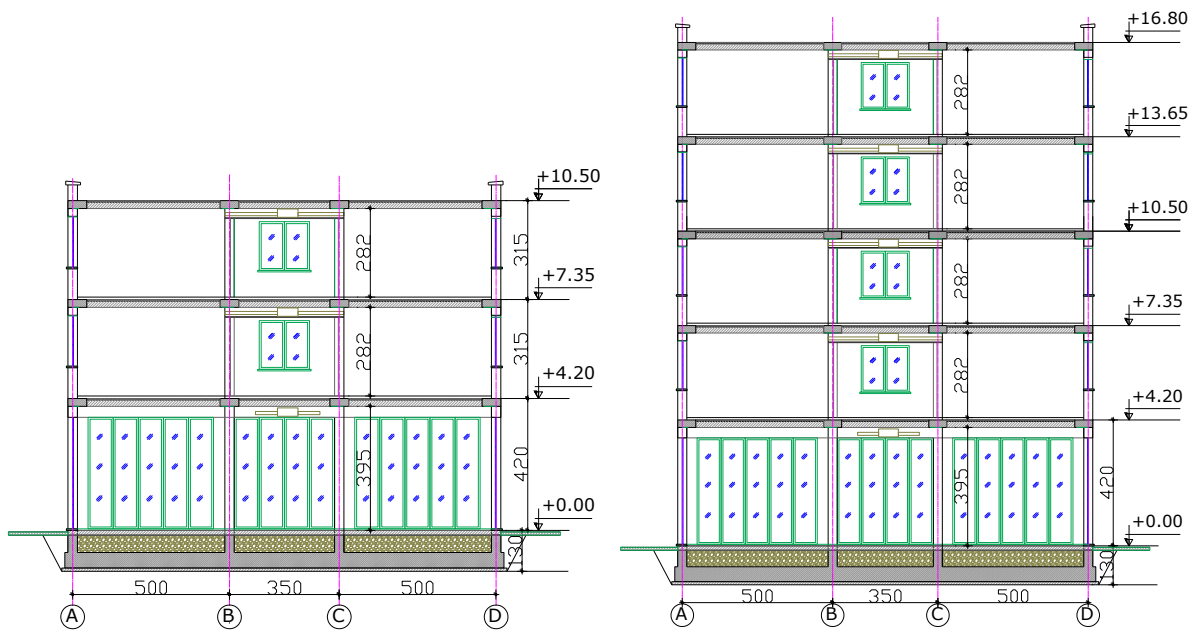


Figure 4 Section of the model (3 floors and 5 floors)

3 VERTICAL LOADS AND SEISMIC ACTION

The permanent loads “G” are represented by the self-weight of the structure and additional permanent load uniformly distributed equal to 3 kN/m². In the case of investigated building (which represents an office building – category B (EN 1991/Table 6.1)), the variable-live load in terms of uniformly distributed load amounts to 2kN/m² (EN 1991/Table 6.2). The variable-live loads are, in a seismic design situation, reduced with a factor of $\Psi_{2i} = 0.3$ (EN 1990/Table A.1.1).

Based on the unit weight of the masonry and plaster a load 9 kN/ml is considered only over the perimeter beams. The self-weight of the vertical and horizontal elements (columns and beams) are automatically generated in program ETABS [2].

For the design of the building the design response spectrum is used (i.e. elastic response spectrum reduced by the behavior factor q).

The reference peak ground acceleration amounts to $a_{gR} = 0.25g$. The values of the periods (T_B, T_C, T_D) and of the soil factor (S), which describe the shape of the elastic response spectrum, amount to $T_B = 0.15s, T_C = 0.5 s, T_D = 2.0 s$ and $S = 1.2$ (EN 1998-1/Table 3.2). The building is classified as importance class II (EN 1998-1/Table 4.3) and the corresponding importance factor amounts to $\gamma_I = 1.0$ (EN 1998-1/4.2.5(5)P). Therefore the peak ground acceleration is equal to the reference peak ground acceleration $a_g = \gamma_I^* a_{gR} = 0.25g$. Using the equation in EN 1998-1/3.2.2.2 the elastic response spectrum was defined for 5% damping.

The floor masses and mass moments of inertia are determined according to EN 1998-1/3.4.2. Complete masses resulting from the permanent load (self-weight of the structure + 3 kN/m²) are considered, whereas the masses from the variable-live load are reduced using the factor $\Psi_{Ej} = \phi \cdot \Psi_{2j}$. Factor Ψ_{2j} amounts to 0.3 in the case of an office building (EN 1990/Table A.1.1).

4 STRUCTURAL MODEL

A three-dimensional structural model is used. The basic characteristics of the model are as follows: All elements are modeled as line elements. Rigid offset for the interconnecting beams and columns elements are taken into account. All elements are fully fixed in foundation. Frames and walls are connected together by means of rigid diaphragms (in horizontal plane) at each floor level. The elastic flexural and shear stiffness properties are taken to be equal to the uncracked elements. Infills are considered in the model on the specified cases.

On the cases where the infill walls with hollow bricks is taken into consideration the equivalent struts concept is used [3]. A different width is suggested on the literature for the equivalent struts. We have considered $0.25d$ (d - length of the struts) and modulus of elasticity $E_{cm} = 1.6GPa$ and Poisson coefficient $\nu = 0.15$. Here below on figure 5 is presented the 3d model constructed and analysed with ETABS program.

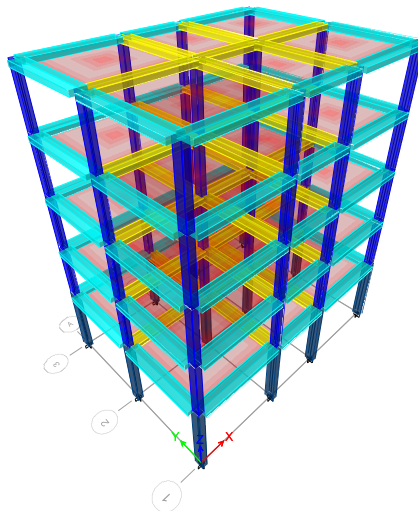


Figure 5 Mathematical models 3d. R/C frame with embedded beams in to the slabs.

5 DETERMINATION OF BEHAVIOR FACTOR

The mathematical model is needed in case of wall systems, for the determination of the structural type of the building. In our case the constructed model have a shear resistance over 65% of the total [4]. So the wall system is defined.

The behavior factor q for each horizontal direction is calculated by equation (EN 1998-1/5.1)

$$q = q_0 \times k_w \quad (1)$$

where q_0 is the basic value of the behavior factor and k_w is the factor associated with the prevailing failure mode in structural system with walls. In case of frame systeme acording we have: $q = 1 \times q_0$ were $q_0 = 3 \times \alpha_U / \alpha_1 = 3 \times 1.3 = 3.9$ so: $q = 1 \times 3.9 = 3.9$.

In case of uncoupled wall system in each of the two horizontal directions and will be designed as a DCM (Ductility Class Medium) structure.

6 MODAL RESPONS SPECTRUM, PERIODS AND NUMBER OF MODS FOR EFFECTIVE MASSES

The first nine modes have been sufficient to satisfy the requirements in EN 1998-1/4.3.3.3(3) (the sum of the effective modal masses amounts to at least 90% of the total mass). For each studiet case we have used the short definitions as below:

FSC- for Frame system clasical (normal beams). FSCW- for Frame system clasical (normal beams) but considering infill walls over ground floor. FSCTW- for Frame system clasical (normal beams) but considering infill walls Total stories. FSE- for Frame system clasical (embedet beams on the slab). FSEW- for Frame system clasical (embedet beams on the slab) but considering infill walls over ground floor. FSETW- for Frame system clasical (embedet beams on the slab) but considering infill walls Total stories. UWS- for uncapped wall system clasical (embedet beams on the slab). UWSW- for uncapped wall system clasical (embedet beams on the slab) but considering infill walls over ground floor. UWSTW- for uncapped wall system clasical (embedet beams on the slab) but considering infill walls Total stories. On the Figure 6 are presentet the modes of vibrations.

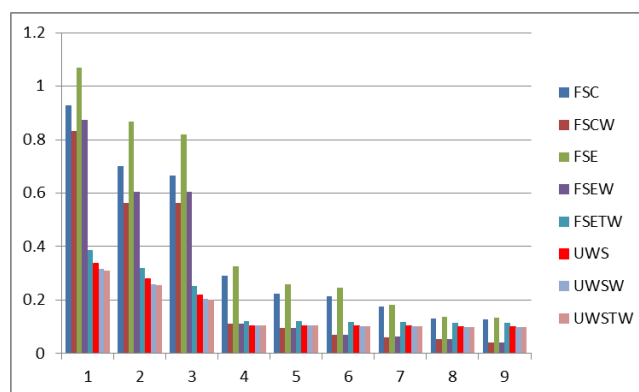


Figure 6 Modal periods for the models with 3 stories

From the above Figure we can conclude that the structure with the reinforced concrete frame that has the beams embeded nto the slab is very flexible. Even the structur with the normal frame is flexible to. This conclusion can be easily drawing if we refer to the easy conservative expresion for modal periods determination as: $T = 0.1 \times N$, were N is the floor number. In case the infills are considered over the ground floor, normaly the periods will be rediused but still they

are far from the normal values. Only when the infill walls are considered on the total building elevation the values of the periods came closer to the normals. The uncapped wall system also present normal value of the periods for all the cases studied.

Here on the Figure 7 below are presented the periods for the models with 5 floors.

The same comment are valid as above for the models with 3 floors.

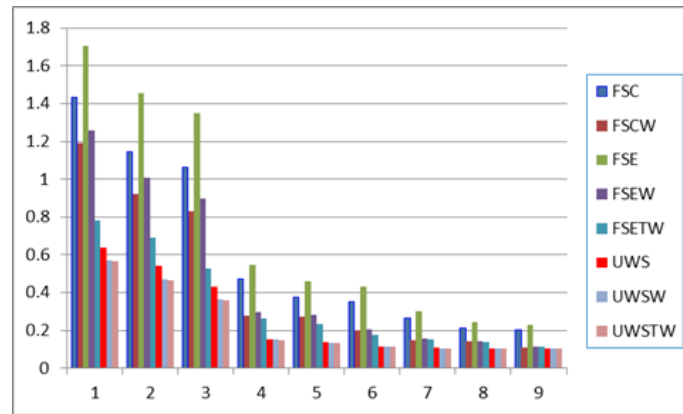


Figure 7 Modal periods for the models with 5 stories

7 DAMAGE LIMITATIONS REQUIREMENTS

The damage limitation requirement should be verified in terms of the interstorey drift (d_r) (EN 1998-1/4.4.3.2) using equation

$$d_r \cdot v \leq \alpha \cdot h \quad (2)$$

Story drift d_r is evaluated as the difference of the average lateral displacements d_s in CM at the top and bottom of the story. The analyzed building is classified as importance class II and the corresponding reduction factor v amounts to 0.5 (EN 1998-1/4.4.3.2(2)). α is factor which takes into account the type of the non-structural elements and their arrangements into the structure. It amounts to 0.005, 0.0075 and 0.01 (EN 1998-1, equations 4.31, 4.32 and 4.33). For a clear presentation are presented with line the three values of α . It can be seen that the most severe drift limit ($\alpha = 0.005$, for building having non-structural elements of brittle materials attached to the structure) is exceeded. The deformation of structural members is connected also to all the elements nonstructural, equipments etc as they are may be connected together. For this reasons this limitations are important to the importance not only on the financial loss but also to the loss of services of important equipment etc.

First we have presented the comparison between the three type of structures FSC, FSE and UWS. Due to the similarity of results and the limited page number of the articles we are presenting here the results only for the X- direction.

Easily from the Figure 8 we can see that the damage limitation requirement according Eurocode is much difficult to be accommodated from the case of the structure FSE. If for the first floor the infills have to be on the ductile nature for FSC and FSE structures for the first floor only the FSE structure have this requirement. The other type UWS show a good performance due to the stiffness presented by r/c walls.

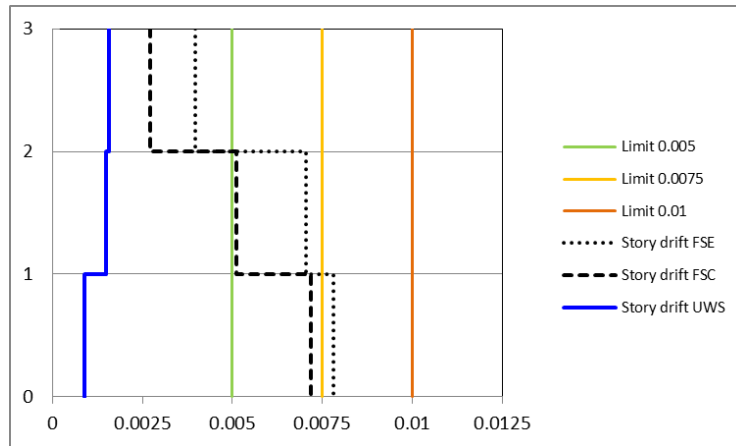


Figure 8 Comparisons of the models FSE, FSC and UWS

Below are presented on Figure 9 the cases where is taken into consideration the infill walls with hollow bricks (without in ground floor). The structures FSCW are FSEW are presenting that the requirement of damages on the ground floor does not correspond to the normal construction practice in Albania (building having non-structural elements of brittle materials attached to the structure) [5]. In fact this case brings attention to the phenomenon of soft story created by the absence of the infills in ground floors. The other case of structure UWSW is presenting much consistent value of damages limitations. The financial loss due to the deformations of the structures UWSW under a frequent earthquake will be not important. Even the structures are of low height we see that the requirement of damages limit state are difficult to accommodate. For buildings that frame structures with embedded beams onto the slab the second criterion of design has much sensitivity than the normal frames.

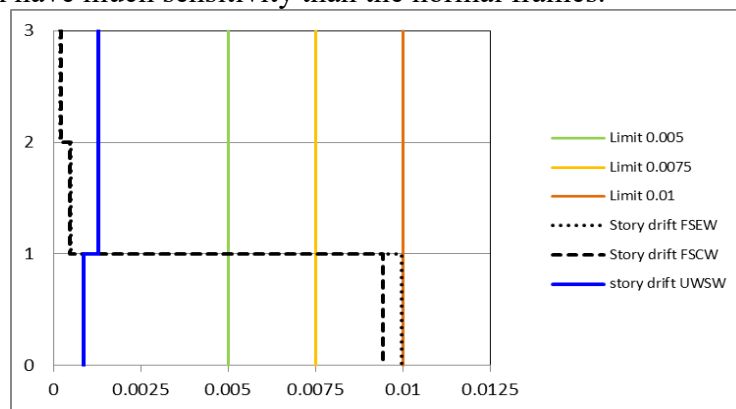


Figure 9 Comparisons of the models FSEW, FSCW and UWSW

For the models where are included in all the floors the infills the interstory drifts are similar. On the literature in fact is mentioned that due to the nature of the masonry infills (heterogeneity of element) this conclusion has to be carefully stated. Experiments have shown that the factors that influence on the total frame and infills reactions are many and this is still a subject that engineers are working on.

Below on the Figure 10 and Figure 11 are presented the results for the models that have 5 floors. The same comments as for the model with 3 floors are valid.

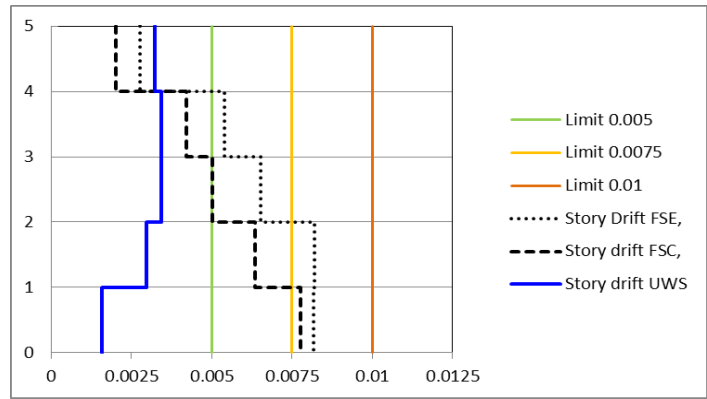


Figure 10 Comparisons of the models FSE, FSC and UWS

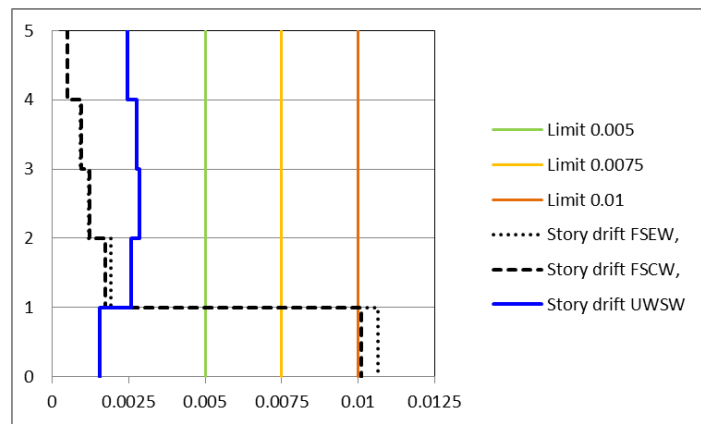


Figure 11 Comparisons of the models FSEW, FSCW and UWSW

8 SECOND ORDER EFFECTS CRITERION P-Δ

The criterion for taking into account the second order effect is based on the interstorey drift sensitivity coefficient θ , which is defined with equation (EN 1998-1/4.4.2.2(2))

$$\theta = P_{tot} \cdot d_r / V_{tot} \cdot h \quad (3)$$

where d_r is the interstorey drift, h is the story height, V_{tot} is the total seismic story shear obtained by modal response spectrum analysis and P_{tot} is the total gravity load at and above the story considered in the seismic design situation ($G + 0.3Q$). On the following figures we are presenting the results only for the direction x.

In the investigated buildings, the second order effects need to be taken into account, mostly in the ground floors and especially when the building does not have infill walls on the ground floor. The 5 floor building analysis with the Frame with embedded beams in the slab is more sensitive to the P-Δ. For wall system, in all the cases the requirements of the second level design are easily fulfilled. In Figure 12 and Figure 13 below are presented only the results in x direction of the model with 5 floors.

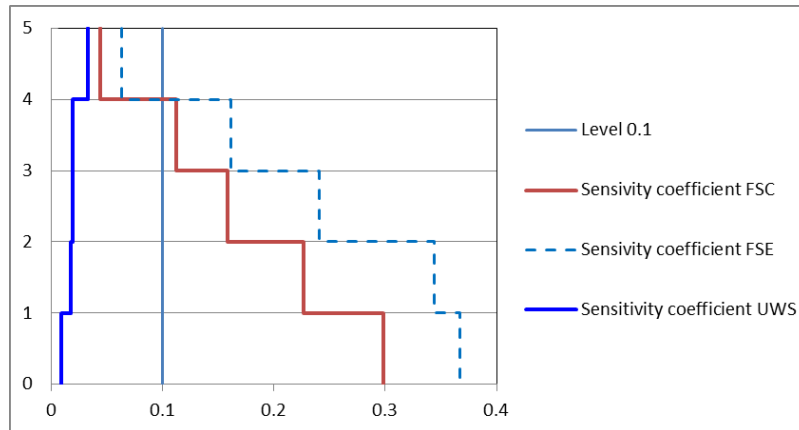


Figure 12 Comparisons of the models FSE, FSC and UWS

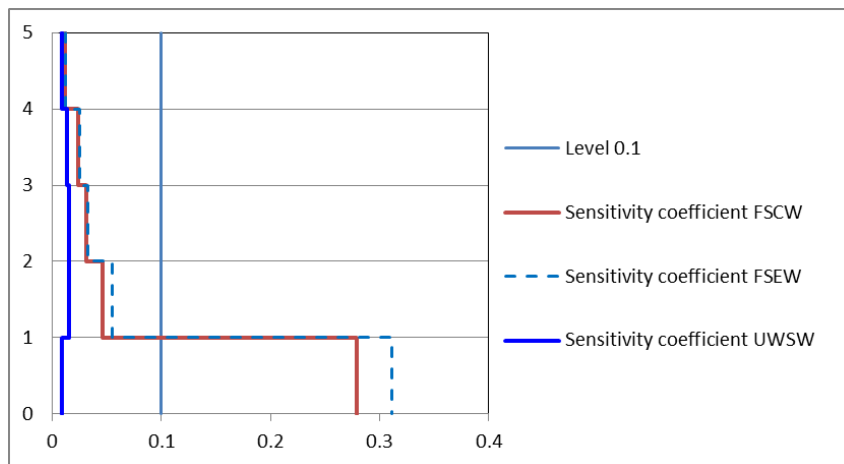


Figure 13 Comparisons of the models FSEW, FSCW and UWSW

For the 5 floor building the sensitivity coefficient has considerable values. The request to increase the shear load design on the vertical elements is bigger for the frame with embedded beams into the slabs.

9 CONCLUSIONS

Based on the linear structural analysis of reinforced concrete frames with two different heights of models, 3 and 5 floors, we conclude:

Frame structures made of reinforced concrete with embedded beam have a higher flexibility than those with the classical frame with the normal beams. The UWS present consistent values for the modal periods on all studied cases.

Interstory drifts of the frame with embedded beams are the highest of the models studied. These facts bring attention to the fulfilment of the damages limitation requirement according eurocodes. The same situation applies with respect to control of the secondary $P-\Delta$ effect. The frame with embedded beams need a higher coefficient to apply for increasing the forces received from the linear analysis.

By consideration of the infills walls, it shows that they have the ability to substantially modify the structure response.

Based on this analysis and on other studies made about this topic, as well as technology implementation and experience in our country (Albania) we suggest that the terminology used

for infill walls with hollow blocks “non-structural elements” is not appropriate [6]. It create confusion in construction practice with the idea that modifications of infills can be easily made. Such modifications may be catastrophic in case of frame with beams embedded into the slabs due to the sensitivity that this typologies present.

Beside the life safety is the damage limitation requirement. For the same life safety fulfilment of different structure typologies different damage limitation capabilities (of course all they should accommodate the minimums required by codes) may be accommodates. For investors is important to know how their investment is exposed to the negative effects of the frequent earthquakes.

REFERENCES

- [1] “Reinforced Concrete Frames and Wall Buildings” by H.Sezen et al. Structural Engineering Reconnaissance of the Kocaeli (Izmit) Turkey Earthquake of August 17 1999. Berkeley: Pacific Earthquake Engineering Research Center, (PEER Report 2000-09), December 2000
- [2] “ ETABS (2013)”, Nonlinear version 13, Extended 3-D analysis of building systems Computers and Structures, Inc.Berkeley, U.S.A
- [3] “ Conceptual Seismic Design Guidance for New Framed Infill Buildings” Shabnam J. Semnani, Stanford University; Janise E. Rodgers, GeoHazards International; Henry V. Burton, Stanford University
- [4] “ Eurocode-8(2004): Design of structures for earthquake resistance” The European Committee for standardization, Final Draft, December 2004
- [5] “ Inxhinieria sizmike “ /Niko Pojani Botime Toena 2003. ISBN 99927-1-747-5
- [6] Seranaj A., Kokona E., Balilaj M.,” REAGIMI I RAMAVE FLEKSIBILE PREJ BETONI TË ARMUAR NËN VEPRIMIN E FORCAVE SIZMIKE “ / Buletini i shkencave teknike, Universiteti Politeknik i Tiranës. Albania

Analysis of Reinforced Concrete Spatial Structures with Different Structural Openings and Forms

Agim Seranaj¹, Erald Elezi², Altin Seranaj²

¹Department of Structural Mechanics, Civil Engineering Faculty, Polytechnic University of Tirana, Albania

²Department of Building Constructions and Transport Infrastructure, Polytechnic University of Tirana, Albania

ABSTRACT

The first reinforced concrete spatial structures date from 1920. Since then, their popularity has increased as a new structural system with widely used materials like reinforced concrete. The building trend of these structures faded near 1970s, because of the high costs in formwork and labor work compared to other structural systems, but also the high calculations difficulty and the lack of knowledge for their structural behavior strongly connected with their form.

The technological evolution of formworks, like air inflated forms or polymer modular formwork, as well as the technological advance of computer and software industry for civil engineering through automation of numerical methods and creation of new algorithms, have helped to reach new levels of expertise during the conceptual and structural design process.

The scope of this analytical study is the use of structural openings to create new lighter, sustainable and architectural forms of structures, using a new approach to the form finding process. The paper includes structure cyclic analysis due to finding the appropriate position and geometrical form of the openings considering stresses, deformations and boundary conditions of specific cases. Optimizations and analysis are made using advanced optimization algorithms of form finding and topological optimization (ATOM – Abaqus Topology Optimization Module ®) and FEM based software for static and seismic analysis.

Based on the analysis data of the case examples for the new designing approach to structural openings and forms, presented on this paper with the use of advanced software technology, we conclude that spatial structural system in 21st century should be considered as the next engineering challenge in conjunction to architectural trends for free, irregular and diverse forms.

Keywords: *Spatial structures, optimization, FEM, static, seismic*

INTRODUCTION

Spatial structures are a type of structural system which cover large areas only with edge supports (column free). This structural system is highly connected with statically stable forms with different thickness mostly found on nature (egg shell, turtle shell etc.)

Due to high labor costs and difficulties in design of these structures they lost their popularity around 1970s. The use of other structural systems which were not as architecturally attractive as shell structures but easier to design and build replaced for a long time this type of structure. Shells stresses and strains are highly connected with their form. With small changes in form a new field of stresses can be obtained.

Due to this relation with form shells are very vulnerable to build errors, material strength and specialization of workers. Other difficulties in designing shells is finding the right ratio between thickness and span. Many authors made recommendations about this ratio but as they are connected to form a proper formula for this ratio cannot be obtained. Logically the larger the span is we expect thicker shells but on the other hand thicker shells mean heavier ones and more vertical forces to this structures can create tensile stresses and large compression ones, one the other hand thin shells can send to element failure due to cracks and material failure.

To obtain small stresses we should design and analyze the proper form. These structures are very attractive to architects due column free forms, different shapes and large spans that they cover. From shells popularity era to nowadays are made a lot of engineering advances in mathematics, material engineering, construction engineering, computer eng. etc. Concrete shells, due to the combination of filling and load carrying capacities are being designed and calculated as 'thin shells', with a radius-to-thickness ratio starting at 200 - 800 or higher. The low consumption of material follows from the fact that concrete shells are very effective in carrying loads that are perpendicular to their surface creating in plane membrane stresses. Concrete shells include single and double curved surfaces which are either synclastic, monoclastic or anticlastic

From the above introduction a primary research questions can be formulated:

Can these structures gain back their popularity with the use of advanced software and computational methods in form finding obtaining new shell forms due to given optimization conditions and boundary conditions, to make the design process easier without losing the architectural approach?

The asked research question is evaluated by using optimization methods (shape and topology) in a simple shell as groin vault, by creating an open path to evaluate and optimize more complicated forms and different spans.

Historic approach

Shell structures have an ancient history. Starting from the Pantheon in Rome and Haiga Sophia in Istanbul these structures made a difference in history of architecture and engineering. For a long time shells were made with bricks or other materials depending on the advances in materials. Reinforced concrete thin shells can be defined as slabs with curvature whose cross dimension (thickness) is very small compared to span dimension or other dimensions as radius and curvature. Concrete shells are a slow evolution form masonry arches and does, which were used from the early days of human construction evolution. The popularity of concrete shells was risen after the WWII. Using concrete made this structures popular because concrete can be cast in any forms. The advantage of concrete shells is that as steel can be used as structural system, but it has the body to cover the space, so it acts like a structural roof.

With the newly developed reinforced concrete in 20th century engineers had new possibilities of creating long span shell forms. Franz Dischinger and Ulrich Finsterwalder designed in 1925 one of the first concrete shell in modern era, the Zeiss planetarium in Germany followed by other engineers as Pier Luigi Nervi, Eduardo Torroja, Anton Tedesko, Nicolas Esquillan, Felix Candela and Heinz Isler who created the most famous shells during 1950s - 1970s. These engineers developed new forms of concrete structures by using and developing known formulas about equilibrium but also by using experimental small scale forms with the use of cement to check the structural reaction of shells due to vertical loading. The surface can be generated by mathematical functions or by form-finding methods such as hanging membranes or pneumatic models. By using hanged models the approach is to create tension free structures, as the hanged model stays and gets a form within the fixed edges (the supports) if we reverse it we will get a total compression form.



Figure 1. Zeiss Planetarium



Figure 2. Hanged membrane model

Numerical and analytical theories of shell study

In the early times there was a difficulty in calculating the internal forces in a cross section for a shell structure. Because of their shape the use of classical formulas was nearly impossible in complicated forms of shells. Mostly the classical theories and solutions depend on General Theory of Elasticity [1] and equilibrium of forces. This theories made a revolution in calculation of plates and shells but they were not enough to solve complicated forms. Mostly this theories are used in simple created shells by regular forms or created by surface of revolution or extrusion (sphere, cylinder, conus etc.).

With the creation of numerical methods for element analysis things changed for shells also. Now with the use of automated numerical methods in advanced computers with faster processing units study of shell stresses, strains, and element forces is made easier. By using FEM (Finite Element Method) based software we can make cyclic analyses of the structure to check it's structural behavior or make sensitivity analyses by changing one of the components (thickness, span, curvature) in it and finding the differences in results.

Optimization Process and Methods

The geometry forms a structural effective shell if the shell is able to develop a prevalent membrane stress field by avoiding bending moments. Optimization techniques, such as shape optimization by minimizing strain energy, may create new structural forms which are more appropriate to structural approach due to stresses and strains. Optimization may be enhanced by advanced computation optimization algorithms such as dynamic relaxation etc. In general the design will lead to a shell with an opening angle between 60 and 90 degrees. The shell thickness is practically bounded by 60 to 80 mm for one- or two-layers of traditional steel reinforcing steel bars. The reinforcement percentages are rather low, approximately 0.15 to 0.4%.

Structural optimization can be defined as a process to create a better structural solution for problems created during the design. The scope is that considering an optimization objective, to create a new optimized structure more efficient than the first one in terms of internal forces, strain energy, volume etc. It is a very simple principle but that includes a lot of various knowledge in many disciplines as structural analysis, design modelling, sensitivity analysis, mathematical and algorithmic programming strongly connected to civil engineering principles. The first steps of structural optimization were taken by *A.G. Michell* who tried to create the most

efficient structure to carry a point load with least possible weight. Michell tried to find the best trajectory for stress distribution among element.

A clear example is how a tree can be seen as a structural system, where the branches have the right angle and thickness and the trunk is thicker near the ground to stand wind forces. Other examples can be found in other shells like turtle shell that can withstand huge forces and create constant distribution of surface stresses, and other organisms that evolved in a form to withstand external forces or threads. The principle of constant distribution of surface stresses (as seen in soap bubbles) can be used itself in optimization of shell structures. Different optimization objectives can send to different shapes and results, so it's very important to choose the right boundary conditions, optimization objectives and constrains. With the use of advanced optimization algorithms we can apply a multi objective optimization, multi single term objectives or single combined ones.

As mentioned shells are a very shape sensitive structures thus with little differences in shape a different structural behavior can be obtained, Sometimes optimization for shells can be very difficult if we optimize by multi-criteria or if we take in count the nonlinear effects on concrete or buckling, dynamic, seismic forces. This process can be easy if we take in count only vertical forces and self-weight of the structure. The optimization of shells can be very sensitive to parameters as shells itself are optimized by form so the risk of not getting correct results over optimization algorithms is very high. Optimization can be categorized in function of the optimization objective and parameters. A categorization includes: shape optimization, topology optimization (structural openings), material optimization, size optimization etc.

In this paper it is used shape and topology optimization. Shape optimization begins with a finite element model which is imported and meshed inside the software, minimizes stress concentrations in the selected areas to redefine the mesh, using the results of a stress analysis to modify the surface geometry of a component until the required stress level is reached. Shape optimization then attempts to reposition the surface nodes of a selected region until the stress across the region is constant.

Cyclic analysis that the software offers (Abaqus ®) makes possible to check every cycle of the optimization process so you can check the advance of the stresses and shape. It is very important to set the correct parameters to optimization because as mentioned before may lead to very different results. Shape optimization is used in double groin vault to find the best shape with different optimization objectives, firstly to minimize surface stresses and secondly to minimize the density of strain energy. Possible shape optimization constraints can be connected with stresses, strain, strain energy density. On the other hand topology optimization means removing finite elements by lowering their relative density and by recalculating the stresses every removal cycle. Topology optimization begins with an initial design, which is assumed to be the maximum physical extent of the component, and determines a new material distribution by changing the density and the stiffness of the elements in the initial design while continuing to satisfy the optimization constraints. General topology optimization uses an algorithm that adjusts the density and stiffness of the design variables while trying to satisfy the objective function and the constraints. The general algorithm is partly described in Bendse and Sigmund (2003). In contrast, condition-based topology optimization uses a more efficient algorithm that uses the strain energy and the stresses at the nodes as input data and does not need to calculate the local stiffness of the design variables. The condition-based algorithm was developed at the University of Karlsruhe, Germany and is described in Bakhtiary (1996) [2]

Also in both types of optimizations used in this paper, geometric constrains are applied to maintain the main architectural form. This is possible in the optimization-FEM software used by using an advanced algorithm to optimize with multiple parameters and constrains.

Both optimization processes pass through the same cycle but with different approach to optimization techniques. Firstly the optimization parameters are set, than the number of cycles

to archive this optimization objective. Constrains or stop conditions may be added and in every cycle of the optimization step it is checked if the constrain is violated or stop condition is reached, if yes the optimization process stops, if no it continues to the next interaction.

Shape optimization

In our paper the initial model is groined vault (also sometimes known as a double barrel vault or cross vault). The example is made using two barrels each with 30m of diameter by creating the classical form of the shell (as seen in the image below) with a height of 10 m. The first optimization process was made for shape optimization using the objective of minimization of main principal stresses. Studying the stresses of this model is easy noticeable the effect of groin (the contact between two barrels). In this part of the structure we can notice an increase of the main principal stresses (as can be checked by the colors after static structural analysis).

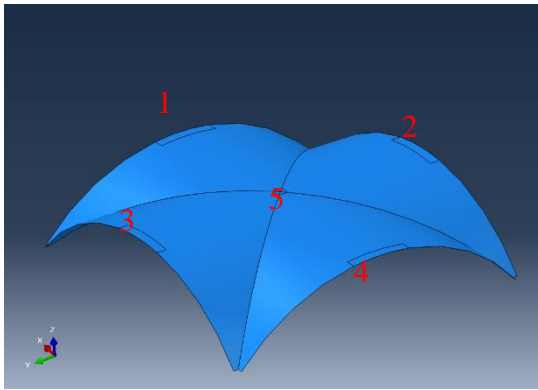


Figure 3. Initial geometry

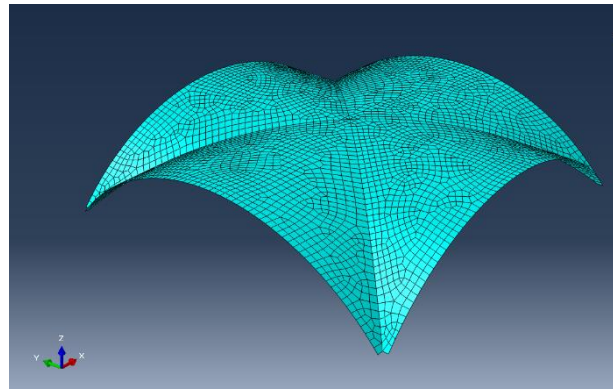


Figure 4. Dense mesh of FE

The models are calculated with dense mesh (*ref. Fig 4*) to get more reliable optimization results. Shape optimization is very connected to mesh density because it is related to node moving to get the best shape.

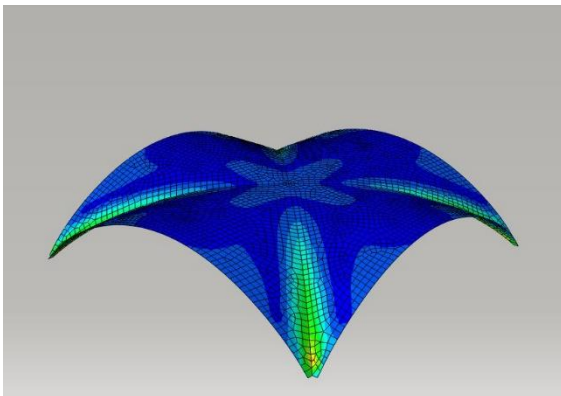


Figure 5. Principal stresses for initial geometry

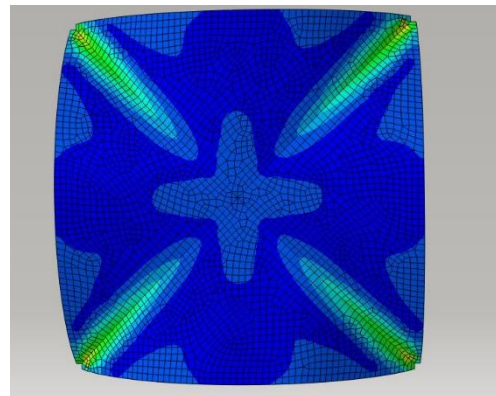


Figure 6. Principal stresses (top view)

Optimization parameters:

Type : Shape Optimization, Design Response : Principal stresses

Design Objective : Minimization of Design Response parameters (stresses)

Geometric Restrictions : Design direction only +/- z (x and y fixed), global coordinates, for areas marked with red numbers (*ref. Fig 3*) to maintain the area covered and not to get a result radically different from the initial architectural shape.

Optimization process is made using a condition based shape algorithm with 30 cycles of optimization by single design parameter with geometrical restriction.

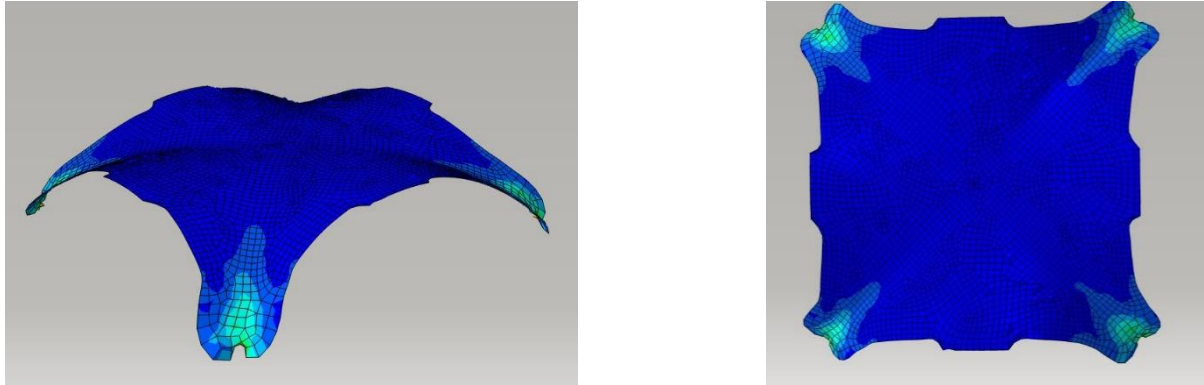


Figure 7. Theoretical shape Optimization results (3D view and Top view)

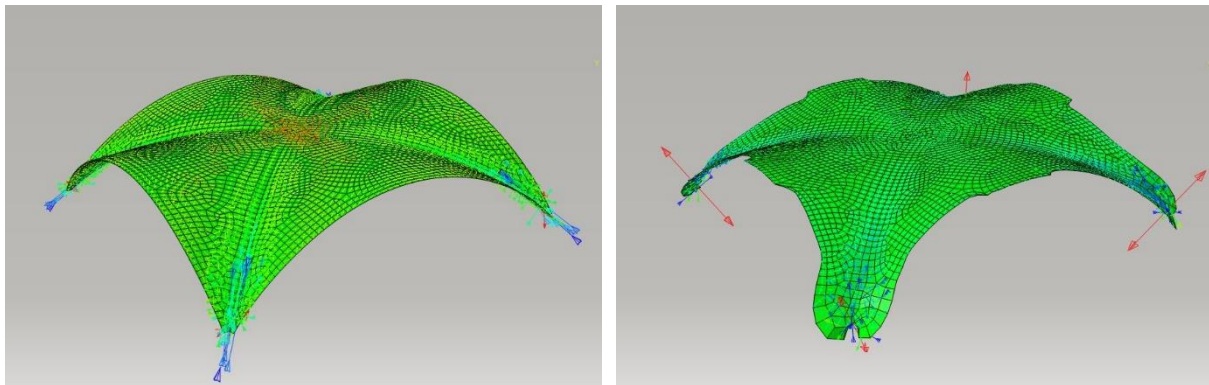


Figure 8. Differences (initial-after opt.) in Smax and Smin (in plane) and Smax (out of plane)

As can be seen by the shape opt. result by using the mesh smoothing by algorithm the increased stresses in the zone of the groin between barrels are minimized as described in the optimization objective, also the fixed regions show clearly the similarity between the optimized shape and the initial one (*ref. Fig 7*). Two main changes can be seen. One – going from a thick edge groin to a smoother one, and two – creating wider zones of elements near the support zones to equally distribute the stresses in this area. Differences in shape (by using nodal displacement) are seen near the top of the structure where can easily be seen how shape opt. algorithm eliminates higher stress zones. On the negative side we have higher out of plane stresses near the support zones, this connected also with the fixed single node for boundary conditions (*ref. Fig 8*). The above mentioned results are reflected in the Table 1 of one side groin edge nodes and graphical explanation.

Table 1 Nodal coordinates for the edge of two groins (contact line)

Node	Original coordinates (global)			After Optimization			Differences		
	x	y	z	x	y	z	dx	dy	dz
215	30530.60	4064.52	1235.09	30556.50	3969.91	1236.02	25.90	-94.61	0.93
216	30500.00	4095.21	1269.18	30514.70	3985.19	1271.04	14.70	-110.02	1.86
217	30468.70	4126.43	1302.28	30495.40	4037.46	1306.44	26.70	-88.97	4.16
218	30437.00	4158.17	1334.40	30463.90	4085.56	1347.16	26.90	-72.61	12.76
219	30404.80	4190.39	1365.55	30432.00	4132.34	1384.22	27.20	-58.05	18.67
220	30372.10	4223.06	1395.72	30400.10	4179.69	1417.04	28.00	-43.37	21.32
221	30339.00	4256.17	1424.93	30357.80	4219.32	1448.12	18.80	-36.85	23.19
222	30305.50	4289.69	1453.19	30313.50	4257.54	1477.43	8.00	-32.15	24.24
223	30271.60	4323.60	1480.51	30266.30	4291.92	1507.11	-5.30	-31.68	26.60
224	30237.30	4357.88	1506.89	30224.10	4333.52	1533.55	-13.20	-24.36	26.66
225	30202.70	4392.50	1532.35	30184.10	4372.76	1558.42	-18.60	-19.74	26.07
226	30167.70	4427.46	1556.89	30145.20	4408.67	1582.54	-22.50	-18.79	25.65
227	30132.40	4462.73	1580.52	30107.90	4443.72	1605.47	-24.50	-19.01	24.95
228	30096.90	4498.29	1603.24	30073.20	4478.76	1626.66	-23.70	-19.53	23.42
229	30061.00	4534.13	1625.08	30038.40	4512.53	1647.83	-22.60	-21.60	22.75
230	30024.90	4570.23	1646.03	30001.30	4545.10	1669.41	-23.60	-25.13	23.38
231	29988.60	4606.59	1666.10	29962.40	4578.32	1690.74	-26.20	-28.27	24.64
232	29952.00	4643.17	1685.31	29925.10	4615.24	1710.03	-26.90	-27.93	24.72
233	29915.20	4679.98	1703.65	29888.90	4654.49	1728.13	-26.30	-25.49	24.48
234	29878.20	4716.99	1721.13	29851.70	4694.31	1745.20	-26.50	-22.68	24.07
235	29841.00	4754.20	1737.77	29812.70	4733.63	1761.18	-28.30	-20.57	23.41
236	29803.60	4791.60	1753.56	29772.60	4772.06	1775.98	-31.00	-19.54	22.42
237	29766.00	4829.16	1768.52	29732.30	4810.38	1789.71	-33.70	-18.78	21.19
238	29728.30	4866.89	1782.65	29692.50	4848.75	1802.31	-35.80	-18.14	19.66
239	29690.40	4904.76	1795.95	29653.00	4887.00	1813.96	-37.40	-17.76	18.01
240	29652.40	4942.77	1808.44	29614.00	4924.85	1824.77	-38.40	-17.92	16.33
241	29614.30	4980.92	1820.11	29575.60	4962.41	1834.83	-38.70	-18.51	14.72
242	29576.00	5019.18	1830.97	29537.80	5000.06	1844.28	-38.20	-19.12	13.31
243	29537.60	5057.55	1841.02	29500.70	5038.33	1853.11	-36.90	-19.22	12.09
244	29499.10	5096.02	1850.27	29463.30	5077.46	1861.38	-35.80	-18.56	11.11
245	29460.60	5134.59	1858.73	29424.60	5117.20	1869.00	-36.00	-17.39	10.27
246	29421.90	5173.24	1866.39	29383.90	5156.90	1875.82	-38.00	-16.34	9.43
247	29383.20	5211.96	1873.26	29342.20	5194.95	1881.39	-41.00	-17.01	8.13
248	29344.40	5250.75	1879.34	29304.80	5235.03	1885.79	-39.60	-15.72	6.45
249	29305.60	5289.59	1884.63	29275.50	5277.50	1888.84	-30.10	-12.09	4.21

The tabulated data are for the points 1 and 1', while the data are taken for points near groin edge 2 and 3, and on the other hand as it is noticed in 1 and 1' that the differences between z coordinate is positive (the edge is risen), also for 2 and 3 the difference in z coordinate is positive, equal, but less than 1' and 1. The position of these points are shown schematically in Figure 9.

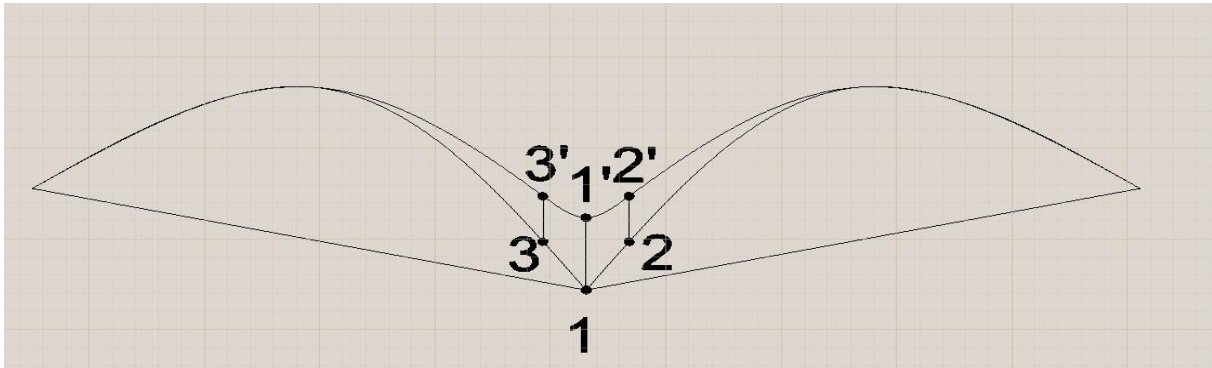


Figure 9. Graphical illustration of node movement after optimization

Topology optimization for different load cases

In this paper is discussed finding the best position for structural openings regarding a given objective also called as topology optimization. Using topology optimization on shells is difficult for their sensitivity on forms and forces direction. Topology optimization (by relative density algorithm) is mostly used in solid objects but using it in shell structures has given good results.

The first topology optimization is made as follows- Optimization parameters:

Type : Topology Optimization, *Design Response* : Strain energy

Design Objective : Minimization of Design Response parameters (strain energy)

Geometric Restrictions : Final optimization form must have 70 % of the initial form volume.

Optimization process is made using a condition based shape algorithm with 30 cycles of optimization by single design parameter with geometrical restriction.

Case 1: Gravity and service loading (distributed)

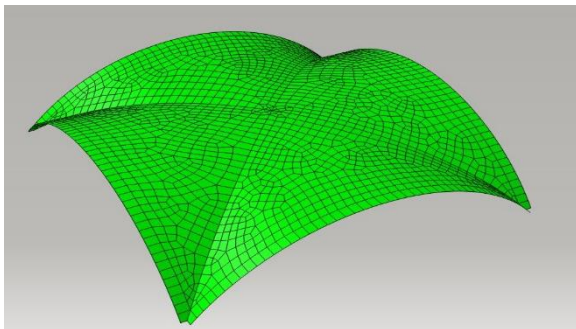


Figure 10. Initial geometry

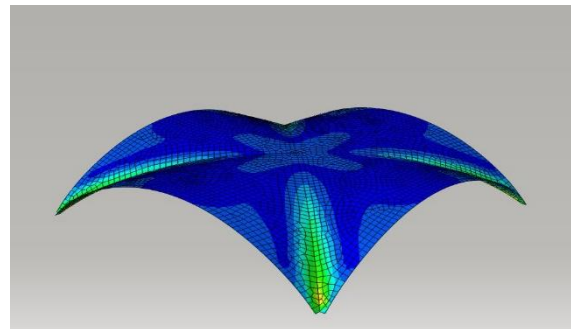


Figure 11. Stresses of initial geometry

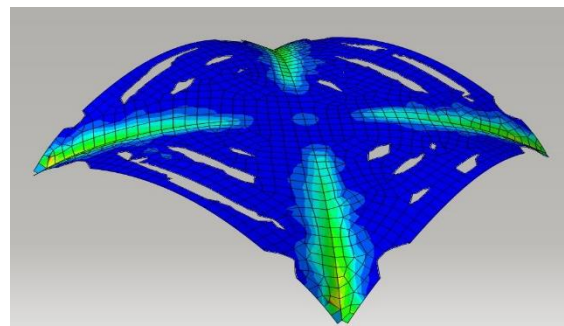
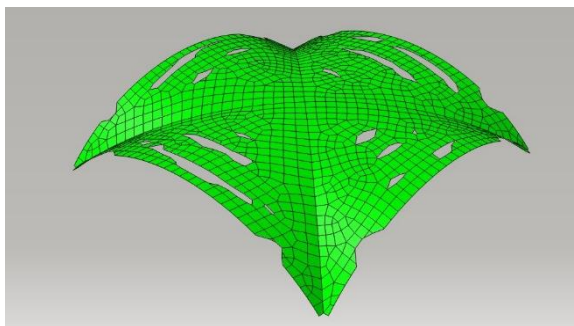


Figure 12. Final theoretical topology geometry

Figure 13. Stresses of final geometry

So it is clearly noticeable that the topology optimization creates structural openings near the less stressed areas. The new structure is 30 % lighter than the first one in terms of weigh but additional material like glass (thinner and lighter) may or should be added in the structural openings so the shell would now loose its purpose as roof (*ref. Fig 12 & 13*).

So we can conclude that the position of the structural opening can be set by using advanced algorithms of topology optimization and for the case studied under gravity loading the structural openings should start in the direction and form of the given areas in the above shown pictures. Of course we expect that for different types of loadings to have different results strongly connected with the sensitivity of shells due to form and vertical loading.

The second topology optimization is made as follows- Optimization parameters:

Type : Topology Optimization, *Design Response* : Strain energy

Design Objective : Minimization of Design Response parameters (strain energy)

Geometric Restrictions : Final optimization form must have 60 % of the initial form volume.

Optimization process is made using a condition based shape algorithm with 30 cycles of optimization by single design parameter with geometrical restriction.

Case 1: Gravity and concentrated force in the center (2000 kN) (*ref. Fig 14&15*)

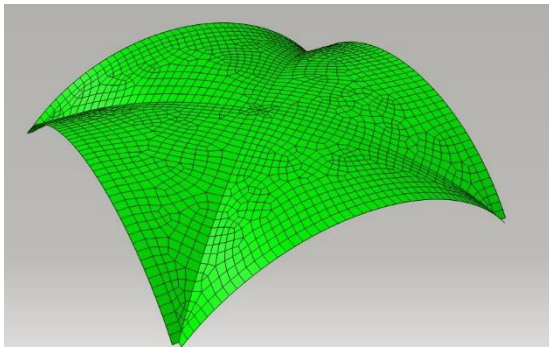


Figure 14. Initial geometry

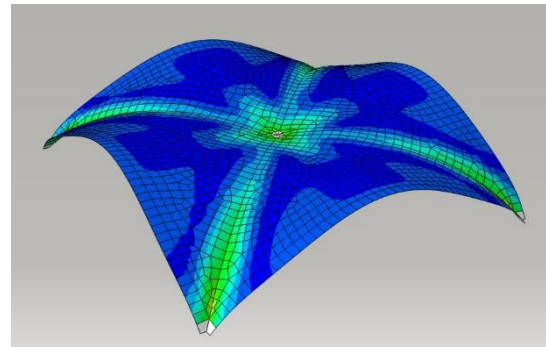


Figure 15. Stresses of initial geometry

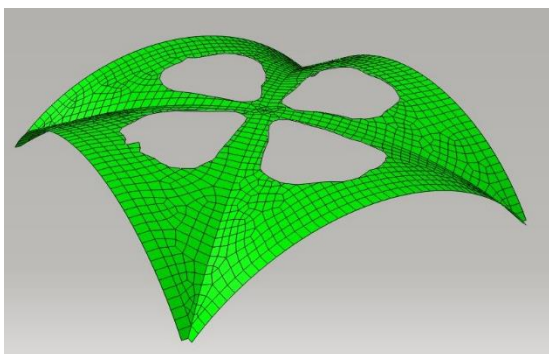


Figure 16. Final theoretical geometry 2

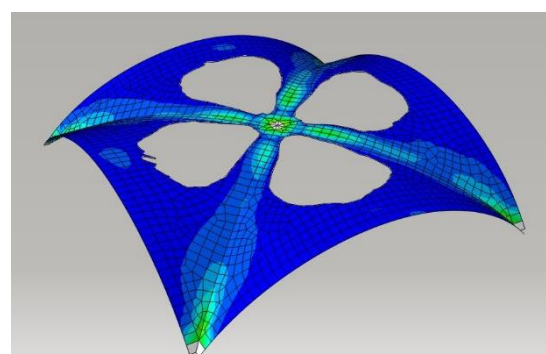


Figure 17. Stresses of theoretical geometry 2

As can be seen from the results the position and size of the openings change from case to case. If we concentrate in the stress field of the initial geometry we can approve that the relative density algorithm used has started removing elements in the shape and position of blue areas (less stressed) and then by analysing the structure cycle after cycle we reach to the final geometry. As mentioned above our structure is 40 % lighter but to maintain the structural function as roof the structural openings can be covered with lighter materials than concrete (*ref. Fig 16 & 17*). Also in this case we got the position and the form of the openings. It is the initial

step of creating structural opening to create more architectural, lighter and statically stable shell roofs.

CONCLUSIONS

Use of new methods in form finding and shape optimization so this structures can have a better structural behaviour regarding different loading and boundary condition. With small changes in shell form we can reach different fields of stresses.

Use of software automated numerical methods to make sensitivity cyclic analysis due to different parameters as stresses, strain energy, strain energy density etc.

Use of advanced optimization algorithms in shape and topology optimization which are capable of calculating optimization problems with multiple objectives, variables, constrains, stop conditions, or geometric restrictions due to given loads and boundary conditions.

Creation of new algorithms with integrated analytical and numerical methods to be more practical and simpler to use by structural engineers for shell structural system, will help the future applications of these structures.

Finding new shapes and use of structural openings can bring to creation of new lighter forms, structurally stable, covering larger surfaces with shells.

Bringing concrete shells to attention again, because of all the technological advances mentioned above, could be the next engineering challenge.

REFERENCES

- [1] S. Timoshenko, S. Woinowsky Krieger - "Theory of plates and shells", McGraw- Hill Book Company, Classic Textbook Reissue, 1989
- [2] Abaqus ® Analysis User's Guide 13.1.1 – Analysis Types and Optimization
- [3] P.C. Varghese – “Design Reinforced Concrete Shells & Folded Plates”, Phi Learning Pvt. Ltd. 2008
- [4] Christian Meyer & Michael H. Sheer – “Do concrete shells deserve another look” – Concrete International, October 2005
- [5] David P. Billington -“Thin Shell Concrete Structures” – 2nd Edition, McGraw Hill Book Co. New York 1982
- [6] Sigrid Adriaenssens, Philippe Block, Diederik Veenedaal, Chris Williams – “Shell Structures for Architecture, Form Finding and Optimization” , Routledge , Taylor and Francis Group, 2014

The Influence of Base Isolation to the Required Ductility of Soft Storey Buildings

Agim Seranaj¹, Mihail Garevski²

¹Department of Structural Mechanics, Civil Engineering Faculty, Tirana, Albania

²Institute of Earthquake Engineering and Engineering Seismology (IZIIS), Skopje, Macedonia

ABSTRACT

The Response Spectrum Analysis of the structures is based on the allowable ductility considered for that structure. In the case of a multi-degree-of-freedom buildings, the required ductility cannot be the same with the allowable ductility; furthermore, the required ductility values are different for different storey. In the case of first soft/weak storey building, the required ductility of this storey is much higher compared to allowable ductility and impossible to achieve. Nowadays there are many cases of existing reinforced concrete structures with the possibility of soft/weak storey. Even new structures are required to have open space at ground floor level as the owners want them for shops or garages usage.

This paper analyses the influence of base isolation to the required storey ductility of weak storey buildings. A five storey shear frame type structure is considered as the model. The elastic and elasto-plastic modelling of the structural elements and bilinear modelling of rubber isolators are used. Linear Response Spectrum analysis and Nonlinear Time History analysis are performed in order to determine the required storey ductility for the existing and new soft/weak storey buildings using the SAP2000 computer program.

The analysis results show the reduction of the required storey ductility due to the application of base isolation not only in new structures, but in existing structures too. This means that the base isolation technique is a good alternative to be applied in buildings with first soft/weak storey structure.

Keywords: *soft/weak storey, required ductility, base isolation*

INTRODUCTION

The seismic response of the structure can be obtained using response spectrum analysis, RSA or time history analyses, THA [1]. Response spectrum analysis is based on the seismic response spectrum which is considered for different values of the allowable ductility of the structure. For the single-degree-of-freedom systems the required ductility is the same as the allowable one, whereas for multi-degree-of-freedom systems these values are different (bigger or smaller).

Ductility depends on several factors. For building structures with storeys it is important to know the relation of the required ductility and the yield strength and stiffness of the storeys. To analyse this relationship we will use the concept of “weak” storey, which has a smaller yield strength compared to the required one, and also the concept of “soft” storey, which has a smaller stiffness compared to the required one.

Base isolation technique was developed as an attempt to reduce the effects on buildings and their structural elements during seismic events, and is becoming one of the most effective methods for a wide range of problems of structures under the seismic action. [2] [3]. In recent decades, based isolation has become one of the most accepted techniques for seismic protection of buildings [4].

In order to study the influence of seismic isolation to the required ductility of a soft storey building, we will consider a five storey building with the first soft/weak storey to be isolated. These buildings can be existing or new structures, thus we will analyze the application of base isolation in both cases. The elastomeric isolation system is used. Mostly they are characterized by high vertical stiffness and low horizontal stiffness [5] [6]. The analysis performed in linear and nonlinear using elastic and elasto-plastic modelling of the structural elements allow us to determine the required ductility and make the comparison with the allowable ductility for different situations of structure. Linear Response Spectrum analysis and Nonlinear Time History analysis are performed in order to determine the required storey ductility using the SAP2000 computer program [7].

The required ductility of soft first storey of the existing structures can be very high and impossible to achieve. Applying base isolation on these buildings can reduce the required ductility to the desired value [8]. Based on the code, in case of base isolation of new buildings, the structure is designed to behave almost within the elastic range with the allowable ductility $\mu_a=1$. If this new structure tends to be soft/weak first storey, the base isolation is shown to be a good alternative to solve the problem.

ALLOWABLE AND REQUIRED DUCTILITY

Based on the response spectrum analysis, the design yield strength is determined, as a function of the allowable ductility by the following expression:

$$f_y = A_y \cdot m$$

where m is the mass of system and A_y is the pseudo-acceleration obtained from response spectrum of the considered allowable ductility.

From the response spectrum analysis, the yield strength (f_y) and yield deformation (Δ_y) are determined using the response spectrum for the corresponding values of the ductility μ_a .

From the time history analysis, based on the elasto-plastic behaviour diagram, and parameters resulting from the response spectrum analysis (k, f_y, Δ_y), we will determine the maximum deformation Δ_m of the structure. The required ductility is determined by the ratio between the maximum deformation and the yield deformation:

$$\mu_r = \frac{\Delta_m}{\Delta_y}$$

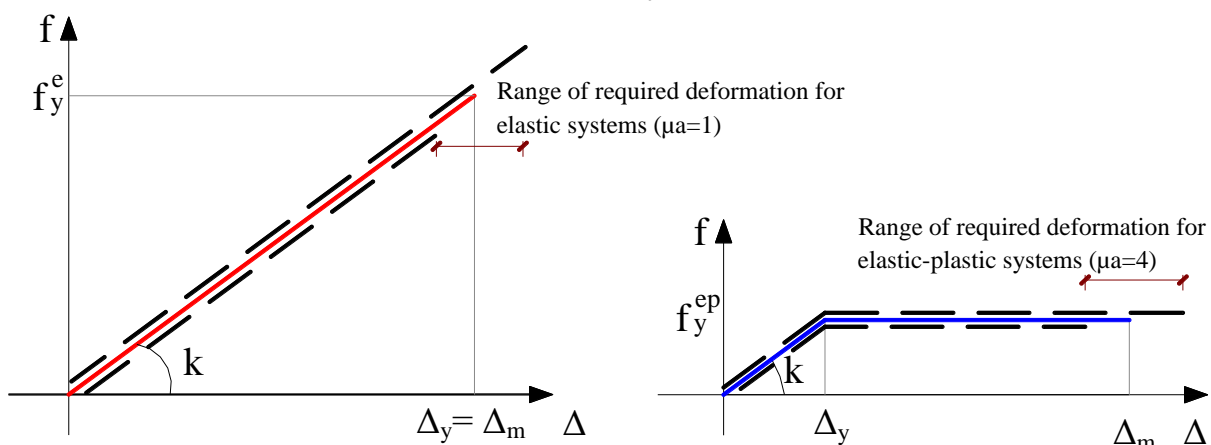


Figure 1: Maximum allowable and required deformation for two systems, $\mu_a=1$ and $\mu_a=4$

Question: Does the required ductility (μ_r) has the same value as the allowable ductility (μ_a)? The response of elasto-plastic elements requires a certain level of the deformations. The required deformation can be bigger or smaller than the structure's deformation capacity [9]. This is schematically shown in Figure 1, for two different cases of the structure; the first with allowable ductility $\mu_a = 1$ and the second with $\mu_a = 4$.

SEISMIC RESPONSE OF MULTI-STOREY BUILDING AND STOREY DUCTILITY

Different models are created to study the seismic response of fixed base or base isolated multi-storey buildings with different storey yield strength and storey stiffness distribution, or with different values of allowable ductility. The TYPE 1 represent the normal structure with uniform storey stiffness. The TYPE 2 represent the soft/weak first storey structure, which is obtained by structure TYPE 1, multiplying the stiffness of storey two to five by 4. TYPE 2a BI and TYPE 2b BI represent the application of base isolation to the structure TYPE 2 in case of new and existing buildings. These models are schematically shown below:

Base situation	Types of structure considered	Analysed cases for each Type
Fixed base structures	TYPE 1 (normal structure) $k_1 \times 1$ and $k_{2-5} \times 1$	$\mu_a = 1$
Fixed base structures	TYPE 2 (soft/weak first storey) $k_1 \times 1$ and $k_{2-5} \times 4$	$\mu_a = 1$ and $\mu_a = 4$
Base isolation of new buildings	TYPE 2a BI $k_1 \times 1$ and $k_{2-5} \times 4$	$\mu_a = 1$
Base isolation of existing buildings	TYPE 2b BI $k_1 \times 1$ and $k_{2-5} \times 4$	$\mu_a = 4$

The shear frame 5 storey structure is considered to analyse as shown in Figure 2:

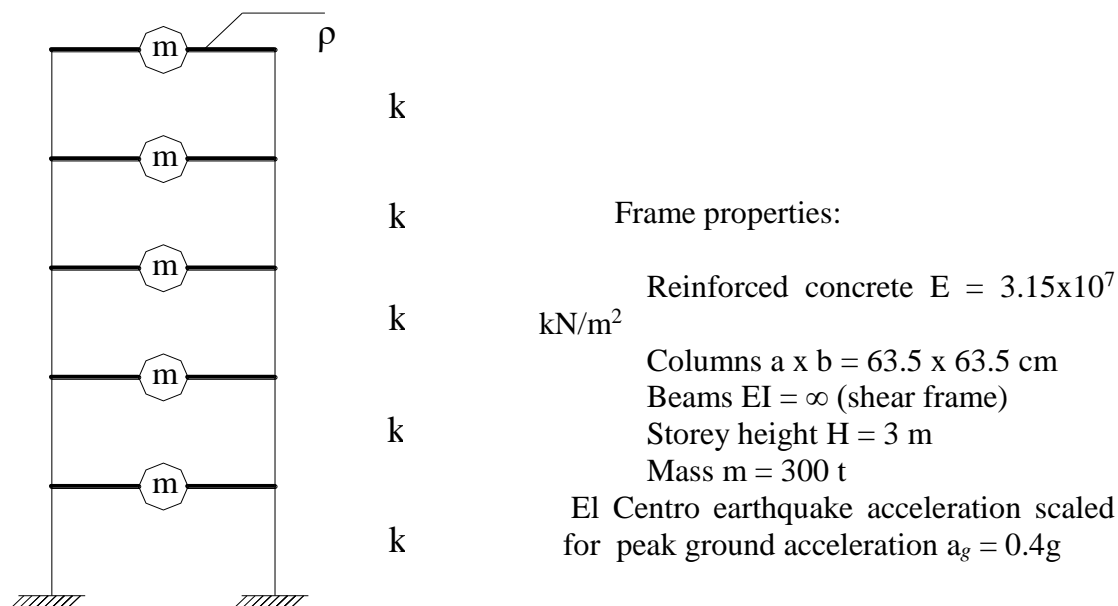


Figure 2: Five-story shear frame of linear elastic model

First we conduct the response spectrum analysis using SAP2000 computer software, in elastic range ($\mu = 1$) with $\eta = 5\%$ damping. From this analysis we obtain the results given in Table 1 below. Since these results represent the yield phase, we note them with the index “y” (yield).

Table 1: Results of linear elastic response of a 5 – storey structure

Storey	Displacement U_{yj} (cm)	Deformation Δ_{yj} (cm)	Shear force $f_{y,j}^e$ (kN)	Storey stiffness k_j (kN/m)
5	11.07	1.82	1149	63132
4	9.25	2.24	1953	57185
3	7.01	2.43	2504	103045
2	4.58	2.42	2937	121364
1	2.16	2.16	3221	149120

where U_{yj} is the yield displacement of storey “j”; $\Delta_{yj} = U_{yj} - U_{y(j-1)}$ is the yield deformation of storey “j”; $f_{y,j}^e$ is the shear force of storey “j”, which in case of elasto-plastic systems, represents the yield strength; and k_j is the stiffness of storey “j”, $k_j = f_{y,j}^e / \Delta_{yj}$. For the time history analysis we will consider a new model of the shear frame in order to perform the analysis in the elasto-plastic range ($\mu > 1$) besides the elastic one ($\mu = 1$). Figure 3 shows this model, where the columns are replaced with elements with infinite stiffness $EI = \infty$ while the elastic parameters are represented by the nonlinear elements NLIN_j, the characteristics of which are the same of the columns they replace. Nonlinear elements NLIN_j are modelled with stiffness k_j and yield strength f_{yj}^{ep} . Figure 4 shows the elasto-plastic diagram of the nonlinear elements NLIN_j. It is obvious that in case of elastic systems $f_{yj}^{ep} = f_{yj}^e$ (because $\mu = 1$), while in case of elasto-plastic systems f_{yj}^{ep} is a function of the allowable ductility.

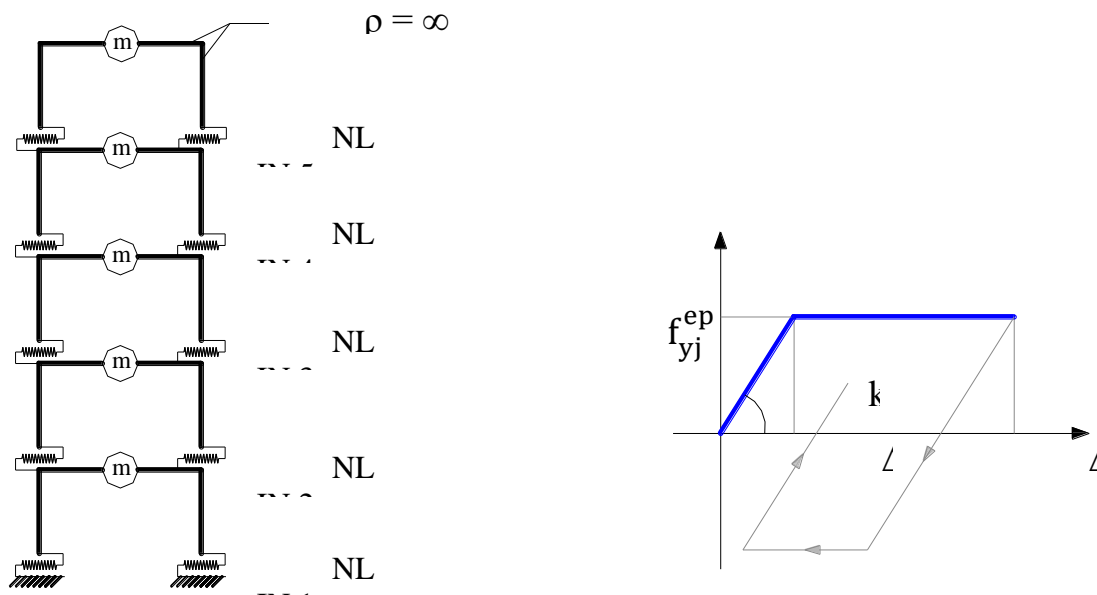


Figure 3: Shear frame of elasto-plastic (nonlinear) model

Figure 4: Elasto-plastic diagram between shear force and storey deformation

Two analysis will be conducted: the response spectrum analysis (RSA) and time history analysis (THA). These analysis will be perform for two different allowable ductility levels: allowable ductility $\mu_a = 1$ (elastic system) and allowable ductility $\mu_a = 4$ (elasto-plastic system).

First, the response spectrum analysis is performed using El Centro earthquake response spectrum with 5% damping for the allowable value of ductility.

With the response spectrum analysis results, the nonlinear elements NLIN_j are modelled in order to continue with the time history analysis, using the same earthquake acceleration with 5% damping. With the nonlinear analysis results we determine the maximum storey displacements U_{mj} , which then are used to calculate the maximum storey deformations (by the difference of maximum storey displacements):

$$\Delta_{mj} = U_{mj} - U_{m(j-1)}$$

Knowing the elastic deformations of the storeys Δ_{yj} and their maximum required deformations, it is possible to calculate their required ductility $\mu_{rj} = \frac{\Delta_{mj}}{\Delta_{yj}}$

MULTI-STOREY BUILDINGS WITH WEAK AND SOFT STOREY

There are reasons the engineers are facing to the situation of soft/weak storey buildings. Mostly, it happens because of architectural requirements to have an open space at ground floor level. To illustrate this relation, let us consider a different structure, called TYPE 2, with soft/weak first storey. Practically, weak storey buildings are also soft storey buildings because this storey will be more flexible than the others. This happens because the strength and the stiffness are inter-related.

The parameters of structure TYPE 2, are performed from above structure, multiplying the stiffness of second to fifth storeys by 4, keeping the same value of the first storey stiffness. By this, the TYPE 2 structure becomes with soft first storey. Using the elasto-plastic model, two types of analyses are conducted: response spectrum analysis and time history analysis, with two different levels of the allowable ductility $\mu_a = 1$ and $\mu_a = 4$.

First the response spectrum analysis is conducted, which gives us the results of the yield strength of the second to fifth storeys.

Then we perform the time history analysis, taking results of the maximum required displacement of the storeys, U_{mj} , to calculate the maximum required deformations, Δ_{mj} , and the required storey ductility μ_{rj} .

The analysis results of the parameters of interest are given in the Tables 2 and 3:

Table 2: Analyses results of structure TYPE 2, with $\mu_a = 1$

Analysis type		Response spectrum analysis (L)			Time – history analysis (NL)		
St orey	k_j	U_{yj} (cm)	Δ_{yj} (cm)	f_{yj}^{ep} (kN)	U_{mj} (cm)	Δ_{mj} (cm)	μ_{rj}
5	25 2528	8.2 4	0.6 6	166 5	5.71	0.35	0 .53
4	34 8740	7.5 8	0.9 2	319 6	5.36	0.47	0 .51
3	41 2180	6.6 6	1.1 0	454 2	4.89	0.53	0 .48
2	48 5456	5.5 6	1.1 6	566 4	4.36	0.53	0 .46
1	14 9120	2.1	2.1	312 6	3.83	3.83	1 .82

Table 3: Analyses results of structure TYPE 2, with $\mu_a = 4$

Analysis type		Response spectrum analysis (L)			Time – history analysis (NL)		
St orey	k_j	U_{yj} (cm)	Δ_{yj} (cm)	f_{yj}^{ep} (kN)	U_{mj} (cm)	Δ_{mj} (cm)	μ_{rj}
5	25 2528	2.0 6	0.1 6	416	8.05	0.04	0 .25
4	34 8740	1.9 0	0.2 3	799	8.01	0.06	0 .26
3	41 2180	1.6 7	0.2 8	113 5	7.95	0.10	0 .36
2	48 5456	1.3 9	0.2 9	141 6	7.85	0.11	0 .38
1	14 9120	1.1 0	1.1 0	781	7.74	7.74	1 4.6

From the results of Tables 2 and 3 it is obvious that TYPE 2 model, represent the structure with soft and weak first storey. The required storey ductility is shown in shown graphically in Figures 5, for the two analyses cases with allowable ductility $\mu_a = 1$ and $\mu_a = 4$:

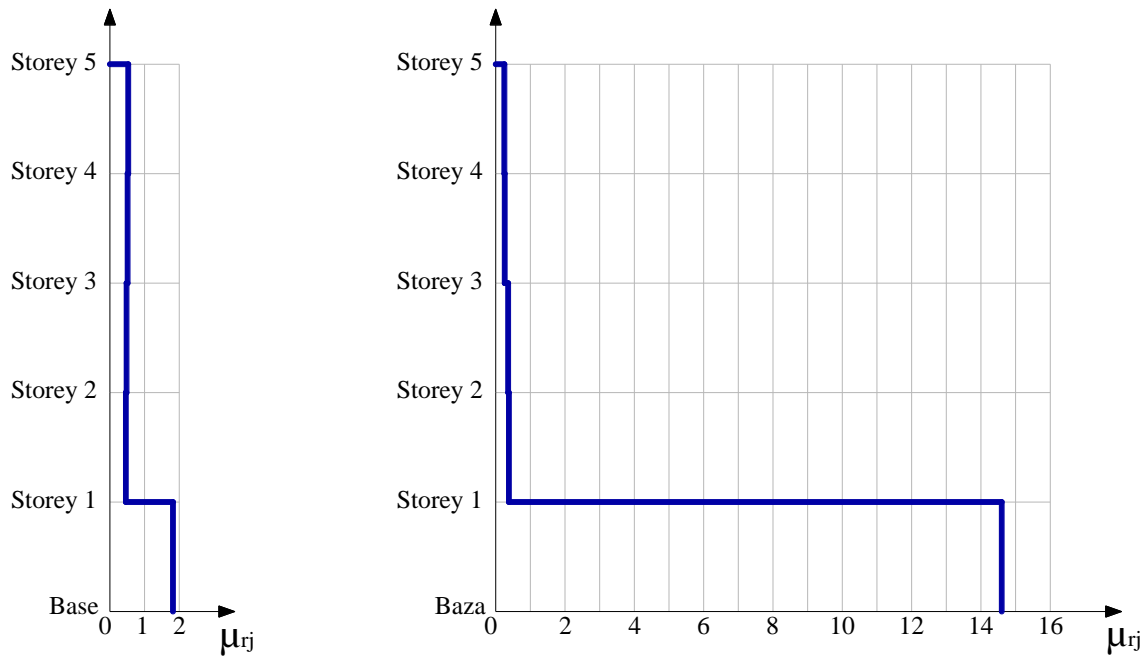


Figure 5. Required story ductility of TYPE 2 structure: a) for $\mu_a=1$, b) for $\mu_a=4$

So, the required ductility of the first storey $\mu_{r1} = 14.6$ is much bigger than the allowable one $\mu_a=4$ and practically impossible to be possessed by conventional structures. Thus, this structure cannot resist the design seismic action.

THE INFLUENCE OF SEISMIC ISOLATION TO THE REQUIRED DUCTILITY

In order to study the influence of seismic isolation to the required ductility of a soft storey building, we will consider the previous structure (TYPE 2), but with a base isolation.

Isolators are considered bilinear and their characteristics are calculated for the given quantities $W= 350$ kN, $T=2.3$ s, $D=0.15$ m, $\beta= 5\%$ and $r=0.1$, the isolators characteristics are:

$$K_{eff} = 5591 \text{ kN/m}; K_1 = 42256 \text{ kN/m}; Q_y = 228 \text{ kN}; u_y = Q_y/K_1 = 0.539 \text{ cm}.$$

First the response spectrum analysis is performed using SAP2000 computer software, for the elastic phase ($\mu = 1$) with $\eta = 15\%$ damping.

For the time history analysis, in order to perform the elasto-plastic nonlinear analysis besides the elastic one, we will use the model with nonlinear elements. Schematically this model is shown in Figure 6.

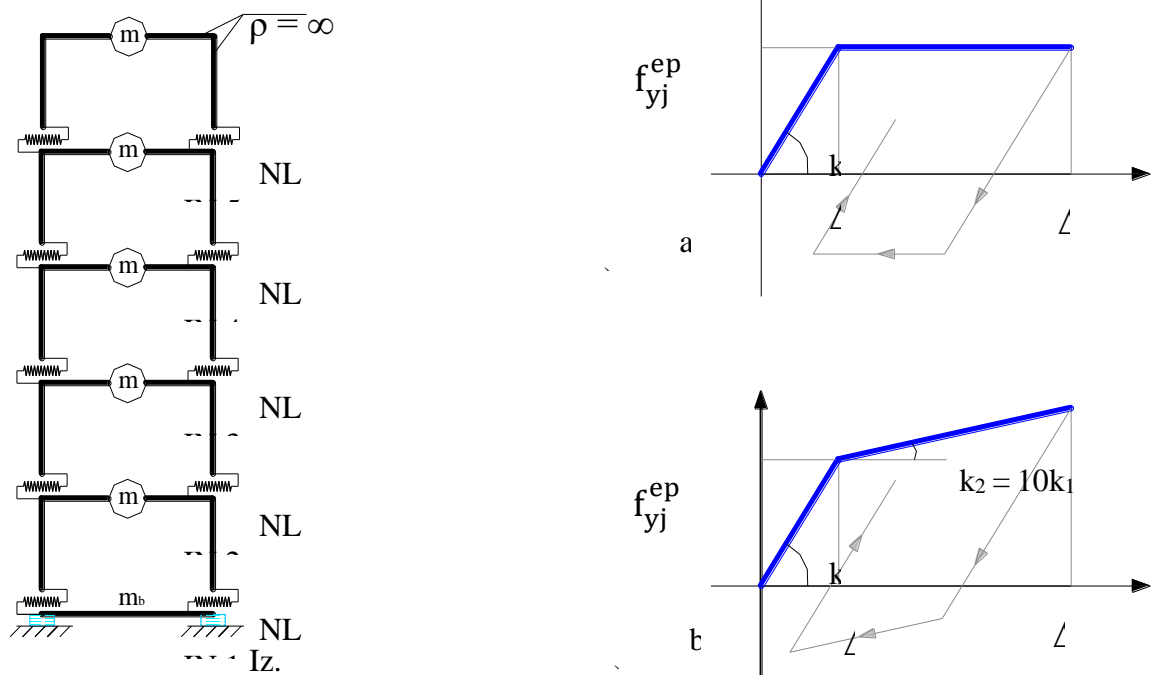


Figure 6: Elasto-plastic (nonlinear) model of base isolated frame

Figure 7: Nonlinear diagram of elements: a) Elasto-plastic diagram between shear force and storey deformation, b) Isolators bilinear diagram

This model represents the replacement of the columns with elements with infinite stiffness $EI = \infty$ and with elastic characteristics of nonlinear elements, $NLIN_j$, which are the same as the characteristics of the column replaced. Practically, the nonlinear elements $NLIN_j$ are modelled with stiffness k_j and yield strength f_{yj}^{ep} . The elasto-plastic diagram of the nonlinear elements, $NLIN_j$, is shown in Figure 7a while the bilinear diagram of the isolators is shown in Figure 7b.

Two types of analyses are conducted with the elasto-plastic model: the response spectrum analysis (RSA) and time history analysis (THA). First, the response spectrum analysis is performed using the El Centro earthquake response spectrum with $\eta = 15\%$ damping (to consider the damping level of the isolators). With the results of this analysis, the characteristics of the nonlinear elements $NLIN_j$ are modelled, further to be used for the time history analysis. Since isolated structures response is within the elastic range, the damping level of the structures is low, thus the nonlinear elements $NLIN_j$ are considered with $\eta = 2\%$ elastic damping. To study the seismic isolation effect on different structures we will analyze the base isolation of new buildings and the base isolation of existing ones.

a) Base isolation of new buildings

Since base isolated structures are designed to behave almost within the elastic range, the allowable ductility for the analyses is accepted level $\mu_a = 1$.

The third model, called structure TYPE 2a BI, represents the seismic isolation of structure TYPE 2 with allowable ductility $\mu_a = 1$. Since the yield strength of this type of structure is accepted to be different from the results of response spectrum analysis, the storeys yield deformation will be calculated by the expression $\Delta_{yj} = f_{yj} / k_j$ for all storeys (as shown in Table 4). For this case, only time history analysis is performed in order to estimate the required deformations and the required ductility of each storey (Δ_{mj} and μ_{rj}). The analyses results of structure TYPE 2a BI, are given in Tables 4.

Table 4: Analysis results of structure TYPE 2a BI, with $\mu_a = 1$

Analysis type		Response spectrum analysis (L)			Time – history analysis (NL)		
St ore y	k_j	U_{yj} (cm)	Δ_{yj} (cm)	f_{yj}^{ep} (kN)	U_{mj} (cm)	Δ_{mj} (cm)	μ_{rj}
5	25 2528	20. 78	0.1 1	223	14.8 9	0.1	0 .91
4	34 8740	20. 67	0.1 4	445	14.7 9	0.1 1	0 .79
3	41 2180	20. 53	0.1 6	655	14.6 8	0.1 3	0 .81
2	48 5456	20. 37	0.1 8	874	14.5 5	0.1 5	0 .83
1	16 2571	20. 19	0.6 6	107 9	14.4 0	0.4 8	0 .73

From the results of the analysis of structure TYPE 2a BI it is concluded that base isolation of the structure with soft (and weak) first storey is very effective to the reduction of storey required ductility

b) Base isolation of existing buildings

If we apply the seismic isolation on existing structures (designed and built in a previous period of time) with soft and weak first storey, we can conclude that the required storey ductility is obviously reduced.

To illustrate the effect of base isolation we consider the five-storey shear frame analyzed before, structure TYPE 2. Supposing that the existing buildings are designed with allowable ductility $\mu_a = 4$. The Isolated structure is called TYPE 2b BI. The characteristics of isolators are the same as those used for structure TYPE 2a BI. The results of the time history analysis are given in Tables 5:

Table 5: Analysis results of structure TYPE 2b BI , with $\mu_a = 4$

Analysis type		Response spectrum analysis (L)			Time – history analysis (NL)		
St orey	k_j	U_{yj} (cm)	Δ_{yj} (cm)	f_{yj}^{ep} (kN)	U_{mj} (cm)	Δ_{mj} (cm)	μ_{rj}
5	25	2.0	0.1	416	14.9	0.0	0
	2528	6	6		1	9	.56
4	34	1.9	0.2	799	14.8	0.1	0
	8740	0	3		2	3	.57
3	41	1.6	0.2	113	14.6	0.1	0
	2180	7	8		5	9	4
2	48	1.3	0.2	141	14.5	0.1	0
	5456	9	9		6	5	5
1	14	1.1	1.1	781	14.4	0.5	0
	9120		0		0	2	.98

To better understand the change of the required ductility values, Figure 8 shows the required ductility of isolated and non isolated structures, for both cases, base isolation of new structures and base isolation of existing structures.

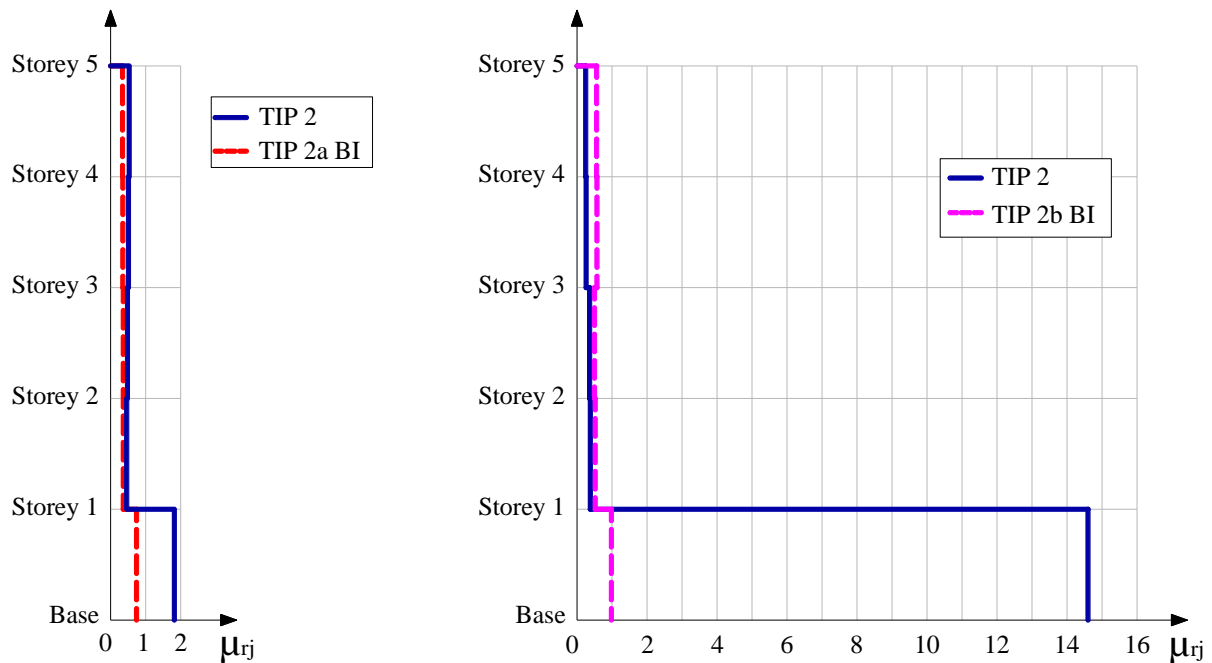


Figure 8: a) The required ductility for each storey of fixed base (TYPE 2) and base isolated (TYPE 2a BI) of new structures designed with allowable ductility $\mu_a = 1$.

b) The required ductility for each storey of fixed base (TYPE 2) and base isolated (TYPE 2b BI) of existing buildings) designed with allowable ductility $\mu_a = 4$

Comparing the results of the required deformation of structural elements of the first storeys, we conclude that for the nonisolated structures the deformation demand is higher, while for isolated structures, structural elements almost does not have deformations, because these deformations are mostly developed on the isolation system.

Seismic isolation of existing buildings with soft first storey (and weak storey) reduces the required ductility of the first storey from $\mu_{r1} = 14.6$ as in the case of structure TYPE 2, to $\mu_{r1} = 0.98$ in the structure TYPE 2b BI. So, with seismic isolation of existing soft storey structures, it is provided that the structure behaves in the elastic range (even the soft storey).

Seismic isolation is used very effectively to improve the required ductility of the structure if it was designed with higher value of the required ductility which in practice is impossible to achieve.

The nonlinear analyses of isolated structures, TYPE 2a BI and TYPE 2b BI, are conducted using the yield strength of the existing storeys. The fact that the required ductility of isolated structures is less than 1, shows that the structure has sufficient strength (because its elastic strength capacity can be higher than needed).

CONCLUSION

In structures that represent the soft storey phenomenon, the seismic isolation manages to improve the structure response and is able to eliminate the defect.

For new base isolated structures, it is possible to design them to behave close to elastic range. So the isolation of buildings calculated in linear phase ($\mu_a = 1$) improves the first storey to develop no plastic deformations.

The benefit of seismic isolation in the reduction of yield strength (shear force) is well known. This study shows another benefit, the reduction of storey ductility of building structures.

If we apply the seismic isolation on existing structures (designed and built in a previous period of time) with soft and weak first storey, it will state that storeys ductility demand will be significantly improved.

Through seismic isolation of existing buildings with soft storey (and weak storey) with high required ductility it is possible to reduce considerably the value of this ductility. By using the seismic isolation, even the soft storey response is within the elastic range.

Seismic isolation is used very effectively to improve the ductility of the structure if it is designed with higher value ductility demand which in practice is impossible to achieve.

REFERENCES

- [1] Chopra, A.K., "Dynamics of Structures: Theory and Application to Earthquake Engineering", 2nd Ed, Pearson Prentice Hall, Upper Saddle River, New Jersey, 2007
- [2] Skinner, R.I., Robinson, W.H., McVerry, G.H., "An Introduction to Seismic Isolation", John Wiley & Sons Ltd., New York, 1993.
- [3] Naeim, F., Kelly, J.M., "Design of Seismic Isolated Structures", John Wiley & Sons, New York, 1999.
- [4] Higashino, M., Okamoto, S., "Response Control and Seismic Isolation of Buildings", Taylor & Francis, New York, 2006
- [5] Kelly, J.M., "Earthquake Resistant Design with Rubber", Springer-Verlag London Limited, 1997.
- [6] Kelly, E, Trevor. "Base Isolation of Structures", Holmes, Consulting Group Ltd, 2001.
- [7] SAP2000®, Integrated Finite Element Analysis and Design of Structures, analysis Reference, Vol. 1&2, Computer and Structures, Inc, Berkeley, California, USA, 2000
- [8] Seranaj, A., "Dynamic Response and Seismic Analysis of Base Isolated Buildings", Monograph, Scholar's Press, www.omniscryptum.com, Germany, 2016
- [9] Seranaj, A., "Reagimi Dinamik dhe Analiza Sizmike e Strukturave të Izoluara në Bazë me Izolator Gome me Fibra", Disertacion Doktorature, Tiranë, Albania, 2015

Probabilistic seismic hazard analysis of events occurred in Albania

Drilona Disha¹, Hektor Cullufi¹, Altin Bidaj¹, Anjeza Gjini¹

¹Department of Mechanic of Structures, Faculty of Civil Engineering, Tirana, Albania

ABSTRACT

Albania is a seismic region so the goal of many earthquake engineers is to ensure the durability of a structure for a given level of ground vibration. There are many uncertainties about magnitude, location and the intensity of the future earthquake. Probability methods allow us to speak quantitatively about variables phenomenon. Probabilistic Seismic Hazard Analysis (PSHA) aims to reveal these uncertain and to produce the distribution of the future earthquakes that may occur. The purpose of this paper is to discuss the calculation involved in PSHA and to give some qualifications about the probability of intense ground vibration at a place and their associated rates of exceedance. The results can be used to identify the ground vibration intensity, which has small probability of being exceeded. In calculation are involved the location and intensity of all the seismic events occurred in Albania.

Keywords: earthquake, PSHA, rates of exceedance, PGA

1.INTRODUCTION

Albania is a seismic region so the goal of earthquake engineering analyses is to ensure the structures for a given ground shaking while maintaining a good performance. The earthquakes are stochastic phenomena so one of the best methods of prediction is a probabilistic method. We know that the seismic events have some uncertainties about the future events expected. These uncertainties include size, location, intensity etc, so the Probabilistic Seismic Hazard Analyses (PSHA) aims to combine these and make a future prediction for the upcoming events. The Probabilistic Seismic Hazard Analysis is a method used in the Eurocode EC8.

The acceleration (PGA) refers to the value of seismic acceleration in a hard rock, who for $P=90\%$ will be not exceeded for $t=50$ years or the acceleration caused by an earthquake with $RP=475$ years (designing earthquake)

The dates of this calculation are used from local or national administrators to minimize the risk, geologist engineers, seismographs, architects and project engineers.

The first thing to do is to determine the annual probability of exceeding some levels of earthquake ground shaking at a site and then to evaluate the risk of a structure.

The purpose of this paper is to discuss the calculation involved in PSHA because probability calculations are a critical part of the procedures described here.

With PSHA we are not looking for worst-case ground motion intensity, but we consider all possible earthquake events that have occurred in Albania along with their associated probabilities of occurrence, in order to find the level of ground motion intensity exceeded.

2. EARTHQUAKE SOURCES

This method is interested in the identification of all the earthquake sources capable of producing ground motions at a site. These sources could be faults, which are planar surfaces identified through observations of past earthquake locations and geological evidence. There are also individual sources of earthquake and if they are not identifiable these sources could be explained as area sources. In Albanian region are active ten seismic source zones described in Table 1.

Table.1 Parameters for the ten seismic source zones

Zone name/Code	Zone area (km ²)	Earthquakes used	β	A (No)	M _x	Rate of M>6 p.a	Rate density
Ohrid-Korca, KO	2760	44	1.44	242	6.9	0.0315	11.4
Kukesi-Peshkopia, KP	1480	21	1.75	481	6.9	0.0104	7.0
Ionian Coast, IC	16600	151	1.40	692	7.0	0.115	6.9
Elbasani-Dibra-Tetova, EDT	2660	46	1.99	3142	6.9	0.0167	6.3
Periadriatic Lowland, PL	7460	75	1.61	914	7.0	0.0458	6.1
Lezha-Ulqini, LU	5140	39	1.52	293	7.2	0.0272	5.3
Skopje, SK	3300	5	2.08	2541	7.2	0.00913	2.8
Shkodra-Tropoja, ST	1570	11	1.99	778	6.9	0.00418	2.7
Peja-Prizreni, PP	1740	5	2.03F	418	6.8	0.00173	1.0
Eastern Albanian Backgr, EAB	57200	75	2.03F	6075	6.5	0.0199	0.35

3. PROBABILISTIC HAZARD ANALYSIS

PSHA is first developed by Cornell (1968) and his methods were adopted for evaluating hazard. The hazard curves obtained from PSHA show the variation of Peak Ground Acceleration against means of annual rate of exceedance. The occurrence of an earthquake is assumed to follow Poisson's distribution. The estimation of seismic hazard values in any region needs the complete details of past earthquakes. In this calculations I have obtained 134 seismic events occurred in Albania from 1905-2014 capable producing damages (considering all

earthquakes with magnitude greater than 5). These data include the depth, magnitude, time etc. The earthquake data are collected from IGJEUM (Institute of Geosciences, Energy, Water and Environment)

3.1 IDENTIFICATION OF MAGNITUDES

Seismic faults are capable producing different scales of earthquakes. Gutenberg and Richter observed the earthquakes magnitudes and they saw that the distribution of earthquake sizes at a site usually follow the law (1):

$$\log \lambda_m = a - bm \quad (1)$$

where, λ_m is the rate of earthquakes with $M > m$ and a, b are constants.

This equation is called Gutenberg-Richter recurrence law. For magnitudes from 3-8, and $a=b=1$, in figure (1) is showed a typical distribution of observed magnitudes, along with Gutenberg-Richter law.

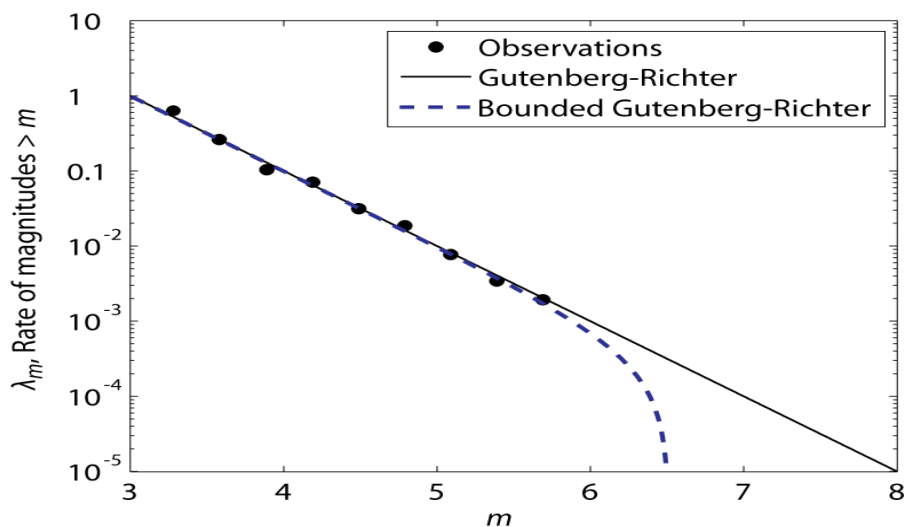


Figure.1 Typical distribution of observed magnitudes

Equation (1) can be used to calculate a Cumulative Density Function CDF for magnitudes greater than minimum m and smaller than maximum M .

$$F_M(m) = \frac{1 - 10^{-b(m - m_{\min})}}{1 - 10^{-b(m_{\max} - m_{\min})}}, \quad m_{\min} < m < m_{\max} \quad (2)$$

While deriving equation (2) we obtain a Probability Density Function PDF

$$f_M(m) = \frac{b \ln(10) 10^{-b(m - m_{\min})}}{1 - 10^{-b(m_{\max} - m_{\min})}}, \quad m_{\min} < m < m_{\max} \quad (3)$$

where, M_{\max} is the maximum magnitude that a source can produce. This limited distribution of magnitude is known as Gutenberg – Richter law. For further equation of PSHA we will convert

the continued distribution of magnitudes in a discrete set of magnitudes. The discrete values can be found through formula (4):

$$P(M = m_j) = F_M(m_{j+1}) - F_M(m_j) \tag{4}$$

where m_j , are the discrete values of magnitudes sorted in a certain way that $m_j < m_{j+1}$. At the Table.2 is showed the CDF for the magnitudes and the PDF as well.

Table.2 CDF and PDF for the magnitudes of the earthquakes

MAGNITUDE	$F_M(m_j)$	$P(M=m_j)$
5	0.000	0.206
5.1	0.206	0.164
5.2	0.369	0.13
5.3	0.499	0.103
5.4	0.602	0.082
5.5	0.684	0.065
5.6	0.750	0.052
5.7	0.801	0.041
5.8	0.842	0.033
5.9	0.875	0.026
6	0.901	0.021
6.1	0.921	0.016
6.4	0.961	0.01
6.6	0.976	0.007
6.7	0.981	0.005
6.8	0.985	0.003
6.9	0.988	0.003
7	0.991	0.002

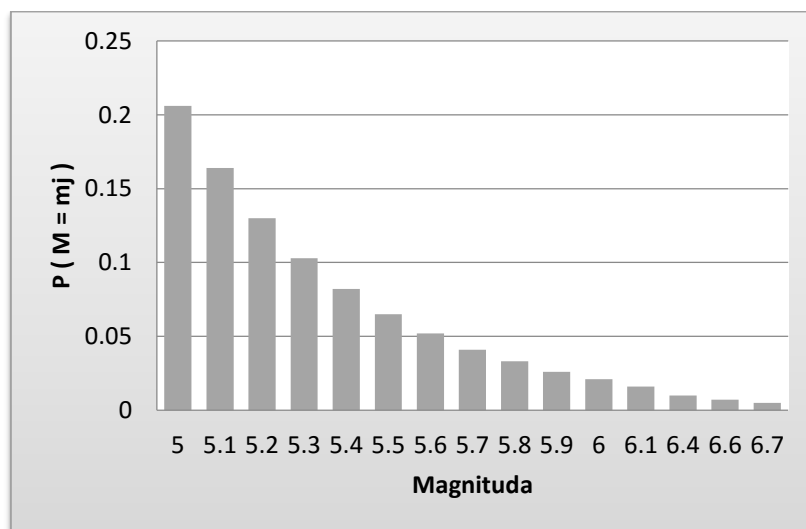


Figure.2 The discrete probability values of PDF from formula (4)

4. EARTHQUAKE DISTANCES

The distribution of the distances from earthquake to the site of interest is important to predict the ground shaking at a site. We assume that for a given earthquake source the probability to occur in any location is equal. According to this, is simple to identify the distribution of source to site distances using the geometry of the sources. This model is appropriate for modeling faults that exist on the boundary of two tectonic plates.

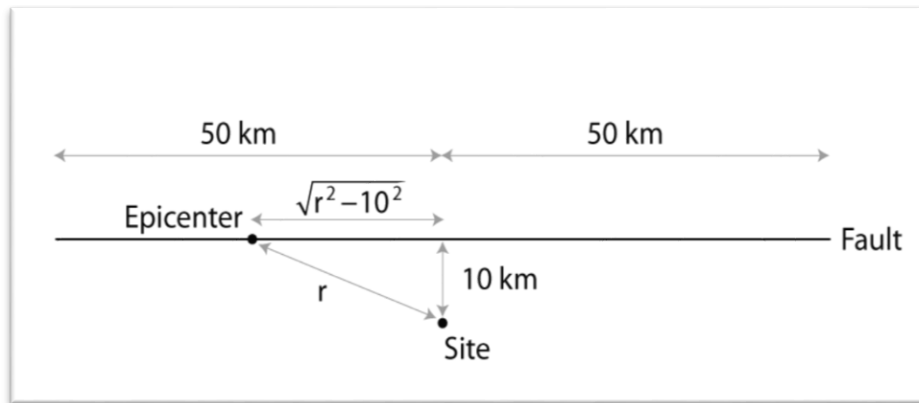


Figure 3. Ilustration of the model of line source

Considering a 100 km fault, with a site located 10 km from the center and in this case the probability to observe a distance of less than r is equal to the fraction of the fault located with a radius of r . So, we can compute the CDF of R

$$F_R(r) = P(R \leq r) = \frac{\text{gjatesia e carjes me distance } r}{\text{gjatesia totale e carjes}} = \frac{2\sqrt{r^2-10^2}}{100} \quad (5)$$

The equation is true for distances less than 10 km and greater than 51 km. Distances out of this range are impossible, so the CDF is:

$$F_R(r) = \begin{cases} 0 & \text{nese } r < 10 \\ \frac{2\sqrt{r^2-10^2}}{100} & \text{nese } 10 \leq r < 51 \\ 1 & \text{nese } r \geq 51 \end{cases} \quad (6)$$

The PDF and CDF are plotted in the figure (4).

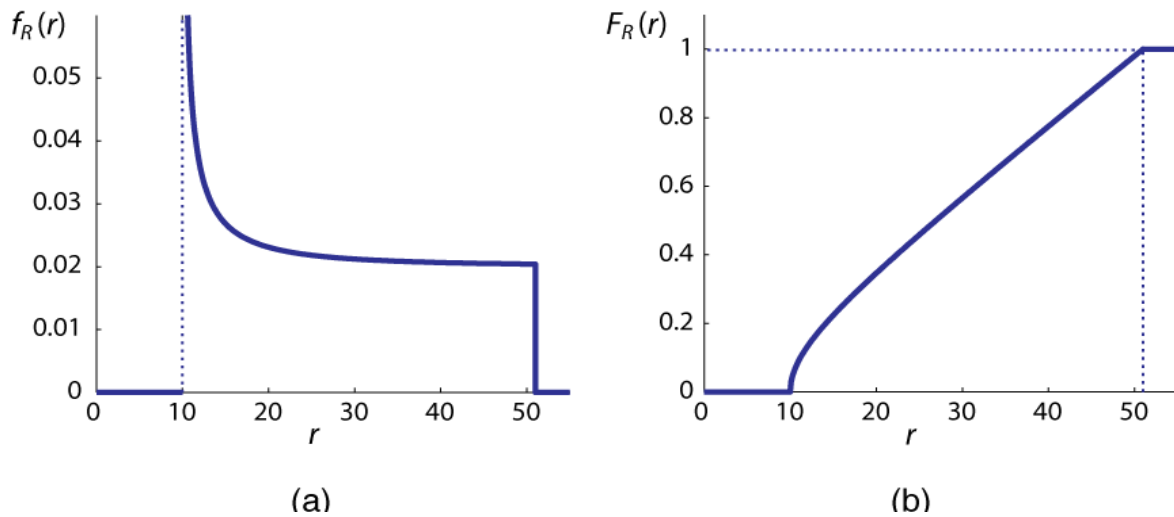


Figure.4. The CDF (a) and PDF (b) of the distance source to site for the future earthquakes

5. GROUND MOTION INTENSITY

The next step is a ground motion prediction model and these models are called attenuation relations. The chosen model predicts the probability of ground motion intensity, as a function of many variables such as: magnitude, distance, faulting mechanism, the near surface site conditions and the potential presence of other effects. To describe the probability distribution, the prediction models are in this form:

$$\ln IM = \overline{\ln IM(M, R, \theta)} + \sigma(M, R, \theta) * \varepsilon \tag{7}$$

where, $\ln IM$ is the natural log of ground motion intensity measure (such as spectral acceleration at a given period). The terms $\overline{\ln IM(M, R, \theta)}$ and $\sigma(M, R, \theta)$, are the output of the ground motion prediction model, the predicted and the standard deviation respectively of $\ln IM$. There are many methods for the mean of PGA, but we choose to use the prediction model for horizontal response spectra in Europe by Ambrasey, Simpson and Bommer (1996). [2]. They predicted the following model for the mean of peak ground acceleration:

$$\ln PGA = -1.09 + 0.238 m - 0.0005r - \log(r) \tag{8}$$

where, $h_o=6\text{km}, \sigma_{\log \varepsilon}=0.28$. The mean depth of the earthquakes in Albania is 10 km, but in Ambrasey relations this parameter is not used, so this will not be part of hazard calculation.

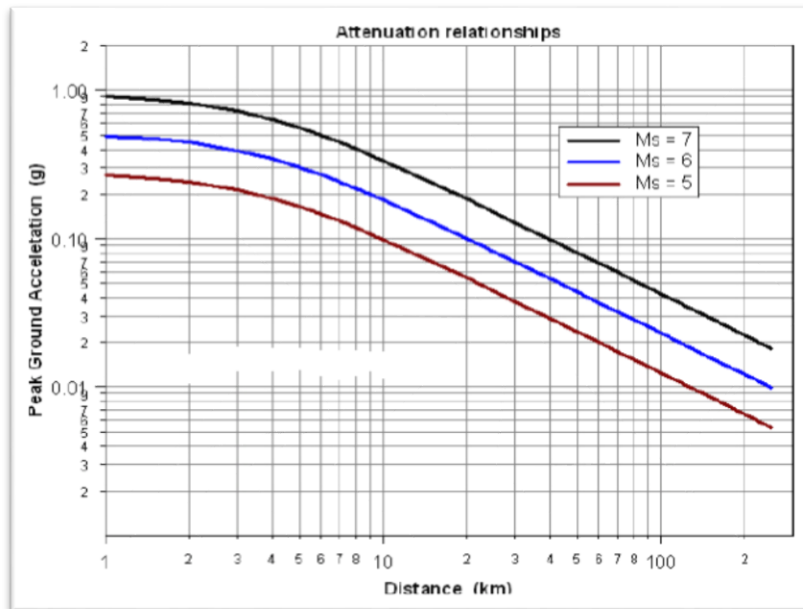


Figure.5 PGA attenuation relationships for European region by Ambrasey, Simpson and Bommer

Table.3 The calculation of a_g with Ambrasey, Simpson and Bommer formulas

(a *)	log(a *)	h_0 (km)	d (km)	m	r (km)	logr	log(D)	ag/g
0.2055217	-0.6871422	6	1	5	6.0827625	0.7841009	0.000	0.0209502
0.0127587	-1.8941923	6	2	5	6.3245553	0.80103	0.301	0.0013006
0.1862257	-0.7299604	6	3	5	6.7082039	0.8266063	0.477	0.0189833
0.1731382	-0.7616072	6	4	5	7.2111026	0.8580017	0.602	0.0176491
0.159746	-0.79657	6	5	5	7.8102497	0.8926649	0.699	0.016284
0.1469234	-0.8329089	6	6	5	8.4852814	0.9286662	0.778	0.0149769
0.1351079	-0.8693192	6	7	5	9.2195445	0.9647095	0.845	0.0137725
0.1244515	-0.905	6	8	5	10	1	0.903	0.0126862
0.1149473	-0.9395013	6	9	5	10.816654	1.0340929	0.954	0.0117174
0.0764895	-1.116398	6	5	5	16.155494	1.2083203	1.176	0.0077971
0.0588595	-1.2301836	6	20	5	20.880613	1.3197432	1.301	0.0059999
0.0397251	-1.400935	6	30	5	30.594117	1.4856379	1.477	0.0040494
0.0297088	-1.5271154	6	40	5	40.447497	1.6068916	1.602	0.0030284
0.023591	-1.627254	6	50	5	50.358713	1.7020746	1.699	0.0024048
0.0194777	-1.7104616	6	60	5	60.299254	1.7803119	1.778	0.0019855
0.0165266	-1.7818159	6	70	5	70.256672	1.8466876	1.845	0.0016847
0.014308	-1.8444204	6	80	5	80.224684	1.904308	1.903	0.0014585
0.0125804	-1.9003054	6	90	5	90.199778	1.9552055	1.954	0.0012824
0.0111977	-1.9508702	6	100	5	100.17984	2.0007803	2.000	0.0011415

It is proved that the values are distributed in a significative way just like the prediction. The ε coefficient extracted from the PGA values grows up in a lognormal law, so $\ln(\varepsilon)$ follows a normal law. The PDF of lognormal variable can be written as:

$$f_2(a_g) = \frac{1}{a_g \sigma_{\ln \varepsilon} \sqrt{2\pi}} \exp \left\{ -\frac{1}{2} \left[\frac{1}{\sigma_{\ln \varepsilon}} \ln \left(\frac{a_g^2}{a_g^*} \right) \right]^2 \right\} \quad (9)$$

Table.4 The PDF of the lognormal variables a_g

a_g	a_g^*	σ	$f_2(a_g)$
0.0001	0.2	0.62	1.49E-29
0.05	0.2	0.62	1.056887
0.1	0.2	0.62	3.445252
0.15	0.2	0.62	3.852881
0.2	0.2	0.62	3.218092
0.25	0.2	0.62	2.413017
0.3	0.2	0.62	1.732354
0.35	0.2	0.62	1.223633
0.4	0.2	0.62	0.861313
0.45	0.2	0.62	0.608042
0.5	0.2	0.62	0.431892
0.55	0.2	0.62	0.30916
0.6	0.2	0.62	0.223189
0.65	0.2	0.62	0.162533
0.7	0.2	0.62	0.11939
0.75	0.2	0.62	0.088444
0.8	0.2	0.62	0.066055
0.85	0.2	0.62	0.049722
0.9	0.2	0.62	0.037709
0.95	0.2	0.62	0.028803
1	0.2	0.62	0.02215

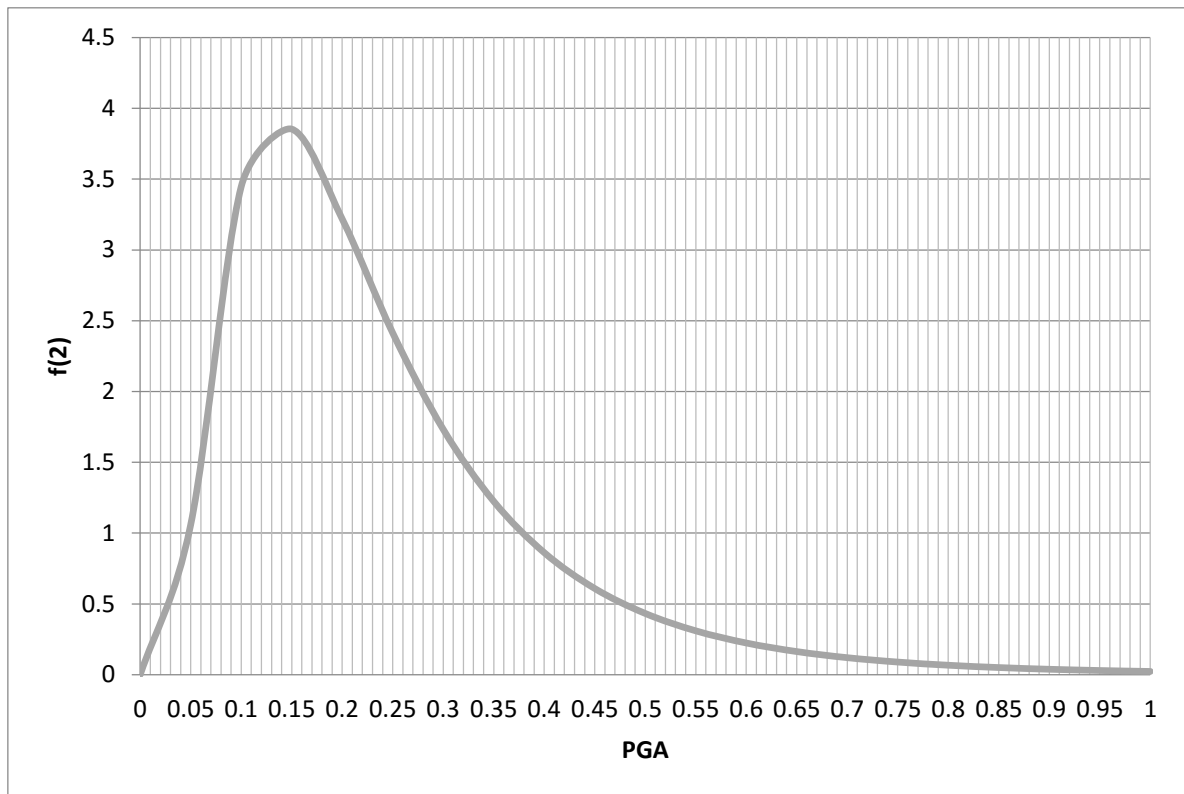


Figure.6 The graphic of lognormal distribution of PGA

6. THE PROPABILITY OF EXCEEDANCE

The probability of exceedance is calculated for three representative earthquakes and the results are calculated with the formula (10) for a period of 1 year and 50 years.

$$P_{TL}(A_g > a_g) = 1 - e^{-w_{TL}} \tag{10}$$

Table .5 Calculating the propability of exceedance

a_g	M=5	M=5	M=5	$w_i = \alpha * P$			
	D=4Km	D=7Km	D=15Km	w_1	w_2	w_3	$w = \sum w_i$
	a_g^*	a_g^*	a_g^*				
	0.2	0.115	0.058				
0.0001	100	100	100	0.210526316	0.210526316	0.210526316	0.631578947
0.05	97.63083114	91.40146	66.44546	0.205538592	0.192424131	0.139885178	0.537847901
0.1	83.0269472	64.11685	18.3465	0.174793573	0.134982852	0.038624206	0.348400631
0.15	57.70567171	33.40739	0.240942	0.121485625	0.070331339	0.000507247	0.192324211
0.2	35.39390019	15.44694	0	0.074513474	0.032519875	0	0.107033349
0.25	20.58017045	6.809861	0	0.043326675	0.014336549	0	0.057663223
0.3	11.78003028	2.852054	0	0.024800064	0.006004324	0	0.030804388

0.35	6.766921278	1.035205	0	0.01424615	0.002179379	0	0.016425529
0.4	3.943388866	0.184193	0	0.008301871	0.000387774	0	0.008689646
0.45	2.348241185	0	0	0.004943666	0	0	0.004943666
0.5	1.437984544	0	0	0.003027336	0	0	0.003027336
0.55	0.911571449	0	0	0.001919098	0	0	0.001919098
0.6	0.602604041	0	0	0.00126864	0	0	0.00126864
0.65	0.41848177	0	0	0.000881014	0	0	0.000881014
0.7	0.30708954	0	0	0.000646504	0	0	0.000646504
0.75	0.238701752	0	0	0.00050253	0	0	0.00050253
0.8	0.196119135	0	0	0.000412882	0	0	0.000412882
0.85	0.169244559	0	0	0.000356304	0	0	0.000356304
0.9	0.152064585	0	0	0.000320136	0	0	0.000320136
0.95	0.140947431	0	0	0.000296731	0	0	0.000296731
1	0.133669923	0	0	0.00028141	0	0	0.00028141

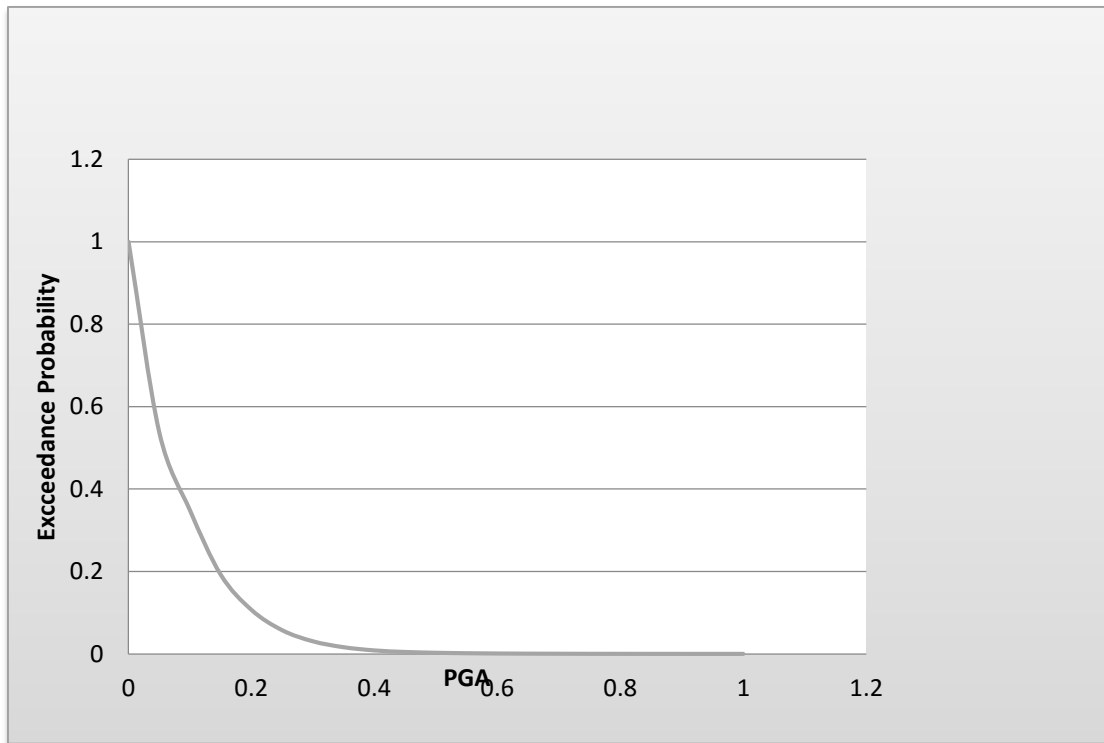


Figure.8 The hazard curve

Table.6 The probabilities of exceedance for three different earthquakes and their summary

	M=5, D=3	a_g*=0.2	w₁
E(0.05)	0.02	0.95	0.019
E(0.1)	0.02	0.75	0.015
E(0.15)	0.02	0.5	0.01
E(0.2)	0.02	0.4	0.008
E(0.4)	0.02	0.075	0.0015
E(0.45)	0.02	0.05	0.001

	M=5, D=9	a_g*=0.115	w₂
E(0.05)	0.02	0.95	0.019
E(0.1)	0.02	0.85	0.017
E(0.15)	0.02	0.50	0.01
E(0.2)	0.02	0.25	0.005
E(0.4)	0.02	0.03	0.0006
E(0.45)	0.02	0.00	0

	M=5, D=50	a_g*=0.06	w₃
E(0.05)	0.02	0.95	0.019
E(0.1)	0.02	0.25	0.005
E(0.15)	0.02	0.15	0.003
E(0.2)	0.02	0.05	0.001
E(0.4)	0.02	0.00	0
E(0.45)	0.02	0.00	0

a_g	w=Σw_i
E(0.05)	0.057
E(0.1)	0.037
E(0.15)	0.023
E(0.2)	0.014
E(0.4)	0.0021
E(0.45)	0.001

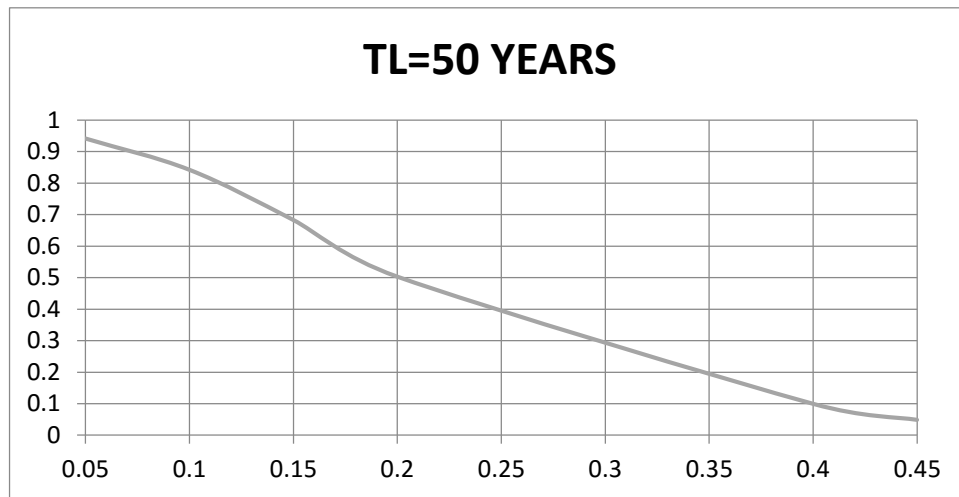


Figure .7 The graphic of propability of exceedance for $T_L=50$ years

T_L (Time Life)	w	0.057	0.037	0.023	0.014	0.0021	0.001
a_g		0.05	0.1	0.15	0.2	0.4	0.45
	50	P	0.942156	0.842762834	0.683363	0.503415	0.099675477
1	P	0.055406	0.036323865	0.022738	0.013902	0.002097797	0.0009995

Table 7. The probability of exceedance for 1 and 50 years

CONCLUSIONS

The concepts and the methodology used in this paper is only a introduction to the propabilistic seismic hazard analysis and the importance at engineering. The work presented here is no way conclusive and intends to make a little introduction to the seismic hazard using PSHA. This method is easy interpreted and can be easily applied to seismic computations.

REFERENCES

- [10] Baker 2008, Intro to the PSHA ,v1-3
- [11] Ambraseys, N.N ,Simpson ,K.A ,Bommer , J.J .1996.Prediction of horizontal response spectra in Europe.*Earthquake Engineering and Structural Dynamics*.
- [12] Baker,J.W., and Cornell,C.A (2006).”Correlation of response spectra values for multi-component ground motions”*Bulletin of the Seismological Society of America*
- [13] Gutenberg ,B., and Richter, C.F (1944).”Frequency of earthquakes in California.”

Comparative analysis of dynamic solutions using Albanian Seismic Code KTP-89 and Eurocode 8

Enkeleda Kokona¹, Helidon Kokona², Hektor Cullufi¹

¹Civil Engineering Faculty, Polytechnic University of Tirana

²Institute of Earthquake Engineering and Engineering Seismology IZIS, Skopje, Macedonia

ABSTRACT

The scope of this presentation is to compare some of principal characteristics of structural dynamic responses computed using Earthquake Resistant Design Regulations KTP-N.2-89, (Albanian Seismic Code) and Eurocode 8 (prEN 1998-1). In this paper are mentioned some of the principal differences between two codes, comprising mainly: Seismic Intensity Classification according to Seismic Zonation Map of Albania, Identification of Ground Types, Reference Peak Ground Acceleration, Elastic and Design Response Spectrum used to present earthquake motion at a given point on the surface. Spectrum Analysis (horizontal and vertical direction), Analysis Methods, etc.

The comparative results of two codes issued by dynamic analysis of reinforced concrete dual system structure chosen are presented along with respective conclusions.

Keywords: seismic, spectrum, shear, displacement, acceleration

INTRODUCTION

The Balkan region is one of the world's most active seismic zones and one in which earthquakes caused heavy losses of life and property throughout history.

In 1970, the countries of the region (except Albania) undertook projects REM/70/172 and REM/74/09 under assistance of UNDP and UNESCO, a survey of seismicity of the region, as a result of which observatory networks and detailed studies of seismicity are improved. Albania took part not formally in some of these activities.

After catastrophic earthquake of 15.04.1979 in Montenegro and northern Albania, the immediate request in developing further earthquake studies was finalized through Project Document RER/79/014/C/01/13 signed by UNDP and UNESCO, where Albania officially joined in November 1981. The project defined the primary long-term and immediate objectives in development of scientific methods for earthquake-resistant design of buildings.

As it is known the most important natural hazard in Albania is earthquake. Thus, the ways and means of reducing consequences from earthquakes is of vital importance.

As result the first seismic code in Albania officially known as Earthquake Resistant Design Regulations KTP-N.2-89, (Albanian Seismic Code) was prepared by Seismic Center, Academy of Science of Albania, Department of Design, Ministry of Construction, Tirana, Albania 1989.

The european standards approved by CEN (European Committee for Standardization) establish a set of harmonised technical rules for the design of buildings. Through standards approved, Eurocode 8 consists of technical rules applied to the design and construction of buildings in seismic regions.

Their overall goal is to make such structures more resistant to earthquakes. Seismic design codes help structural engineers to design structures that will not be damaged in minor shaking and will avoid serious damage or collapse in a major earthquake.

The philosophy of earthquake design for structures other than essential facilities has been well established and proposed as follows:

- to prevent non- structural damage in frequent minor ground shaking
- to prevent structural damage and minimize non- structural damage in occasional moderate ground shaking.
- To avoid collapse or serious damage in rare major ground shaking

THE DESIGN SEISMIC ACTION IS EXPRESSED IN TERMS OF:

A) THE REFERENCE SEISMIC ACTION A_{GR} , ASSOCIATED WITH A REFERENCE PROBABILITY OF EXCEEDANCE, P_{NCR} , IN 50 YEARS OR A REFERENCE RETURN PERIOD, T_{NCR} , AND

b) the importance factor γ_I , to take into account reliability differentiation. An importance factor γ_I is assigned to each importance class.

The scope of this paper is to compare Earthquake Resistant Design Regulations KTP-N.2-89, (Albanian Seismic Code) with Eurocode 8 (EC-8).

In advance, there are some of the principal difference between two codes:

- Classification of Seismic Intensity and division of Albanian Seismic Zone
- Classification of Soil Category
- Spectrum Analysis, (horizontal and vertical direction)
- Classification of structures for importance coefficient.
- Methods of analysis
- Load combination
- Design of Foundation
- Classification of Ductility
- Seismic control joints
- Detailing rules

1. some principal rules according to eC- 8 and Ktp-89

1.1 Classification of Seismic Intensity and division of Albanian seismic Zone

For the purpose of EN 1998, national territories shall be subdivided by the National Authorities into seismic zones, depending on the local hazard. By definition, the hazard within each zone is assumed to be constant.

For most of the applications of EN 1998, the hazard is described in terms of a single parameter, i.e. the value of the reference peak ground acceleration on type A ground, a_{gR} .

The reference peak ground acceleration, chosen by the National Authorities for each seismic zone, corresponds to the reference return period T_{NCR} of the seismic action for the no-collapse requirement (or equivalently the reference probability of exceedance in 50 years, P_{NCR}) chosen

by the National Authorities. An importance factor γ_I equal to 1,0 is assigned to this reference return period. For return periods other than the reference, the design ground acceleration on type A ground a_g is equal to a_{gR} times the importance factor γ_I ($a_g = \gamma_I a_{gR}$).

In Earthquake Resistant Design Regulations KTP-N.2-89, (Albanian Seismic Code) the division in zone of Albanian map is made by intensity seismic scale MSK-64. There are three seismic intensity category VII, VIII, IX (MSK-1964). (Fig. 1b). A probabilistic seismic hazard map of Albania, (Fig. 1a) is presented by Duni & Kuka in 2010 from Albanian Seismic Center.

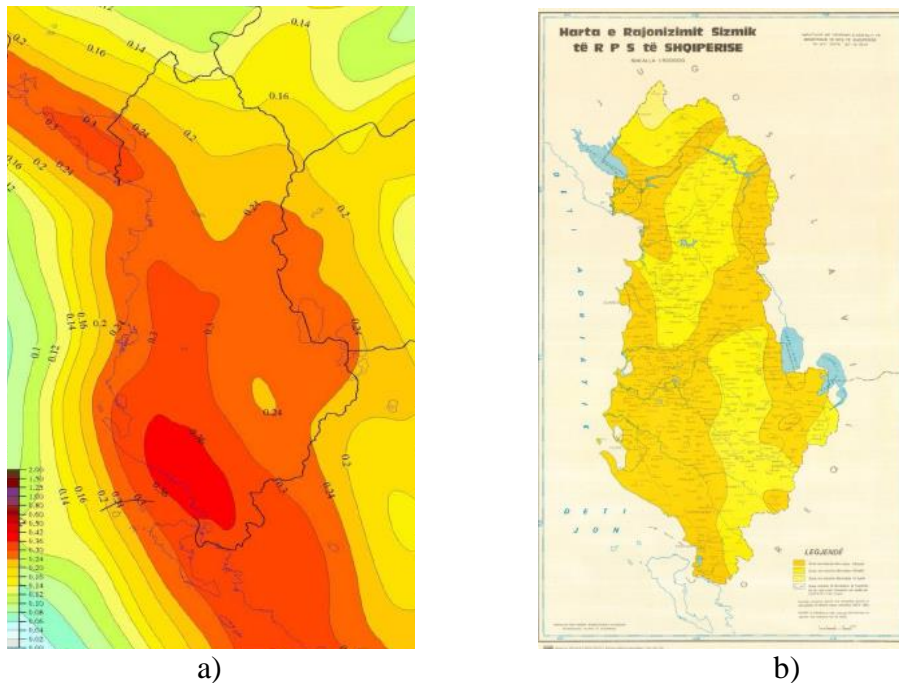


Figure 1. a) Probabilistic seismic hazard map of Albania (Duni & Kuka 2010)
 a_{gR} - reference peak ground acceleration; $T_{NCR} = 475$ years, $P_{NCR} = 10\%$
 b) Seismic zonation map of Albania (Sulstarova 1980)

1.2. Classification of Soil Category

Ground types A, B, C, D, and E, in Eurocode 8 are described by the stratigraphic profiles and parameters given in Table 3.1 (prEN 1998), may be used to account for the influence of local ground conditions on the seismic action. This may also be done by additionally taking into account the influence of deep geology on the seismic action.

In Earthquake Resistant Design Regulations KTP-N.2-89, (Albanian Seismic Code) the classification of soils is made by 3 category; (I, II, III-d category of soils according to Table 1 KTP-89)

1.3. Spectrum Analysis, (horizontal and vertical direction)

In Eurocode 8 spectrum analysis is divide in Horizontal elastic response spectrum and Vertical elastic response spectrum.

The values of the periods T_B , T_C and T_D and of the soil factor S describing the shape of the elastic response spectrum depend upon the ground type (Table 3.2 prEN 1998).

The vertical component of the seismic action shall be represented by an elastic response spectrum, $S_{ve}(T)$. (Table 3.4 prEN 1998)

In KTP-89 vertical response spectrum is equal to horizontal response spectrum multiply by coefficient $2/3$.

1.4. Design ground displacement

According to EC-8, the design ground displacement d_g , corresponding to the design ground acceleration, may be estimated by expression:

$$d_g = 0,025 \cdot a_g \cdot S \cdot T_C \cdot T_D \quad \text{with } a_g, S, T_C \text{ and } T_D \text{ as above.}$$

Displacement according to KTP-89 $u_{ki} = k_E \cdot k_r \cdot \psi \cdot \beta_i \cdot \eta_{ki} \cdot g \cdot (T_i/2\pi)^2$

1.5. Classification of structures for importance coefficient.

Buildings are classified in 4 importance classes (prEN-1998), depending on the consequences of collapse for human life, on their importance for public safety and civil protection in the immediate post-earthquake period, and on the social and economic consequences of collapse.

The importance classes are characterised by different importance factors γ_I .

Table 4-a in KTP-89 gives the building importance coefficient k_r , where the buildings are classified in V category.

1.6. Methods of analysis

The seismic effects and the effects of the other actions included in the seismic design situation may be determined on the basis of the linear-elastic behaviour of the structure.

- The reference method for determining the seismic effects shall be the modal response spectrum analysis, using a linear-elastic model of the structure and the design spectrum.

- Depending on the structural characteristics of the building one of the following two types of linear-elastic analysis may be used:

a) the "lateral force method of analysis"

b) the "modal response spectrum analysis", which is applicable to all types of buildings

- As an alternative to a linear method, a non-linear method may also be used, such as:

c) non-linear static (pushover) analysis;

d) non-linear time history (dynamic) analysis,

In general the horizontal components of the seismic action shall be taken as acting simultaneously.

$$\text{a) } E_{Edx} \text{ "+" } 0,30E_{Edy} \quad \text{b) } 0,30E_{Edx} \text{ "+" } E_{Edy}$$

E_{Edx} , E_{Edy} - action effects due to the application of the seismic action along the chosen horizontal axis x , y respectively of the structure;

If the structural system or the regularity classification of the building in elevation is different in different horizontal directions, the value of the behaviour factor q may also be different.

The sign of each component in the above combinations shall be taken as being the most unfavourable for the particular action effect under consideration.

1.7. Load combination

In Albanian Seismic Code, in combinations of actions for seismic design situations partial factors are defined as follows:

seismic load partial factor is equal to 1,0.

dead load partial factor is equal to 0,9;

live load (long term) partial factor is equal to 0,8;

live load (short term) partial factor is equal to 0,4 (Table 3, KTP-89)

According to EC-8, the inertial effects of the design seismic action shall be evaluated by taking into account the presence of the masses associated with all gravity loads appearing in the following combination of actions:

$\Sigma G_{k,j} \text{ "+" } \Sigma \psi_{E,i} \cdot Q_{k,i}$ where $\psi_{E,i}$ is the combination coefficient for variable action i . (Recommended values of $\psi_{E,i}$ factors for buildings Table A1.1 peEN-1990)

The combination coefficients $\psi_{E,i}$ take into account the likelihood of the loads $Q_{k,i}$ not being present over the entire structure during the earthquake. These coefficients may also account for a reduced participation of masses in the motion of the structure due to the non-rigid connection between them.

2. Analysis of reinforced concrete structures

IN THE EXAMPLE BELOW IT IS SHOWN THE DYNAMIC ANALYSES RESULTS OF DUAL REINFORCED CONCRETE SYSTEM FOR THE BUILDING STRUCTURE.

DYNAMIC ANALYSIS

ACTIVE LOADS THAT ARE TAKEN INTO ACCOUNT ARE:

- | | | |
|----------------|----|---|
| • Dead Load | DL | G |
| • Live Load | LL | P |
| • Seismic Load | EL | S |

LOAD COMBINATIONS

IN ADDITION TO THE DEAD LOAD G AND LIVE LOAD P, THE STRUCTURE IS SUBJECTED TO EARTHQUAKE FORCES S, AND CONSIDERING THAT EARTHQUAKE FORCES ARE SUBJECT TO REVERSALS, THE FOLLOWING LOAD COMBINATIONS MIGHT HAVE TO BE CONSIDERED:

$$1.35 \text{ DL} + 1.50 \text{ LL} \quad (\text{EC2 2.3.3})$$

$$1.0 \text{ DL} + 1.5 \cdot 0.3 \text{ LL} \pm 1.0 \text{ EL} \quad (\text{EC2 2.3.3})$$

These default loading combinations are produced for persistent and transient design situations (EC2 2.2.1.2) by combining load due to dead, live, and earthquake loads according to the simplified formula (EC2 2.3.3.1) for ultimate limit states.

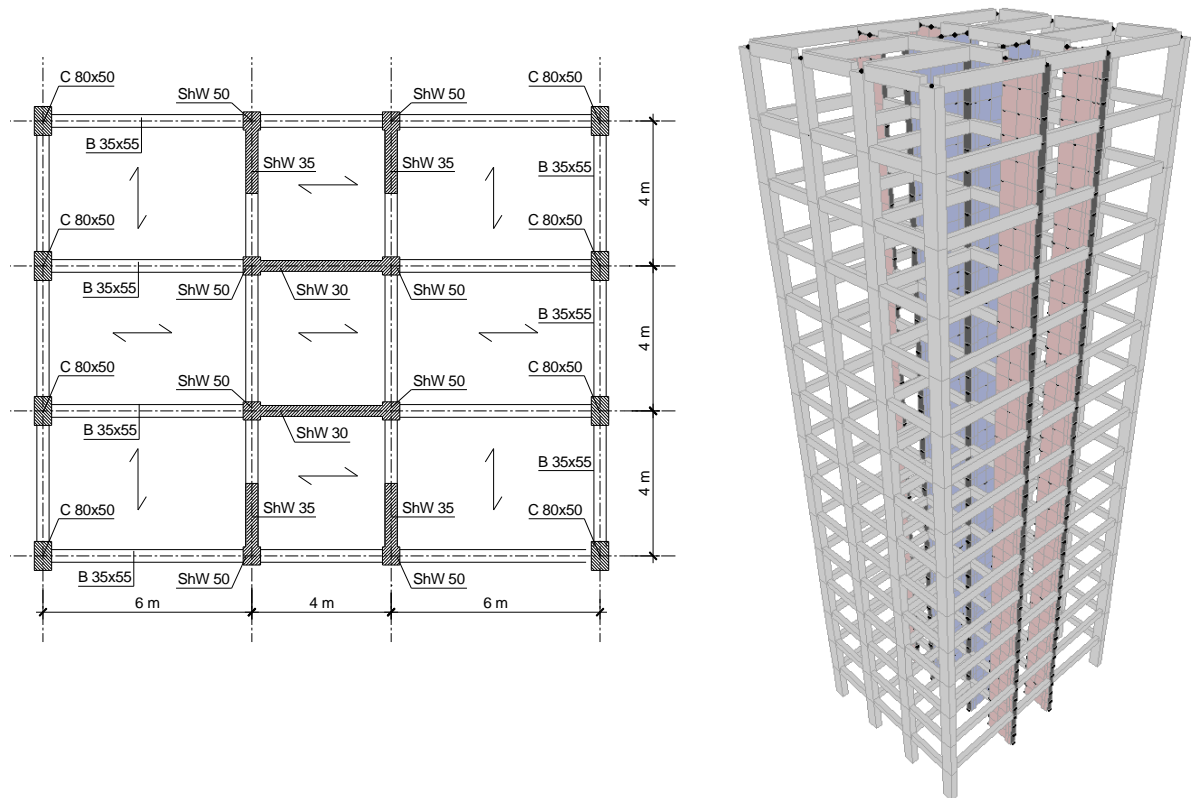


Figure 2. Planimetri and 3D model of reinforced concrete building

Seismic Force according to KTP- N.2-89

Seismic horizontal force in the storey level is defined by formula:

$$E_{ki} = k_E k_r \psi \beta_i \eta_{ki} Q_k$$

$k_E=0.36$ - seismic coefficient, (Tab 2, KTP-N.2-89 Albanian Seismic Code) is presented below Table 1.

Table 1. Seismic coefficient according to soil category and seismic intensity (MSK-1964)

Soil category	Seismic coefficient k_E		
	Intensity VII	Intensity VIII	Intensity IX
I	0.08	0.16	0.27
II	0.11	0.22	0.36
III	0.14	0.26	0.42

$k_r=1.0$ - importance coefficient, Tab 4-a, KTP-N.2-89 Albanian Seismic Code

$\psi=0.28$ - structure coefficient, Tab 5, KTP-N.2-89 Albanian Seismic Code

β_i - dynamic coefficient (Fig.3)

$$1. 0.65 \leq \beta_i = \frac{0.7}{T_i} \leq 2.3 \quad \text{for soil category I}$$

$$2. 0.65 \leq \beta_i = \frac{0.8}{T_i} \leq 2.0 \quad \text{for soil category II}$$

$$3. 0.65 \leq \beta_i = \frac{1.1}{T_i} \leq 1.7 \quad \text{for soil category III}$$

$$\eta_{ki} = \phi_{ki} \frac{\sum_{j=1}^n Q_j \phi_{ji}}{\sum_{j=1}^n Q_j \phi_{ji}^2} \quad \text{- seismic force distribution coefficient}$$

According to Eurocode 8: for ground type - B, Type 1 elastic response spectra (Tab 3.2 pEN 1998 we have this values of parameters:

S=1.2, T_B(s)=0.15, T_C(s)=0.5, T_D(s)=2, for PGA=0.32g, Importance factor γ_I=1, a_g=3.14; Ductility q=3 (Fig.3)

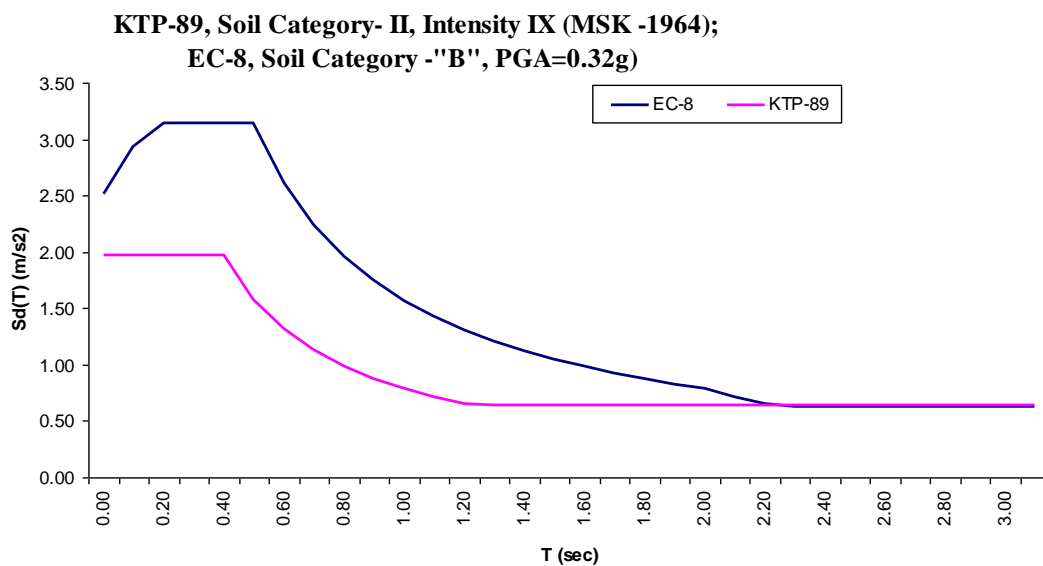


Figure 3. Design response spectrum according KTP-89 & EC-8

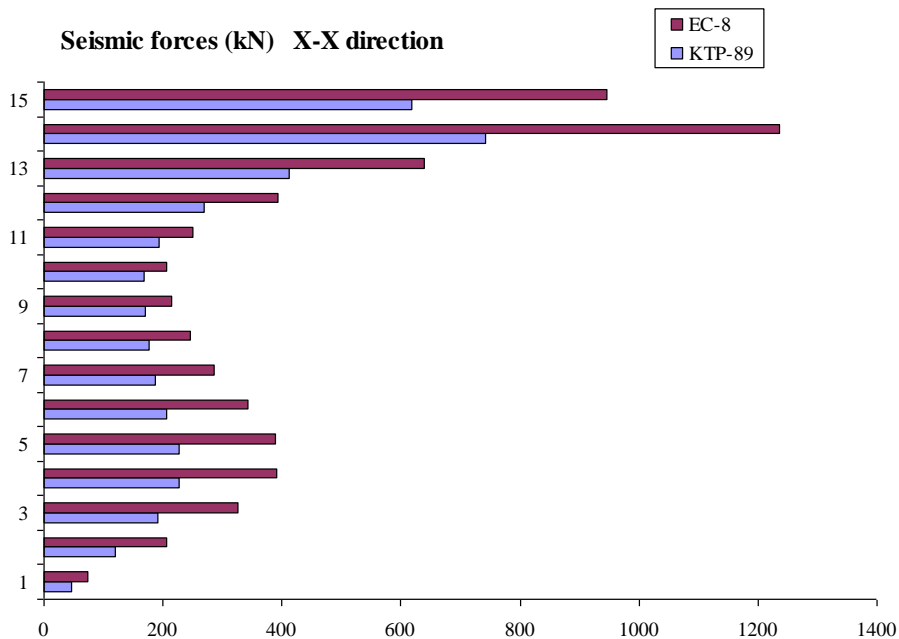


Figure 4. Seismic force in X-X direction according KTP-89 & EC-8

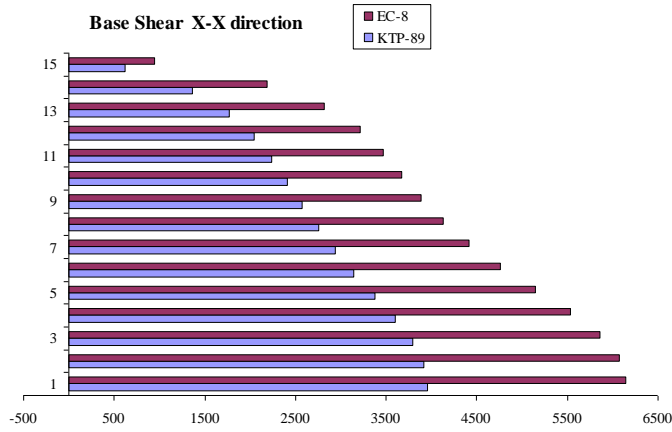


Figure 5. Base shear in X-X direction according KTP-89 & EC-8

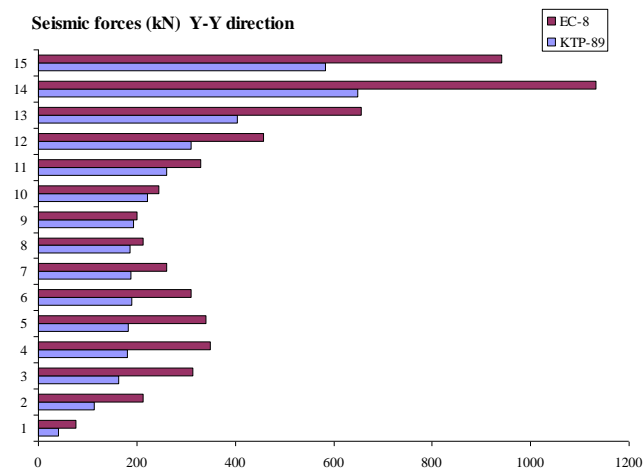


Figure 6. Seismic force in Y-Y direction according KTP-89 & EC-8

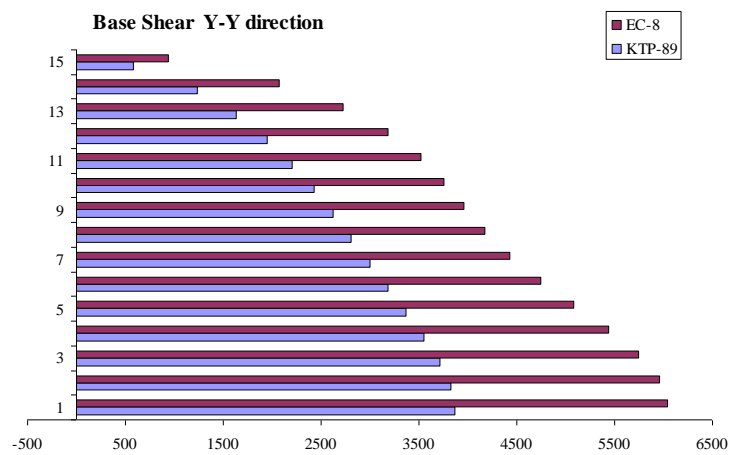


Figure 7. Base shear in Y-Y direction according KTP-89 & EC-8

Table 2. Results for some element in structural model

Elementi 25 (Beam)		
	KTP-89	EC-8
Axial force	0 kN	0 kN
Shear force	21 kN	33 kN
Moment	81 kN×m	123 kN×m

Shear wall		
	KTP-89	EC-8
Axial force	1750 kN	2720 kN
Shear force	2460 kN	3655 kN
Moment	19752 kN·m	30056 kN·m

Elementi 23 (Column)		
	KTP-89	EC-8
Axial force	750 kN	1124 kN
Shear force	31 kN	48 kN
Moment	95 kN·m	146 kN·m

Displacement of the top level		
	KTP-89	EC-8
Joint 1764	6.25 cm	9.36 cm

CONCLUSION

- Design response spectrum input values according to Earthquake Resistant Design Regulations KTP-N.2-89, (Albanian Seismic Code), are considerably lower compared to respective values taken of EC-8 formulations. In structures with low values of fundamental frequency this difference is negligible.
- analyses according to EC-8 presents approximately 30% higher values of seismic loads and base shear in both X,Y horizontal directions compared to respective values based on Earthquake Resistant Design Regulations KTP-N.2-89, (Albanian Seismic Code).
- Generally, structural response under the seismic design situation defined based on EC-8 consists in higher forces and displacements values compared to respective values based on Earthquake Resistant Design Regulations KTP-N.2-89, (Albanian Seismic Code).
- In despite of structural assesment of buildings erected prior to the adaption of Earthquake Resistant Design Regulations KTP-N.2-89, (Albanian Seismic Code), structural examination and reassessment of all buildings according to Eurocode-8 rules must be developed.

Finally, should be mentioned that a properly engineered structure does not necessarily have to be extremely strong or expensive. It has to be properly designed to withstand the seismic effects while sustaining an acceptable level of damage. Basic concepts of the earthquake engineering, implemented in the major building codes, assume that a building should survive a rare, very severe earthquake by sustaining significant damage but without globally collapsing. On the other hand, it should remain operational for more frequent, but less severe seismic events.

REFERENCES

- [1] Seismic Risk Reduction in the Balkan Region, “ Project findings and recommandations”; Terminal UNDP/RER/ 79/014; Serial No. FMNWSC/ OPS/84/228/(UNDP) Paris 1984
- [2] EN 1990 Eurocode : Basis of structural design
- [2] EN 1991 Eurocode 1:Actions on stuctures
- [4] EN 1992 Eurocode 2: Design of concrete stuctures
- [5] EN 1998 Eurocode 8: Design of Structures for Earthquake Resistance.
- [6] Earthquake Resistant Design Regulations: Seismic Center, Academy of Science of Albania. Department of Design, Ministry of Construction. KTP-N.2-89, Tirana, Albania 1989
- [7] Anil K. Chopra, “Dynamic of Structures; Theory and Aplications to Earthquake Engineering”, Prentice Hall, New Jersey, USA 1995.
- [8] T. Paulay and M.J.N. Priestley, “Seismic Design of Reinforced Concrete and Masonry Buildings”, San Diego, USA, 1981.

Monitoring the Condition of a Bridge using a Traffic Speed Deflectometer Vehicle Travelling at Highway Speed

Eugene J. OBrien^{1,2}, Enrique Sevillano¹, Daniel Martinez¹

¹*School of Civil Engineering, University College Dublin, Ireland*

²*Roughan O'Donovan Innovative Solutions, Consulting Engineers, Ireland*

ABSTRACT

The Traffic Speed Deflectometer (TSD) is a vehicle incorporating a set of laser Doppler vibrometers on a straight beam to measure the relative velocity between the beam and the pavement surface. This paper describes a numerical study to see if a TSD could be used to detect damage in a bridge. From this measured velocity it is possible to obtain the curvature of the bridge, from whose analysis, it will be demonstrate that information on damage can be extracted.

In this paper a Finite Element model is used to simulate the vehicle crossing a single span bridge, for which deflections and curvatures are calculated. From these numerical simulations, it is possible to predict the change in the curvature signal when the bridge is damaged. The method looks promising and it suggests that this drive-by approach is more sensitive to damage than sensors installed on the bridge itself.

Key words: Bridge, TSD, Doppler Laser, vibrometer, dynamics, deflection, curvature, damage, SHM, Instantaneous Curvature, IC.

INTRODUCTION

Many efforts have been put in recent years to develop monitoring methodologies in order to enhance and complement the health inspections of a wide range of engineering infrastructures, bridges among them. Most of these approaches are based on structural vibration data, so that conclusions about damage existence can be inferred from the measurable changes in the dynamic properties of the bridge (natural frequencies, mode shapes, etc.). However, the main drawback of all these methods is the necessity of a high number of sensors directly installed on the bridge.

Bridge monitoring traditionally relies on visual inspections. While this is arguably still the best means of confirming structural condition, there are issues with the objectivity of inspectors. There have been considerable efforts in recent years to develop systems of sensors to complement or replace the information obtained by the inspector. Some authors [1] have suggested that visual inspection alone may not be adequate for bridge health monitoring. In countries like Japan, which is prone to natural disasters, it is recommended that monitoring of engineering infrastructure should be conducted continuously [2].

A popular SHM approach is the use of structural vibration data for damage assessment. The principle is that if damage occurs in a structure, its physical properties change, (e.g. local loss of stiffness) which cause measurable changes in the bridge's dynamic properties. Based on which dynamic properties or damage features are considered, such damage identification methods can be categorized as [3]: (i) natural frequency-based; (ii) mode shape-based; (iii) modal curvature-based or (iv) other approaches based on modal parameters. Methods based on curvature are particularly promising but require a great number of sensors on the bridge if damage is to be detectable at all points.

In that sense, 'drive-by' monitoring has risen in importance as an alternative to the sensor network based solutions, given its capability to derive the dynamic properties of bridge structures from the dynamic response of a passing vehicle. The idea of drive-by monitoring, in which the dynamic properties of bridge structures are inferred from the dynamic response of a passing vehicle, is proposed by Yang et al. [4, 5]. While the vehicle may be expensive, this approach is low cost as it can be applied throughout the fleet without the need to install any sensors on the bridges themselves. It involves a vehicle instrumented with sensors through which dynamic properties of the bridge are extracted. Through interaction between the bridge and vehicle, the moving vehicle can be considered as both exciter and receiver. The feasibility of this method in practice was experimentally confirmed by Lin and Yang [6] by passing an instrumented vehicle over a highway bridge in Taiwan.

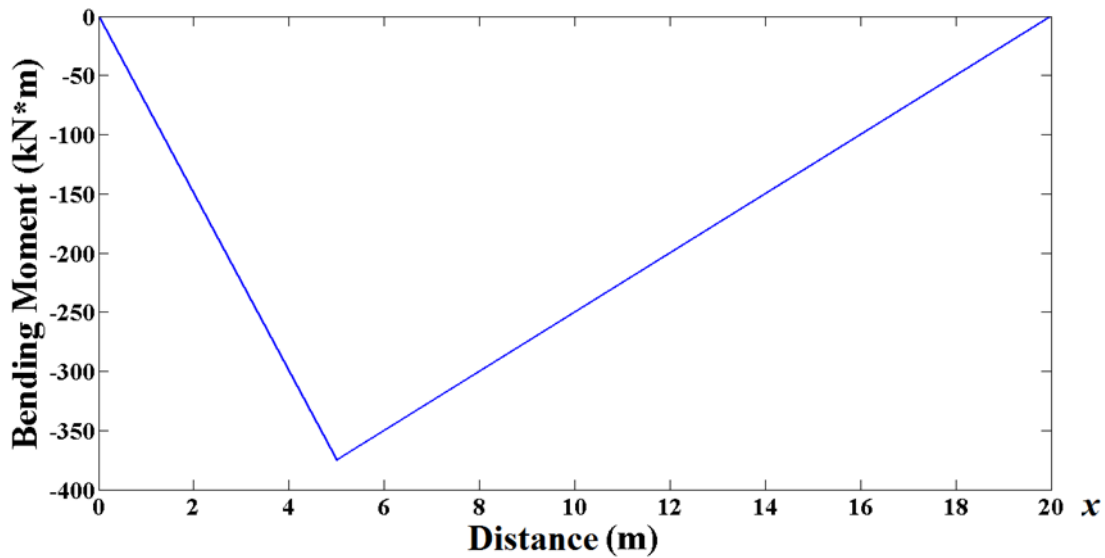
Falling Weight Deflectometers are traditionally used to measure pavement stiffness, but the vehicle is stationary and there are concerns about safety and traffic disruption. As a result, the Traffic Speed Deflectometer (TSD) has been developed as an alternative means of measuring pavement stiffness using a vehicle travelling at full highway speed. OBrien & Keenahan [7] were the first to propose the idea of using a TSD for bridge monitoring. While the concept has yet to be proven, this paper will demonstrate that there is considerable potential, provided measurements of sufficient accuracy can be obtained [8]. However, the number of measurements is affected by the time the vehicle is on the bridge, making it harder to develop an indicator that is sensitive to damage. A TSD uses a set of laser vibrometers to accurately measure the derivative of the distance between the vehicle and the road surface profile [9, 10]. In the case of the TSD travelling over a bridge, this distance will include a combination of vehicle movements, road surface profile and bridge vibrations. The latter information, when separated from the other components, has the potential to be sensitive to damage in the bridge.

static response to passing load

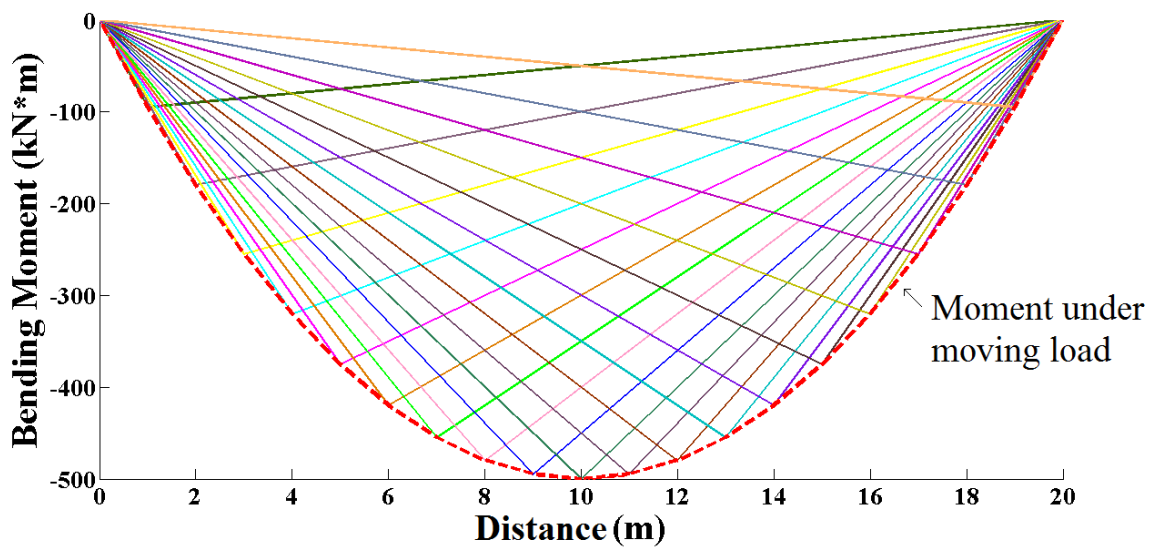
The simplest case is considered first: the static response to a point force crossing a beam (Figure 1(a)). The bending moment diagram due to a point force at a fixed point is illustrated in Figure 1(b) and the bending moment diagrams due to a moving point force (various values of x) are illustrated in Figure 1(c). In a TSD, the sensors constitute moving references so a sensor located at the force would always sense data corresponding to the maximum bending moment. This corresponds to the peaks of the bending moment diagrams of Figure 1(c). This peak bending moment varies smoothly from the start to the finish.



(a) Force at a fixed point, x , on the beam with $P=100kN$.



(b) Bending moment diagram due to force at a fixed point, x



(c) Bending moment diagrams due to moving load

Figure 6. Bending moment response to point force on a beam

Curvature, the second derivative of deflection, is given by M/EI , where M is moment and EI is stiffness, product of modulus of elasticity, E , and second moment of area, I . Hence, for a beam of constant stiffness, curvature varies smoothly and in proportion to the peak moments illustrated in Figure 1(c). Hence, if there is a local loss of stiffness, as would occur if a beam

were damaged, there will be a sharp local increase in curvature. An example is illustrated in Figure 2, where stiffness has been reduced by 20% locally at quarter-span and mid-span.

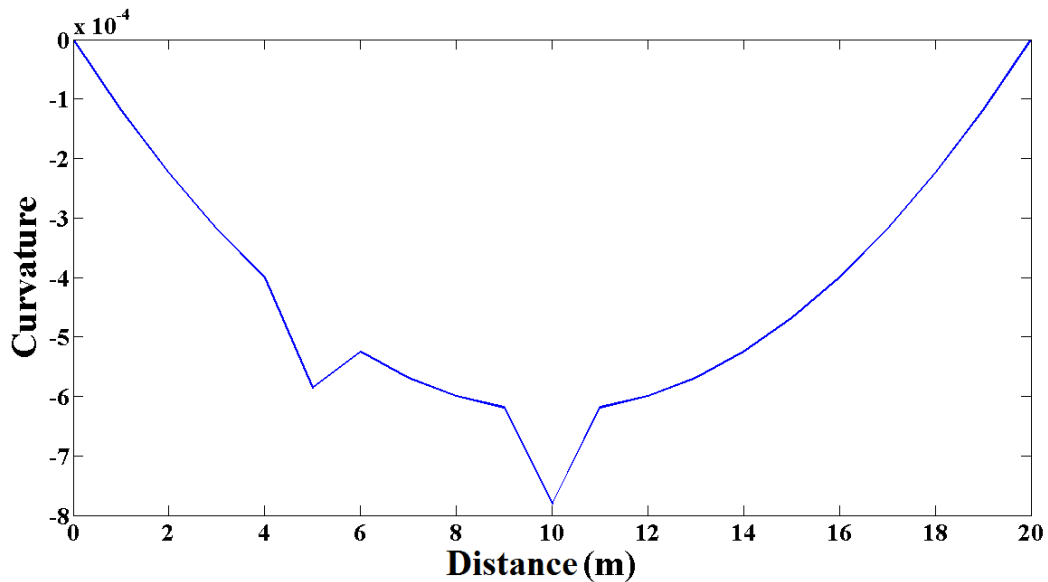


Figure 2. Curvature, calculated numerically from deflections at adjacent points, under a moving point force in a beam with 20% local stiffness reductions at quarter- and mid-span

vehicle bridge interaction model

A vehicle/bridge dynamic interaction model has been developed in MATLAB. The half-car (HC) vehicle model of Figure 3 has been developed using the vehicle properties listed in Table 1. The HC model has 4 degrees of freedom (DOFs): sprung mass bounce translation, pitch rotation and the two unsprung mass (axle hop) translations. Some of the Traffic Speed Deflectometer (TSD) characteristics have been taken into account in the model, in view of its potential as a drive-by monitoring vehicle [8]. A high velocity is chosen to represent highway conditions.

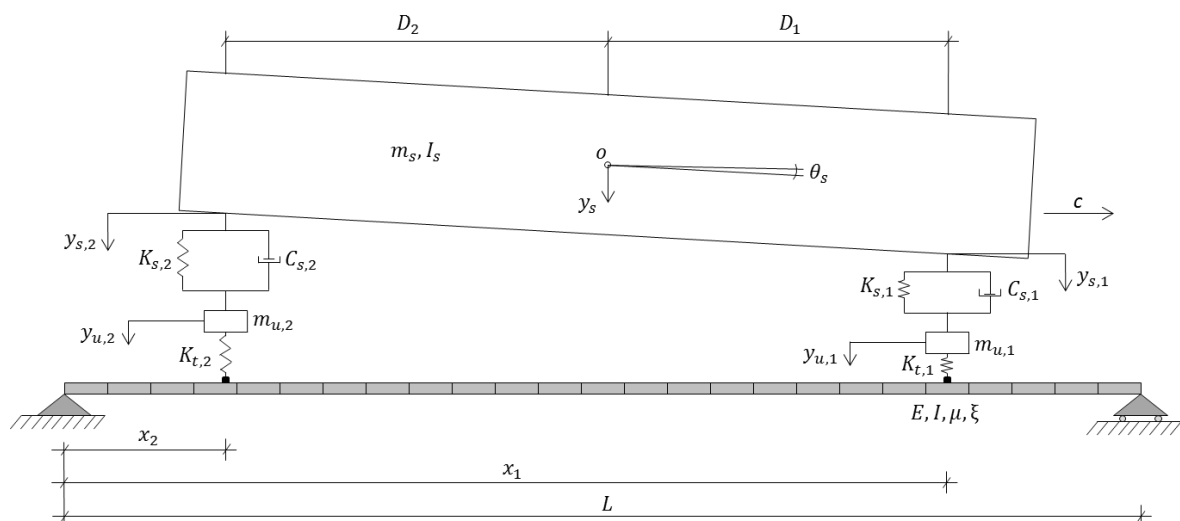


Figure 3. Half-car model, adapted from [11]. (Notation given in Table 1)

Table 1. Geometrical and mechanical properties of the modelled HC vehicle

Property and notation	Notation	Value
Weight of the sprung mass	m_s	18 t
Unsprung mass axle 1	m_{u1}	1000 kg
Unsprung mass axle 2	m_{u2}	1000 kg
Length of the vehicle	L_v	11.25 m
Tyre 1 stiffness	$K_{t,1}$	1.75×10^6 N/m
Tyre 2 stiffness	$K_{t,2}$	3.5×10^6 N/m
Damper 1 stiffness	$K_{s,1}$	4×10^5 N/m
Damper 2 stiffness	$K_{s,2}$	10^6 N/m
Damper 1 damping	$C_{s,1}$	10^3 Ns/m
Damper 2 damping	$C_{s,2}$	2×10^3 Ns/m
Distance of centre of gravity from axle 1	D_1	3.8 m
Distance of centre of gravity from axle 2	D_2	3.8 m
2 nd moment of area	h	3.76 m
Velocity	c	80 km/h (22.22 m/s)

The bridge is modelled as a beam with 1-dimensional finite elements. Contact is imposed at each time step between the axles and the relevant points on the bridge. A smooth road surface profile has been used for this example. It is acknowledge that this removes the influence of road profile thereby greatly improving the prospects of damage detection. The healthy bridge has the properties listed in Table 2.

Table 2. Geometrical and mechanical properties of the modelled bridge

Bridge Property	Value
Number of elements	20
Frequency	1000 Hz
Length	20 m
Young's modulus	35×10^6 kN/m ²
2 nd moment of area	1.26 m ⁴
Mass per unit length	37500 kg/m
Damping	3%
First natural frequency	4.26 Hz
Length of the approach	100 m

RESULTS AND DISCUSSION

Damage is represented in this example as a 20% loss of stiffness over a 2m length, 7.5 m from the left support of the 20 m long bridge as shown in Figure 4. It can be seen in Figure 5 that (assuming that vehicle motion can be removed) there is a clear difference in the absolute bridge displacements under the axles between the healthy and damaged cases. It is not apparent from this figure where the damage is located. Furthermore, the quantity of the damage is difficult to estimate, as the influence of damage propagates through the entire beam and damage

near the centre causes more displacement than damage near the supports. Due to this influence, damage location and the maximum increase in deflection do not correspond in the figures. For the first axle in particular, there is little difference in the displacements at the damage location. It is only when the first axle is near three quarter-span and the second axle reaches the damage location that the difference between the signals becomes large. Both axles interact and it causes the change of curvature at the first stage in Figure 5a due to the entrance of the second axle and the second stage in Figure 5b when the first axle leaves the bridge.

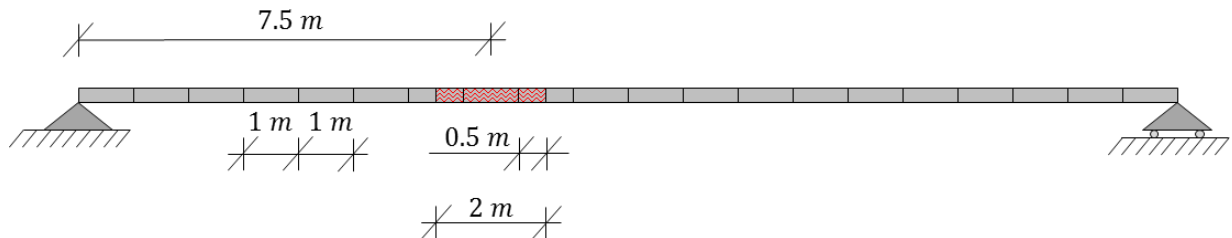


Figure 4. Bridge displacements at axle location, a) first axle, b) second axle.

Fortunately, while translation under the moving reference is not a good indicator of local damage location, curvature is much better. This is illustrated in Figure 6 which shows the Instantaneous Curvatures (ICs), i.e., the 2nd derivatives with respect to distance (calculated at fixed points in time) of the calculated displacements under or near the moving load. These derivatives are calculated numerically, assuming three laser measuring devices at 1 m intervals that record simultaneously.

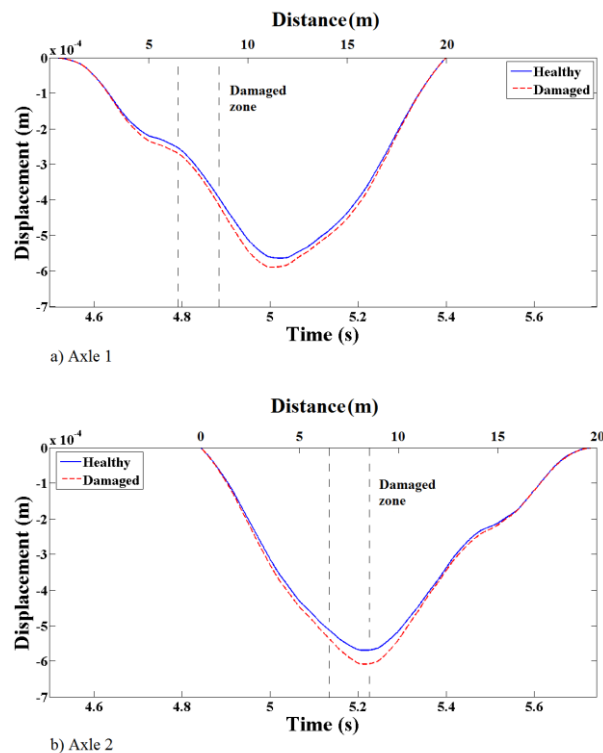


Figure 5. Bridge displacements at axle location, a) first axle, b) second axle.

The damage can be easily detected by IC in Figure 6, since the change in the curvature matches exactly with the damaged location in the bridge. Hence, this approach is able not only to identify damage in the bridge, but also to accurately localize it. Furthermore, just by calculating the difference between the healthy and the damaged bridge ICs, it is easy to check that the maximum relative error is 23% for the first axle's curve and 26% for the second one; in both cases around 8 m from the left support of the 20 m long bridge. As $1/0.8=1.25$, this constitutes a fairly good prediction of the induced 20% loss of stiffness, as specified above. Hence, quantification of damage magnitude is also possible when using IC as a damage indicator. Finally, focusing on the healthy and damaged curvatures at any point outside of the damaged region, it is shown in Figure 6 they match almost perfectly for the rest of the length of the bridge. In Figure 4, on the other hand, this does not happen, especially from the instant when the second axle arrives to the bridge, due to some dynamic effects.

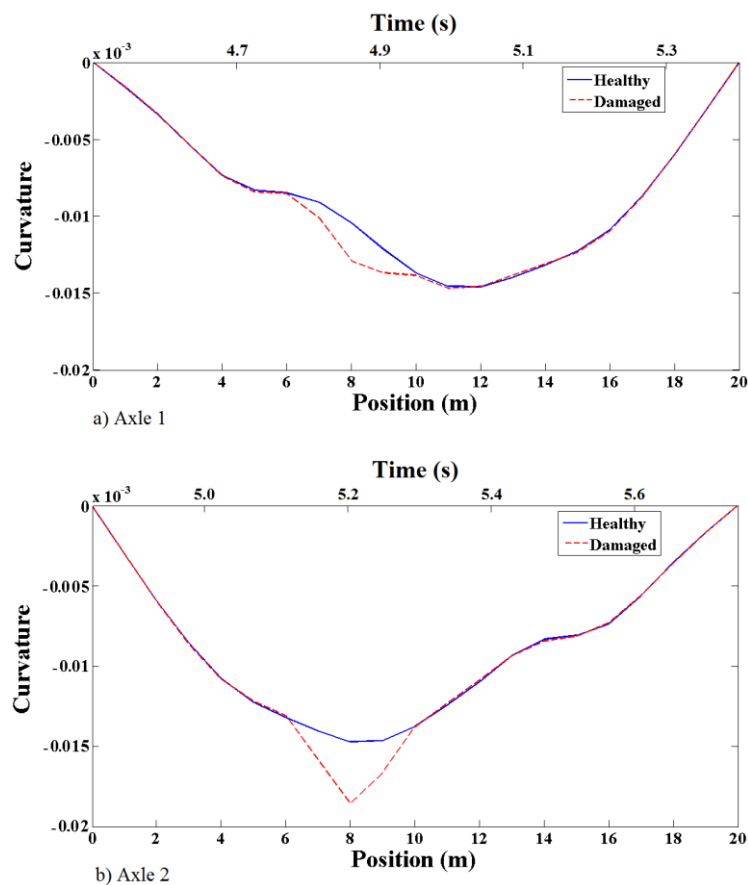


Figure 6. Instantaneous curvatures at axle location, a) measured at first axle, b) measured at second axle.

It is important to note that IC is not the 2nd derivative of the curves shown in Figure 5. These are moving reference translations so successive points represent different points in both space and time. IC is, by definition, the 2nd derivative with respect to distance at a *fixed* point in time. Figure 7 shows the 2nd derivatives of the curves in Figure 5 which can be seen to be quite different from the curves of Figure 6. While there are clear differences between the healthy and damaged cases in Figure 7, some of these differences are the result of bridge vibration under the moving axles.

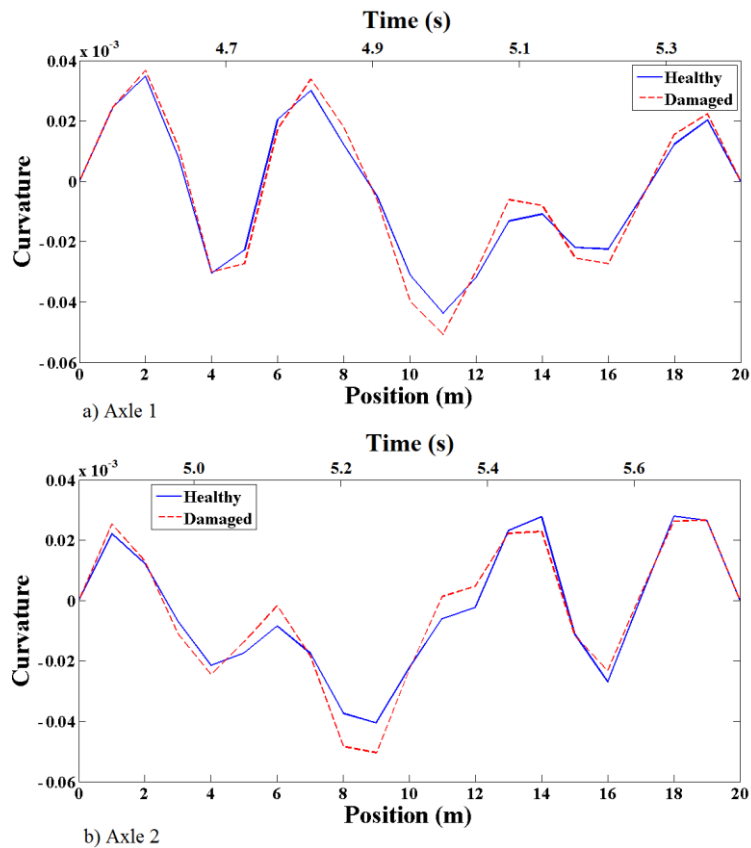


Figure 7. Second derivatives of moving reference translation: a) measured at first axle, b) measured at second axle, as they are influenced by the time.

CONCLUSIONS

IC is a promising parameter for use as a damage indicator. The differences between healthy and damaged curves are clearly greater around the damage location when using curvatures rather than deflections. Of course measuring curvature is considerably more difficult than measuring translation. As a second derivation, it is much more sensitive to measurement noise. However, the TSD already measures the curvature of the deflection ‘trough’ under the heavy weight for pavement stiffness assessment purposes. Further, curvature is independent of the road profile. In addition, as demonstrated with the example studied in this work, curvature enables damage identification at three levels: damage identification, location and quantification, which was not possible when using deflection measurements to estimate damage. Furthermore, healthy and damaged bridge curves suffer small or negligible differences from each other in non-damaged locations, which means that this approach can also lead to a reduction in the number of false warnings in the damage prediction procedure.

ACKNOWLEDGEMENTS



The authors acknowledge the support for the work reported in this paper from the European Union’s Horizon 2020 Research and Innovation Programme under the Marie Skłodowska-Curie grant agreement No. 642453.

REFERENCES

- [1] Chupanit, P. and Phromsorn, C. (2012) The Importance of Bridge Health Monitoring. *International Science Index*, **6**,135-138.
- [2] Fujino, Y, Siringoringo, D.M. (2011) Bridge monitoring in Japan: the needs and strategies. *Structure & Infrastructure Engineering*, **7**, 597-611.
- [3] Fan, W. and Qiao, P.Z. (2011) Vibration-based Damage Identification Methods: A Review and Comparative Study, *Structural Health Monitoring*, **10**, 83-111.
- [4] Yang, Y.B. Lin, C.W. and Yau, J.D. (2004) Extracting bridge frequencies from the dynamic response of a passing vehicle, *Journal of Sound and Vibration*, **272**, 471-493.
- [5] Yang, Y.B. and Lin, C.W. (2005) Vehicle-bridge interaction dynamics and potential applications, *Journal of Sound and Vibration*, **284**, 205-26.
- [6] Lin, C.W. and Yang, Y.B. (2005) Use of a passing vehicle to scan the fundamental bridge frequencies: An experimental verification, *Engineering Structures*, **27**, 1865-1878.
- [7] OBrien, E. J., & Keenahan, J. (2015). Drive-by damage detection in bridges using the apparent profile. *Structural Control and Health Monitoring*, **22**(5), 813-825.
- [8] Rada G.R., Nazarian S., Visintine B.A., Siddharthan R.V., Sivaneswaran N. (2015) Use of High-Speed Deflection Devices in Network-Level PMS Applications: Are We Ready? *9th International Conference on Managing Pavement Assets*, Alexandria, Virginia, USA, Diefenderfer B. & Katicha M., pp. 12.
- [9] Rassmussen S., Aagaard L., Baltzer S., Krarup J. (2008) A comparison of two years of network level measurements with the Traffic Speed Deflectometer. *Transport Research Arena Europe*, Znidaric A., ZAG Ljubljana, Ljubljana, Slovenia, 1-8.
- [10] Malekjafarian A., McGetrick P. J., OBrien E. J. (2015) A Review of Indirect Bridge Monitoring Using Passing Vehicles. *Shock and Vibration*, 2015:16.
- [11] McGetrick, P. Kim, C.-W. Gonzalez, A. (2013) Dynamic axle force and road profile identification using a moving vehicle, *International Journal of Architecture, Engineering and Construction*, **2**(1), 1-16.

Seismic Displacement Demand of a Mid-Rise RC Building Considering Soil Structure Interaction

Bayram Tanik Cayci¹ and Mehmet Inel¹

¹Department of Civil Engineering, Pamukkale University, Denizli, Turkey

ABSTRACT

This study aims to evaluate the effect of soil structure interaction and the differences in linear and nonlinear modelling of the structure on seismic response. For this purpose, SSI and fixed base models of 7-story building were used. Both linear and nonlinear behavior of the building are taken into account for comparison.

The findings obviously indicate large variation in displacement demands depending on ground motion record, soil type, consideration of soil structure interaction and linear and nonlinear structure modelling. The displacement demands tend to increase for softer soils except few cases, especially for fixed base models. Significant differences are obvious for linear and nonlinear building models of fixed base case. The evaluation of obtained results and observations in the current study clearly indicate that the effects of SSI approach depend on dynamic characteristics of soil and structure. While soil deformations influence the seismic demands of structure in positive way for linear models, these effects are more complex for nonlinear models. It is difficult to mention about certain trend for nonlinear models. It should be also kept in mind that linear fixed base models are inappropriate for dynamic analysis due to high sensitivity of dynamic amplification and the use of fixed base linear models may cause inaccurate seismic demand estimates.

The outcomes and observations emphasize that the demand estimates are independent from the fixed base or SSI approaches and linear or nonlinear models for stiffer soils. All combinations provide reasonable demand estimates. However, the modelling approach becomes extremely important for softer soils. The best approach seems to be SSI with nonlinear modelling. The fixed base with nonlinear modelling also provides acceptable estimates.

Keywords: Fixed Base; Linear Analysis; Nonlinear Analysis; RC Building; Seismic Demand; Soil Structure Interaction (SSI); Time History Analysis

INTRODUCTION

Seismic response of structures is directly influenced by soil behavior under dynamic loads. Soil deformations and rotations at the base of structure may change the dynamic behavior of buildings. It is well known that building input motion and free-field motion can differ due to the presence of structure as well as the frequency content and amplitude of motion. These effects are more pronounced for softer soil profiles and stiffer superstructures.

The interaction between soil and structure is generally neglected with the fixed base assumption. However, soil structure interaction is an important issue for the behavior of structures on soft soils. Soil Structure Interaction (SSI) approach includes much more complexity compared to fixed base assumption inherently [1-3]. Soil properties, characteristics of input motions and transmitting boundary conditions are significantly effective parameters in modelling. Therefore, it is important to define SSI problem with minimum error and as simple as possible.

This study aims to evaluate the effect of soil structure interaction and the differences in linear and nonlinear modelling of the structure on seismic response. For this purpose, SSI and fixed base models of 7-story building were used. Both linear and nonlinear behavior of the building are taken into account for comparison.

The selected 7-story building was designed according to modern Turkish Earthquake Code [4] considering both gravity and seismic loads. 7 ground motion records and 4 soil types with different stiffness were taken into account during linear and nonlinear time history analyses.

METHODOLOGY

In this study, direct approach with finite element method (FEM) was preferred and three-dimension linear and nonlinear time history analysis has been performed using general-purpose structural analysis program Sap2000 [5]. Schematic illustration of a direct method model of soil-structure interaction problem is given in Figure 1a. Three dimensional frame system of building and Solid FEM model of soil were simultaneously taken into account in mathematical model and analysis in single step [6]. The equation of motion can be written as follows:

$$[M]\{\ddot{u}\} + [C]\{\dot{u}\} + [K]\{u\} = -[M]\{\ddot{u}_g\}$$

where $\{\ddot{u}_g\}$ represents the input motion of model, $[M]$, $[C]$ and $[K]$ are respectively the mass, viscous damping and stiffness matrix of the total system, $\{\ddot{u}\}$, $\{\dot{u}\}$ and $\{u\}$ are respectively acceleration, velocity and displacement vectors.

Viscous boundary approach was used to eliminate propagating waves [7] and the bottom of soil layer is assumed to be on the rock as defined as fixed at the bottom in the models. Mesh length of soil is taken as 0.5 m and 2 m at adjacent to building and distant locations, respectively.

Four different soil types were considered during analyses by taking into soil classification of FEMA. Soil dimensions are taken as 80 m in X, 70 m in Y directions and 20 m in depth. Although there might be differences, soil layer profile was assumed to be uniform throughout depth. Detailed information about soil properties are given in Table 1. The 3-D view of soil-structure model is shown in Figure 1.b.

Free-field motions recorded on rock were used in the current study. The records were applied at the bottom of soil layer were processed to obtain soil amplified records at the top layer. This is an accepted assumption as mentioned in literature; SAP2000 program, using the SOLID element, can be used to calculate either the one, two or three dimensional free-field motions at the base of a structure if the soil material is considered as linear [8]. The amplified records were used for the fixed base models as input motion while the records were directly applied at the bottom of soil layer for SSI cases.

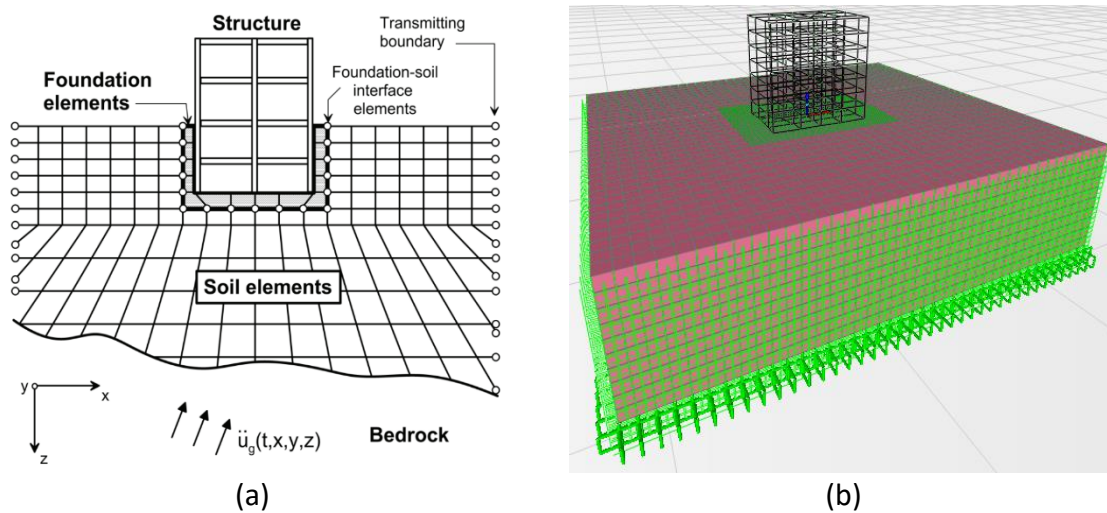


Figure 7 (a) Schematic illustration of a direct approach [9], (b) 3D view of soil-structure model

Table 2 Soil Properties

Soil:	Shear Wave Velocity, V_s (m/s)	Soil Profile Type (FEMA)	Density (kN/m ³)	Poisson Ratio	Damping (%)
S1	800	B	2.25	0.25	%5
S2	400	C	2.15	0.30	%5
S3	200	D	1.80	0.40	%5
S4	150	E	1.60	0.40	%5

Building Models

A 7-story RC building was selected to represent mid-rise residential buildings located in the high seismicity region of Turkey in the current study. Building model is typical beam-column RC frame building with no shear walls. Plan view of model can be seen in Figure 2a. The selected reference model was designed according to modern Turkish Earthquake Code considering both gravity and seismic loads. A design ground acceleration of 0.4 g and soil class Z3 that is similar to class C soil of FEMA-356 [10] was assumed.

Nonlinearity of structural models was defined with lumped plasticity by defining plastic hinges at both ends of beams and columns. As shown in Figure 2b, five points labelled A, B, C, D and E define force-deformation behaviour of a typical plastic hinge. The typical nonlinear static analysis has a decrease in lateral load carrying capacity at point C. In this study the decrease at point C is ignored for numerical problems in SAP2000. The values assigned to each of these points vary depending on type of element, material properties, longitudinal and transverse steel content, and axial load level on the element. Plastic hinge length is assumed to be equal to half of the section depth as recommended in 2007 Turkish Earthquake Code [11] and other documents (such as ATC-40 [12], FEMA-356 etc.). Also, effective stiffness values are obtained per the code; 0.4EI for beams and values between 0.4 and 0.8EI depending on axial load level for columns. Shear hinges were also defined at the middle of columns to reflect brittle behaviour of members. Shear hinges were not effective on results in the scope of this study since none of column members reached the shear capacity.

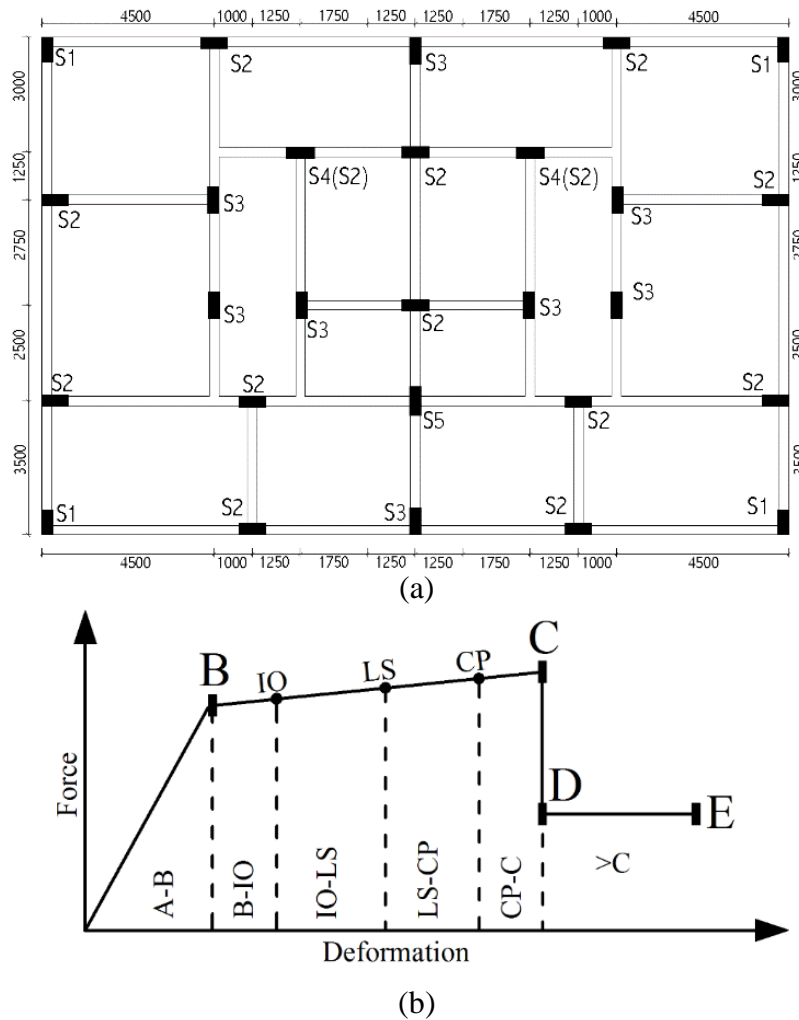


Figure 8 (a) Plan view of the 7-story building, (b) Force-deformation relationship for a typical plastic hinge

Ground Motion Records

Ground motions recorded on rock soil were used during dynamic time history analyses. For this purpose, 7 records were taken from the stations with shear velocity values greater than 750 m/s. Table 2 lists the records considered in this study [13,14].

Results

Roof displacement demands and displacement profiles of SSI and fixed base approaches are compared for both linear and nonlinear models to understand the effects of soil structure interaction and linear or nonlinear modelling of structures on seismic behavior. Table 3 illustrates roof displacement demands of 7-story building models with fixed base and SSI approaches for linear and nonlinear cases. The table obviously indicates large variation in displacement demands depending on ground motion record, soil type, consideration of soil structure interaction and linear and nonlinear structure modelling. The displacement demands

tend to increase for softer soils except few cases, especially for fixed base models. Significant differences are obvious for linear and nonlinear building models of fixed base case.

Table 2 Information about ground motion records used in the study

Identifier	Earthquake	Date	Magnitude	Station	Comp.	PGA	PGV	Dist.
		(dd/mm/yy)			(°)	(g)	(m/s)	(km)
IR80STUR.000	Irpinia Italy	23.11.1980	M _w = 6.5	Sturno	360°	0.251	0.37	32.00
IR80STUR.270	Irpinia Italy	23.11.1980	M _w = 6.5	Sturno	270°	0.358	0.527	32.00
KB95KBU.000	Kobe	16.01.1995	M _w = 6.9	Kobe Univ.	360°	0.29	0.53	0.90
KC99IZT.090	Kocaeli	17.08.1999	M _w = 7.4	Izmit	90°	0.22	0.298	4.80
LP89G01.090	Loma Prieta	18.10.1989	M _w = 6.9	Gilroy Array 1	90°	0.473	0.339	11.20
LP89G01.000	Loma Prieta	18.10.1989	M _w = 6.9	Gilroy Array 1	360°	0.411	0.316	11.20
NR94GPO.270	Northridge	17.01.1994	M _w = 6.7	USGS Griffith Park Obs.	270°	0.246	0.211	23.80

Table 3 Roof displacement demands of the 7-story building (mm)

Linear								
Record:	SSI				Fixed Base			
	S4	S3	S2	S1	S4	S3	S2	S1
IR80STUR.000	95.7	91.1	61.4	53.7	259.1	144.5	64.4	53.8
IR80STUR.270	87.2	70.2	56.5	43.6	171.4	104.3	61.0	42.5
KB95KBU.000	152.5	113.4	96.1	85.6	272.4	123.5	85.2	79.8
KC99IZT.090	82.8	60.8	54.6	43.7	203.4	80.0	56.5	42.8
LP89G01.000	83.9	85.3	60.2	39.4	155.2	147.5	75.2	39.8
LP89G01.090	75.6	148.0	69.3	61.3	187.3	263.6	84.6	64.7
NR94GPO.270	157.7	137.6	99.5	88.1	294.4	198.2	92.7	85.5
Nonlinear								
Record:	SSI				Fixed Base			
	S4	S3	S2	S1	S4	S3	S2	S1
IR80STUR.000	129.9	91.0	60.5	49.6	129.6	128	63.7	51.5
IR80STUR.270	109.9	100.9	84.7	53.2	112.5	105.5	101.5	65.8
KB95KBU.000	315.8	194.2	131.9	113.9	266.9	161.5	114.8	100.9
KC99IZT.090	104.4	60.8	54.0	39.7	104.4	59.8	61.9	47.0
LP89G01.000	75.7	87.0	53.7	35.4	61.7	86.1	54.6	37.2
LP89G01.090	101.9	160.4	85.8	54.6	126.0	141.1	87.5	63.2
NR94GPO.270	176.9	96.9	76.8	67.8	157.8	110.4	65.1	57.1

Figure 3 plots displacement demand ratio of SSI and fixed base cases for linear and nonlinear models, separately. The scatter in linear building model is evident indicating significant differences between fixed base and SSI models. The fixed base model estimates are extremely higher than the SSI estimates except Kobe and Northridge records for S1 and S2 soils. This means that the fixed base model tends to overestimate displacement demands especially on softer soils for linear behavior. The fixed base and SSI models give reasonable estimates only for stiffer soil S1. As the soil gets softer, the discrepancy in estimates of the fixed base and SSI models increases for linear building behavior.

The average displacement demand ratios of SSI and fixed base models for 7 ground motions are also plotted on the figure. It is interesting that the average ratios of linear behavior is close to unity for S1 and S2 soils, indicating similar demand estimates of both models. This is expected behavior because as the soil gets stiffer it approaches to the fixed base model. However, the average of fixed base model estimates exceeds twice of SSI estimates for S4 soil type. Figure 3 obviously illustrates that both variation and the difference between fixed base and SSI approach estimates tend to decrease with increasing soil stiffness in linear behavior. It is well accepted that SSI approach in linear models estimates smaller displacement demands for softer soils due to energy dissipated by soil movement and base rotations. The observations in Figure 3 are compatible with the common view about soil structure interaction effects.

Although similar scatter to linear behavior is observed in nonlinear behavior, the ratio of SSI and fixed base estimates ranges around unity, having values of about 0.7 to 1.2. It is hard to mention about the positive influence of SSI approach for nonlinear behavior. It is also interesting that the average ratios of 7 records are very close unity meaning that both SSI and fixed base approaches give similar displacement demand estimates in average sense. It is hard to conclude a clear tendency related to the performance of SSI or fixed base approach for nonlinear behavior. Besides, there is no clear soil type dependence in estimates. Nevertheless, fixed base model displacement demand estimates is acceptable in average sense when nonlinear behavior of building is considered.

Plastic deformations change seismic response of structure and phase shift due to deviation of dynamic response may cause increment or decrement on relative structure displacement demands. Thus, the effect of SSI for nonlinear models is a much more complex problem compared to linear models. This phenomenon is highly depended by soil and structural properties as well as frequency content of input motion.

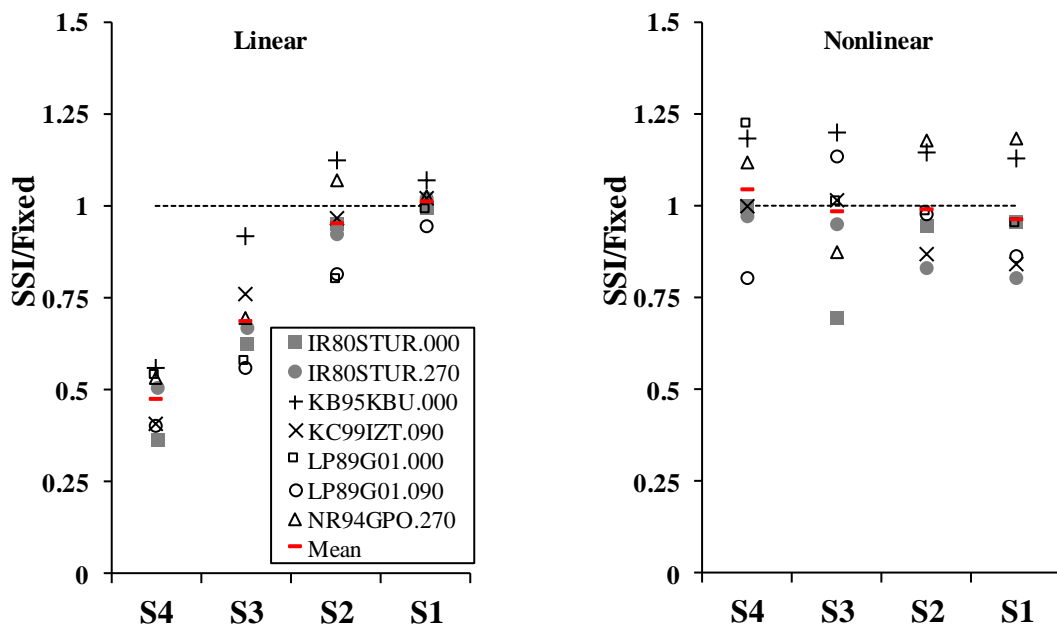


Figure 9 Comparisons of roof displacement demand ratios of SSI and fixed base approaches for linear and nonlinear models

Figure 4 compares linear and nonlinear model estimates of the fixed base and SSI approaches. The linear model tends to give lower estimates for softer soils when soil structure interaction is taken into account. The ratio of linear to nonlinear model estimates vary below and above unity with relatively good average values for stiffer soils. The meaning of this observation is that both linear and nonlinear models provide reasonable demand estimates when SSI is accounted in modelling. Similar observation is valid for the fixed base model when the soil type is S1 or S2. However, the variation significantly increases as the soil gets softer. All estimates of linear model with the fixed base approach are greater than nonlinear model estimates for soil type S4, having ratios up to 2.5. Figure 4 obviously illustrates that linear models give extremely higher estimates for soil types S3 and S4.

The outcomes and observations from Figure 4 indicate that the demand estimates are independent from the fixed base or SSI approaches and linear or nonlinear models for stiffer soils. All combinations provide reasonable demand estimates. However, the modelling approach becomes extremely important for softer soils. The best approach seems to be SSI with nonlinear modelling. The fixed base with nonlinear modelling also provides acceptable estimates.

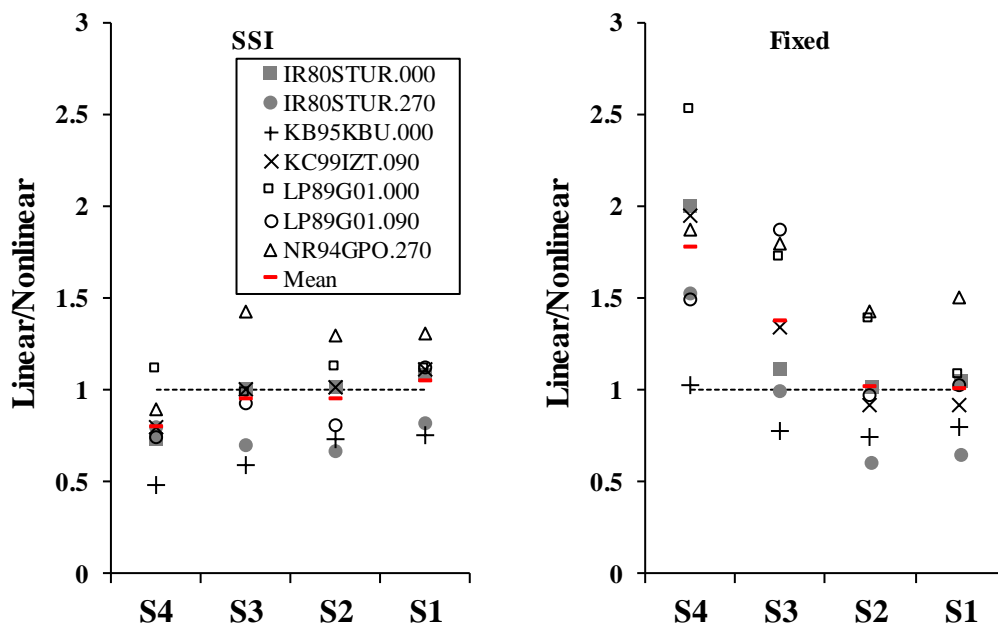


Figure 10 Comparisons of roof displacement demand ratios of linear and nonlinear models for SSI and fixed base approaches

Displacement profile along the building height is an indicator for interstory drift ratios. It also shows sudden changes of story displacement for irregular structures. The displacement profiles of the selected building are compared for the fixed base and SSI approaches at maximum roof displacement. Figures 5 and 6 plots the average displacement profiles of 7 records for linear and nonlinear models, respectively. The displacement profiles of the fixed base and SSI approaches are similar for S1 and S2 soil types for linear models. The profiles start to deviate for softer soils due to extremely higher estimates of the fixed base case.

Similarity of average displacement profiles of SSI and fixed base approaches is obvious for nonlinear models. The observations for average displacement profiles point out that the linear fixed base models are more sensitive to dynamic amplifications for softer soils (i.e. S3 and S4 soil types).

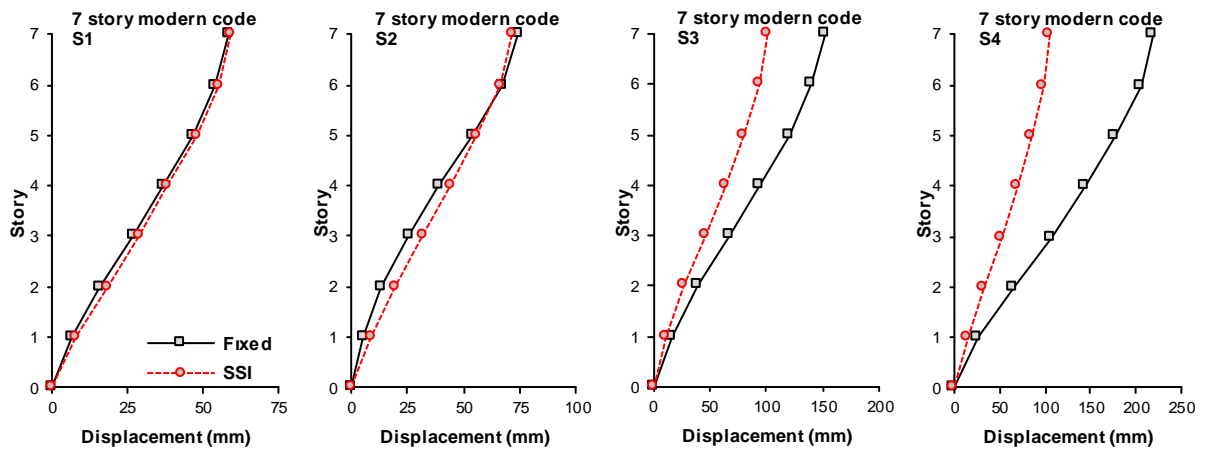


Figure 11 Comparisons of average displacement profiles of linear 7-story modern code building for SSI and fixed base approaches

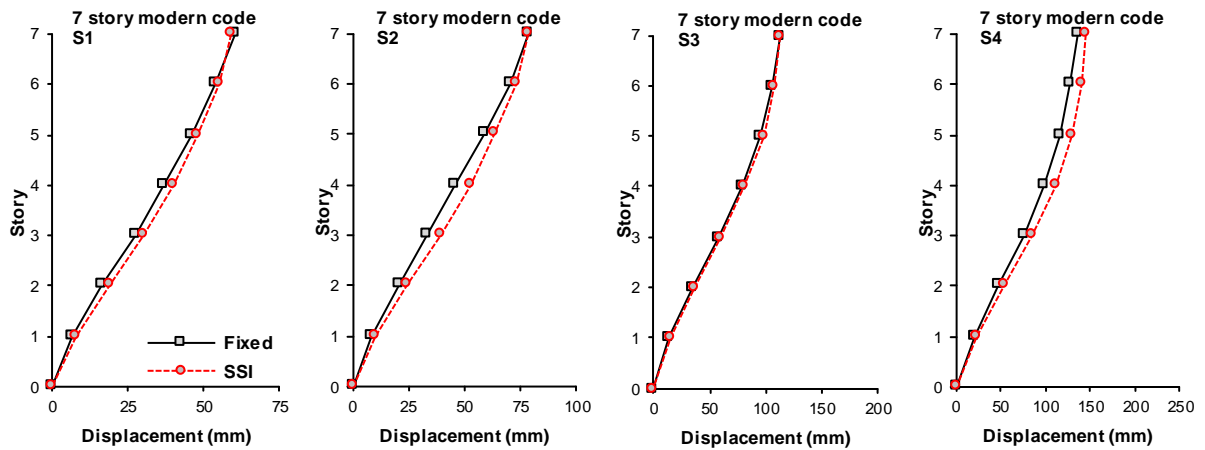


Figure 12 Comparisons of average displacement profiles of nonlinear 7-story modern code building for SSI and fixed base approaches

Although the average displacement profiles of fixed base and SSI approaches match reasonably well for nonlinear models, there are differences for individual records. Figure 7 shows the displacement profiles for KB95KBU.000 and IR80STUR.000 records on soil type S4 and S3 respectively. The differences and opposite trend are obvious for the considered records.

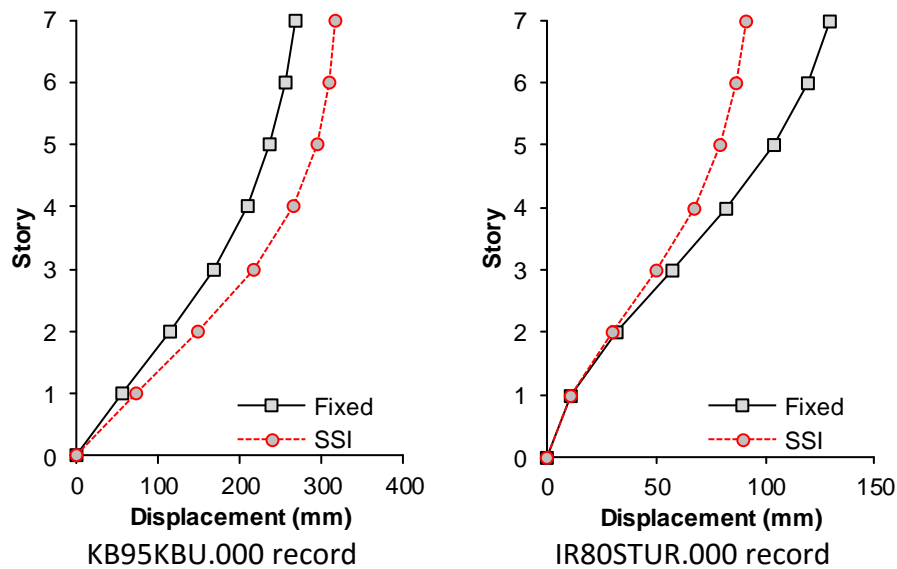


Figure 7 Comparison of displacement profiles of nonlinear for SSI and fixed base approaches subjected to KB95KBU.000 and IR80STUR.000 records

CONCLUSION

This study evaluates the effect of soil structure interaction and the differences in linear and nonlinear modelling of the structure on seismic response. For this purpose, SSI and fixed base models of 7-story building were used. Both linear and nonlinear behavior of the building were taken into account for comparison.

Roof displacement demands and displacement profiles of SSI and fixed base models were compared for both linear and nonlinear models to understand the effects of soil structure interaction and linear or nonlinear modelling of structures on seismic behavior. The findings obviously indicate large variation in displacement demands depending on ground motion record, soil type, consideration of soil structure interaction and linear and nonlinear structure modelling. The displacement demands tend to increase for softer soils except few cases, especially for fixed base models. Significant differences are obvious for linear and nonlinear building models of fixed base case.

The evaluation of obtained results and observations in the current study clearly indicate that the effects of SSI approach depend on dynamic characteristics of soil and structure. While soil deformations influence the seismic demands of structure in positive way for elastic models, these effects are more complex for nonlinear models. It is difficult to mention about certain trend for nonlinear models.

It should be also kept in mind that linear fixed base models are inappropriate for dynamic analysis due to high sensitivity of dynamic amplification which is not compatible with nonlinear behaviour since the dynamic properties change by plastic deformations. Therefore, the use of fixed base linear models may cause inaccurate seismic demand estimates. Another important point is that the average dynamic analysis results do not reflect characteristic properties of the records. This may mislead to understand the effect of specific ground motion like near fault or forward directivity. Even the average values tend to be in similar range for nonlinear models, seismic demands vary in a wide range for ground motion records.

As concluding remarks, the outcomes and observations emphasize that the demand estimates are independent from the fixed base or SSI approaches and linear or nonlinear models

for stiffer soils. All combinations provide reasonable demand estimates. However, the modelling approach becomes extremely important for softer soils. The best approach seems to be SSI with nonlinear modelling. The fixed base with nonlinear modelling also provides acceptable estimates.

ACKNOWLEDGEMENT

The authors acknowledge partial support provided by Scientific and Technical Research Council of Turkey (TUBITAK) under Project No: 214M639 and support of Pamukkale University Research Fund Unit (PAU-BAP) under Project No: 2015FBE011.

REFERENCES

- [1] Wolf J.P. (1985) *Dynamic Soil-Structure Interaction*, 1st Ed., Prentice-Hall, New Jersey.
- [2] Saez E., Caballero F.L., Razavi A.M.F. (2013) Inelastic dynamic soil-structure interaction effects on moment-resisting frame buildings, *Engineering Structures*, **51**, 166-177.
- [3] Kutanis M. (2001) *Dynamic Soil-Structure Analysis*, Ph.D. Thesis, Sakarya University.
- [4] Ministry of Public Works and Settlement, Turkish Earthquake Code (1997). Specifications for structures to be built in disaster areas. Ankara, Turkey (in Turkish); 1997.
- [5] Sap2000, CSI., Integrated Software for Structural Analysis and Design, Computers and Structures Inc., Berkeley, USA.
- [6] Kramer S.L. (1996) *Earthquake Geotechnical Engineering*, 1st Ed., Prentice-Hall, New Jersey.
- [7] Lysmer J., Kuhlemeyer R.L. (1969) Finite dynamic model for infinite media. *Journal of Engineering Mechanics Division*, ASCE 1969;95(4):759–877.
- [8] Wilson E.L. (2002) *Three Dimensional Static and Dynamic Analysis of Structures*, 3th Ed., Computers and Structures, Inc., Berkeley.
- [9] NIST GCR 12-917-21 (2012) *Soil Structure Interaction for Building Structures*, NEHRP Consultants Joint Venture.
- [10] American Society of Civil Engineers (Asce). *Prestandard and Commentary for The Seismic Rehabilitation of Buildings*. Fema-356. Washington Dc; 2000.
- [11] Turkish Earthquake Code (2007-TEC) (2007) “Specifications for Buildings to Be Built in Seismic Areas”, Ministry of Public Works and Settlement Ankara, Turkey. [In Turkish].
- [12] Applied Technology Council (Atc). *Seismic Evaluation and Retrofit of Concrete Buildings*. Volumes 1 And 2. Report No. Atc-40, Redwood City (Ca), 1996.
- [13] Pacific Earthquake Engineering Research Center (PEER), Ground Motion Database: <http://ngawest2.berkeley.edu/>
- [14] Strong-Motion Virtual Data Center (VDC): <http://strongmotioncenter.org/vdc/scripts/default.plx>

Self-Equilibrium state of V-Expander Tensegrity Beam

Pilade Foti¹, Aguinaldo Fraddosio¹, Salvatore Marzano¹, Gaetano Pavone¹, Mario Daniele Piccioni¹

¹ Department of Civil Engineering and Architecture, Politecnico of Bari, Italy

ABSTRACT

In this paper, we study an innovative class of tensegrity beams, obtained by a suitable assembly of elementary V-Expander tensegrity cells along a longitudinal axis in the three-dimensional space.

Tensegrity structures, made by struts in compression and cables in tension, are an innovative structures by itself: they are similar only in appearance to conventional pin-joint structures (trusses), and their mechanics is strongly related to initial feasible self-stress states induced in absence of external loads. In particular, from a kinematical point of view these self-stress states avoid the activation of possible infinitesimal mechanisms.

By a numerical study, we analyze the feasible self-stress states for lightweight tensegrity beams made by a suitable assembly of V-Expander elementary cells. Moreover, we analyze the influence on the feasible self-stress states of the addition of struts or cables starting from the simplest V-Expander configuration.

Keywords: tensegrity beam; self-equilibrium; force density method; numerical methods

INTRODUCTION

Tensegrity structures are an innovative class of lightweight structures, which have gained the interest of researchers in many different fields, including but not limited to engineering. In particular, the interest for tensegrity structures in structural engineering, as well as in architecture, is due to their aesthetic value, their large stiffness-to-mass ratio, the possible deployability, together to their reliability and controllability. The tensegrity concept has found applications within architecture and civil engineering, such as towers, large dome structures, stadium roofs, temporarily structures and tents [1].

Tensegrity is a pin-connected free-standing framework composed of struts in compression and cables necessarily in tension. Usually, the structural analysis of a tensegrity preliminarily requires a form-finding process, since the shape of a tensegrity structure is strictly related to the self-stress in its elements.

In this paper, we show a numerical study of a class of tensegrity beams, obtained by a suitable assembly of elementary V-Expander tensegrity cells along a longitudinal axis in three-

dimensional space [2]. The overall performance of this kind of beam is strongly dependent on the way the different elementary cell are connected. By applying a numerical method, we study the self-equilibrium states for the V-Expander tensegrity beam, and we analyze the structural behavior as the pattern of the elements changes.

FORM-FINDING OF TENSEGRITY STRUCTURES

Basic assumptions

Tensegrity structures can be defined as a discontinuous set of elements in compression within a continuous network of tensile elements; this definition is described by well-known expression: “island of compression in an ocean of tension” [3].

The following assumptions are considered in this study: (i) elements are connected by pin joints; (ii) members of the structure are rectilinear; (iii) the connection between the struts is possible only at their extremities; (iv) topology, i.e. the connectivity between the nodes and elements, and the geometrical configuration are known; (v) self-weight of elements is neglected and no external load is applied; (vi) buckling of the strut is not considered; (vii) the structure is free-standing.

From the assumptions, only axial forces are carried by the elements, i.e. there are only two types of elements: struts in compression and cables in tension.

The geometrical configuration of the structure is described in terms of nodal coordinates. Since the structure is free-standing no supports are needed.

A tensegrity structures is a system in a stable self-equilibrated state. The self-equilibrium state refers to the initial mechanical state of the structure before any load, even gravitational, are applied. In this initial state, there is a self-stress state in the elements.

Furthermore, if tensegrity structure possesses any infinitesimal mechanisms, these are stabilized by the self-stress state in the elements. The stability of the structure is defined as the ability of the system to return in equilibrium configuration after a small perturbation [4].

Geometry and topology

In three-dimensional space, a tensegrity structure has e elements: c cables and s struts, ($c + s = e$). The elements of the structure are jointed at n nodes. In the cable-net structures, apparently similar to the tensegrity structures, there exist some fixed nodes due to fact that only tension is carried into the cables. Tensegrity structures are free-standing, for assumption, and therefore there exist only free nodes in three-dimensional space. In order to define the geometrical configuration of a tensegrity structures we define \mathbf{x} , \mathbf{y} and \mathbf{z} ($\in \mathbb{R}^n$) as the nodal coordinate vectors of the free nodes in three directions \mathbf{e}_x , \mathbf{e}_y , \mathbf{e}_z of an orthogonal reference system $O\{\mathbf{e}_x, \mathbf{e}_y, \mathbf{e}_z\}$.

The topology of the tensegrity structures can be defined by a *connectivity matrix* \mathbf{C} ($\in \mathbb{R}^{e \times n}$). If member k connects nodes i and node j , with $i < j$, then in the k th row of \mathbf{C} we set 1 and -1 at the i th and j th position, respectively.

Therefore, the connectivity matrix can be defined as follows:

$$[\mathbf{C}]_{k,p} = \begin{cases} +1 & \text{if } p=i \\ -1 & \text{if } p=j \\ 0 & \text{otherwise.} \end{cases} \quad (1)$$

Let \mathbf{u} , \mathbf{v} and \mathbf{w} ($\in \mathbb{R}^e$) the vectors of coordinate differences of elements k in x , y , z directions respectively:

$$\begin{cases} \mathbf{u} = \mathbf{C}\mathbf{x} \\ \mathbf{v} = \mathbf{C}\mathbf{y} \\ \mathbf{w} = \mathbf{C}\mathbf{z} \end{cases} \quad (2)$$

and let \mathbf{l} the vector ($\in \mathbb{R}^e$) which collects the lengths of the elements. Let \mathbf{U} , \mathbf{V} , \mathbf{W} and \mathbf{L} ($\in \mathbb{R}^{e \times e}$) be the diagonal form of \mathbf{u} , \mathbf{v} , \mathbf{w} and \mathbf{l} , respectively.

The diagonal matrix \mathbf{L} can be expressed:

$$\mathbf{L}^2 = \mathbf{U}^2 + \mathbf{V}^2 + \mathbf{W}^2 \quad (3)$$

In this way, the geometrical configuration and the topology of the tensegrity structure are completely defined.

Self-Equilibrium state

When geometrical configuration and topology of tensegrity structure are defined, the equilibrium equations in each directions can be set as developed by Scheck [5]. The nonlinear equilibrium equations for unknown locations of the nodes are transformed to a set of linear equations by introducing the so-called force density q_k as the internal axial force to length ratio for each k elements. Note that $q_k > 0$ for cables and $q_k < 0$ for struts.

This condition is associated to the unilateral mechanical behaviour of elements, i.e. cable are in tension, and struts are in compression. In absence of the external loads, the self-equilibrium equations for a general pin-jointed structure can be written as:

$$\begin{cases} \mathbf{C}^T \mathbf{Q} \mathbf{C} \mathbf{x} = \mathbf{0} \\ \mathbf{C}^T \mathbf{Q} \mathbf{C} \mathbf{y} = \mathbf{0} \\ \mathbf{C}^T \mathbf{Q} \mathbf{C} \mathbf{z} = \mathbf{0} \end{cases} \quad (4)$$

where \mathbf{Q} ($\in \mathbb{R}^{e \times e}$) is the diagonal matrix collecting the force densities ratios of all elements. By introducing the *force density matrix* \mathbf{D} , ($\in \mathbb{R}^{n \times n}$) as

$$\mathbf{D} = \mathbf{C}^T \mathbf{Q} \mathbf{C} \quad (5)$$

the equilibrium equations in (4) can be written as

$$\begin{cases} \mathbf{D}\mathbf{x} = \mathbf{0} \\ \mathbf{D}\mathbf{y} = \mathbf{0} \\ \mathbf{D}\mathbf{z} = \mathbf{0} \end{cases} \quad (6)$$

Noting that $diag(\mathbf{b})\mathbf{f} = diag(\mathbf{f})\mathbf{b}$, with \mathbf{b} and \mathbf{f} are a generic vectors, and by introducing the so called *equilibrium matrix* \mathbf{A} ($\in \mathbb{R}^{3n \times e}$), (4) can be rewritten as

$$\begin{bmatrix} \mathbf{C}^T diag(\mathbf{C}\mathbf{x}) \\ \mathbf{C}^T diag(\mathbf{C}\mathbf{y}) \\ \mathbf{C}^T diag(\mathbf{C}\mathbf{z}) \end{bmatrix} \mathbf{q} = \mathbf{0} \quad (7)$$

where the equilibrium matrix is defined as

$$\mathbf{A} = \begin{bmatrix} \mathbf{C}^T diag(\mathbf{C}\mathbf{x}) \\ \mathbf{C}^T diag(\mathbf{C}\mathbf{y}) \\ \mathbf{C}^T diag(\mathbf{C}\mathbf{z}) \end{bmatrix} \quad (8)$$

From the equations in (7), the unknown basis of the vector space of the unknown force densities in the elements lie in the null space of \mathbf{A} . The *feasible self-stress state* $\tilde{\mathbf{q}}$, ($\in \mathbb{R}^e$) is defined as a state of self-stress that satisfies (7) and should be in accordance with the unilateral behaviour of the elements. In [6] it is shown that $\tilde{\mathbf{q}}$, ($\in \mathbb{R}^e$), which can be expressed as a linear combination of the basis of the vector space of the force densities, can be written according to the geometrical symmetry of the structure. In particular, elements in symmetric position have the same force density and then they can be collected in a group.

Let r_A and \bar{r}_A , the rank and the dimension of the null space of the equilibrium matrix, hence, there exist \bar{r}_A independent states of self-stress.

$$\bar{r}_A = e - r_A \quad (9)$$

As above mentioned, $\tilde{\mathbf{q}}$ can be written as

$$\tilde{\mathbf{q}} = \lambda_1 \mathbf{q}_1 + \lambda_2 \mathbf{q}_2 + \dots + \lambda_{\bar{r}_A} \mathbf{q}_{\bar{r}_A} \quad (10)$$

where λ_i , $i=1,2,\dots, \bar{r}_A$, are real coefficients. Furthermore, let h , the number of groups of the symmetry, vector $\tilde{\mathbf{q}}$ can also be written as

$$\tilde{\mathbf{q}} = \mathbf{e}_1 q_1 + \mathbf{e}_2 q_2 + \dots + \mathbf{e}_h q_h \quad (11)$$

where \mathbf{e}_i ($\in \mathbb{R}^e$), $i=1,2,\dots, h$, is a vector composed of a unit in the i th position if the element belongs to the group and zero otherwise. From (10) and (11), a new matrix $\tilde{\mathbf{G}}$ ($\in \mathbb{R}^{e \times (\bar{r}_A+h)}$), and new vector $\bar{\mathbf{p}}$ ($\in \mathbb{R}^{(\bar{r}_A+h)}$), can be written, which collects the vectors \mathbf{q}_i and \mathbf{e}_i , and the real λ_i and q_i , respectively as

$$\tilde{\mathbf{G}} = [\mathbf{q}_1, \mathbf{q}_2, \dots, \mathbf{q}_{\bar{r}_A}, -\mathbf{e}_1, \mathbf{e}_2, \dots, \mathbf{e}_h] \quad (12)$$

$$\bar{\mathbf{p}} = [\lambda_1, \lambda_2, \dots, \lambda_{\bar{r}_A}, q_1, q_2, \dots, q_h] \quad (13)$$

In this way, in order to find the feasible self-stress state, can be written the follows equation

$$\tilde{\mathbf{G}}\bar{\mathbf{p}} = \mathbf{0} \quad (14)$$

A Singular Value Decomposition (SVD) should be carried out to find all solutions of (14). These solutions lie in the null space of $\tilde{\mathbf{G}}$. If the dimension of the null space of $\tilde{\mathbf{G}}$ is unit, a tensegrity structure possess a single initial mode of self-stress which is compatible with the unilateral behaviour of the elements, and is in according to the symmetry of the structure in the self-equilibrium.

If the dimension of the null space of $\tilde{\mathbf{G}}$ is equal to zero (14) has only trivial solutions; if the dimension of the null space of $\tilde{\mathbf{G}}$ is more than unit (14) has more than one non-trivial solutions. It is clear that the first \bar{r}_A terms of $\bar{\mathbf{p}}$ are the real coefficients of the linear combination in (10) and the last h terms are the force densities in the groups.

The initial force vector, in the self-equilibrium state, $\bar{\mathbf{f}}_i$ ($\in \mathbb{R}^e$) can be express as

$$\bar{\mathbf{f}} = \mathbf{L}\bar{\mathbf{q}} \quad (15)$$

The Euclidean norm of the vector of unbalanced force $\bar{\mathbf{f}}_u$ ($\in \mathbb{R}^{3n}$) can be used to evaluate the accuracy of the self-equilibrium conditions

$$\bar{\mathbf{f}}_u = \mathbf{A}\bar{\mathbf{q}} \quad (16)$$

Infinitesimal mechanisms

Let $\boldsymbol{\varepsilon}$ ($\boldsymbol{\varepsilon} \in \mathbb{R}^e$), and \mathbf{d} ($\mathbf{d} \in \mathbb{R}^{3n}$) be the vector of the axial strains of the elements and the vector of the nodal displacements, respectively.

By the principle of virtual works

$$\mathbf{A}^T \mathbf{d} = \boldsymbol{\varepsilon} \quad (17)$$

Infinitesimal mechanism \mathbf{d}_m ($\mathbf{d}_m \in \mathbb{R}^{3n}$), is the vector of the nodal displacements which are related to null axial strains, i.e.

$$\mathbf{A}^T \mathbf{d}_m = \mathbf{0} \quad (18)$$

By (18), infinitesimal mechanisms lie in the null space of the transpose of the equilibrium matrix. The dimension of the null space of \mathbf{A}^T , which is the multiplicity of infinitesimal mechanisms is

$$\bar{r}_{A^T} = 3n - r_A \quad (19)$$

Rank deficiency conditions

Let r_D the rank of the force density matrix, the dimension of the null space of \mathbf{D} is

$$\bar{r}_D = n - r_D \quad (20)$$

The dimension of the null space of \mathbf{D} , in order to create a space of the solution of (6) with at least four dimensions, should be equal or more than four. Furthermore, dimension of the null space of \mathbf{A} should be equal or more than unit. These conditions ensure the possibility to build a non-degenerate self-equilibrated tensegrity structure in three-dimensional space.

V-Expander tensegrity beam

In this paper, we study how the feasible self-stress state $\tilde{\mathbf{q}}$ changes when the number of the elements increases. The V-Expander Tensegrity beam is obtained by assembling three V₂₂-Expander tensegrity cell as shown in Fig. 1. Here, the V-Expander Tensegrity beam is studied as the geometrical parameters d (m) and h (m) change. Therefore, the feasible self-stress-state is calculated and plotted for $d = 1$ m and $h = 0.5$ m. The first analysed V-Expander beam is composed of sixteen struts and twenty-seven cables; twenty-two nodes connect the elements (nodes and elements are labelled in view of geometrical symmetry of the structure). Then, more complex V-Expander beams are analysed, with the following outline:

- *Case 1*, forty-three elements,
- *Case 2*, fifty-three elements,
- *Case 3*, fifty-seven elements,
- *Case 4*, fifty-nine elements,
- *Case 5*, sixty-three elements,
- *Case 6*, sixty-seven elements,
- *Case 7*, seventy-one elements.

In all the above cases, the tensegrity beam is capable of being enclosed in a parallelepiped, the dimensions of which are $6d$, $2d$ and h , in x , y and z direction respectively. For example, in Figure 1 is shown the top view of the V-Expander beam of *Case 1*. In the V-Expander Tensegrity beam, as shown in Fig. 2, referred to *Case 7*, the initial struts are labelled from 48 to 63.

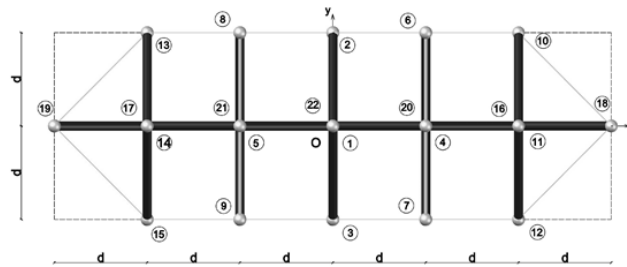


Figure 1 Top view of V-Expander beam in Case 1.

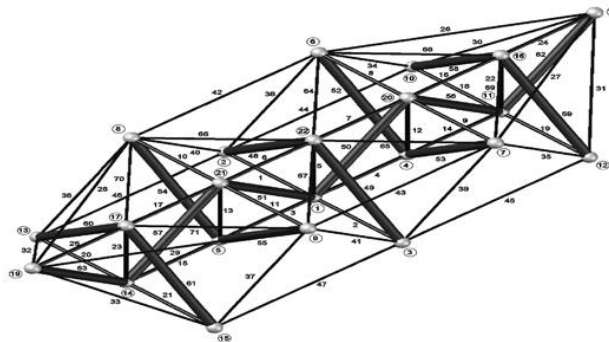


Figure 2 Perspective view of V-Expander beam in Case 7.

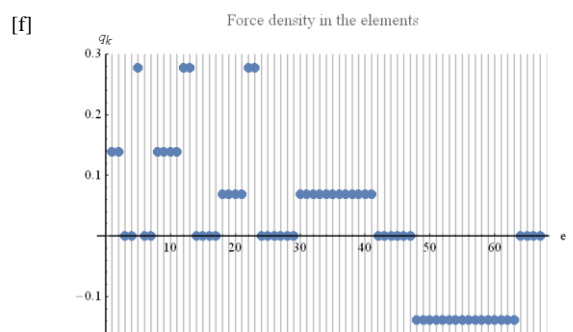
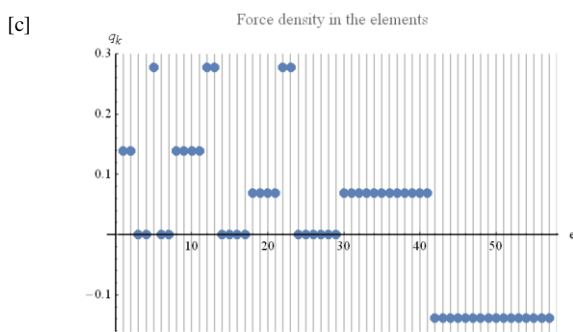
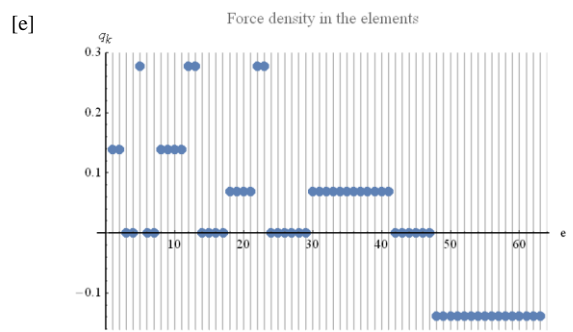
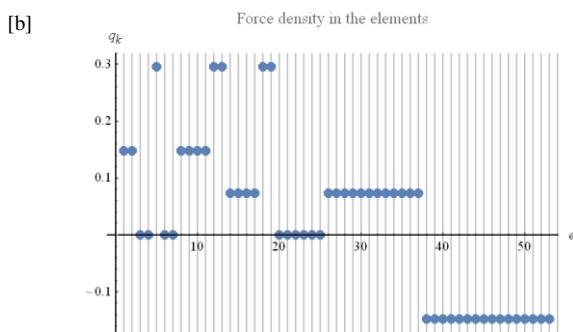
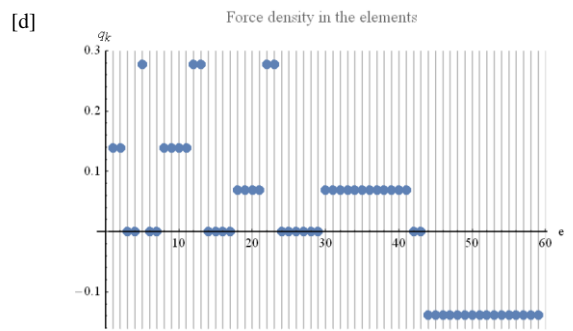
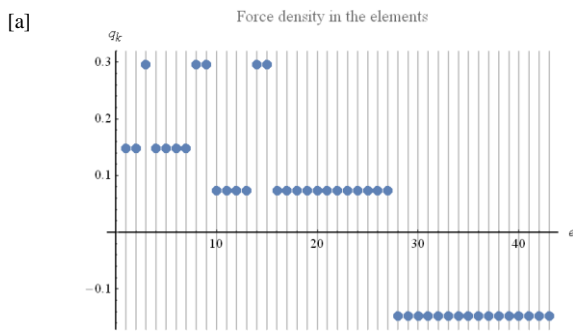
When the number of the elements increases, the rank of the equilibrium matrix A increases and, then, the number of the independent self-stress states also increases. Furthermore, the number of the infinitesimal mechanisms of the V-Expander tensegrity beam decreases. In particular, *Case 1* possesses eighteen infinitesimal mechanisms when the six rigid-body motions in three-dimensional space are opportunely constrained; *Case 7* does not possess any

infinitesimal mechanisms when the rigid-body motions are excluded. The first case analysed, *Case 1*, is composed of:

- Twenty-seven cables (1, 2, 5, 8, 9, 10, 11, 12, 13, 18, 19, 20, 21, 22, 23, 30, 31, 32, 33, 34, 35, 36, 37, 38, 39, 40, 41) and sixteen struts, which are labelled as mentioned above.

The other cases analysed are obtained, starting from *Case 1*, by addition of the elements (addition respects geometrical symmetry of the structure) as follow:

- *Case 2*, ten elements (3, 4, 6, 7, 24, 25, 26, 27, 28, 29);
- *Case 3*, four elements (14, 15, 16, 17);
- *Case 4*, two elements (42, 43);
- *Case 5*, four elements (44, 45, 46, 47);
- *Case 6*, four elements (64, 65, 66, 67);
- *Case 7*, four elements (68, 69, 70, 71).



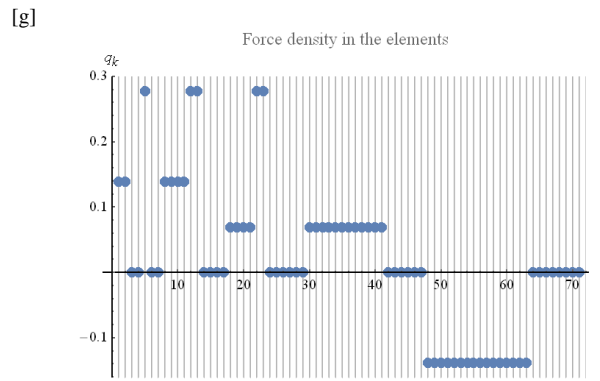


Figure 3 Feasible self-stress states of V-Expander beam [a] Case 1, [b] Case 2, [c] Case 3, [d] Case 4, [e] Case 5, [f] Case 6, [g] Case 7.

In Figure 3 are listed the feasible self-stress states of the seven cases analysed; notice that as the complexity increases, some force densities assume values near to zero. In Figure 4 is shown the number of the independent self-stress states and the number of the infinitesimal mechanisms for every V-Expander beam studied.

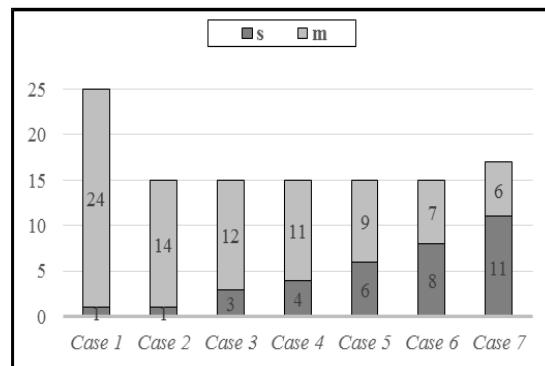


Figure 4 Number of independent self-stress states s and number of infinitesimal mechanisms m of V-Expander beams.

In Table 1 are listed the properties of the seven V-Expander beams studied.

Table 1 Properties of the seven V-Expander beams.

Case		1	2	3	4	5	6	7
Properties of V-Expander beam	\mathbf{C} ($\in \mathbb{R}^{e \times n}$)	43 x 22	53 x 22	57 x 22	59 x 22	63 x 22	67 x 22	71 x 22
	\mathbf{A} ($\in \mathbb{R}^{3n \times e}$)	66 x 43	66 x 53	66 x 57	66 x 59	66 x 63	66 x 67	66 x 71
	r_A	42	52	54	55	57	59	60

In Table 2 are listed the real coefficients of the linear combination in (10) for Case 7.

Table 2 Real coefficients of the linear combination for *Case 7*.

	<i>Case 7</i>											
Real coefficients λ_i ($i=1,2,\dots,11$)	-0.24499	-0.09704	-0.47821	-0.02461	0.00749	-0.51210	-0.037932	0.06266	0.45970	0.16743	0.27318	

CONCLUSIONS

In this paper, we analyse the influence on the feasible self-stress states of the addition of elements (struts and/or cables) starting from an initial configuration of a tensegrity V-Expander beam. In *Case 1* there are possible twenty-four independent infinitesimal mechanisms which lie in the kernel of the transpose of the equilibrium matrix of the structure. Furthermore, in this case, there exists only one independent self-stress state.

From *Case 1* to *Case 7* we observe a redistribution of the force densities in the elements; in particular, we find that the force densities in the vertical cables, i.e. elements 5, 12, 13, 22, 23, decrease from 0.3 to 0.28. Simultaneously, we observe that the force densities in the struts increase until they reach the value -0.138, starting from a value, in *Case 1*, equal to -0.147.

Additional elements “stiffen” the V-Expander tensegrity beam: indeed, disregarding rigid-body motions, the number of infinitesimal mechanisms decreases, and it becomes zero in *Case 7* (the most complex examined beam).

As natural extension of the present work, the mechanical behaviour of the V-Expander tensegrity beam under the action of external loads will be analysed in forthcoming papers.

REFERENCES

- [1] Gilewsky, W. and Klosowska, J. and Obara, P. (2015) Applications of tensegrity structures in civil engineering. *Procedia Engineering*, **111**, 242-248.
- [2] Raducanu, V. and Motro, R. (2011) STABLE SELF-BALANCING SYSTEM FOR BUILDING COMPONENT. *Patent*, **WO02081832**.
- [3] Fuller, R. B. (1975) Synergetics. Explorations in the Geometry of Thinking. *Macmillan Publishing*, New York, NY, USA.
- [4] Motro, R. (2003) Tensegrity: Structural Systems for the Future. *Kogan page Science*, London, UK.
- [5] Scheck, H. J. (1975) The force density method for form finding and computation of general networks. *Comput. Methods Appl. Mech. Eng.*, 115-134.
- [6] Tran, H.C. and Lee, J. (2010) Initial self-stress design of tensegrity grid structures. *Computers & Structures*, **88**, 558-566.
- [7] Tran, H.C. and Lee, J. (2010) Self-stress design of tensegrity grid structures with exostresses. *International Journal of Solids and Structures*, **47**, 2660-2671.
- [8] Foti, P. and Fraddosio, A. and Marzano, S. and Pavone, G. and Piccioni, M. D. (2016) On self-stress design in V-Expander tensegrity structures. in press.

- [9] Zhang, J. Y. and Ohsaki, M. (2007) Stability conditions for tensegrity structures. *International Journal of Solids and Structures*, **44**, 3875–3886.
- [10] Gómez-Jáuregui, V. (2010) Tensegrity structures and their application to architecture. *Universidad de Cantabria. Servicio de Publicaciones*.

Effects of Soft storey Irregularity on RC building Response

Rezarta Uruci¹, Huseyin Bilgin¹

¹Department of Civil Engineering, Epoka University, Albania

ABSTRACT

Albanian building stock is composed of reinforced concrete and masonry buildings. Most of these buildings are designed with Old Albanian Codes (KTP Codes) and some of them are constructed without any project. Considering these facts and the observations done in Albanian construction industry, presence of structural irregularities is very common in these buildings. Irregularities are weak points in the building which may cause fail of one element or total collapse of the building during an earthquake. Irregularities encountered in Albanian construction practice consist of short column, large and heavy overhangs, reinforcement details and soft story irregularity. Since Albania is a high seismic country which has been hit many times from earthquakes of different magnitudes establishes the need to study the effect of irregularities. Among all these irregularities in this study is taken in consideration the soft story effect under seismic loads in low and mid-rise buildings of Albanian construction practice. In order to get the effect of soft story irregularity in RC buildings several number of Nonlinear Static (Pushover) Analyses are done for regular frames, frames with soft story because of higher height and lack of masonry infill walls in ground story or because of the presence of both cases for the two types of structures, 3 and 6-story frames representing low and mid-rise buildings respectively. The analysis has been performed by ETABS software. The results of the analyses indicate that low and mid-rise structures with soft story irregularity due to absence of infill walls and higher height of ground story are more vulnerable during earthquakes.

Keywords: *Low and Mid-Rise RC buildings, Soft Story, Nonlinear Static Pushover Analysis.*

INTRODUCTION

The inadequate performance and the huge number of collapsed buildings during past earthquakes because of diverse structural irregularities determines the idea to analyse the buildings with dissimilar irregularities in order to understand the effect of them in RC buildings under the seismic effect. Different researchers [1, 2] have studied altered vertical and horizontal irregularities with different methods of analysis such: nonlinear static (pushover) analysis, dynamic analysis and time history analysis, etc. and realized which type of them are more risky during an earthquake and what should be taken in consideration from the designers during the design process. This study aims to get the seismic performance of low and mid-rise frames, which are more vulnerable during earthquake, with soft stories by using nonlinear static analysis. Soft story irregularity is one of the main irregularities affecting the damages of the buildings during an earthquake, it has also been studied from different researchers. [1, 3] Soft story irregularity in most of the cases occurs because of the lower stiffness of first story of the buildings which may be originated as a result of non-uniform distribution of masonry infill walls or because of the higher height of one story compared to the other ones which in most of the cases is done for commercial reasons. In this study both cases are taken into consideration,

lack of infill walls and higher story height, for low and mid-rise buildings. The considered cases will be studied separately and composed, firstly the masonry infill walls will be removed from the first story, and then story height will be 4.5m instead of 3m normal height. Capacity curves of the considered cases are obtained by using nonlinear static analysis, which are performed by using ETABS software. Frame elements, beams and columns are modelled as nonlinear elements with lumped plasticity by defining plastic hinges at both ends of them. Masonry infill walls are modelled as diagonal strut, with specifications from FEMA-356. [4] Effect of soft story in low and mid-rise RC buildings is evaluated in observation of capacity curves which are very beneficial to understand its effect during earthquakes.

AIM AND SCOPE

This study aims to assess the seismic performance of the major portion of low and mid-rise building stock in Albanian construction practice. Seismic performance of the selected buildings is done by considering reinforced concrete elements and as well as masonry infill walls. Selected buildings are modified to have the structural deficiency like soft story, created because of non-uniform distribution of masonry infill walls and because of higher story height compared to the other ones or because of both of them, even though soft story may also arise as a result of changes in load carrying and slab system, observed in damaged buildings during the last earthquakes in Albania and worldwide. The most frequent reason of soft story creation is the abrupt change of masonry infill walls between different stories since infill walls are not considered as part of load carrying system, so they are considered in the structural behaviour of the frame. For this reason, most of the civil engineers don not give attention to the creation of soft story because of infill walls. In order to increase the level of knowledge and achieve the aim of this study a 3 and 6-story reinforced concrete buildings are selected to represent the reference low and mid-rise buildings. The certain buildings are typical RC frame buildings with no shear walls in which the irregularities will be implemented.

BUILDING MODELS

The selected 3 and 6-story frame buildings are regular 20m by 16 m in plan as shown in Figure 1 below. They have 5 bays by 4m along X direction and 4 bays by 4m along Y direction (Figure 1). Typical floor height is 3m. The location of masonry infill walls in plan is shown by the hatch of beams (Figure 1). The selected buildings have the plan view as shown in Figure 1:

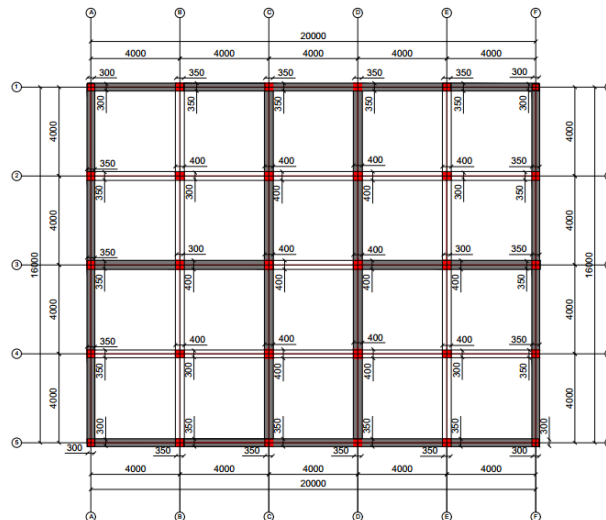


Figure 1 Structural Plan view of 3, 6-Story frame (units in mm)

Beam and column dimensions of the reference buildings represent the most common frame elements for low and mid-rise frames in Albanian construction practice. The 3-story frame consists of 300mm x 300mm corner columns and 350mm x 350mm outside columns, identified as C1 and C2 respectively, 300mm x 400mm, 400mm x 300mm and 400mm x 400 mm inside columns, identified as C5, C4 and C3 respectively, as shown in Figure 2. Beams have all the same section for the 3-story frame which consists of 300mm x 400 mm, Figure 4. The 6-story consists of 400mm x 400 mm corner columns and 500mm x 500 mm outside columns, identified as C3 and C6 respectively, and 600mm x 600mm, 500mm x 400mm and 400mm x 500 mm inside columns, identified as C7, C8 and C9 respectively, as shown in Figure 3 and the beams have all the same section 300mm x 400 mm, Figure 4.

Material properties are based on most common materials used in Albanian construction practice; it is assumed 20 MPa for the concrete compressive strength and 355 MPa for the yield strength of reinforcement. Then in order to get the effect of soft story structural irregularity in reinforced concrete structures the selected buildings are modified to have above-mentioned structural deficiency, soft story. The cases which will be analysed are:

- 1- Reference regular building, infilled frame, (Ref), Figure 5a
- 2- Reference regular building without masonry infill walls, bare frame, (RefWW), Figure 5c
- 3- Soft story due to increased ground story height (3 m to 4.5 m) (SSH), Figure 5e
- 4- Soft story due to absence of walls at ground story (SSW), Figure 5b
- 5- Soft story due to increased height and absence of walls at ground story (SS-H-W), Figure 5d

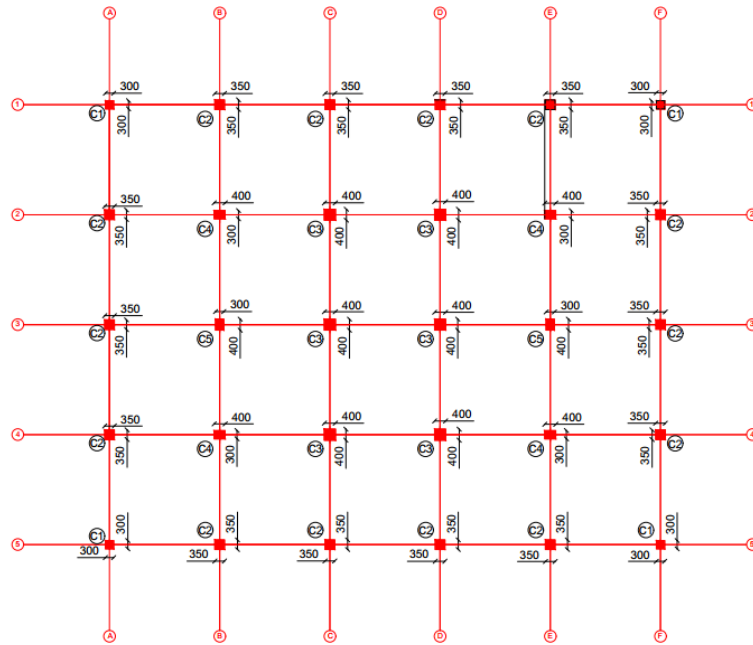


Figure 2 Column plan view of 3 Story frame (units in mm).

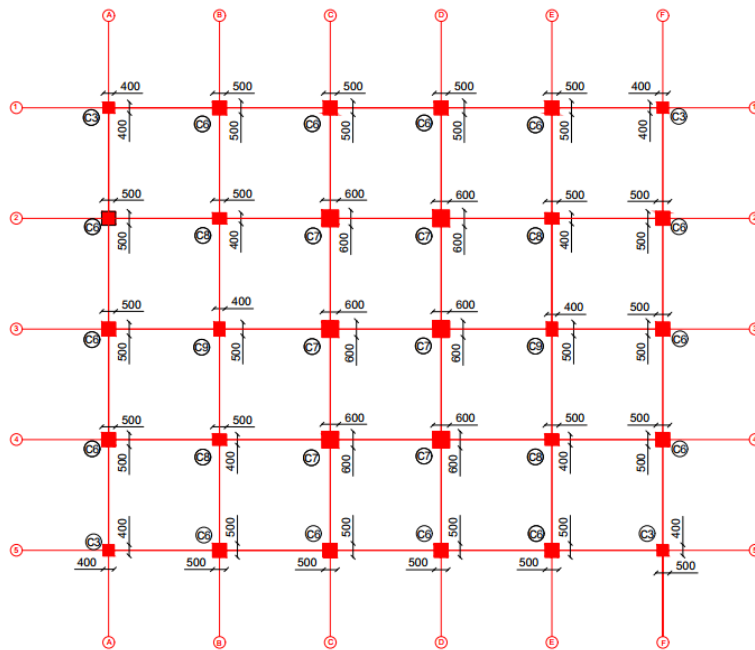


Figure 3 Column plan view of 6 Story frame (units in mm)

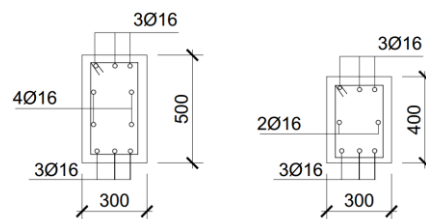


Figure 4 Beam Sections (units in mm)

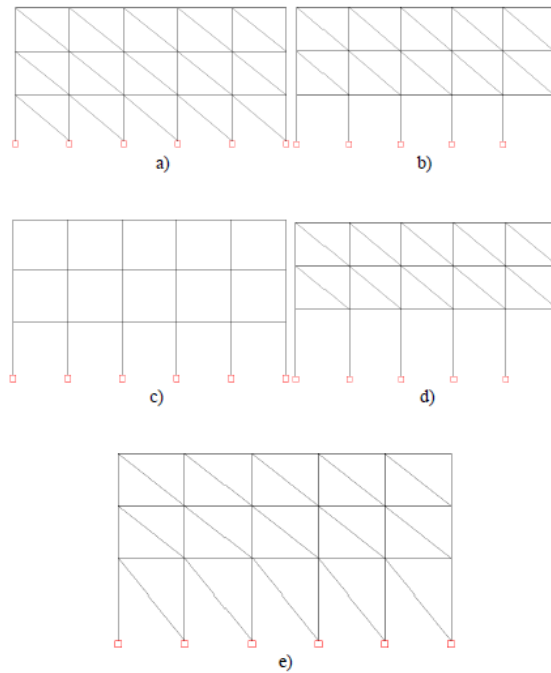


Figure 5 : Elevation view of building models a) Ref, b) SSW, c) RefWW, d) SS-H-W, e) SS-H

PUSHOVER ANALYSIS

Nonlinear static pushover analysis is a type of analysis which is performed by subjecting a monotonically increasing pattern of lateral loads in the structure which represents the forces that the structure may experience during an earthquake. Under incrementally increasing loads various structural elements may yield sequentially. Consequently, at each event, the structure experiences a loss in stiffness. Using a pushover analysis, a characteristic non-linear force displacement relationship can be determined. Guidelines like FEMA 356 have mentioned the modelling procedures, acceptance criteria and analysis procedures for the pushover analysis. (FEMA, 2000) This code defines the force-deformation criteria for possible locations of lumped inelastic behaviour defined as plastic hinges in the pushover analysis. In figure 6 is shown the plastic hinge force-deformation behaviour by using five points labelled as A, B, C, D, and E and three point's labelled IO (Immediate Occupancy), LS (Life Safety) and CP (Collapse Prevention) are used to define the acceptance criteria for the hinge.

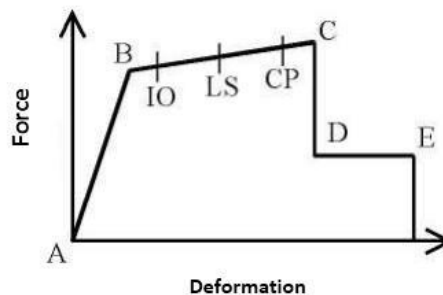


Figure 6 Pushover Curve (FEMA, 2000)

The values assigned to each of these points vary depending on the type of member as well as many other parameters, such as the expected type of failure, the level of stresses with respect to the strength, or code compliance.

ANALYSIS RESULTS

Pushover analysis has been conducted for the 10 building models. The material nonlinearities are assigned as hinges; M3 flexural hinges for beams and PM2M3 flexural hinges for columns. Infill panels are modelled by one nonlinear strut elements, which only has compressive strength. Then each lateral load pattern is applied and static pushover analyses results of the case study buildings are generated. Behaviour of the structure is represented by capacity curves that represents the base shear force and displacement of the roof. Figures 7-10 illustrates capacity curves obtained from the pushover analysis of the 3 and 6-story frames. In x-axis is shown the roof drift ratio that is roof displacement normalized by the building height and in y-axis is shown the shear strength coefficient that is the base shear force normalized by the seismic weight.

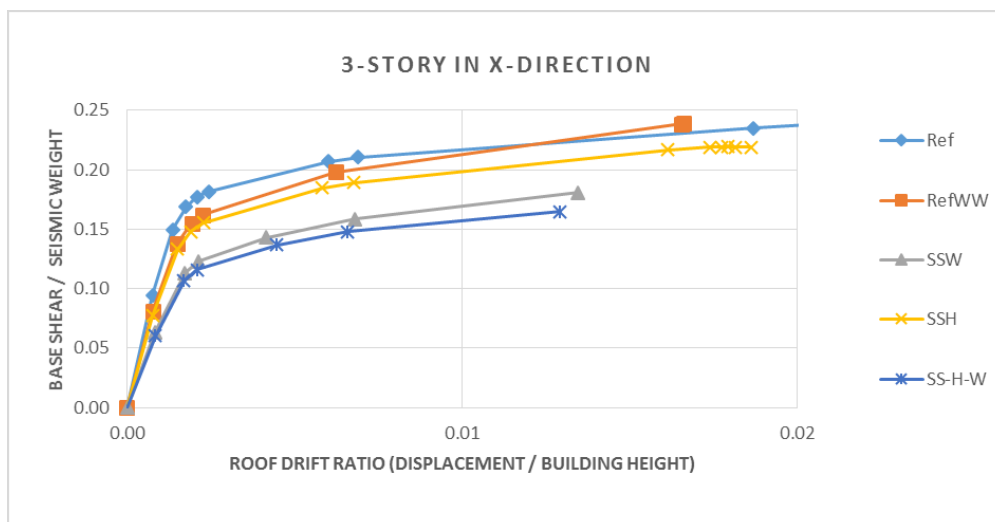


Figure 7 Capacity Curve of 3- story Frame, X-direction

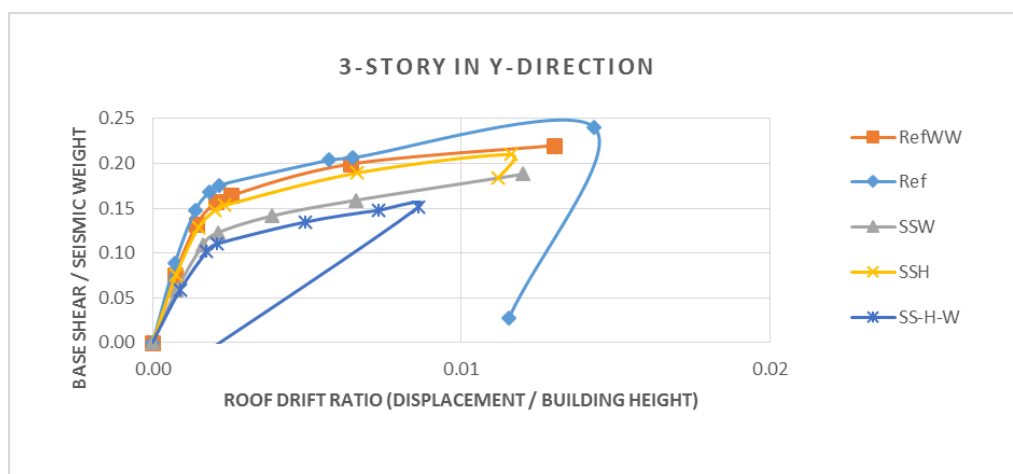


Figure 8 Capacity Curve of 3- story Frame, Y-direction

From the normalized graphs (see Figures 7-10) is showed that presence of masonry infill walls for both frames increases both stiffness and strength of the frames. Infilled (Ref) frame has shown approximately a stiffness of 1.4 and strength of 1.2 that of bare frame for the 3 story case and a 1.2 strength and 1.3 stiffness of the bare frame for the 6 story case. From the normalized graphs, presence of soft story irregularity effects the seismic performance of the frame, it both weakens and softens the system as shown in Figures (7- 10) below. Soft story due to absence of masonry infill walls at the ground story is found to be more damaging than the soft story due to greater height of the ground story in both cases low and mid-rise buildings, 3-and 6-story respectively. Soft story due to absence of infill has shown approximately 1.2 lower strength than soft story due to higher story height and 1.4 lower strength than the Ref building.

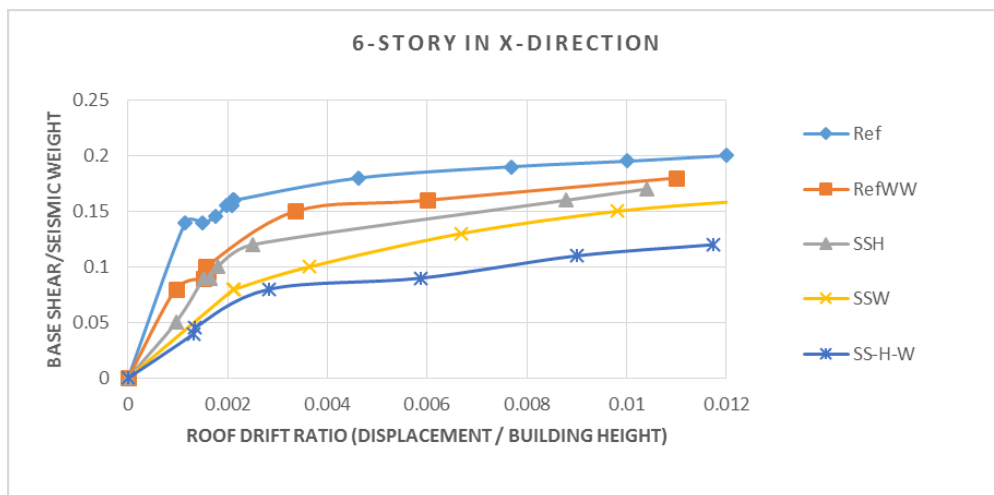


Figure 9 Capacity Curve of 6- story Frame, X-direction

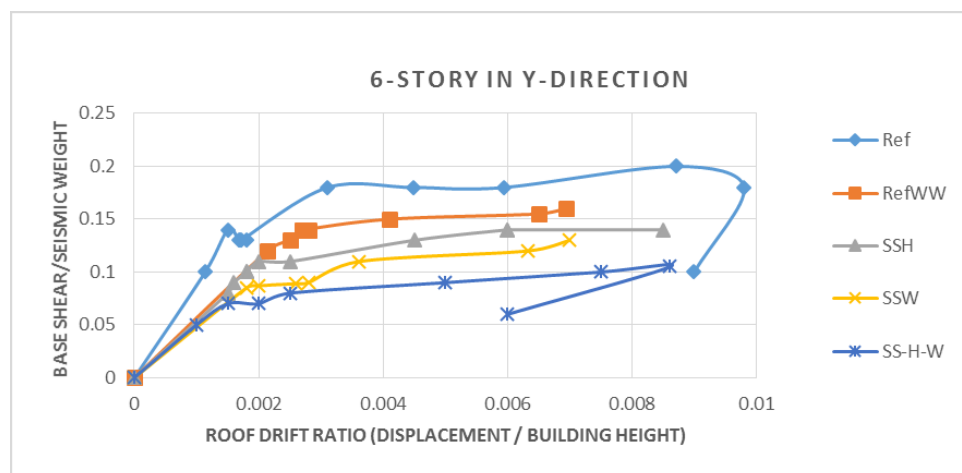


Figure 10. Capacity Curve of 6- story Frame, Y-direction

But the most unfavourable case is soft story due to both absence of infill walls and higher height of the ground story. The capacity curve of 6-story SS-H-W building has shown approximately 1.7 lower strength and 1.2 lower stiffness than Ref building, and capacity curve of 3 story SS-

H-W building has shown 1.6 lower strength and 1.9 lower stiffness than capacity curve of Ref building.

The drift ratios obtained in this study (see Figure 7-10) obviously show that the demands of 3-story buildings are higher than those of 6-story ones.

CONCLUSION

This study assesses the seismic performance of bare and masonry-in filled RC frames, frames with soft story due to absence of masonry infill walls and higher height of the ground story considering the cases separately and composed for the two types of structures low and mid-rise buildings.

Results of pushover analysis show an increase in initial stiffness, strength, and energy dissipation of the infilled frame (Ref), compared to the bare frame (RefWW), despite the wall's brittle failure modes.

Presence of soft story irregularity effects the seismic performance of the frame, it both weakens and softens the system.

Soft story due to absence of masonry infill walls (SSW) at the ground story is found to be more destructive than the soft story due to greater height (SSH) of the story in both cases low and mid-rise buildings, 3-and 6-story respectively.

The most unfavourable case is soft story due to both absence of infill walls and higher height of the ground story (SS-W-H).

Drift ratios shown in capacity curves Figures 7-10, visibly show that the demands of 3-story buildings are higher than those of 6-story.

REFERENCES

- [1] Altuntop, M. A. (2007). Analysis of building structures with soft stories. Turkey: Atelim University.
- [2] Varadharajan. (2014). Study of Irregular RC Buildings under Seismic effect. Kurukshetra: National Institute of Technology Kurukshetra.
- [3] Matjaz Dolsek, P. F. (2000). Soft story effects in uniformly infilled reinforced concrete frames. Ljubljana: University of Ljubljana.
- [4] Engineers (FEMA), A. S. (2000). Prestandart and commentary for the seismic rehabilitation of buildings (FEMA-356). Washington, D.C.: Federal Emergency Management Agency.
- [5] Sonmez, E. (2013). Effect of infill wall stiffness on the behaviour of reinforced concrete frames under earthquake demands. İzmir: Graduate School of Engineering and Sciences of İzmir Institute of Technology.
- [6] Shabnam J. Semnani, J. E. (2014). Conceptual Seismic Design Guidance for New Reinforced Concrete Framed Infill Buildings.

Earthquake Performance Assessment of a Low-rise URM Building

Hüseyin Bilgin¹, Ergys Huta¹

¹Department of Civil Engineering, Epoka University, Albania

ABSTRACT

In the present paper, seismic performance assessment of a typical low-rise unreinforced masonry (URM) building, which has been built in accordance with template designs in Albania, has been performed. For this purpose, one of the most widely used template designed URM building typology has been selected as a good representatives of residential building stock. This type shows some particular features, typical of the traditional construction techniques at that time which could be identified as the additional potential damage sources. The building was designed and constructed in 1960 and contains details which are typical of that construction period of the region. Material properties are assessed based upon experimental test results. Then, the buildings is modeled and analyzed as 3-D assembly of finite elements. The earthquake ground motion to be used in performance assessment is determined through probabilistic seismic hazard assessment. The seismic response of the buildings has been evaluated for various earthquake levels based on Eurocode 8 and FEMA 440 guidelines. Upon the evaluation of the obtained results here for the earthquake performance of this type of buildings, useful conclusions are drawn on the strength and nonlinear behavior of masonry subjected to earthquake actions.

Keywords: *Unreinforced masonry walls, earthquake performance assessment, pushover analysis, template projects.*

INTRODUCTION

Unreinforced masonry is one of the most common structural types for low-rise construction in the Albania. Particularly, Bilgin and Korini 2012, [1] have showed that the most representative typology of essential facilities (i.e., schools, hospitals, residential buildings, police stations, .etc.) of the country corresponds to URM, which are distributed throughout the region. The construction of these buildings took place during the communist period (1944-1990). Most of these existing URM have been designed considering only gravity loads without any consideration of seismic criteria [2]. Moreover, past studies [3-6] and earthquake reconnaissance team reports have suggested that URM structures are highly prone to seismic actions. Therefore, this type of structures has high seismic vulnerability over the region. This implies that a moderate or over size earthquake might cause a disastrous result associated with the URM buildings in the country.

Recently, a group of researchers have carried out the seismic hazard of Albania, approaching the problem from both deterministic and probabilistic point of views [7]. For the scope of the study, two types of response spectra are used: Eurocode 8 [8] and Albanian seismic code [9]. Mechanical properties of the case study building have been determined experimentally and adopted for the nonlinear analysis. Seismic performance evaluation of the building has been performed by N2 method proposed by Fajfar [10]. Then, using the obtained spectral

displacement and damage states suggested by Calvi [11] for URM structures, damage grades and thus the performance of the building is determined.

DESCRIPTION of the REPRESENTATIVE URM STRUCTURE

Typical URM essential facilities in Albania are template designs of low and mid-rise buildings. The structure is mainly composed of two components, namely the URM bearing walls and floor and roof diagrams. The walls are stiff with many openings and the diaphragms are usually constructed of reinforced concrete slabs. For the scope of the study, a benchmark building is selected as a representative of existing URM low-rise buildings in the region. The typical URM building, which has been studied, has three stories, brick walls of 250 mm for the load bearing walls and 120 mm for other partition walls. It has 21,85 m x 10,70 m dimensions in plan with a storey height of 2,8 m (Figure 1). Solid bricks with (250 mm x 125 mm x 60 mm) dimensions connected with cement mortar are used to build the masonry walls. The slabs are in-situ concrete ones with a height of 150 mm and a flat roof. In order to ensure a better distribution of vertical and horizontal loads, ring beams are built to create a better connection between slabs and load bearing walls.

In order to truly represent the strength and structural integrity of the case building, mechanical properties of the masonry material are obtained from the experimental tests conducted on the case study building [12]. The experimental tests are performed according to ASTM C67-09 guidelines [13]. According to the test results, clay bricks and the mortar have the 4.35 MPa and 3.88 MPa resistances, respectively and the $E = 4350$ MPa. The load bearing walls thickness is kept constant as 250 mm over the height of the structure.

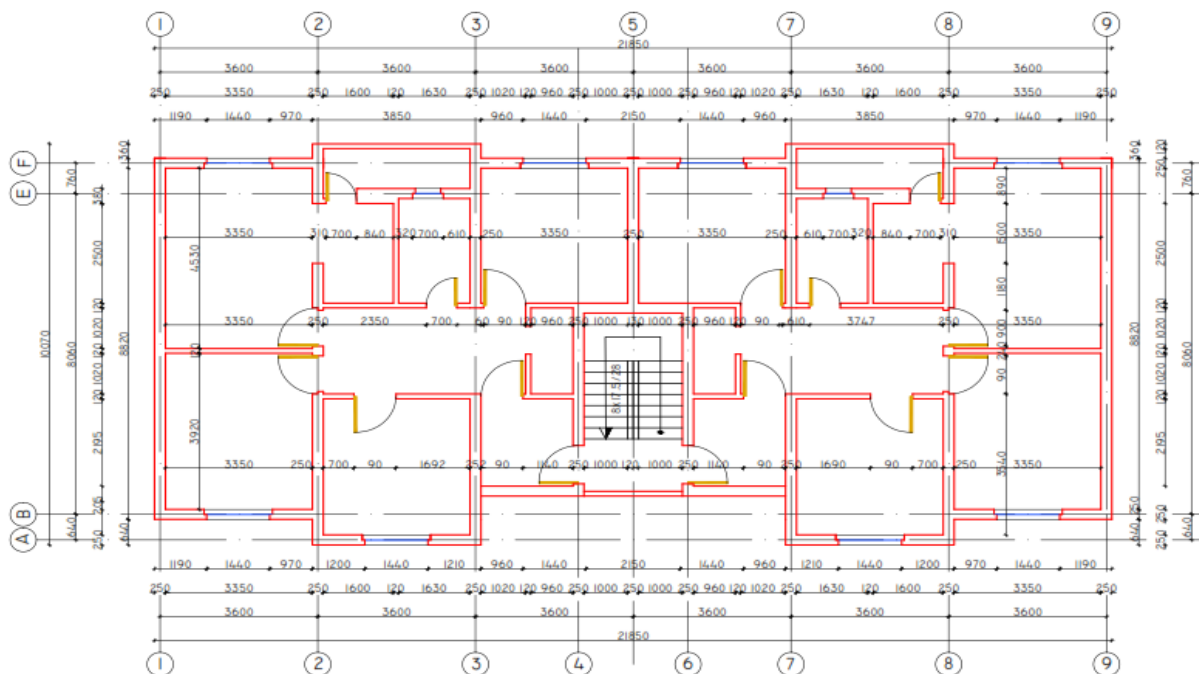


Figure 13 Typical plan view of the URM building

SEISMIC DEMAND

Albania, known with its high seismic activity, is situated on the tectonic rift that starts in South Italy, near the city of Napoli, continues with the Channel of Otranto, the cities of Vlore, Himar, Sarande, then in Thessaloniki and extends to Northern Turkey.

Earthquake loads are commonly represented by response spectrum functions. In this study, the result of a seismic hazard assessment for Lapraka area, where the building is located, is used [14]. The PGA is calculated for stiff soil conditions for two levels of probability: 10% probability of exceedance in 10 years and 10% in 50 years that correspond to two periods of 95 and 475 years repeating earthquakes. Thus, the PGA values are estimated 0.25 g for stiff soil conditions and the probability of exceedance 10%/50 years [7]. The results are summarized in Table 1.

Table 3 PGA and Spectral Acceleration [14]

PGA	S _a (0.2s)	S _a (0.5s)	S _a (1.0s)	S _a (2.0s)
0.248 g	0.595 g	0.341 g	0.173 g	0.077 g

In this study, the demand calculations for the seismic assessment of the considered building are performed considering the soil Type B with a moderate seismicity (0.248 g) according to Eurocode 8 [8].

STRUCTURAL CAPACITY

Modeling the URM Building

Masonry is a heterogeneous material composed of two components: the masonry bricks and the mortar. Its mechanical characteristics depend upon the inherent properties of its constituents. Masonry response can be very complex under simple static loadings. In order to simulate the response of URM structure, several assumptions are made and numerical models are proposed in the literature [15].

Due to the complexity on the case study, several assumptions on the material properties and the necessity of having advanced performance computers to process the analysis, macromodeling technique is considered in this study (Figure 2). DIANA v 9.6 [16] software is deployed to conduct the numerical analysis.

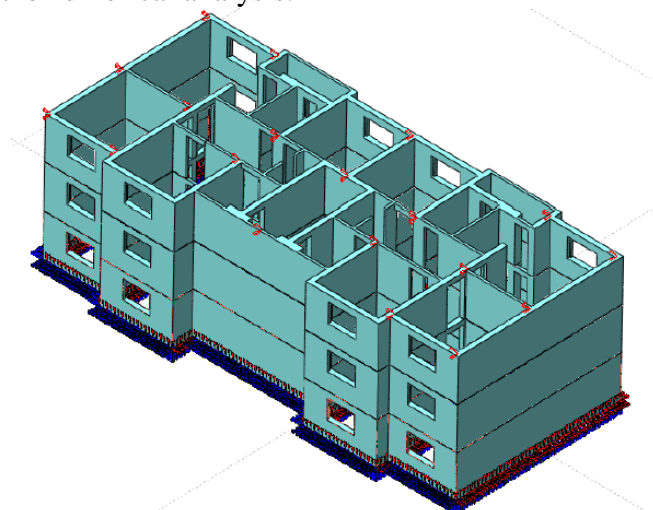


Figure 14 3D view of three storey unreinforced masonry building (DIANA v.9.6)

According to the previous experience and suggestions from the software, curved shell elements are used for modeling (Figure 3).

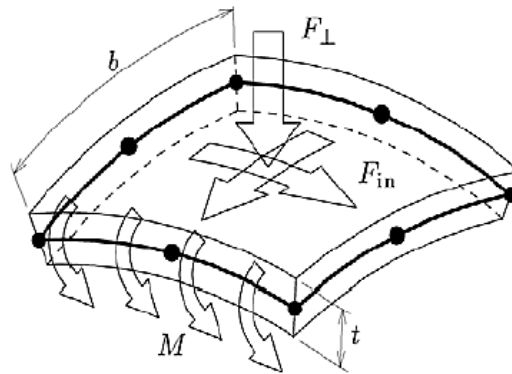


Figure 15 Curved shell element used for modeling (DIANA v.9.6)

Earthquake capacity of the URM building is obtained by pushover analysis. For nonlinear analysis, material properties are determined from experimental tests. Member sizes are used to model the selected building without making any simplifications.

ANALYSIS RESULTS

Damage Limit States

A performance level is a limit stage on the capacity curve that is used to quantify the damage. There are different approaches to damage limit states classification for masonry. Researchers like Calvi (1999) have introduced inter-storey drift ratios with three limit states. Calvi (1999) proposed three damage limit states for masonry structures as follows (Figure 6):

LS2 - Minor structural damage and/or moderate non-structural damage; the building can be utilized after the earthquake, without any need for significant strengthening and repair to structural elements. The suggested drift limit is 0.1%.

LS3 - Significant structural damage and extensive non-structural damage. The building cannot be used after the earthquake without significant repair. Still, repair and strengthening is feasible. The suggested drift limit is 0.3%.

LS4 - Collapse; repairing the building is neither possible nor economically reasonable. The structure will have to be demolished after the earthquake. Beyond this LS global collapse with danger for human life has to be expected. The suggested drift limit is 0.5%.

Below is shown a schematic capacity spectrum with the corresponding damage limit states.

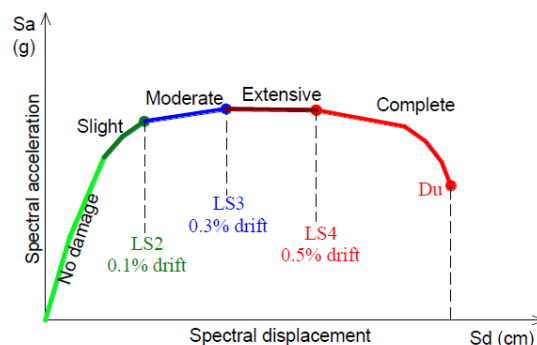


Figure 16 Damage limit states according to Calvi (1999)

Capacity Evaluation

The pushover analysis is a performance based analysis procedure which allows defining the structural response under the horizontal seismic loads and vertical gravity ones acting on the structure. The response of the structure is presented through the capacity curve which usually gives the relation between the base shear and roof displacement. It can be also plotted in ADRS format together with the demand curve and determine the top displacement under the design earthquake (performance point). The amplitudes of the seismic loads are increased in a stepwise fashion in order to observe the yielding sequences and the progress of the overall capacity curve of the structure. A non-linear static analysis is performed at each step until the structure becomes unstable.

The extended N2 method and CSM represent an assessment tool for the non-linear static analysis. However, these methods do not provide any criteria to classify the damage according to the performance point. There are various approaches to damage limit states classification for the masonry [2]. In this study are used the damage thresholds provided Lagomarsino and Penna [17] and Calvi [11]. According to Lagomarsino and Penna [17], yield point and ultimate displacement are firstly identified. After that the capacity curve is split into 5 parts (Fig. 4). Classification of damage state according to spectral displacement is provided in Table 2.

Table 2. Performance levels and criteria provided by Lagomarsino and Penna [17]

Damage state	Spectral displacement, Sd
No damage	$Sd < 0.7 Dy$
Slight	$0.7 Dy < Sd < Dy$
Moderate	$Dy < Sd < Dy + 0.25(Du - Dy)$
Extensive	$Dy + 0.25(Du - Dy) < Sd < Du$
Complete	$Sd > Du$

Two types of load distributions are applied for the pushover analysis, namely a linear distribution pattern and a modal distribution pattern. Capacity curves of the building with the corresponding damage limits states under both load patterns are given below (Figure. 5)

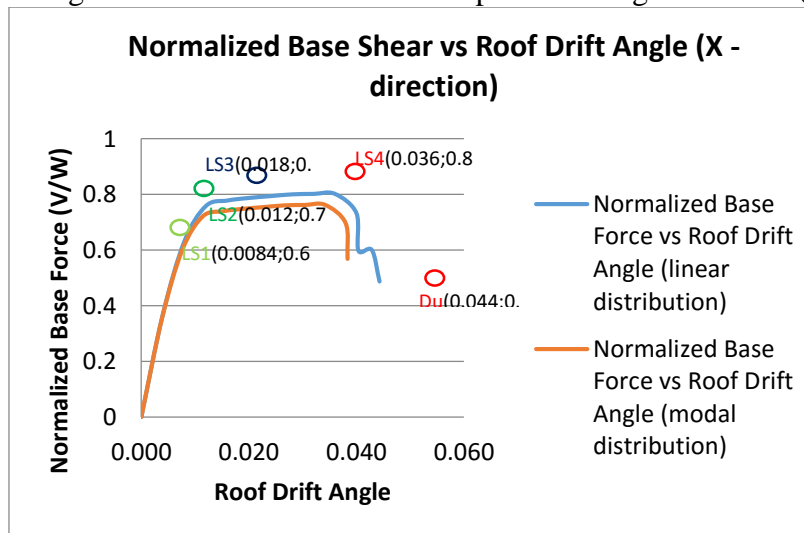


Figure 17 Capacity curve with the corresponding limit states (x- direction)

The linear distribution shows a more ductile behaviour of the structure than the modal one. Although the results state a ductile behaviour of the structure, the appearance of LS4 indicates an extensive damage state.

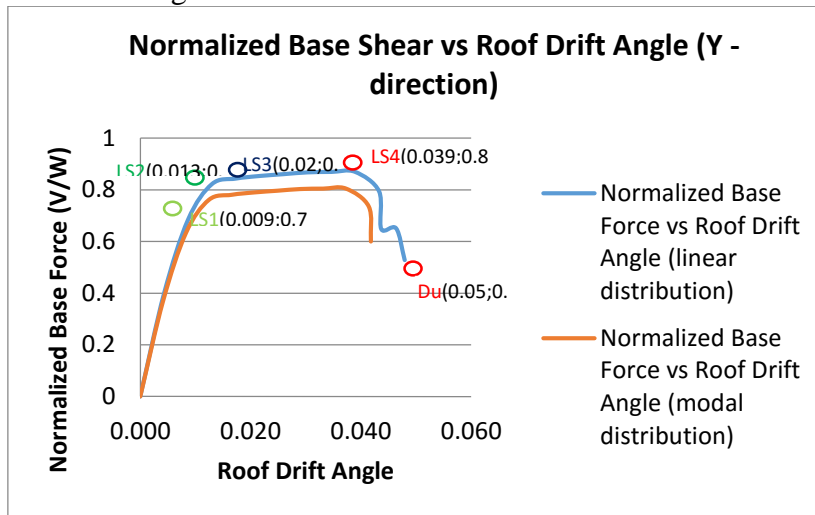


Figure 18 Capacity curve with the corresponding limit states (y- direction)

As in the *x*-direction, the linear distribution shows a more ductile behaviour of the structure than the modal one. Even in this direction the appearance of LS4 indicates an extensive damage state. A reason for this similarity is the distribution of the load bearing walls. They are distributed symmetrically in the two directions.

SEISMIC PERFORMANCE ASSESSMENT

As described previously, the performance point of the structure in *x*-direction is obtained through the extended N2 [10] and FEMA440 guidelines [18]. Capacity curves obtained by these two methodologies are plotted below for both directions (Figure 7-8).

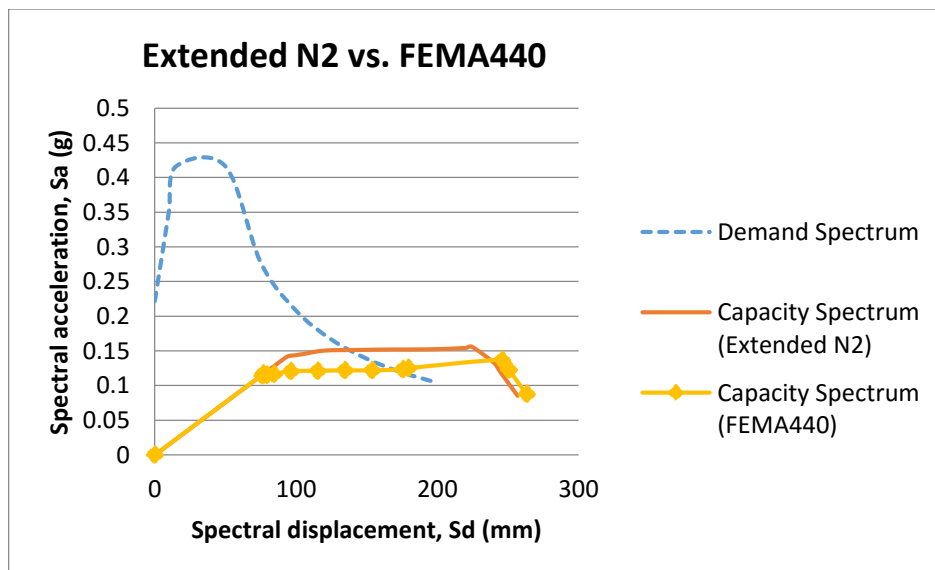


Figure 19 Performance point of URM building: Comparison of the two methodologies (*x* – direction)

FEMA440 tends to indicate a more ductile behaviour of the structure but the performance point obtained with this method is lower than the one obtained with the extended N2 method. However, both methods indicate a poor structure performance from seismic loads. This is justified by the position of the performance point: It stands between LS3 and LS4 for both spectrums.

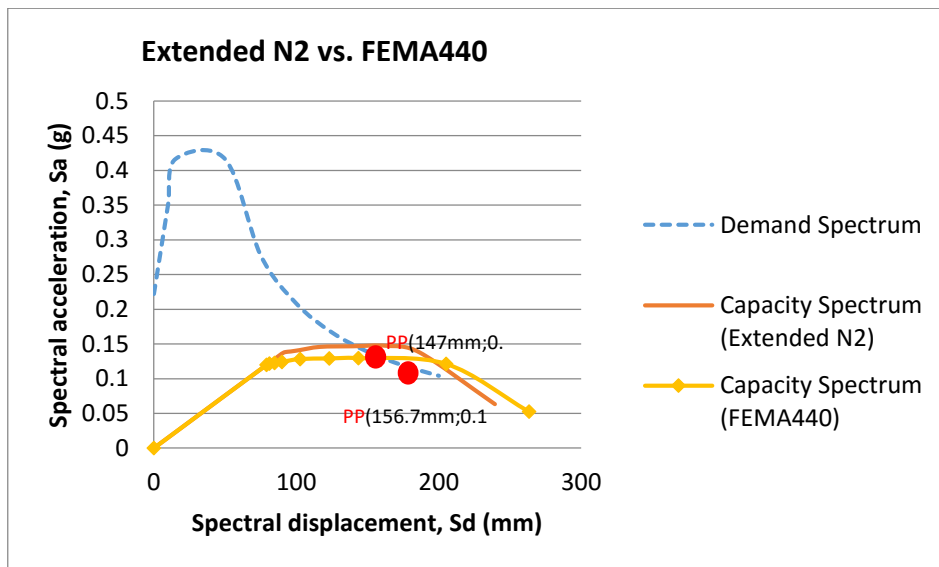


Figure 20 Performance point of URM building: Comparison of the two methodologies (y – direction)

Both codes indicate low stiffness in y-direction with a high risk of collapse. Intervention to improve the seismic capacity of the building is not economically reasonable.

CONCLUSIONS

The seismic performance of a typical 3-storey URM building of the Albanian masonry stock has been analyzed. The capacity of the building was calculated by a structural model that uses macro elements for masonry panels. The expected demand has been defined by two response spectra proposed by the EC8 [8]. The mechanical properties of the materials used are obtained from experimental tests. DIANA v.9.6 software (TNO DIANA) [10] was employed to perform the numerical analysis phase.

Damage thresholds were determined by Lagomarsino and Penna recommendations [17], while drift limits were provided by Calvi suggestions [11]. The performance points were obtained by the extended N2 methodology [10], adopted by Eurocode 8 [8] and Capacity Spectrum Method (CSM) presented in FEMA440 [18]. According to the analysis results; capacity curves obtained by non-linear static analysis demonstrate that URM building poorly performs under earthquake loads. The presence of Limit State 4 (LS4) performance stage indicates an extensive damage state according to Lagomarsino and Penna damage thresholds.

REFERENCES

- [1] Bilgin, H. and Korini, O.: Seismic capacity evaluation of unreinforced masonry residential buildings in Albania, *Nat. Hazards Earth Syst. Sci.*, 12, 3753-3764, doi:10.5194/nhess-12-3753-2012, 2012.
- [2] Korini, O. (2012). “*Seismic Assessment of Albanian Masonry Buildings Using Nonlinear Procedures*”, MSc thesis, 150 pages, Epoka University, Tirana, Albania.
- [3] Inel, M., Ozmen, H. B., & Bilgin, H. (2008). Seismic performance evaluation of school buildings in Turkey. *Structural Engineering and Mechanics*, 30(5), 535-558.
- [4] Yilmaz, S., Tama, Y. S., & Bilgin, H. (2012). Seismic performance evaluation of unreinforced masonry school buildings in Turkey. *Journal of Vibration and Control*, 1077546312453190.
- [5] Bilgin, H. (2013). Fragility-based assessment of public buildings in Turkey. *Engineering Structures*, 56, 1283-1294.
- [6] Bilgin, H. (2015). Generation of Fragility Curves for Typical RC Health Care Facilities: Emphasis on Hospitals in Turkey. *Journal of Performance of Constructed Facilities*, 04015056.
- [7] Aliaj, S., Koçiu, S., Muço, B., Sulstarova, E.: *Sizmiciteti, Sizmotektonika dhe Rreziku sizmik i Shqipërisë*, Albanian Academy of Science, Tirana, 2010 (In Albanian).
- [8] KTP-N2-89, *Albanian seismic design code*. (1989) (In Albanian).
- [9] EN 1998-1. European seismic design code. (2004). Design of structures for earthquake resistance. Part 1: General rules, seismic actions and rules for buildings.
- [10] Fajfar, P., Marušić, D., Perus, I.: *The extension of the N2 method to asymmetric buildings*, proceedings of the 4th European workshop on the seismic behaviour of irregular and complex structures, Thessaloniki, 2005.
- [11] Calvi, G. M., (1999). A displacement-based approach for vulnerability evaluation of classes of buildings. *J Earthquake Eng* 3(3):411–438.
- [12] Huta, E. (2015). “*Earthquake Performance of Low and Mid-Rise Masonry Buildings in Albania*”, MSc thesis, 149 pages, Epoka University, Tirana, Albania.
- [13] American Association State Highway and Transportation Officials Standard, Designation: C67 – 09: *Standard Test Methods for Sampling and Testing Brick and Structural Clay Tile.*, 2008.
- [14] Aliaj, S., Allkja, S.: *Studim inxhinierë-sizmologjik i sheshit të ndertimit të objektit me laretsi 2 - 7 kate me 1 kat nëntokë në rrugën “Don Bosko”, në zonën e Laprakes*, Tirana, Albania, 2014 (In Albanian).
- [15] Lourenço, PB. Computations on historic masonry structures. *Progress in Structural Engineering and Materials* 2002; 4(3):301-319.
- [16] DIANA, Finite Element Analysis: *User’s Manual, Concrete and Masonry Analysis.*, Netherlands, 2014.
- [17] Lagomarsino, S., Galasco, A., and Penna, A., (2007), Nonlinear macro element dynamic analysis of masonry buildings. In: *Proceedings of the ECCOMAS thematic conference on computational methods in structural dynamics and earthquake engineering*, Rethymno, Crete.

- [18] Federal Emergency Management Agency, Fema-440, (2005). Improvement of Nonlinear Static Seismic Analysis Procedures, Applied Technology Council.

Usage of ferrocement jacketing for strengthening of damaged unreinforced masonry (URM) walls

Enea Mustafaraj¹, Yavuz Yardim²

¹Department of Civil Engineering, Epoka University, Albania

²Department of Civil Engineering, University of Nizwa, Oman

ABSTRACT

In this paper, it is presented the usage of ferrocement jacketing technique as an effective method to improve structural performance of unreinforced masonry panels. Nine diagonal compression tests were conducted on plain, pre-cracked repaired and reinforced masonry panels on six specimen with nominal dimensions of 1.2 x 1.2 x 0.25 m, built and tested in laboratory. The results of the diagonal compression tests were compared in terms of increase in shear strength, drift and the mode of failure.

Additionally, finite element modelling using discrete micro-modelling and non-linear analyses were performed using midas FX+ for DIANA 9.6 commercial software to simulate the behavior of plain and reinforced panels.

As a result, it was observed that ferrocement jacketing made a considerable improvement in shear strength and deformation capacity for both, repaired and reinforced masonry panels.

Keywords: *ferrocement jacketing, URM, DIANA, diagonal compression test, repaired masonry, reinforced masonry*

INTRODUCTION

Unreinforced masonry (URM) buildings are one to the most used construction types in the world. Generally, these types of buildings have been designed (often not designed at all) to only resist gravitational loads and have been realized by rules of common practice. During their existence, many of those structures have suffered from the combined effects of inadequate construction techniques, seismic and wind loads, foundation settlements and deterioration of construction materials [1].

During an earthquake, the walls are subjected to a combination of lateral seismic forces, induced by the earthquake, that are in the form of out-of-plane or in-plane loading depending on the orientation of the building with respect to the earthquake epicenter. They manifest a brittle behavior and are very weak when subjected to such types of loads. The overall seismic performance of URM buildings depends on the capacity of in-plane walls to safely transfer the lateral loads to foundations. In this way, the masonry walls provide the post-earthquake stability necessary to avoid collapse of the entire structure [2].

As a result, it is the response of in-plane loaded wall that governs the global seismic performance of a URM building. In order to improve deficiencies related to poor structural performance of URM structures under seismic actions, various strengthening techniques have been developed and applied throughout history of construction. The main aim of the strengthening techniques is to increase low parameters of masonry such as tensile and shear strength as well as vulnerability against lateral loads. Traditional techniques such as: i) filling

cracks and voids by grouting; ii) stitching of large cracks and weak areas with metallic or brick elements; iii) external or internal post-tensioning with steel ties; iv) shotcrete jacketing; v) ferrocement and vi) center core are available for retrofitting of existing masonry structures [3-4].

The main focus of this study is the ferrocement jacketing technique which is applied by embedding closely spaced meshes of fine rods with reinforcement ratio of 3-8% in high strength (15-30 MPa) cement-mortar layer of 10-50 mm thickness. The typical mortar mix consists of cement: sand ratios of 1: (1.5-3) with a w/c ratio of 0.4 [5]. It causes considerable increase in stiffness. Strengthening of pre-damaged URM walls can restore the original capacity and stiffness. Ferrocement can control crack formation as it has high flexural and shear strength.

It has been subject of many studies for both unreinforced masonry as well as concrete structures [6-9]. Kaushik et al.[10], observed that ferrocement provided an increase of strength and ductility for columns in both axial and eccentric loading conditions, improvement of cracking resistance [11], increased stiffness and ultimate load carrying capacity [12].

Some of the advantages of ferrocement such as considerably low price and ability to be completed with unskilled workers, make it an ideal solution for low cost housing.

It has been observed that the mesh helps to confine the masonry unit after cracking and it improves in-plane elastic deformation capacity. Abrams et al.[13], observed that the in-plane lateral resistance was increased 1.5 times during a static cyclic test. The out-of-plane behavior (arching action and out-of-plane stability) is improved too, as the ferrocement increases the wall height-to-thickness ratio [14-15].

In this paper, it is presented the usage of ferrocement jacketing technique as an effective method to improve structural performance of unreinforced masonry panels, its effectiveness in improving the structural performance of URM panels in diagonal compression testing following ASTM E 519-07 [16].

MATERIALS AND METHODS

The methodology followed in this study consists of destructive tests on masonry panels in order to determine the main mechanical properties of bricks, mortar and masonry assemblage. The testing procedures are the ones defined in American Society for Testing and Materials (ASTM) where are defined all the steps to be followed. These standards have been used by many researchers who have experimented with unreinforced clay brick masonry all over the world [1] [17-19].

Plain Panels

All the panels, were built using two leaf, English bond and new clay bricks with typical nominal dimensions of 243.4 mm x 118.9 mm x 56.8 mm with 15 mm thick mortar joints made of hydraulic cement mortar of type "N" with a volumetric mix ratio of cement: lime: sand, 1:1:6 (Figure 21). The specimen are part of a wider experimental campaign conducted by the authors for a research project at Epoka University.



Figure 21. Construction process of plain walls.

Ferrocement jacketing reinforced panels

W-10-FC, W-11-FC and W-12-FC panels were reinforced using ferrocement jacketing; attachment of a double-layered galvanized steel mesh on both sides of the plain wall (**Error! Reference source not found.**). The mesh is fixed to the wall by means of mechanical anchors and common mortar. The dimensions of the steel mesh are equal to the plain wall (1.2 m x 1.2 m). Allowance of 1.5-2 cm on each side shall be made in order to have a proper jacketing of the wall. The galvanized steel mesh is fixed using anchors (threaded bolts of diameter 8 mm and length 70 mm with washers, mounted on previously drilled holes, having 10-mm wall plugs on the bricks at a distance of 30 cm). The spacing of the connections was slightly changed depending on the brick arrangements, in order to make sure that the connection was done on the brick and not on the mortar joint. The process of mounting the steel mesh on the faces of the wall should be done carefully in order to lay the layers properly, as well as to provide a 5-10 mm allowance between mesh and the bricks for plaster mortar. The mortar mix is prepared using cement: sand 1:4, by volume and water/cement ratio of 0.4.

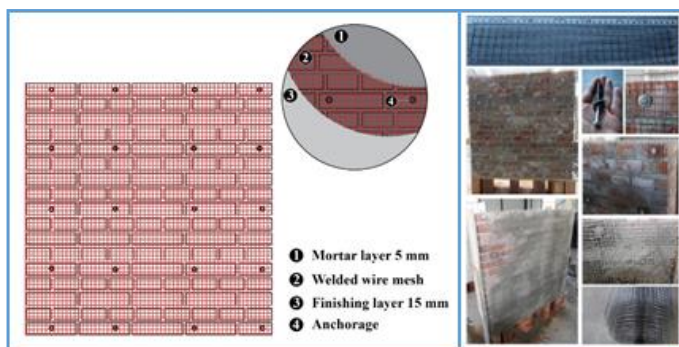


Figure 2. Plastering process with ferrocement jacketing (FC) (schematic view and application) (left) and repairing with ferrocement (right).

Ferrocement jacketing repaired panels

The procedure of repairing of the damaged walls with ferrocement is the same as strengthening of the plain walls. The only difference is application of an extra layer of galvanized steel mesh along the diagonal cracks of the damaged wall (Figure 2). This layer is fixed using extra anchors drilled every 30 cm along the diagonal.

Determination of Diagonal Tensile Strength

ASTM E 519-07 [16] is a test method used to determine the diagonal tensile or shear strength of 1.2 by 1.2 m masonry assemblages by loading them in compression along one diagonal, thus causing a diagonal tension failure with the specimen splitting apart parallel to the direction of load (Figure 3).

The movable test set-up consists of two loading shoes placed on two diagonally opposite corners of the panel connected by four high strength steel rods positioned along the compressed diagonal. The 50-tonne-capacity hydraulic jack was incorporated between the top loading shoe and a metallic plate connected to the steel rods, which when loaded, developed tension forces on the four steel rods connecting the loading shoes, compressing the wall diagonally, providing the desired failure mode; diagonal cracking and/or bed joint sliding failure.

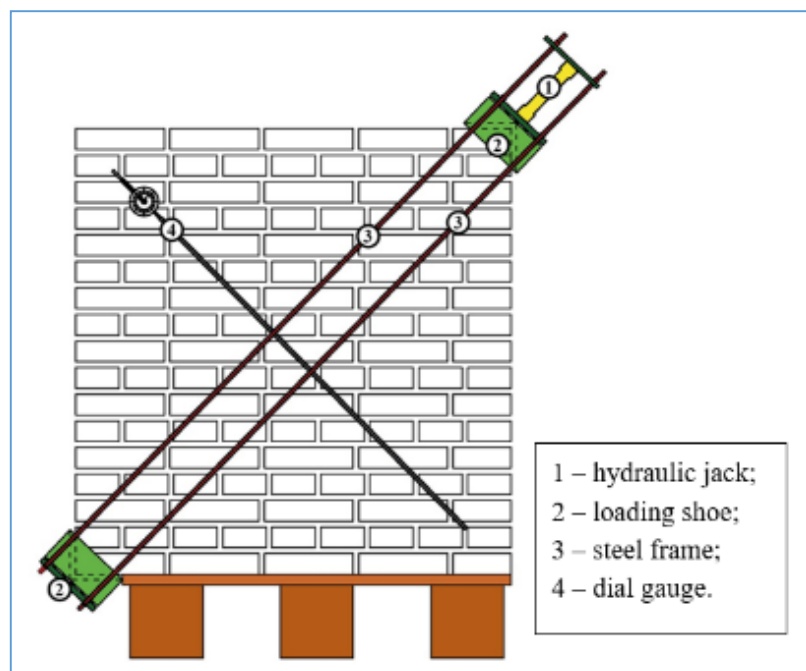


Figure 3. Diagonal compression test set-up.

Numerical modelling

The model was created in midas FX+ for DIANA 9.6. The mesh of the model was done following three main stages: firstly the half-brick was created with interface elements to represent the brick crack and the brick joint, then the basic brick was duplicated in order to create the two-brick model with all the interface elements required for simulation. Lastly, the two-brick model was replicated in horizontal and vertical direction in order to achieve the required dimensions of 1.2 x 1.2 m. In this modelling strategy, the material in the bricks and

brick crack interface were kept as linear indicating that the cracks would be developed only in the mortar joints (as it was clearly seen during the experimental stage of the campaign). In order to effectively apply the load and to simulate the shear behavior of masonry, the bottom edges of the model were constrained in horizontal and vertical direction, whereas for the top edges, only for vertical direction. Additionally, in order to prevent horizontal deformation of the upper edge, a multi-point constraint was applied.

The loading consists of application of a unit horizontal displacement along the top of the panel which would be transferred uniformly along the entire upper edge due to the multi-point constraint applied earlier (Figure 5). The strengthened panels were modelled using an additional reinforcement layer made of a reinforcement grid

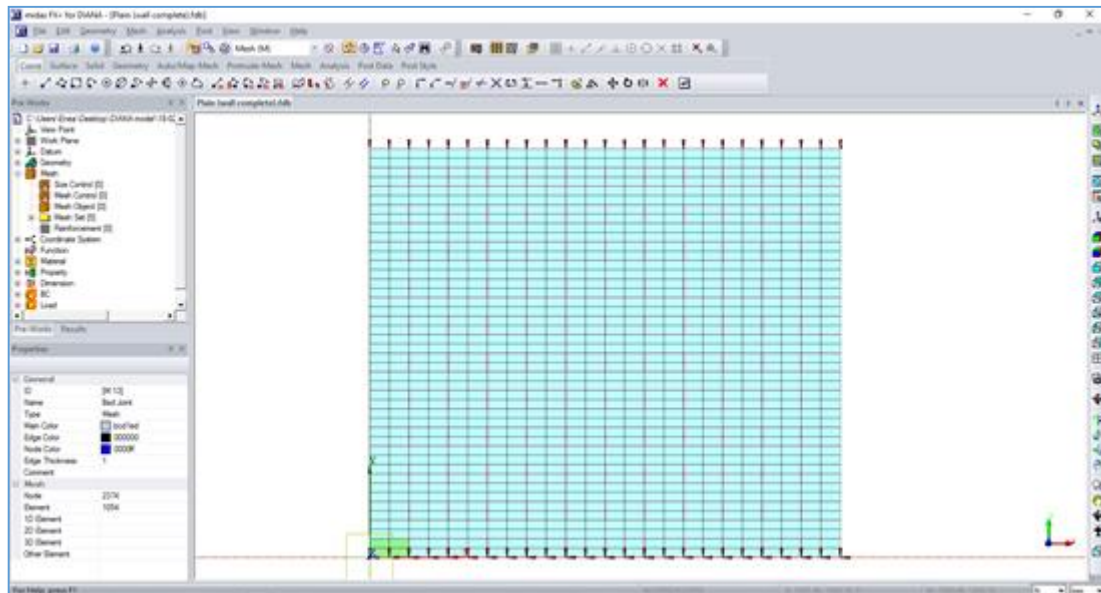


Figure 5. The finished model in midas FX+ for DIANA.

EXPERIMENTAL RESULTS

The main outcome of the experimental results was the type of failure mode for both types of panels: plain and reinforced, shear stress-strain diagrams and maximum shear stress and ultimate drift. The experimental results showed that all the tested specimens presented a similar failure mode, mainly characterized by a step-like crack along one of the diagonals.

The plain wall panels had a similar failure mode; it was observed that cracking occurred along the compressed diagonal, predominantly through the mortar joints. Nevertheless, in some cases, sliding along the mortar bed joints, following by diagonally extended cracks was observed (Figure 6). The overall failure mode can be categorized as tension failure followed by shear-sliding along the compressed diagonal in a step-like pattern.

The plain panels (W-06, W-07, W-08) exhibited similar failure modes; a step-like pattern along the compressed diagonal. The cracks occurred in the mortar joints.



Figure 6. Failure mode of plain, ferrocement strengthened and repaired panels.

Ferrocement jacketing reinforced panels (W-X-FC)

In the ferrocement jacketing reinforcement panels while loading, hair-like cracks were observed, mainly in the compressed diagonal. From the tests, it was observed no splitting in the head or bed joints. The total failure of the wall after the reinforcing ferrocement-plastering layer yielded, is attributed to the loss of bond between the plastering layer and the wall (Figure 6). The connection failure is the main cause of loss of adhesion of the strengthening layer that caused the overall failure of the panels.

In W-11-FC apart from the diagonal and hair-like cracks that were developed in the plaster layer, after exceeding the materials' resisting capacities, due to high tensile stresses, connection failure was observed, which resulted in thick radial cracks around the unloaded upper and bottom edges of the panel. In W-12-FC, connection failure resulted in debonding of the mesh reinforced plaster layer.

Despite the various final cracks of the panels, it was observed that the reinforcing layer had quite a satisfactory behaviour with respect to the strengthened panel. Until the ultimate

strength was reached, no debonding of the mesh and wall panel was observed. For such a composite structure, made of heterogeneous and anisotropic material, the most important properties are ductility and shear strength, thus, in such a case, the performance of this technique is deemed successful.

Repaired walls with Ferrocement jacketing (W-X-R-FC)

The crack pattern of the ferrocement jacketing repaired panels of both series were similar to the corresponding W-FC reinforced panels. Before failure, after unloading, the diagonal cracks were not visible to the naked eye. Because of this reason, during testing stage, all the developed cracks were marked with a graphite pencil at various loading stages. Apart from the usual cracking mode, debonding of the repairing plaster layer was observed.

Shear stress-strain response

The shear stress-strain response is presented in Figure 7. For all the wall panels, the experimental curve was approximately linear prior to crack initiation, followed by a nonlinear portion of the curve up to the maximum strength. This similar behaviour was also observed in other studies [20-24].

As it can be seen, the plain wall panels of both are very brittle, and the stress-strain response is very short. The change in stiffness was observed usually for load values close to the ultimate load, as the first crack develops but it cannot expand due to the presence of the external reinforcement.

For the reinforced panels, on the other hand, stress-strain curve starts with a steep slope indicating the linear stage of masonry, whereas the second stage indicates the plastic phase and it is almost horizontal that usually started after the cracks became visible to naked eye. In this stage, the degraded stiffness can be observed (Figure 7).

From the stress-strain diagrams of the ferrocement jacketing repaired panels compared to their homologous pre-cracked panel. As it may be seen from the graphs, after repair, there is a considerable improvement of ductility and shear strength of the repaired panels.

Mechanical parameters

For the plain panels, the average shear strength was 0.337 MPa, with a maximum value of 0.423 MPa occurring at W-06 and a minimum value of 0.282 MPa occurring at W-07. Another parameter to be taken into consideration while analysing the behaviour of URM is the ultimate drift and ductility. The average drift was calculated to be 0.103%, with a maximum value of 0.150% occurring at W-07 and a minimum of 0.078% occurring at W-08. The average shear and elastic moduli were 365 and 912 MPa, respectively.

The panels reinforced with ferrocement jacketing resulted in maximum shear strength of 0.892 MPa (at W-10-FC) and a drift of 0.890% (at W-12-FC). As it may be seen from Table 4, average shear strength was 2.439 times higher than the plain panel, whereas the ultimate drift was 6.718 times higher. The average shear and elastic moduli were 126 and 315 MPa, respectively.

The repaired panels with ferrocement jacketing exhibited considerable improvement of shear strength and ultimate drifts when compared to their plain counterparts. The average values of ultimate diagonal load, shear strength and ultimate drift are 255.743 kN, 0.603 MPa and 1.366%, respectively. The maximum ultimate load and shear strengths were achieved from W-

06-R-FC (288.956 kN and 0.681 MPa), whereas the minimum values were recorded from W-07-R-FC (209.244 kN and 0.493 MPa). Nevertheless, W-07-R-FC achieved the highest ultimate drift of 2.229%.

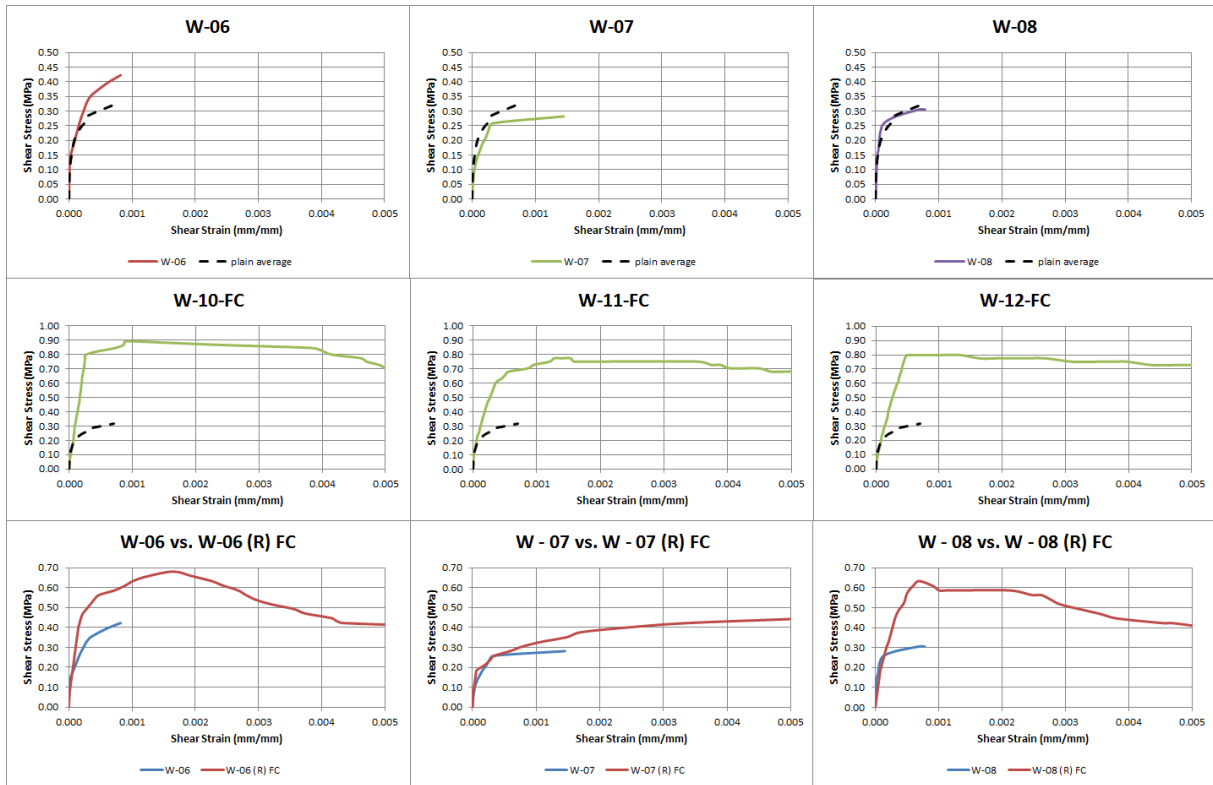


Figure 7. Summary of shear stress vs. shear strain of plain, ferrocement jacketing reinforced and repaired panels.

Table 4. Summary of mechanical parameters of tested specimen.

Wall panel	P_{max} (kN)	v_{max} (MPa)	v_{max}/v_0	δ_u (%)	δ_u/δ_0	G (MPa)	E (MPa)
W-06	179.352	0.423		0.082		515.488	1288.720
W-07	119.568	0.282		0.150		187.880	469.700
W-08	129.532	0.305		0.078		391.359	978.397
W-X	142.817	0.337	-	0.103	-	364.909	912.272
W-10-FC	378.632	0.892		0.512		174.238	435.596
W-11-FC	328.812	0.775		0.675		114.800	287.000
W-12-FC	338.776	0.798		0.890		89.708	224.270
W-X-FC	348.740	0.822	2.439	0.692	6.718	126.249	315.622
W-06-R-FC	288.956	0.681	1.610	1.075	13.110	63.346	158.365
W-07-R-FC	209.244	0.493	1.748	2.229	14.860	22.123	55.307
W-08-R-FC	269.028	0.634	2.079	0.794	10.179	79.864	199.660
(W-X-R-FC)	255.743	0.603	1.789	1.366	13.262	55.111	137.777

P_{max} - ultimate load, v_{max} - ultimate shear strength, δ_u - ultimate drift, G-shear modulus, E- Modulus of Elasticity

Experimental vs Numerical comparisons

In this section a comparison between experimental and numerical results is discussed. The main parameter that was used to understand the trend of the behavior of the panels is the comparison between stress-strain diagrams. The stress-strain diagram obtained after nonlinear analysis showed that the plain panels, as expected exhibited a very brittle behavior and much lower values in both analyses; 0.228 MPa shear strength and a maximum strain of 0.0012.

The ferrocement strengthened specimens achieved the highest shear stress of 0.937 MPa and a maximum strain of 0.0050, considerably higher than other two panels.

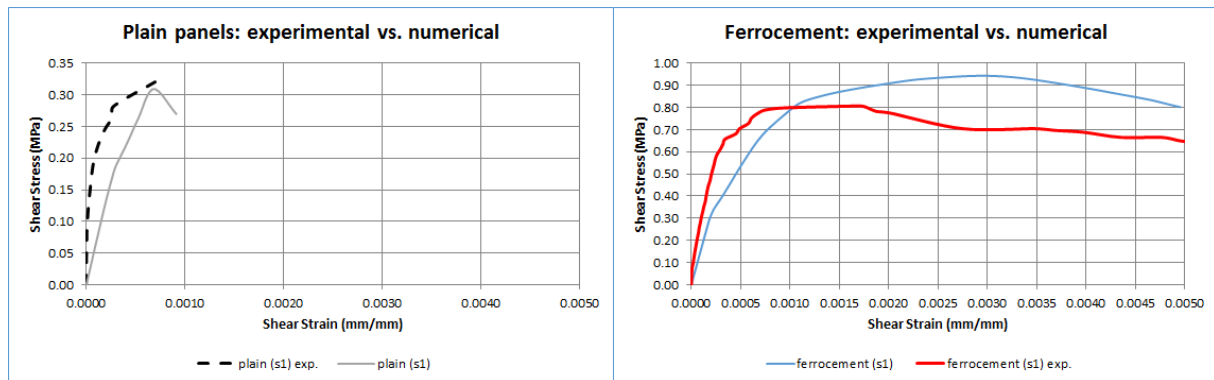


Figure 8. Comparison between experimental and numerical results of plain and ferrocement strengthened panels.

In Figure 8 it is presented the individual comparison between each of the investigated panel types. It was observed that all the modelled panels were more ductile. It may be explained by the linearity assumptions of assumed the material properties used for modelling.

CONCLUSION

In this paper nine diagonal compression tests were performed, three on plain panels and three on ferrocement jacketing reinforced panels to observe the structural behaviour of masonry and investigate the performance of ferrocement jacketing technique. Diagonal cracking was observed to be the main failure mode for both types of the specimen. The unreinforced walls exhibited a very brittle behaviour and low shear strength. The reinforced panels, on the other hand, demonstrated a much ductile behaviour, large deformation capacity and higher shear strength. This strengthening technique was proven to be an effective way to improve the overall structural performance of URM walls.

Acknowledgement

As these panels are part of a wider research project, the authors would like to thank Epoka University for the financial and logistic support, and Malvino Turku for his valuable help during the testing of the panels in laboratory.

REFERENCES

- [1] Faella, C; Martinelli, Nigro, E and Paciello, S. "Shear capacity of masonry walls externally strengthened by a cement-based composite material: An experimental campaign," *Construction and Building Materials*, vol. 24, p. 84–93, 2010.
- [2] Lourenço, P.B. "Computational strategies for masonry structures," Delft University of Technology, Delft, Netherlands, 1996.

- [3] Kalali A. and Kabir, M.Z. "Experimental response of double-wythe masonry panels strengthened with glass fiber reinforced polymers subjected to diagonal compression tests," *Engineering Structures*, vol. 39, pp. 24-37, 2012.
- [4] Triantafillou, T.C. "Strengthening of masonry structures using epoxy-bonded FRP laminates," *ASCE Journal of Composites for Construction*, vol. 2, pp. 96-104, 1998.
- [5] Montes, P. F. A. "Behaviour of a hemispherical dome subjected to wind loading," *Journal of Wind Engineering and Industrial Aerodynamics*, vol. 89, pp. 911-924, 2001.
- [6] Rosenthal, I. "Precast ferrocement columns," *Journal of Ferrocement*, vol. 16, pp. 273-284, 1986.
- [7] Winokur, A and I. Rosenthal, I. "Ferrocement in centrally loaded compression elements," *Journal of Ferrocement*, vol. 12, pp. 357-364, 1982.
- [8] Razvi, S. and Saatcioglu, M. "Confinement of reinforced concrete columns with welded wire fabric," *ACI Structural Journal*, vol. 86, pp. 615-623, 1989.
- [9] Mourad S. M. and Shannag, M. J. "Repair and strengthening of reinforced concrete square columns using ferrocement jackets," *Cement & Concrete Composites*, vol. 34, pp. 288-294, 2012.
- [10] Kaushik, S., Prakash, A. and Singh, A. "Inelastic buckling of ferrocement encastred columns," in 5th International Symposium on Ferrocement, 1990.
- [11] Ahmed, T., Ali, S. and Choudhury, J. "Experimental study of ferrocement as a retrofit material for masonry columns," in 5th International Symposium on Ferrocement, 1990.
- [12] Nedwell, P., Ramesht, M. and Tabhanaki, R.S. "Investigation into the repair of short square columns using ferrocement," in 5th International Symposium on Ferrocement, 1990.
- [13] Abrams, D., Smith, T., Lynch, J., and Franklin, S. "Effectiveness of rehabilitation on seismic behavior of masonry piers," *ASCE Journal of Structural Engineering*, vol. 133, no. 1, pp. 32-43, 2007.
- [14] Forta Ferro Corporation, "Forta for Concrete," September 2015. [Online]. Available: www.forta-ferro.com.
- [15] American Concrete Institute, "State-of-the-art Report on Fiber Reinforced Concrete," ACI, 2002.
- [16] Wood, W.A., "Load distribution of masonry walls subject to concentrated loads over openings," University of Pittsburgh, Pittsburgh, USA, 1998.
- [17] Drysdale, R., Hamid, A. and Baker, L. "Masonry Structures: Behaviour and Design," The Masonry Society, 1999.
- [18] Croci, G., *The conservation and structural restoration of the architectural heritage*, Southampton, UK: Computational Mechanics Publications, 1998.
- [19] Mustafaraj, E. *Assessment of historical structures: A case study of five Ottoman mosques in Albania.*, Germany: LAP Lambert Academic Publishing., 2014.
- [20] Kaushik, H.B., Rai, D. C. and Jain, S.K "Uniaxial compressive stress-strain model for clay brick masonry," *Current Science*, vol. 92, no. 4, pp. 497-501., 2007.
- [21] Lumantarna, R. "Material characterization of New Zealand clay brick unreinforced masonry buildings," University of Auckland, Auckland, New Zealand, 2012.
- [22] Karaman, S. Gunal, H. and Ersahin, S. "Assesment of clay bricks compressive strength using quantitative values of colour components," *Construction and Building Materials*, vol. 20, no. 5, pp. 348-354, 2006.
- [23] Elert, K, Cultrone, G., Navarro, R. C. and Pardo, E.S. "Durability of bricks used in the conservation of historic buildings - influence of composition and microstructure," *Journal of Cultural Heritage*, vol. 4, no. 2, pp. 91-99, 2003.
- [24] ASTM, "ASTM C 62-04 Standard Specification for Building Brick (solid masonry units made from clay or shale)," ASTM International, West Conshohocken, PA, 2004.

